Natural abundance stable isotope values as a tool to link microbial processes and geochemistry applied to boreal forest soils and serpentinization associated springs

by

© Lukas Kohl

A thesis submitted to the
School of Graduate Studies
in partial fulfilment of the
requirements for the degree of
Doctor of Philosophy

Department of Earth Sciences
Memorial University of Newfoundland

September 2016

St. John's Newfoundland

Abstract

Naturally occurring variations in stable isotope ratios provide a tool to study biogeochemical cycles in the absence of disturbance, including amended labelled substrates. This thesis followed two such approaches to study microbial processes in two contrasting ecosystems, ultra-basic, reducing springs and boreal forest soils along a climate transect.

First, the fact that the carbon stable isotope ratios of biomass represent the stable isotope ratio of the carbon source of an organism ("You are what you eat") was exploited to investigate substrate use pattern of microorganisms in undisturbed forest soils. On a pedon scale, fungal and bacterial specific fatty acid biomarkers were isotopically distinct but exhibited no variation with depth in contrast to the increasing $\delta^{13}C$ of the bulk soil C. This suggests a common substrate supporting microorganisms across soil horizons. Further, the carbon isotope ratio of the total microbial community, determined using ubiquitous fatty acid biomarkers, appeared to be dictated by the proportion of ^{13}C-enriched bacterial relative to ^{13}C-depleted fungal biomass in the community. This suggests that the decrease of fungi:bacteria ratio with depth likely contributes to the widely observed increase in $\delta^{13}C$ of bulk soil organic carbon with depth.

Geochemical analyses of soils from across a boreal forest climate transect indicate that climate history and diagenesis can influence distinct chemical properties of soil organic matter. Patterns in these distinct properties across climates indicate that distinct litter inputs rather than soil organic matter diagenesis controls the climate effects on soil chemistry in these forests. First, a warmer climate led to a decrease of moss litter relative to coniferous litter, thus changing the composition of the total litter inputs. Second, a warmer climate led to an increase in nitrogen concentration, which in turn led to a shift in microbial substrate use patterns and to distinct changes of litter chemistry during early litter decomposition. Together, these indirect climate effects led to the establishment of less bioreactive organic matter in warmer climate soils.

Second, the investigation of ultra-basic, reducing springs, in this thesis provides the first microcosm experimental evidence of microbial methanogenesis in this environment. Furthermore, this thesis exploited the distinct isotope fractionation factors associated with the two main metabolic pathways of methanogenesis demonstrating that carbonate, rather then acetate, was the main precursor of microbial methane in this environment. This result suggests that CO_2 injections for carbon capture and storage, which have been proposed for similar sites, might stimulate methanogenesis.

Overall, this thesis made contributions to the understanding of each of the studied ecosystems, and demonstrates the great potential and flexibility of the application of natural abundance stable isotope analysis for reconstructing microbial processes in undisturbed or hard-to-access environments.

Contents

Chapter 1

General Introduction

1.1 Microbial processes dominate geochemical cycles on the surface of Earth

Microorganisms are ubiquitous. Life on Earth is dominated by unicellular organisms, both in terms of cell numbers and biomass [Whitman et al., 1998]. Since the first observations of unicellular organisms by renaissance era researchers equipped with newly invented primitive microscopes , the range of environments in which microbial life has been detected has continued to expand. Living microorganisms are continually found in settings previously thought uninhabitable, and few proclaimed limits for microbial life have stood the test of time.

Microbial growth has been detected at temperatures of up to 121 °C [Kashefi, 2003], under the extreme drought of the Atacama dessert [Navarro-González et al., 2003], and in frozen soils with temperatures as low as -10 °C [Clein and Schimel, 1995]. Microbial life has been found in acid mine drainage fluids with pH values <1 [Johnson, 1998] as well as in in serpentinization-associated springs and hydrothermal vents with pH values >11 [Schrenk et al., 2013]. Even the clean rooms of hospitals and space craft assembly sites host microorganisms adapted to the harsh conditions applied regularly to sterilize these locations [Li and Hou, 2003, La Duc et al., 2007]. Recently, living microorganisms have been detected

at kilometers depth below both the terrestrial surface and the marine seafloor, in sediments that are hundred of millions of years old, and in crystalline rocks of low permeability [Colwell and D'Hondt, 2013].

Microorganisms efficiently harvest chemical energy and contribute to the global cycling of elements. With ubiquitous microbial life, it is not surprising that microorganisms effectively harvest (geo)chemical energy wherever available. Nearly all non-equilibrium electron transfer reactions that occur on Earth's surface are catalyzed by microorganisms, or, more specifically, by a small number of complex enzymes that developed at an early step in the evolution of life and have been highly conserved [Falkowski et al., 2008].

Microbial metabolisms are diverse and have adapted to a wide range of geochemical conditions. This is most impressively exemplified by 'energetic niches', i.e., chemical disequilibria where geochemical energy is available to power yet unknown metabolisms. Two examples of 'energetic niches' that were proposed based upon thermodynamic calculations long before microorganisms that exploit them were found in nature are the anaerobic oxidation of methane and ammonium by anaerbic methane oxidizing (ANME) archaea [Valentine, 2001] and anaerobic ammonix oxidizing (ANAMMOX) bacteria [Kuenen, 2008], respectively.

This thesis focuses on the biogeochemistry of microbial processes. Such research investigates how microorganisms, through their metabolic activity, change their chemical environment, and thereby contribute to the global geochemical cycling of elements. In most ecosystems, microbial metabolisms exceed the activities of animals and plants, constituting a 'microbial loop', in which the majority of organic matter is cycled based on microbial metabolisms alone [Bonkowski, 2004, Fenchel, 2008]. The cycling of organic matter by microorganisms in terrestrial and aquatic ecosystems was long underestimated, but has received increased attention over the last three decades as research focused on understanding the global carbon cycle and its disturbance by anthropogenic activities [Bonkowski, 2004,

Fenchel, 2008].

Narrow and broad processes. Investigating the microbial contributions to geochemical cycles requires some understanding of the composition and physiology of the microbial communities grouped by the major process they perform, as typically investigated by microbial ecology. Microbial processes can be divided into narrow and broad processes [Schimel and Schaeffer, 2012]. Examples of such processes are provided in Table 1.1. "Narrow" processes are conducted by small number of specialized taxa. Examples for narrow processes include methanogenesis and methanotrophy, as well as most steps of the nitrogen cycle including nitrogen fixation, nitrification, and denitrification. Narrow processes rely on the presence of 'competent' microbial actors, independent of thermodynamic conditions. Process rates are therefore affected by community composition and physiological properties of the taxa present in a given ecosystem [Schimel and Schaeffer, 2012].

"Broad" processes, in contrast, can be conducted by a wide range of microbial and non-microbial taxa, and microbial communities typically exhibit a strong functional redundancy in regards to these processes. Examples of such processes include photosynthesis and organic matter decomposition. Broad processes are typically not influenced by microbial community composition or the physiology of individual taxa, but rather by environmental conditions and physiological principals (e.g. the temperature dependence of carbon use efficiency) common to broad groups of microorganisms (e.g. fungi or bacteria) [Schimel and Schaeffer, 2012].

Table 1.1 Examples for broad and narrow microbial processes.

Broad processes	**Narrow Processes**
Photoautotrophic carbon fixation	Methanogenesis, aerobic methanotrophy, and ANME
Heterotrophic respiration	N fixation, nitrification, denitrification, ANAMMOX
	Sulfide oxidation and sulfate reduction
	Pollutant degradation

1.2 Studying microbial processes

Genomic, transcriptomic, proteomic approaches. Studies of the role of microorganisms in global biogeochemical cycles are challenging because many microbial processes occur at very slow rates, because microorganisms are acting on very dilute reservoirs of substrates, and because many key taxa cannot be cultivated under laboratory conditions. Over the last 20 years, however, novel analytical methods like high throughput sequencing, single cell sequencing, or proteomics have allowed incredible advances in molecular biology and microbial ecology [e.g. Bastida et al., 2009, Reuter et al., 2015, Gawad et al., 2016]. The combination of genomic, transcriptomic, and proteomic analysis has enabled the reconstruction of microbial metabolisms of many uncultured taxa in extreme habitats [e.g. Brazelton et al., 2012]. These approaches furthermore allowed the identification of which microbial taxa conduct specific geochemical transformations [Stokke et al., 2012, e.g.], which allows researchers to attempt to isolate these taxa to conduct more detailed physiological studies in culture [e.g. Suzuki et al., 2014]. In complex ecosystems that contain dense and diverse microbial communities like soils [de Vrieze, 2015] changes in microbial community structure and function have been used as early indicators of disturbance and anthropogenic impacts [e.g. Brookes, 1993, Yang et al., 2006]. Metagenomic, metatranscriptomic, and metaproteomic analyses are powerful tools to assess whether microbial communities are competent of conducting a specific metabolic pathway. These methods, however, generate only very limited insight into whether these metabolic pathways are actually occurring. They cannot inform about the process rate of pathways, an information necessary to assess microbial contribution to geochemical cycles.

Stable isotope based approaches. Stable isotope based methods can provide information about the actual rates of geochemical reactions, and thus provide insights that are complementary to (meta)genomic approaches.

Stable isotopes of an element have the same number of protons, but distinct numbers of neutrons. For example, about 98.9% of carbon nuclei consist of 6 protons and 6 neutrons (^{12}C), while roughly 1.1% of carbon nuclei consist of 6 protons and 7 neutrons (^{13}C). The distinct stable isotopes of the same element behave chemically identical. Molecules that contain the heavier isotope (e.g. ^{13}C), however, can exhibit slightly slower reaction rates compared to those that contain the lighter isotope (e.g. ^{12}C) this is termed 'kinetic isotopic fractionation'. Furthermore, the heavier and lighter isotopes can be unequally distributed among educts and products in equilibrium state, termed 'equilibrium isotopic fractionation'. Together, these two processes lead to per mil-scale variations in the stable isotope ratios (e.g., ^{13}C/^{12}C) in different species of an element (e.g., organic and inorganic carbon), and in different reservoirs (e.g., carbon in atmospheric CO_2 and in fossil fuels) [Sharp, 2007, Des Marais, 2001, Anderson and Arthur, 1983].

Stable isotope ratios are typically measured on dedicated gas-source mass spectrometers (isotope ratio mass spectroscopy; IRMS), and are denoted in the delta-notation, which expresses stable isotope ratios relative to ' reference materials (equation 1.1).

$$\delta^n X = \frac{R_{sam}}{R_{std}} - 1 \tag{1.1}$$

In this equation, X stands for the element (e.g., C, H, N, or O), n for the heavy isotope (13, 2, 15, 18, respectively) of the element, and R_{sam} and R_{std} are the ratio of heavy to light isotopes for the sample and standard, respectively [Coplen, 2011]. The number calculated in 1.1 is typically further multiplied by 1000 for easier interpretation, which is indicated with a per mille symbol (‰).

Similar to genomic methods, stable isotope analysis has undergone rapid technological advances over the last three decades. Three such developments are worth mentioning here. First, the development of continuous flow isotope ratio mass spectroscopy (IRMS) has al-

lowed the coupling of the IRMS to a range of peripheral instruments that separate individual analytes and convert them into gases that can be analyzed by IRMS (CO_2, CO, H_2, SO_2). Such combinations of IRMS to gas chromatography, liquid chromatography, or elemental analyzers allows for the rapid analysis of stable isotope ratios within individual compounds ('compound-specific') and bulk samples [e.g. Hayes et al., 1990, Brenna et al., 1998, Dias et al., 2002, Sessions et al., 2005]. Second, cavity-ring down laser spectroscopy (CRDS) allows for continuous optical measurements of stable isotope ratios [Wahl et al., 2006]. This technique is particularly useful when applied in combination with micro-meteorological measurements ('Eddy-covariance') to measure the flux and isotope composition of gaseous emissions of a given land surface like the release of CO_2, CH_4, or N_2O from soils [e.g. Griffis et al., 2008]. Third, the development of advanced IRMS and CRDS instruments has allowed for the measurement of the ratio in which molecules contain multiple rare isotopes ('clumped isotopes'). This allowed for measurements of isotopic equilibria within a single compound (e.g. carbonate or methane) [Eiler et al., 2014, Ono et al., 2014, Stolper et al., 2015], providing, for example, a palaeothermometer that is not dependent upon assumptions about the isotopic composition of other compounds (a common limitation of classical ^{18}O-in-carbonate palaeothermometry [Sharp, 2007, Eiler, 2011]).

Isotope labelling studies. Stable isotope analysis has become are a key tool in environmental microbiology. As the stable isotopes of an element behave largely similar, they are incorporated into microbial biomass in the same way. Stable isotope probing experiments provide microbial communities with substrates of distinct stable isotope ratios ('labelled substrate'; e.g., ^{13}C-enriched glucose). Microorganisms that consume these substrates have biomass that represents the stable isotope ratio of their substrates (e.g., ^{13}C enriched biomass), following the edict "you are what you eat". The stable isotope analysis of biomarkers that are specific to distinct microbial groups allows the determination which of these

groups have taken up a given substrate and incorporated it into their biomass, and therefore to trace which members of a complex microbial community consume a given substrate ("Stable isotope probing", SIP) [Neufeld et al., 2007].

Stable isotope probing experiments can trace the incorporation of isotopically labelled substrates into a different biomarkers with distinct limitations in regards to phylogenetic resolution and the precision of stable isotope ratio measurements [Neufeld et al., 2007]. Phospholipid fatty acids (PLFA) are a compound class that is commonly used to trace the incorporation of ^{13}C into microbial biomass. Unlike DNA, RNA, or protein based SIP, PLFA-SIP can only distinguish between broad groups of microorganisms like fungi, Gram negative bacteria, Gram positive bacteria, actinobacteria. Stable carbon isotope ratios of individual PLFA, however, can be analyzed by gas chromatography – combustion – IRMS (GC-IRMS), which can measure these ratios with great precision compared to the techniques applied to DNA, RNA, or protein (i.e., density gradient centrifugation and liquid chromatography mass spectroscopy). PLFA-SIP can therefore detect the parts per million level incorporation of ^{13}C into biomass. This low detection limit allows us to study processes like the oxidation of atmospheric methane by high-affinity methanotrophs in soil [Bull et al., 2000]. This approach was used by [Morrill et al., 2014] to study the incorporation of carbon monoxide into microbial biomass.

Not all isotope labelling studies measure the incorporation of a labelled substrate into biomass. Such experiments can also be used to detect and quantify the transformations of a certain compound in nature. Chapter 5 of this thesis reports on experiments in which microcosms were amended with ^{13}C-labelled substrates like acetate or bicarbonate, followed by measuring the stable carbon isotope ratio of methane in the microcosms' headspace to demonstrate that the amended substrate was converted to methane.

Isotope pool dilution assays are another type of labelled-substrate experiments. In microcosms, changes in the concentration of a certain compound can only indicate the net

production or consumption of this compound. If production and consumption occur simultaneously, such net measurements underestimate gross conversion rates. Ammonium in soils, for example, is simultaneously produced through the mineralization of organic nitrogen, and consumed by microbial uptake and nitrification. Isotope pool dilution assays address this by adding a known amount of the investigated compound with an isotopic label, e.g., 15N labelled ammonium. By measuring the change in concentration and the stable isotope nitrogen ratio of ammonium, gross production and consumption rates can be calculated [Schimel, 1996, Di et al., 2000]. This thesis make use of this approach in Chapter 5 to demonstrate the simultaneous production and consumption of volatile organic acids in a microcosms experiment.

Isotope labelling studies have specific advantages and limitations. These techniques allow a clear attribution of the measured differences and changes in stable isotope value to distinct chemical processes, i.e., the uptake of a single, labelled substrate, or one specific geochemical conversion. Furthermore, the amended labelled compounds might have stable isotope ratios that strongly differ from their naturally occurring counterparts (e.g., up to 99% ^{13}C). This enables the detection of ^{13}C in compound classes not amendable to IRMS analysis, like DNA or protein. The amendment of a labelled compound, however, is always associated with the disturbance of the studied system. In soils, for example, stable isotope labelling typically requires the removal of soil from its natural setting, homogenization, the amendment of substrates that are typically not present in this form in nature, exclusion of other substrates present naturally (e.g., plant exudates), and incubation under laboratory conditions that are distinct from natural conditions (e.g., constant temperature and moisture). Such manipulation can change the studied system, and results of such experiments therefore might not be representative of undisturbed ecosystems. Stable isotope labelling techniques are therefore ideally combined with passive *in situ* measurements, as exemplified in Chapters 2, 4, and 5 of this thesis.

Natural abundance studies Microbial processes can also be studied through natural variations in stable isotope ratios. Such approaches eliminate the need to introduce a labelled substrate to the studied system, thus eliminating the artificial disturbances to the studied ecosystems. The three main approaches of natural abundance studies include; (1) the manipulation of ecosystems to introduce source materials with distinct stable isotope values; (2) the use of naturally occurring differences in the stable isotope values of the available substrates; and (3) measuring biogeochemical process rates through quantifying the naturally occurring isotopic fractionation.

Natural abundance studies are commonly applied to ecosystems that feature well understood differences in the isotopic signatures of distinct reservoirs of the studied elements. One common strategy to generate such isotopically distinct reservoirs are C3/C4 crop change experiments [Glaser, 2005]. C3 and C4 plants feature distinct carbon fixation pathways with distinct isotopic fractionation factors. C3 plants like wheat typically have $\delta^{13}C$ values that are depleted by about $20‰$ relative to drought-adapted C4 plants like corn. If a long-term wheat planted field is switched to corn plantation, researchers can follow how the distinct carbon reservoirs (plant biomass, plant litter, soil microorganisms, soil organic matter) successively become more enriched in ^{13}C [Glaser, 2005]. This allows tracing the introduction of newly assimilated carbon into the soil ecosystem, and to calculate turn-over times of different carbon reservoirs, including microbial biomass [e.g. Kramer and Gleixner, 2006, 2008]. Similar studies were conducted at sites of free air CO_2 enrichment (FACE) experiments, which increase ambient CO_2 concentrations by releasing fossil fuel derived CO_2 that is typically depleted in ^{13}C relative to atmospheric CO_2 [e.g. Billings and Ziegler, 2005, 2008, Streit et al., 2014]. FACE thus generate newly fixed organic carbon that is depleted in ^{13}C relative to older carbon that was fixated before the start of the experiment. Stable isotope analysis can therefore trace the quantities of new and old carbon degraded by soil microorganisms.

Other natural abundance approaches do not rely on indirect labelling, but explore nat-

ural variations in stable isotope ratios. For example, methane is highly depleted in ^{13}C in many ecosystems. Methanotrophic microorganisms can therefore be identified through their unusually negative $\delta^{13}C$ values [e.g. Schubotz et al., 2011, Mills et al., 2013]. Distinct $\delta^{13}C$ values of land plants and aquatic primary producers can distinguish between dissolved organic carbon of terrestrial and organic origin in marine and freshwater ecosystems [e.g. Thornton and McManus, 1994, Graham et al., 2001]. Isotope fractionation also occurs during plant metabolism, resulting in differences in the stable carbon isotope values of the distinct plant biomolecules of up to 14‰ [Glaser, 2005]. These differences among plant compounds could provide a powerful tool to trace changes in the substrate use patterns of microbial degraders of plant detritus and plant derived soil organic matter. Soil incubations at greater temperature, for example, have led to the release of more ^{13}C depleted CO_2, indicating that soil microorganisms shift their soil substrate use when incubated at greater temperature [Andrews et al., 2000, Biasi et al., 2005]. Conversely, soil microbial biomass became more ^{13}C enriched after nitrogen fertilization, consistent with a decrease in lignin decomposition [Cusack et al., 2011]. In Chapters 2 and 4 of this thesis, I explore such subtle variations in the $\delta^{13}C$ values of microbial biomass in boreal forest soils.

Stable isotope analysis has also become a key tool to understand the origin or processing of molecules like methane and in doing so provides a means to access the biogeochemistry of inaccessible environments, such as aquifers. The sources of methane can (often) be distinguished using the analysis of the carbon hydrogen and carbon isotopes. This allows us to distinguish between methane produced by microorganisms from methane produced through thermogenic or abiogenic processes, and even further identify the metabolic pathway used by methanogens (carbonate reduction or acetate fermentation; see Chapter 5) [Whiticar, 1999, Etiope and Sherwood Lollar, 2013].

The natural abundance approach can also be used to reconstruct the biogeochemistry of ecosystems of limited accessibility. Microorganisms that conduct biogeochemical cycling in

deep aquifers, for example, might be immobilized in biofilms on the rock fracture surfaces, such that the sampling of microbial cells from the groundwater through wells or springs provides only a limited picture of the belowground ecosystem. Stable isotope values of compounds in groundwaters provide a basis upon which biogeochemical processes that occurred in the groundwater can be reconstructed. This approach has been used to measure the degree to which nitrate is converted to N_2 by denitrification, methane is oxidized by methanotrophs, pollutants like perchlorethene are degraded by microorganism in groundwaters [Wassenaar, 1995, Whiticar, 1999, Morrill et al., 2005]. This approach was applied by [Morrill et al., 2014], where the microbial oxidation of carbon monoxide (CO) in a microcosm experiment was studied by monitoring the enrichment of ^{13}C in the remaining CO.

1.3 Two case studies

This thesis focuses on the application of natural abundance stable isotope approaches to the study of how microbial processes affect the geochemistry of two contrasting ecosystems, i.e., (1) boreal forest soils in a climate transect in western Newfoundland to southeastern Labrador (Chapters 2, 3, and 4), (2) serpentinization-associated ultra-basic, reducing springs in an ophiolite located in California (Chapters 5), which is compared to a similar study conducted at an ophiolite located in Newfoundland [Morrill et al., 2014]. This section introduces these two ecosystems, followed by a brief comparison.

1.3.1 Soil organic matter cycling in a boreal forest climate transect

Soil organic matter (SOM) is the largest reservoir of reduced carbon in terrestrial ecosystems [Intergovernmental Panel on Climate Change, 2013]. Estimates of the total amount of carbon stored as SOM vary substantially (1500 to 2400 Pg), but all estimates agree that more carbon is stored in SOM than in the biosphere and in atmospheric CO_2 combined [Intergovernmental Panel on Climate Change, 2013]. SOM accumulates most strongly under cold and wet

conditions, as found in boreal and arctic ecosystems [Post et al., 1985, Schlesinger, 1997, Jobbágy and Jackson, 2000, Scharlemann et al., 2014]. As climate change models predict that these high latitude ecosystems will undergo above-average warming [Intergovernmental Panel on Climate Change, 2013], studies of how high latitude SOM will be affected by future climate change are sorely needed, because a net release of CO_2 from SOM due to warming would constitute a positive feedback of global warming [e.g. Schlesinger and Andrews, 2000].

Climate transects allow us to study future climate change by comparing field sites along natural gradients of expected climate changes [Billings et al., 2012]. The work presented in this thesis is based upon one such gradient, the Newfoundland and Labrador Boreal Ecosystem Latitudinal Transect (NL-BELT), which is shown in Figure 1.1. This transect features permanent field sites with established research plots available to researchers from various disciplines. Field sites were selected among mature balsam fir (*Abies balsamea*) forest stands on well-drained podzolic soils [Ziegler et al., 2017]. This represents managed forests in which the dominant tree species is determined during afforestation, but where the understory vegetation is allowed to develop freely in response to the local climatic conditions. The mesic nature of this transect distinguishes it from previous boreal transect studies that were located in more continental locations characterized by negative correlations between mean annual temperature (MAT) and precipitation (MAP). The NL-BELT is characterized by both increased MAT and MAP with decreased latitude akin to predictions for the region in the coming century [Intergovernmental Panel on Climate Change, 2013], and resulting in sites exposed to similar moisture regimes across the transect. NL-BELT sites receive 1070-1505 mm MAP, whereas comparable studies so far focused on sites that typically receive $<$600 mm MAP (Table 1.2). This transect is therefore especially valuable as an opportunity to study the effect of increasing temperatures in the absence of increasing moisture limitation.

The research in this thesis focuses on the organic soil horizons (L, F, and H), also referred to as forest floor, and representing a diagenetic continuum enabling the study the sequestra-

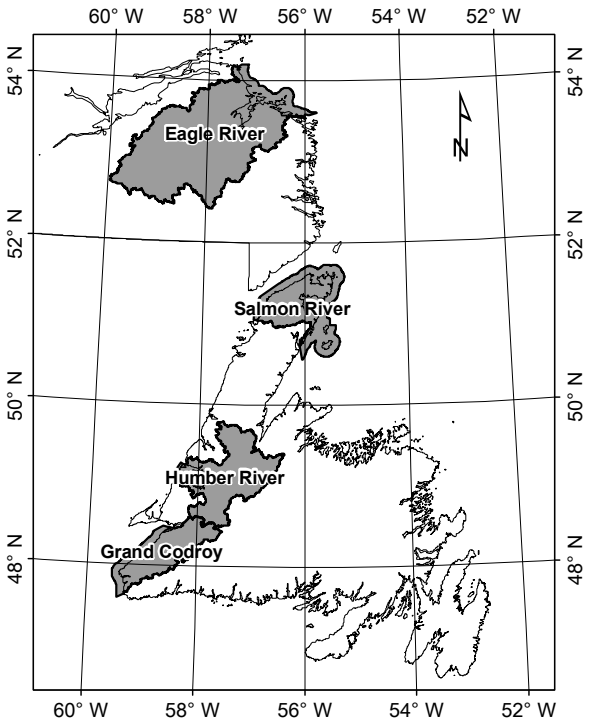

Figure 1.1 Map depicting the location of the four regions that form the Newfoundland and Labrador Boreal Ecosystem Latitudinal Trasect (NL-BELT). Samples from three transect regions (Eagle River, Salmon River, Grand Codroy) have been analyzed as part of this thesis.

tion of plant litter into soil organic matter [Melillo et al., 1989]. These soil horizons consist of relatively fresh plant material. Soil microorganisms in the forest floor consume plant derived carbon, and convert a fraction into their biomass, which is a key step in transforming relatively labile plant compounds into stabilized organic matter [Schurig et al., 2012, Cotrufo et al., 2013]. Understanding carbon cycling in soil therefore requires us to understand which fraction of carbon is removed by microbial degradation, and which secondary compounds are formed by microbial metabolisms [Schimel and Schaeffer, 2012]. In the absence of a mineral phase, SOM in organic soil horizons is not physically stabilized through mineral adsorption or aggregate incorporation. Instead, its persistence relies on its chemical stability alone [von Lützow et al., 2006], along with climatic conditions adverse to decomposition and large quan-

Table 1.2 List of published boreal forest climate transect studies with key climate data. MAT and MAP are stated north to south [where possible]. n.a.; not available.

Transect Name	Location	MAT range (°C)	MAP range (mm)	Dominant species	References
NL-BELT	Canada (NL)	0.0 to 5.2	1074 to 1505	*Abies balsamea*	Ziegler et al. [2017]
BFTCS	Canada (SK & MT)	-3.5 to +0.5	544 to 398	*Picia mariana, Pinus banksiana*	Norris et al. [2011], Preston et al. [2006]
	Norway and Sweden	n.a.	304 to 473	*Betula pubescens*, tundra	Sjögersten et al. [2003]
	Finland	n.a.	500 to 629	*Pinus silvestris, Picia abies*	Hilli et al. [2008]
	Alaska	-2.2 to +0.3	n.a.	*Picia mariana*	Kane et al. [2005]
	Eastern Europe	-1 to +8	450 to 750	*Pinus silvestris*	Vucetich et al. [2000]

tities of litter inputs to these soils. Turn-over rates of SOM in these soil horizons is therefore relatively fast, with radiocarbon measurements suggesting ages of approximately 5-10 years (L horizon) and 50-100 years (H horizon) [Li et al., 2012]. Climate induced changes in the quantity and quality of SOM in organic soil horizon are therefore likely to materialize within our lifetimes.

SOM in the NL-BELT sites was quantified in previous studies, and a number of incubation experiments quantified the response of respiration rates of soils from the L, F, and H horizons to temperature [Laganière et al., 2015, Podrebarac et al., 2016] and the variation in total soil respiration with climate along the NL-BELT [Ziegler et al., 2017]. These studies showed that warming will lead to the accelerated turnover of SOM, but not to a decrease in SOM stocks [Ziegler et al., 2017]. This persistence of similar SOM stocks despite greater respiration rates can be attributed to two main factors; (1) greater primary productivity of vegetation in a warmer climate [Ziegler et al., 2017], and (2) climate-induced changes in SOM properties that lead to a decrease of SOM decomposition rates at a given temperature (SOM bioreactivity), as illustrated in Fig. 1.2.

This thesis investigates the origin and geochemical nature of this difference in SOM bioreactivity. I addressed this question through two major approaches. First, I exploit the natural variations in the $\delta^{13}C$ values of plant biomolecules [Benner et al., 1987, Hobbie and Werner, 2004, Glaser, 2005] by studying the variations in the $\delta^{13}C$ values of microbial biomarkers. The $\delta^{13}C$ value of microorganisms represents the $\delta^{13}C$ value of the substrates consumed by the organism. I therefore assume that changes in microbial substrate use would be accompanied by changes in $\delta^{13}C$ values of microbial biomass and – in turn – biomarkers of living microbial biomass like phospholipid fatty acids (Chapters 2 and 4). Second, I characterized the chemical composition of SOM from the distinct field sites and soil horizons with a range of geochemical methods including elemental, isotopic, total hydrolysable amino acids, and solid state nuclear magnetic resonance analysis. By doing so, I link the observed

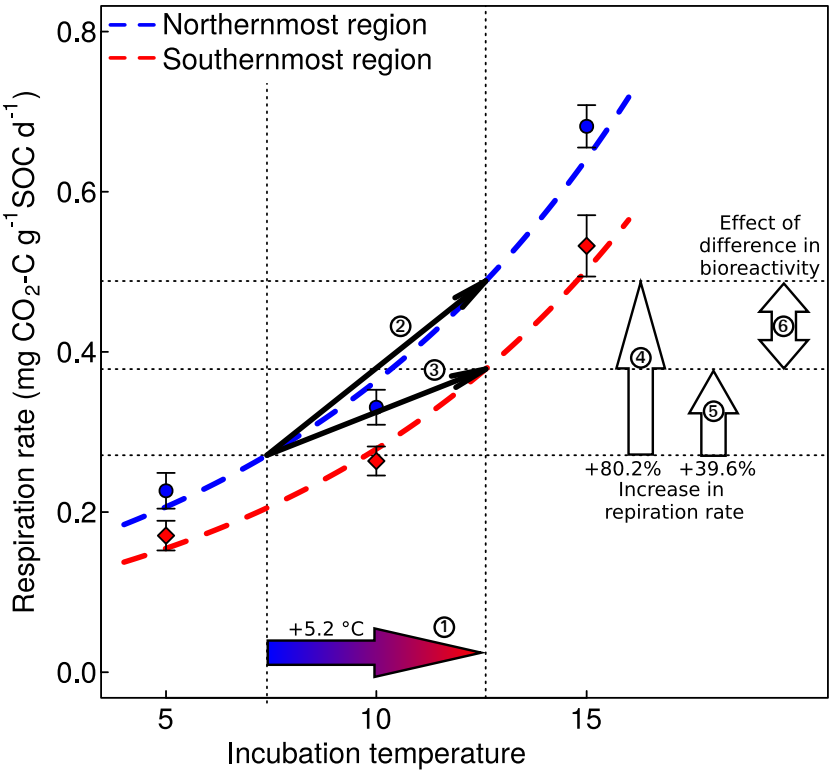

Figure 1.2 Conceptional figure exploring the effects of medium term (months) and long term (decades) of warming on soil respiration rates. The presented data depicts the empirical relation between temperature and respiration rates in intact soil cores consistent of the organic soil horizons (L, F, and H horizon) from the two most extreme regions of the NL-BELT that were incubated for 467 days at 5, 10 or 15 °C. Data from Podrebarac et al. [2016]. Blue and red points depict the average daily respiration rate, with error bar depicting one standard errors among soil cores form distinct sampling plots (n=9). Red points depict results from the southernmost region, which is characterized by a mean annual temperature 5.2 °C warmer than the northernmost region, depicted in blue. The dashed lines depict exponential fits for each region ($R(T) = R_{10} \times Q_{10}^{T/10-1}$). The figure depicts the use this data to explore the effect of medium term warming was simulated by comparing incubations of the same soil at distinct temperatures (2). Long term warming, in contrast, was simulated by comparing the incubation of soil from the cold region at a cooler temperature to the incubation of soil from a warmer region at a warmer temperature (3), thus capturing both direct temperature effects on the decomposition process, but also long-term changes in SOM properties. These two warming scenarios have different effects on soil respiration (4, 5)) because soils that developed under a warmer climate are characterized by lower bioreactivity, i.e., respiration rates at a given temperature. As a result, long term effect of warming on soil respiration rates are about 50% lower than medium term effects (6). In this thesis I explore the chemical properties of soil organic matter responsible for this regional difference in bioreactivity, and the ecosystem processes that produce them.

differences in SOM bioreactivity to explicit geochemical measures (Chapter 3). Finally, I trace these geochemical differences along a latitudinal transect back to identify the ecosystem processes through which climate affects SOM properties (Chapters 3 and 4).

This thesis therefore addresses the following research questions specific to boreal forests:

1. **How do δ^{13}C values of microbial biomass vary with depth, latitude, and microbial group in this transect?** Can differences in these δ^{13}C values be exploited to understand C cycling at these sites?

2. **How do chemical and biological properties of SOM differ with depth and latitude?** Which processes cause regional differences?

3. **Can differences in microbial biomass δ^{13}C values constrain how climate-induced in SOM properties develop?**

1.3.2 Serpentinization-associated ultra-basic, reducing springs

Serpentinization is the reaction of ultra-mafic rocks with water. This reaction was common on the early Earth and still occurs in marine hydrothermal vents,in the deep continental crust [Sherwood Lollar et al., 2007], and in the groundwaters of ophiolites (i.e., geological settings where marine seafloor has been abducted upon a continent) [Barnes et al., 1967], and . In this reaction, olivine and pyroxene are altered to serpentine minerals, as described by reactions 1.2 and 1.3 for olivine and pyroxene endmembers [Schulte et al., 2006].

$$Fe_2SiO_4 + 5Mg_2SiO_4 + 9H_2O \rightarrow 3Mg_3Si_2O_5(OH)_4 + Mg(OH)_2 + Fe(OH)_2 \quad (1.2)$$

$$Mg_2SiO_4 + MgSiO_3 + 2H_2O \rightarrow Mg_3Si_2O_5(OH)_4 \quad (1.3)$$

In a further step, water is reduced to molecular hydrogen through the oxidation of iron hydroxide to magnetite (reaction 1.4) [Schulte et al., 2006].

$$3Fe(OH)_2 \rightarrow Fe_3O_4 + 2H_2O + H_2 \tag{1.4}$$

Serpentinization generates Ca-OH type groundwaters that are characterized by their high pH (11-12), highly reducing conditions (Eh <-600 mV), high concentrations of Ca2+ cations, and low concentrations of inorganic carbon [Barnes et al., 1967]. Molecular hydrogen, a by-product of the serpentinization reaction, is present in millimolar concentrations [Sleep et al., 2004]. Many serpentinization associated fluids furthermore contain elevated concentrations of hydrocarbons (methane to hexane) and volatile fatty acids (VFA; mainly formate and acetate) [Lang et al., 2010]. At many sites of serpentinization, methane and other alkanes are the product of abiogenic synthesis through Fischer-Tropsch-type (FTT) reactions [e.g. McCollom and Seewald, 2007, McCollom, 2013]. These alkanes, however, can also be the product of microbial or thermogenic methanogenesis, i.e., of biogenic origin. The origin of VFA remains poorly understood [Schrenk et al., 2013].

The origin of organic compounds at sites of serpentinization is the subject of intense research because it's relevant to understanding (1) the origin of life on Earth and the potential for below-ground life on Mars [Sleep et al., 2004, Schulte et al., 2006, Sherwood Lollar et al., 2007, Russell et al., 2010, McCollom, 2013]; (2) the limits of microbial life [Schrenk et al., 2013]; (3) proposed carbon sequestration projects in terrestrial ophiolites [Kelemen and Matter, 2008]. So far, two approaches have been taken towards sourcing methane at sites of serpentinization. First, the microbial communities at sites of serpentinization were studied by metagenomics methods to investigate if microbial taxa present at such sites resemble known methanogens [e.g. Brazelton et al., 2012, Suzuki et al., 2013]. Second, geochemical analysis, including the analysis of stable carbon and hydrogen isotope values in methane and

the ratio of methane and C2-C6 alkanes, has been applied to investigate if alkanes exhibit similar composition and stable isotope values as gases from known biogenic or abiogenic sources [e.g. Morrill et al., 2013, Szponar et al., 2013].

In this thesis, I investigated The Cedars, a site of present day serpentinization located in the Franciscan subduction zone in Sonoma county, California, USA. This site has been the subject of previous geochemical studies [Morrill et al., 2013], which led to very different conclusions than the study of a similar site in Newfoundland [The Tablelands, Szponar et al., 2013]. Methane and other hydrocarbons found in springs at The Tablelands exhibit geochemical properties typical for gases of predominantly abiogenic origin, which is similar to other ophiolitic springs [Szponar et al., 2013]. At The Cedars, however, microbial geochemical properties indicate that microbial methanogenesis likely contributes significant proportions of the methane found [Morrill et al., 2013]. These findings are consistent with contrasting results from microbiological studies of these two sites: the metagenome of The Tablelands contain no indication of microbial methanogens [Brazelton et al., 2012], whereas a potentially methanogenic archaeal operational taxonomix unit (OTU) has been identified at The Cedars [Suzuki et al., 2013].

Metagenomic data and the geochemical properties of methane, however, provide only indirect evidence for the presence or absence of microbial methanogenesis. Microcosm experiments with isotopically labelled substrates, however, can provide direct evidence that microbial communities in a given ecosystem are capable of conducting a metabolic process like methanogenesis. This thesis contributes to the ongoing research at The Cedars through a range of microcosm experiments with material collected at both sites (spring fluids and carbonate sediments) that were conducted to test if the distinct natural abundance stable isotope values of methane at these sites correctly predict the presence of microbial methanogens at The Cedars, contrasting their absence at The Tablelands [Morrill et al., 2014].

This thesis therefore addresses the following research questions specific to serpentinization

associated springs:

1. **Are microbial communities in serpentinization associated spring fluids and sediments capable of conducting methanogenesis, acetogenesis, and/or carbon monoxide fixation?**

2. **Do microbial communities from The Cedars and The Tablelands differ in their metabolic potential?** Do these results support the differences observed in methane stable carbon and hydrogen isotope values observed at these two sites? Are they consistent with the composition of the microbial communities at each site?

1.4 Comparison between the two projects

The two ecosystems investigated in this thesis are strikingly different, as summarized in Table 1.3. Soils in boreal forests and elsewhere contain billions of microbial cells per cubic centimeter, and host some of the most divers communities on earth [Schimel and Schaeffer, 2012]. Microbial communities in ultra-basic springs can contain as little as 10 cells per milliliter, and are dominated by a handful of taxa [Brazelton et al., 2013, Suzuki et al., 2013]. Similarly, the chemical environment of soils is one of the most complex known to us, with thousands of distinct organic compounds present in soil pore water [Malik et al., 2016]. The dissolved organic carbon (DOC) in serpentinization associated springs, in contrast, is dominated by a few alkanes and volatile fatty acids (VFA). Yet, the two projects covered in this thesis feature similar questions and approaches. In each case, I studied natural abundance stable isotope values in contrasting sites, i.e., along a climate transect; in two contrasting ophiolites in Newfoundland and California. I then observed how these stable isotope values can be explained by differences in the biogeochemistry of the distinct sites. Overall, this thesis therefore evaluates the potential of studying naturally occurring variations in stable isotope values, in the absence of any added labelled substrates, to better understand

Table 1.3 Comparison between the two ecosystems studied in this thesis.

	Boreal forest soils	Serpentinization-associated springs
Big questions	• How does climate impact soil organic matter (SOM) chemistry? • Does climate change in microbial community composition or physiology? • Do these effects lead to a change in microbial substrate use patterns, which ultimately changes SOM chemistry?	• What are the origin of methane and acetate in ultrabasic spring fluids? • Which carbon substrates are accessed by microorganisms in these fluids and associated sediments? • Are these microorganisms capable of conducting methanogenesis, acetogenesis, and/or carbon monoxide fixation?
"Natural gradient"	Climate transect	Two contrasting sites in Newfoundland and California
Microbial communities	Complex (millions of microbial species)	Simple (dominated by a few taxa)
Microbial processes	'broad' processes: Soil organic matter formation & decomposition	'narrow' processes': Methanogenesis, actetogenesis, carbon monoxide fixation/oxidation
Stable isotope measurements	$\delta^{13}C$ of microbial lipids (PLFA) as a proxy for biomass	$\delta^{13}C$ and $\delta^{2}H$ of methane; $\delta^{13}C$ of acetate, $\delta^{2}H$ and $\delta^{18}O$ of water, $\delta^{13}C$of PLFA as a proxy for biomass
Geochemical measures	SOM characterized by elemental analysis, bulk stable isotope analysis, solid state NMR and total hydrolysable amino acid analysis	pH, Eh, conductivity, dissolved organic carbon species (alkanes, volatile organic acids), dissolved cations and anions, and other analysis
Questions addressed in this thesis	• How do microbial biomass $\delta^{13}C$ values vary with depth and latitude in a boreal forest transect? • How do SOM chemistry vary along these gradients? • Can differences in biomass $\delta^{13}C$ values constrain the microbial processing of SOM?	• Are microbial communities in serpetinization associated springs capable of conducting methanogenesis, acetogenesis, and carbon monoxide fixation? • Is the presence or absence of methanogenesis well predicted by natural abundance $\delta^{13}C$ and $\delta^{2}H$ values of methane?
Thesis chapters	Chapters 2, 3, and 4	Chapter 5

the microbial cycling of organic compounds in natural environments.

1.5 Overview of thesis chapters

Chapters 2-5 cover original research undertaken as part of this thesis and address the broad research goals laid out above (1.4). Each of these four chapters consists of a manuscript that is either intended for publication (Chapters 3 and 4) or has already been published (Chapters 2 and 5). The thesis is organized in two sections. Manuscripts covering boreal forest soils are presented first (Chapters 2-4), followed by a manuscript covering microbial processes in serpentinization-associated springs (Chapter 5).

Chapter 2 investigates how $\delta^{13}C$ values of the biomass of broad microbial groups (fungi, Gram positive bacteria, Gram negative bacteria) – analyzed through compound-specific stable isotope analysis of their phospholipid fatty acids – varies with depth and among microbial groups. While I analyzed samples from across the climate transect described above, this chapter is focused upon common trends observed in soils in both of the two most extreme regions of this transect.

I show that fungal and bacterial biomarkers exhibit distinct $\delta^{13}C$ values, which are constant through the soil profile and therefore are more ^{13}C-depleted relative to the more ^{13}C-enriched soil organic carbon (SOC) at greater depth. Any overall increase in microbial biomass $\delta^{13}C$ resulted from a change in microbial community composition, i.e., greater proportions in ^{13}C-enriched bacteria relative to ^{13}C-depleted fungi at greater depth. These findings have some important implications for carbon cycling in these soils. First, the lack of an increase of fungal or bacterial biomass $\delta^{13}C$ values with the $\delta^{13}C$ value of the bulk SOC indicates that microorganisms likely access a common pool of carbon substrates across soil horizons despite the change in bulk soil $\delta^{13}C$ values. Such common pools of available carbon may include percolating dissolved organic carbon (DOC), as well as fresh root litter inputs

and root exudates, all of which are distinct from 'bulk SOC'. Second, the decrease of fungi to bacteria ratios with greater depth likely contributes to the widely observed increase in the $\delta^{13}C$ value of bulk SOC with depth as microbial necromass contributions to SOC are more enriched in ^{13}C at greater depth. This chapter shows that along soil profiles, the $\delta^{13}C$ values of microbial biomass might control the $\delta^{13}C$ values of bulk SOC, rather than conversely.

Chapter 3 investigates how chemical properties of SOC chemistry vary with climate history. This chapter is based upon the synthesis of both published and new geochemical data for these field sites, and strives to provide an explanation for the higher SOC bioreactivity (i.e., respiration rate at a given temperature) observed in the northern sites. In particular, I investigate if the regional differences in SOC chemistry result from distinct plant litter inputs to SOM or are acquired over time as SOM is exposed to different rates of diagenesis supported by the different climates.

I found that in these soils, depth and latitude affect different SOM properties, and that regional differences in SOM chemistry do not increase with depth. I therefore concluded that regional differences in SOM chemistry resulted from distinct inputs to soil, as opposed to being acquired over time with the persistence of SOM in the soil. I furthermore found that regional differences in SOM chemistry can be explained by three processes, i.e., (1) differences in plant litter composition, (2) distinct proportions of moss litter relative to vascular plant litter, and (3) potentially differences in how plant litter decomposition changes litter chemistry. Consequently, I find that SOM chemistry is correlated with bioreactivity, and that moss inputs are the most important driver of differences in both SOM chemistry and bioreactivity . The ratio of moss litter relative to vascular plant litter is likely to decrease with warming, which will lead to a decrease in SOM bioreactivity in the future.

Chapter 4 investigates how (1) how the chemical composition of needle litter changes in each region in a one-year litterbag experiment; and (2) how microbial community composition

(fungi:bacteria ratios) and microbial biomass $\delta^{13}C$ values vary across the transect in the top soil horizon (L). I report that plant litter decomposition is associated with distinct changes in litter chemistry in the different regions of the transect. Matching these differences, more southern soils contained greater proportions of bacteria relative to fungi, and microbial biomass in more southern soils exhibited higher $\delta^{13}C$ values suggesting the consumption of greater proportions of carbohydrates relative to lignin. These difference in microbial community composition and substrate use can explain the stronger accumulation of lignin during litter decomposition suggested in Chapter 3. The differences in microbial community composition and microbial substrate use were only detected in the most shallow soil horizon (L), consistent with our finding that litter chemistry changes in distinct way in the different regions of the transect during early litter decomposition, but not during the diagenetic alteration of the soil organic matter.

Chapter 5 investigates if microorganisms at The Cedars are capable of (1) conducting methanogenesis and (2) aerobic carbon monoxide (CO) oxidation. Microbial communities at this site were capable of methanogenesis based on a range of organic and inorganic substrates, whereas I found no evidence for CO oxidation. Stable isotope values of the microbially produced methane suggest that regardless of substrate amendments, methanogens primarily convert inorganic carbon to methane. This finding is important for proposed carbon sequestration projects at sites similar to The Cedars: CO_2 injections likely alleviate the inorganic carbon limitation of methanogens at these sites, thus stimulating CH_4 production. Since the global warming potential of CH_4 is approximately 30 times stronger than that of CO_2, the conversion of injected CO_2 to methane could easily lead to a net negative green-house gas balance of such projects.

1.6 Co-authorship statement

The work presented in this thesis could have never been done by one person alone, and I am very grateful for all the work of my co-authors and collaborators, upon which this thesis is based. Their contributions are highlighted in the following list.

Chapters 2-4 (Boreal forest soils). The work presented in these three chapters in based upon a common dataset derived from soil and vegetation samples collect from across the NL-BELT transect. The NL-BELT transect was originally conceptualised by Susan E. Ziegler (SEZ) and Sharon A. Billings (SAB) but actually realised in collaboration with Kate A. Edwards (KAE) of the Atlantic Forestry Center (Natural Resources Canada), with significant support from Darrell Harris and Andrea Skinner (AS) as well as other Canadian Forest Service employees and students.

The three chapters are based on data from a field sampling campaign conducted in June 2011. The campaign was conceptionalized by SEZ, SAB, KAE, and Jerome Laganiere (JL), field work was conducted by KAE, JL, Ronald Benner (RB), Mike Philben (MP), Thalia Soucy-Giguere, and Frances A. Podrebarac (FAP). Initial work-up of soil samples for chemical analysis was conducted by JL, FP, and Jamie Warren (JW). JW, JL, and FAP conducted EA/IRMS measurements supported by Alison Pye. Additional samples were EA/IRMS measurements were analyzed by the G.G. Hatch Laboratory at University of Ottawa. MP conducted THAA analyses. JW conducted NMR measurements supported by Celine Schneider. All PLFA analysis was conducted by myself, with support from Geert van Biesen (GVB).

Litter traps were installed and maintained by KAE with support of AS, Sara Thompson, Danny Pink, and Amanda Baker. KAE, SAB and SEZ planned the litterbag experiment while KAE and AS carried out the ongoing litterbag experiment used in Chapter 4. Chemical analysis of litter samples was conducted by KAE and JW. The incubation experiments

included in Chapter 3 were planned by SEZ, SAB, and JL, and carried out by JL and FAP. Using this dataset, I conceptualized all three chapters in close collaboration with SEZ and Penny L. Morrill (PLM; Chapter 2). I conducted the data analysis and wrote initial draft for each of the manuscripts, which were then revised based upon several rounds of feedback from SEZ and comments from all co-authors. The soil profile pictures used in the conceptional figure in Chapter 2 were taken by FAP.

Chapter 5. The two microcosm experiments covered in this chapter were conceptualized by PLM and set up by Emily Cummings (EC) and Alison Cox (AC) as part of their honours projects. EC, AC, and myself analyzed headspace gas concentrations. The compound specific analysis of stable carbon and hydrogen isotope analysis of methane was conducted by GVB. The compound specific analysis of stable carbon isotopes in volatile organic acids was conducted by myself. Samples for the analysis of stable carbon isotope analysis of dissolved organic carbon and total inorganic carbon were prepared by me and analyzed by Alison Pye. Samples for the analysis of hydrogen and water isotopes were conducted by an external commercial laboratory. Liam Morrissey provided a literature review of methane stable isotope values. I conducted the data analysis and wrote the manuscripts with inputs from all co-authors.

Chapter 2

Distinct fungal and bacterial $\delta^{13}C$ signatures as potential drivers of increasing $\delta^{13}C$ of soil organic matter with depth

Lukas Kohl[1], Jérôme Laganière[1,2], Kate A. Edwards[3], Sharon A. Billings[4], Penny L. Morrill[1], Geert Van Biesen[1], Susan E. Ziegler[1]

[1]Department of Earth Sciences, Memorial University, 300 Prince Philip Dr., St. John's, A1B 3X5, NL, Canada

[2]Natural Resources Canada, Canadian Forest Service, Laurentian Forestry Centre, 1055 Rue du P.E.P.S., Québec, G1V 4C7, QC, Canada

[3]Natural Resources Canada, Canadian Forest Service, Atlantic Forestry Centre, 26 University Drive, Corner Brook, A2H 6J3, NL, Canada

[4]Department of Ecology and Evolutionary Biology, Kansas Biological Survey, University of Kansas, 2101 Constant Ave., Lawrence, 66047, KS, USA

This chapter was originally published in Biogeochemistry 124:13-26. [Kohl et al., 2015]. Online Resources 2.1 to 2.7, which were provided in support of the original publication, can be found on pages 49 to 58.

Abstract

Soil microbial biomass is a key source of soil organic carbon (SOC), and the increasing proportion of microbially derived SOC is thought to drive the enrichment of ^{13}C during SOC decomposition. Yet, little is known about how the $\delta^{13}C$ of soil microbial biomass differs across space or time, or with the composition of the microbial community. Variation in soil microbial $\delta^{13}C$ may occur due to variation in substrates used by soil microorganisms, and variation in how different microorganisms synthesize biomass. Understanding these variations in soil microbial $\delta^{13}C$ would enable more accurate interpretation of patterns in the $\delta^{13}C$ of SOC. Here, we report the variation in $\delta^{13}C$ values of individual phospholipid fatty acids (PLFA) within podzolic soils from mesic boreal forests characterized by steep decreases in fungal to bacterial (F:B) ratios. By comparing trends in $\delta^{13}C$ of PLFA indicative of either fungi or bacteria to those PLFA common across both microbial groups, we tested the hypothesis that the enrichment of ^{13}C in bacterial relative to fungal biomass represents a mechanism for the increase of bulk SOC $\delta^{13}C$ with depth. We demonstrate that PLFA derived from fungi were consistently depleted in ^{13}C (-40.1 to -30.6 ‰) relative to those derived from bacteria (-31.1 to -24.6 ‰), but unlike bulk SOC the $\delta^{13}C$ of PLFA from either group did not vary significantly with depth. In contrast, the $\delta^{13}C$ of PLFA produced by both fungi and bacteria, which represent the $\delta^{13}C$ of soil microbial biomass as a whole, strongly increased with depth (increase of 7.6 to 8.4 ‰) and was negatively correlated with the fungi/(fungi + bacteria) ratio (r^2 >0.88). The steep increase of the $\delta^{13}C$ of general PLFA with depth cannot be explained by an increase in the $\delta^{13}C$ of either fungal or bacterial biomass alone since the PLFA indicative of those groups did not vary with depth. Instead, these data demonstrate that the increase in soil biomass $\delta^{13}C$ with depth is driven by a change in the proportion of bacterial relative to fungal biomass. We suggest that the increased proportions of soil bacterial relative to fungal biomass with depth may represent an important mechanism

contributing to increasing $\delta^{13}C_{SOC}$ with depth via contributions from 'necromass' to SOC.

2.1 Introduction

Since the establishment of isotope-ratio mass spectroscopy (IRMS), the analysis of natural abundance stable isotope composition (isotopic signatures) has led to key insights into the ecophysiology and food webs of macroscopic organisms [e.g. Ehleringer et al., 1985, Peterson et al., 1985, Fry et al., 1978]. Yet for the study of microbial communities and their processes, stable isotope analysis remains largely limited to labeling approaches (stable isotope probing), even though well established methods for the compound-specific isotopic analysis of microbial biomarkers in environmental samples exist [e.g. Hayes et al., 1990, Abrajano et al., 1994, Silfer et al., 1991].

Soil microorganisms mediate both the formation and mineralization of soil organic carbon (SOC). They not only act as gatekeepers of the respiratory release of CO_2 from SOC [Schlesinger and Andrews, 2000], but are also considered an important source or precursor of SOC [Grandy and Neff, 2008, Bol et al., 2009, Miltner et al., 2011]. Soil microorganisms therefore exert crucial control on key feedbacks in the global carbon cycle. Linking microbial formation and degradation of SOC to the isotopic signatures of SOC and microbial biomarkers in soils could provide a tool for the investigation of these microbial processes in relatively undisturbed soils. This is sorely needed, given that most studies on microbial substrate use and SOC formation are based on laboratory incubations with labeled substrates [e.g. Waldrop and Firestone, 2004, Rinnan and Bååth, 2009] or labeled microbial biomass [Miltner et al., 2009]. Such stable isotope probing experiments typically require severe manipulations of the soils, including the removal of the soils from their in situ location, homogenization, addition of substrates often above ambient concentrations, and the exclusion of many C sources available to soil microorganisms in situ, like litter leachates or root exudates. The patterns of C cycling found in such experiments therefore can differ drastically from in situ measurements of the same soil [Phillips et al., 2013].

The relation between the $\delta^{13}C$ signature of soil microbial biomass and $\delta^{13}C_{SOC}$, however, is bi-directional (Fig. 2.1b). As precursors to SOC, microbial biomass $\delta^{13}C$ signatures have the potential to contribute to changes in $\delta^{13}C_{SOC}$. Given that the fungi:bacteria ratio (F:B) decreases with depth in most soils [e.g. Schnecker et al., 2015], an increase in the $\delta^{13}C$ of microbial necromass inputs to SOC from shallow horizons dominated by potentially ^{13}C depleted fungi to deep horizons dominated by potentially ^{13}C enriched bacterial necromass could, for example, represent a further mechanism for the increase in $\delta^{13}C_{SOC}$ with depth. Fungi and bacteria often fulfill different roles in soil biogeochemistry [e.g. Strickland and Rousk, 2010] and may generate chemically and perhaps isotopically distinct biomass and therefore necromass [Schimel and Schaeffer, 2012]. Such distinct signatures may occur due to the utilization of different substrates [e.g. Baum et al., 2009] or distinct metabolic fractionations [Hayes, 1993]. Although potentially useful in tracing contributions of necromass to soil, it remains unclear whether distinct biomass isotopic signatures exist between broadly defined soil microbial groups (e.g. fungi and bacteria). Our knowledge about the variations in $\delta^{13}C$ of soil microorganisms so far remains largely limited to the isotopic signatures of the microbial biomass as a whole, as analyzed after chloroform fumigation extraction, without differentiation between microbial groups [e.g. Dijkstra et al., 2006, Werth and Kuzyakov, 2010].

Phospholipid fatty acids (PLFA) have long been analyzed as a proxy for the abundance, composition and $\delta^{13}C$ of microbial biomass in soils [Frostegård et al., 2010]. Some PLFA predominantly occur in specific functional or operationally defined groups of microorganisms (e.g. fungi, Gram positive-, Gram negative- or Actinobacteria) and allow for the measurement of the $\delta^{13}C$ of these groups [Ruess and Chamberlain, 2010, and references therein]. Other PLFA are produced by a broad range of microorganisms and therefore report an integrated $\delta^{13}C$ of the microbial community as a whole [e.g. Cifuentes and Salata, 2001]. The application of $\delta^{13}C_{PLFA}$ in natural abundance studies so far remains largely limited to case

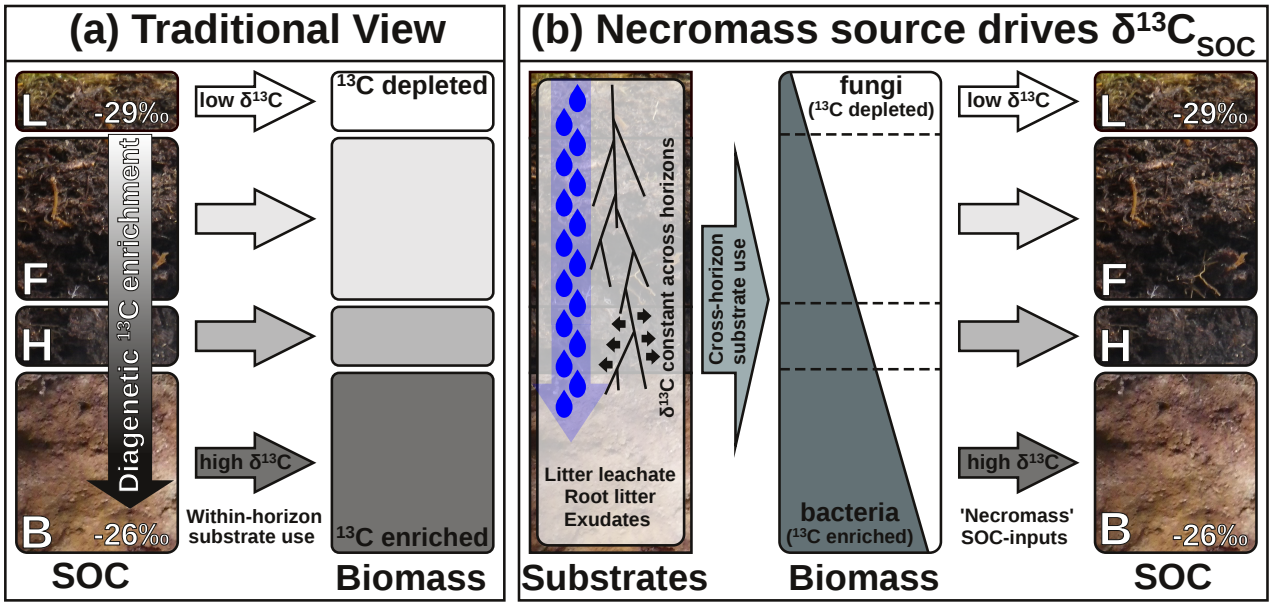

Figure 2.1 Conceptional figure depicting how diagenesis and microbial substrate use and are typically assumed to drive the δ^{13}C of soil organic carbon (SOC) and microbial biomass in soil profiles (a) versus the more complex exchange suggested by the results of this study (b). While the traditional view is that soil microorganisms primarily consume the SOC from 'their' own soil horizon and that $\delta^{13}C_{biomass}$ therefore increases with depth along with $\delta^{13}C_{SOC}$, we demonstrate that fungal and bacterial biomass have distinct δ^{13}C values and that the fungi:bacteria ratio dictate the overall $\delta^{13}C_{biomass}$ through the profile. We further suggest that the depletion of ^{13}C fungi-dominated biomass in shallow horizons and the enrichment of ^{13}C in bacteria-dominated biomass in deeper soil horizon can contribute to the development of distinct $\delta^{13}C_{SOC}$ signatures in the different horizons.

studies where major contrasts in the isotopic composition of potential substrates occur naturally (e.g. methanotrophy; Cifuentes and Salata [2001]) or were experimentally introduced (e.g. C3/C4 crop change experiments; Kramer and Gleixner [2006]; or free-air in situ CO_2 enrichment (FACE) experiments; Billings and Ziegler [2008], Streit et al. [2014]). Consequently, few studies have investigated the natural variations of $\delta^{13}C_{PLFA}$ to assess potential variation in microbial δ^{13}C [Baum et al., 2009, Cusack et al., 2011, Churchland et al., 2013].

Here, we report the variation in δ^{13}C values of individual PLFA within soil profiles characterized by steep decreases in F:B ratios and increases bulk $\delta^{13}C_{SOC}$ with depth. We invoked variation in $\delta^{13}C_{PLFA}$ values within profiles to test the hypothesis that the enrichment of ^{13}C in bacterial biomass relative to fungal biomass drives an increase of the overall δ^{13}C of soil microbial biomass with depth, representing a further mechanism contributing to the

increasing bulk $\delta^{13}C_{SOC}$ with depth. If in fact the biomass of these two groups were consistently distinct in their $\delta^{13}C$ we would expect the $\delta^{13}C$ of 'general' PLFA—derived from both bacteria and fungi—to be negatively correlated to the F:B ratio, and increase with depth. To attribute such a trend in general PLFA $\delta^{13}C$ to an enrichment of ^{13}C in bacterial relative to fungal biomass, the $\delta^{13}C$ of 'specific' PLFA—derived from either fungi only or bacteria only—would not only need to be distinct from each other but remain invariant with depth relative to the $\delta^{13}C$ of general PLFA.

2.2 Methods

All field sampling was conducted in June 2011. Field sites were located in the end member regions of a latitudinal transect of mesic boreal forests in Atlantic Canada (Newfoundland and Labrador Boreal Ecosystem Latitudinal Transect; NL-BELT) in south-western Newfoundland and southern Labrador. In each region, three locations ('sites') were selected for similarity in vegetation, stand type, class and age, and elevation (Online Resource 2.1). Within each site, three soil profiles were collected at random locations within a 10 m diameter circular as described in Laganière et al. [2015]. For each profile, two adjacent samples with an area of 10x10 cm were cut out of the organic layer. After removal of all live vegetation, organic layer samples were immediately separated into L, F, and H horizons (corresponding to the Oi, Oe, and Oa subhorizons in the U.S. soil nomenclature). Where present, the eluviated A horizon was removed and two 10 cm long cylindrical soil cores from the B horizon were taken using a 5.1 cm diameter corer. L, F, H, and B horizon samples were pooled to the plot level in the field resulting in two paired sets of 24 composite samples (2 regions, 3 sites, 4 horizons), which were designated for chemical analysis and PLFA extraction.

Bulk $\delta^{13}C_{SOC}$ values were analyzed by elemental analysis/isotope ratio mass spectroscopy (EA/IRMS). PLFA were extracted by an optimized protocol based on Ziegler et al. [2013].

The recovery of PLFA was determined in each extraction batch through duplicate extractions of samples from the F and B horizons with one replicate spiked with 130 µg di-17:0-phosphatidylcholine as described in Ziegler et al. [2013]. We recovered $\geq$ 73 % of this phospholipid with no significant differences between soil horizons or extraction batches. PLFA were quantified by gas chromatography/flame ionization detection (GC/FID), compound specific stable isotope ratios were measured by gas chromatography-combustion-isotope ratio mass spectroscopy (GC/IRMS), and peak identities were confirmed by gas chromatography/mass spectroscopy (GC/MS) analysis of selected samples. A detailed description of our analytical methods is provided in Online Resource 2.2.

We detected a total of 45 individual PLFA which were assigned to microbial groups based on Ruess and Chamberlain [2010]. Briefly, we assigned 18:2ω6,9 and 18:3ω3,6,9 to fungi and branched PLFA, monounsaturated PLFA (except 18:1ω9cis), cyclopropylated PLFA, and straight chained PLFA with an uneven number of C atoms to bacteria. A complete list of PLFA and their assignment to microbial groups is provided in Online Resource 2.3. Based on this assignment we calculated the ratio of mol% fungal to mol% bacterial PLFA, which we also transformed to fungal/(fungal + bacterial) PLFA in representation of a two-pool mixing model. For a multivariate analysis of the composition of PLFA we conducted a non-metric multi-dimensional scaling (NMDS) based on Bray-Curtis distances of the mol% of each PLFA in each sample to visualize how community structure varies with soil horizon and region. Based on this ordination, we then calculated linear fittings for the mol% of the sum of fungal or bacterial PLFA using the function 'envfit' in vegan (see below).

Carbon isotopic signatures were analyzed for nine individual PLFA that were properly separated and sufficiently abundant in all samples. Seven of the nine PLFA were specific to broad microbial groups including fungi (18:2ω6,9) or bacteria. Among bacteria, i15:0 and a15:0 are specific to Gram positive bacteria, while 16:1ω7, 18:1ω7, cy17:0, and cy19:0 occur predominantly but not exclusively in Gram negative bacteria (Grogan and Cronan

1997). The other two PLFA were general biomarkers produced by both fungi and bacteria (16:0 and 18:1ω9cis; Ruess and Chamberlain [2010], Frostegård et al. [2010]). In addition, we determined $\delta^{13}C$ values of the fungal PLFA 18:3ω3,6,9 in the fungi-rich L horizons but not in deeper soil horizons, where low concentration of this PLFA inhibited reliable measurements. Together, these 9 or 10 PLFA made up 61-74 mol% of the total PLFA content of the samples.

Preliminary analysis showed that the differences in $\delta^{13}C_{PLFA}$ between the two study regions (typically <1 ‰) were minor compared to differences among soils horizons or among microbial groups. We therefore tested for significant differences among soil horizons in the $\delta^{13}C_{PLFA}$ of each individual PLFA using a mixed effect model with 'soil horizon' as a fixed effect and 'site' as a random effect followed by pair-wise comparison of soil horizons with Tukey HSD post hoc tests as described by Hothorn et al. [2008]. The same analysis was conducted for SOC normalized $\delta^{13}C_{PLFA}$ values (i.e. $\Delta^{13}C_{PLFA\text{-}SOC}$) to test whether PLFA were more or less enriched relative to the surrounding bulk SOC in the different soil horizons. Furthermore, we tested whether $\delta^{13}C_{PLFA}$ co-varied with $\delta^{13}C_{SOC}$ by calculating the correlation coefficients (R) between these two measures for each individual PLFA. Because of the relatively low $\delta^{13}C_{PLFA}$ in L horizon samples, we repeated the analysis excluding the L horizon samples to further test whether $\delta^{13}C_{PLFA}$ was correlated with $\delta^{13}C_{SOC}$ in the deeper soil horizons. All statistical analyses were performed with the software and statistical computing environment R (Version 3.0.2) using the packages 'nlme' (Version 3.1-113), 'multcomp' (Version 1.3-7), and 'vegan' (Version 2.0-7). All results are stated as means of six field sites ± one standard deviation unless indicated otherwise.

2.3 Results

The soil horizons contained a highly stratified microbial community as characterized by proportions of fungal and other eukaryotic PLFA decreasing with depth and proportions of

bacterial PLFA increasing with depth. The overall PLFA concentration varied little relative to bulk SOC among soil horizons (3.5 ± 0.4 to 3.8 ± 0.5 µmol g^{-1} SOC; Online Resource 2.4). The concentration of fungal PLFA decreased relative to bulk SOC from 0.97 ± 0.11 µmol g^{-1} SOC in L horizons to 0.075 ± 0.013 µmol g^{-1} SOC in B horizons. In contrast, concentrations of bacterial PLFA increased from 1.18 ± 0.14 µmol g^{-1} SOC in L horizons to 2.84 ± 0.36 µmol g^{-1} SOC in B horizons. The ratio of fungal to bacterial PLFA therefore decreased from 0.82 ± 0.10 in the L horizon to 0.027 ± 0.002 in the B horizon, corresponding to fungal/(fungal + bacterial) ratios of 0.45 ± 0.03 and 0.027 ± 0.002, respectively (Fig. 2.2a). Neither PLFA concentration nor PLFA composition (mol% fungi or bacteria) exhibited a significant difference between the two regions. Multivariate analysis (NMDS) resulted in samples clustering by soil horizon, suggesting that microbial community composition varied strongly between soil horizon but little between the studied regions (Online Resource 2.5). Carbon isotopic signatures of bulk SOC increased with depth from -29.2 ± 0.3 ‰ in L horizons to -26.4 ± 0.2 ‰ in B horizons. $\delta^{13}C_{PLFA}$ was more variable relative to the SOC and ranged from -40.1 to -22.4 ‰ (Figs. 2.2b), varying by 8 to 10 ‰ among individual PLFA within a sample. The $\delta^{13}C$ of general and group-specific PLFA exhibited contrasting patterns (Fig. 3). Total variation in $\delta^{13}C$ among specific PLFA, that is individual PLFA produced by only one microbial group (i15:0, a15:0, 16:1ω7, cy17:0, 18:1ω7, cy19:0, and 18:2ω6,9), was captured by variation in the $\delta^{13}C$ of PLFA produced by Gram positive bacteria (G+) and fungi (Figs. 2.2b, 2.3a). In all samples, PLFA produced by fungi (18:2ω6,9 and 18:3ω3,6,9) exhibited the lowest $\delta^{13}C$ values while those PLFA produced by G+ bacteria (i15:0 and a15:0) were highest. In contrast to this range in $\delta^{13}C$ among PLFA by source organism, the $\delta^{13}C$ of each specific PLFA showed remarkably little variation with depth (Fig. 2.3a) or within the entire dataset (Fig. 2.2b). If the bulk soil substrate $\delta^{13}C$ had any influence on microbial biomarker $\delta^{13}C$ the $\delta^{13}C_{PLFA}$ would have increased with depth in parallel with $\delta^{13}C_{SOC}$. However, 4 of the 7 specific PLFA (i15:0, 18:1ω7, cy19:0, 18:2ω6) exhibited no

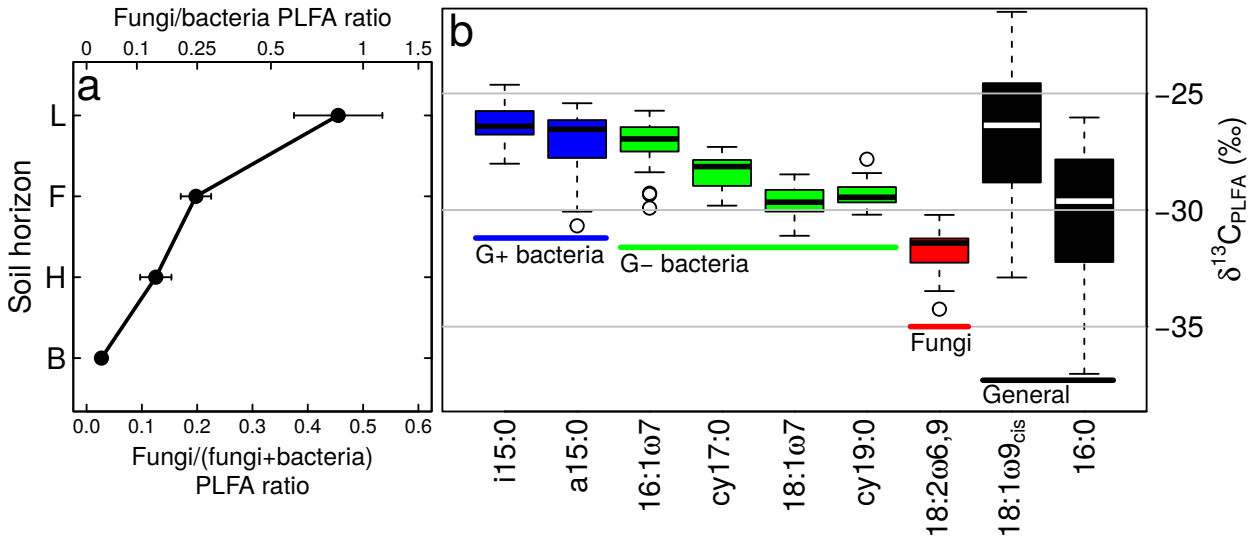

Figure 2.2 (a) Depth profile of fungal vs. bacterial abundance, expressed as fungal/(fungal + bacterial) PLFA. The plotted value represent the means of 6 field sites with error bars indicatng the standard deviations of these means. (b) Overall range of the δ^{13}C of individual PLFA in the organic (LFH) and mineral (B) soil horizons of boreal forest soils (n=24). Note the higher variance of the δ^{13}C of general PLFA (black) compared to PLFA specific to an individual microbial group (in color) and the consistent enrichment in ^{13}C within bacterial PLFA relative to fungal PLFA.

significant difference in δ^{13}C among soil horizons. The other 3 specific PLFA (a15:0, 16:1ω7, cy17:0) varied in δ^{13}C by horizon and exhibited a significant correlation between $\delta^{13}C_{PLFA}$ and $\delta^{13}C_{SOC}$ ($R = 0.71$ to 0.77; $p < 0.001$), but these correlations were primarily driven by low $\delta^{13}C_{PLFA}$ values in the L horizons (Table 2.1) and were lost or largely diminished when L horizon samples were excluded (Online Resource 2.6). While the δ^{13}C of specific PLFA exhibited little difference between soil horizons in absolute terms, these PLFA were more ^{13}C-depleted relative to the surrounding bulk SOC at greater depth, as indicated by significantly lower $\Delta^{13}C_{PLFA\text{-}SOC}$ values in deeper soil horizons compared to more shallow horizons in 6 of 7 specific PLFA (Table 2.1), providing further evidence that $\delta^{13}C_{PLFA}$ signatures of group-specific PLFA were not directly affected by the increase of $\delta^{13}C_{SOC}$ with depth.

Unlike specific PLFA, general PLFA, that is PLFA produced by both bacteria and fungi (18:1ω9 and 16:0), varied by over 10 ‰ among samples (Fig. 2.2b) and became more enriched in ^{13}C with depth, both in absolute terms and relative to bulk SOC (Table 2.1;

Table 2.1 Carbon isotopic signatures of 9 individual PLFA by soil horizon, presented both in absolute terms ($\delta^{13}C_{PLFA}$) and relative to the surrounding SOC ($\Delta^{13}C_{PLFA\text{-}SOC}$). The presented values are given as the average among six field sites with the standard deviations of these averages provided in brackets. Different superscript letters indicate significant differences between soil horizons across of region (Tukey HSD). Furthermore, test metric (F) and significance level (***, p<0.001; **, p<0.01, *, p«0.05; n.s., p>0.05) for soil horizon effect on PLFA isotopic signatures.

PLFA	L	Soil Horizon				Soil horizon effect[1]
		F	H	B		$F_{F3,15}$
i15:0	$\delta^{13}C_{PLFA}$	-26.7 (1.1)	-26.0 (0.3)	-25.7 (0.9)	-26.6 (0.2)	3.1
(G+ bacteria)	$\Delta^{13}C_{PLFA\text{-}SOC}$	2.4 (1.0)a	2.3 (0.3)a	1.7 (0.9)a	-0.3 (0.5)b	19.6***
a15:0	$\delta^{13}C_{PLFA}$	-28.9 (1.7)a	-27.1 (0.6)b	-26.5 (0.9)b	-26.2 (0.2)b	11.9***
(G+ bacteria)	$\Delta^{13}C_{PLFA\text{-}SOC}$	0.3 (1.4)	1.2 (0.5)	0.9 (0.9)	0.2 (0.6)	2.3
16:1ω7	$\delta^{13}C_{PLFA}$	-28.7 (0.9)a	-26.8 (0.4)b	-26.5 (0.8)b	-26.6 (0.3)b	30.9***
(G- bacteria)	$\Delta^{13}C_{PLFA\text{-}SOC}$	0.4 (0.7)a	1.5 (0.4)b	0.8 (0.6)a	-0.3 (0.6)c	16.7***
cy17:0	$\delta^{13}C_{PLFA}$	-29.4 (0.4)a	-28.4 (0.5)b	-27.9 (0.6)b	-27.8 (0.3)b	16.2***
(G- bacteria)	$\Delta^{13}C_{PLFA\text{-}SOC}$	-0.3 (0.7)a	-0.1 (0.3)a	-0.6 (0.6)a	-1.5 (0.4)b	8.9***
18:1ω7	$\delta^{13}C_{PLFA}$	-29.8 (0.9)	-29.5 (0.5)	-29.8 (0.6)	-29.5 (0.8)	0.4
(G- bacteria)	$\Delta^{13}C_{PLFA\text{-}SOC}$	-0.7 (0.3)a	-1.2 (0.5)a	-2.4 (0.6)b	-3.2 (0.6)c	29.0***
cy19:0	$\delta^{13}C_{PLFA}$	-29.1 (0.8)	-29.5 (0.5)	-29.4 (0.6)	-29.4 (0.3)	0.9
(G- bacteria)	$\Delta^{13}C_{PLFA\text{-}SOC}$	0.0 (0.5)a	-1.2 (0.3)b	-2.0 (0.5)c	-3.0 (0.4)d	83.7***
18:2ω6,9	$\delta^{13}C_{PLFA}$	-32.0 (0.8)	-31.6 (0.6)	-31.0 (1.5)	-31.3 (0.5)	1.3
(Fungi)	$\Delta^{13}C_{PLFA\text{-}SOC}$	-2.8 (0.6)a	-3.3 (0.6)a	-4.7 (1.6)b	-4.9 (0.5)b	11.5**
18:3ω3,6,9[2]	$\delta^{13}C_{PLFA}$	-37.2 (1.8)	–	–	–	
(Fungi)	$\Delta^{13}C_{PLFA\text{-}SOC}$	-8.0 (1.5)	–	–	–	
16:0	$\delta^{13}C_{PLFA}$	-35.0 (1.5)a	-30.7 (0.5)b	-28.7 (0.2)c	-26.7 (0.4)d	176.1***
(General)	$\Delta^{13}C_{PLFA\text{-}SOC}$	-5.9 (1.2)a	-2.4 (0.4)b	-1.4 (0.4)bc	-0.4 (0.6)d	148.8***
18:1ω9	$\delta^{13}C_{PLFA}$	-31.0 (1.0)a	-27.4 (0.4)b	-25.3 (0.5)c	-23.4 (1.2)d	129.0***
(General)	$\Delta^{13}C_{PLFA\text{-}SOC}$	-1.9 (1.2)a	1.0 (0.5)b	2.0 (0.6)bc	2.9 (1.5)c	33.8***

[1] Soil horizon effects on $\delta^{13}C_{PLFA}$ and $\Delta^{13}C_{PLFA\text{-}SOC}$ were tested in mixed effects model with soil horizon as a fixed effect and site as a random effect.

[2] $\delta^{13}C$ values of 18:3ω3,6,9 could not be analyzed in F,H, and B horizons due to the low concentrations of this PLFA in these horizons.

Fig. 2.3b). The increase in $\delta^{13}C$ of general PLFA with depth and lack of such change in any group-specific PLFA (fungal or bacterial) was exhibited in all soil profiles analysed (Online Resource 2.7). The $\delta^{13}C$ of general PLFA co-varied with the proportion of fungal versus bacterial PLFA given as the ratio fungal/(fungal + bacterial) PLFA (R = -0.96 and -0.94 for 16:0 and 18:1ω9 cis ; $p < 0.001$; Fig. 2.4a) consistent with the idea that $\delta^{13}C$ of these general PLFA was largely attributed to the proportion of fungi to bacteria PLFA present in the soil and these groups' distinct $\delta^{13}C$ signatures (Figs. 2.3b). No such relationship with fungal/(fungal + bacterial) PLFA was observed for any specific PLFA (Fig. 2.4b). The $\delta^{13}C$ of general PLFA co-varied with $\delta^{13}C_{SOC}$ (R = 0.87-0.92, $p < 0.001$; Online Resource 2.6), but slopes of $\delta^{13}C_{PLFA}/\delta^{13}C_{SOC}$ were significantly greater than one (2.57 ± 0.23 (standard error) and 2.27 ± 0.27 for 16:0 and 18:1ω9cis; t = 6.56 and 4.67; both $p < 0.001$; n = 24) indicating that the $\delta^{13}C$ of general PLFA exhibited a much steeper increase with depth than $\delta^{13}C_{SOC}$ (Fig. 2.3b).

2.4 Discussion

2.4.1 Fungal biomass is depleted in ^{13}C relative to bacterial biomass

Our data suggest that fungal PLFA in these soils are depleted in ^{13}C relative to bacterial PLFA. This is consistent with most previous studies from which we could retrieve such data demonstrating key fungal PLFA (typically 18:2ω6,9 as used here) are typically deplete in ^{13}C relative to bacterial PLFA (Table 2.2a). One noteworthy exception to this generally consistent pattern was one study that found fungal PLFA enriched in ^{13}C relative to bacterial PLFA in soils from a glacial forefield chronosequence [Esperschütz et al., 2011]. The lower $\delta^{13}C$ values observed in fungal PLFA in the current study are not an artefact of fungal PLFA selection; indeed, 18:2ω6,9 is generally enriched in ^{13}C relative to other fungal PLFA and fungal biomass in culture (-0.3 to +2.5 ‰; Abraham and Hesse [2003]). Furthermore we

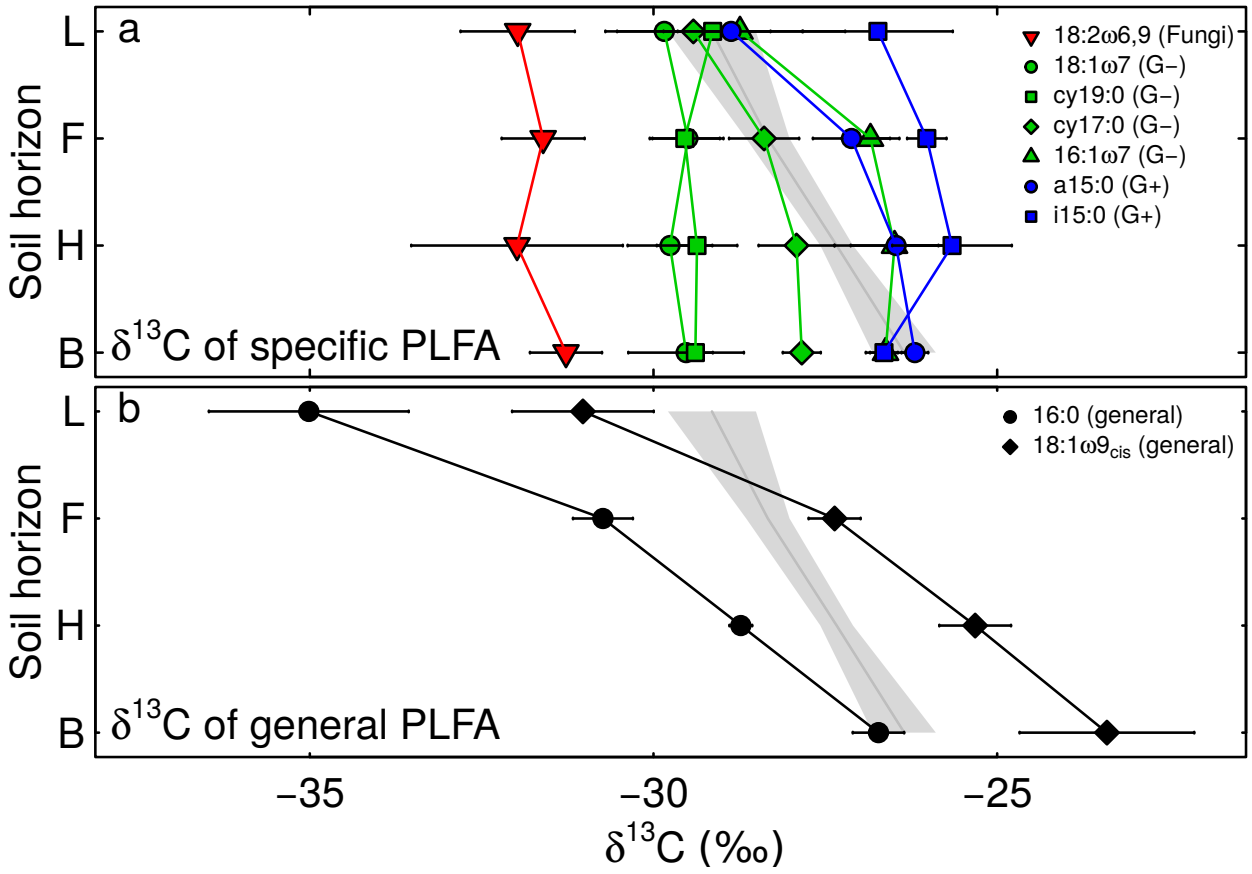

Figure 2.3 Within-profile variation of the δ^{13}C of phospholipid fatty acids (PLFA) in boreal forest soils. δ^{13}C profiles are presented for 4 PLFA indicative of Gram positive bacteria (G+), Gram negative bacteria (G-), or fungi (a); and for 2 general PLFA (b). The δ^{13}C of bulk soil organic carbon printed in the background (grey line). All values are given as means among six field sites with error bars and the areas indicating one standard deviation of these means.

observed highly ^{13}C depleted values for the second fungal PLFA 18:3ω3,6,9 analyzed in the L horizon soils across sites where it was abundant enough to analyze (Table 2.1).

The increasing trend with depth in $\delta^{13}C_{PLFA}$ produced by both fungi and bacteria (16:0 and 18:1ω9cis) further supports our observation of the ^{13}C depletion of fungal relative to bacterial PLFA in these soils. The depth trend in these two PLFA was best explained by the proportion of fungal to bacterial PLFA abundance in these soils (Fig. 2.4a). The negative correlation between soil F:B ratio and the δ^{13}C of 16:0 and 18:1ω9cis implies that in a given sample the same individual PLFA was more enriched in ^{13}C when produced by bacteria than when produced by fungi. Because we found that the δ^{13}C of PLFA indicative

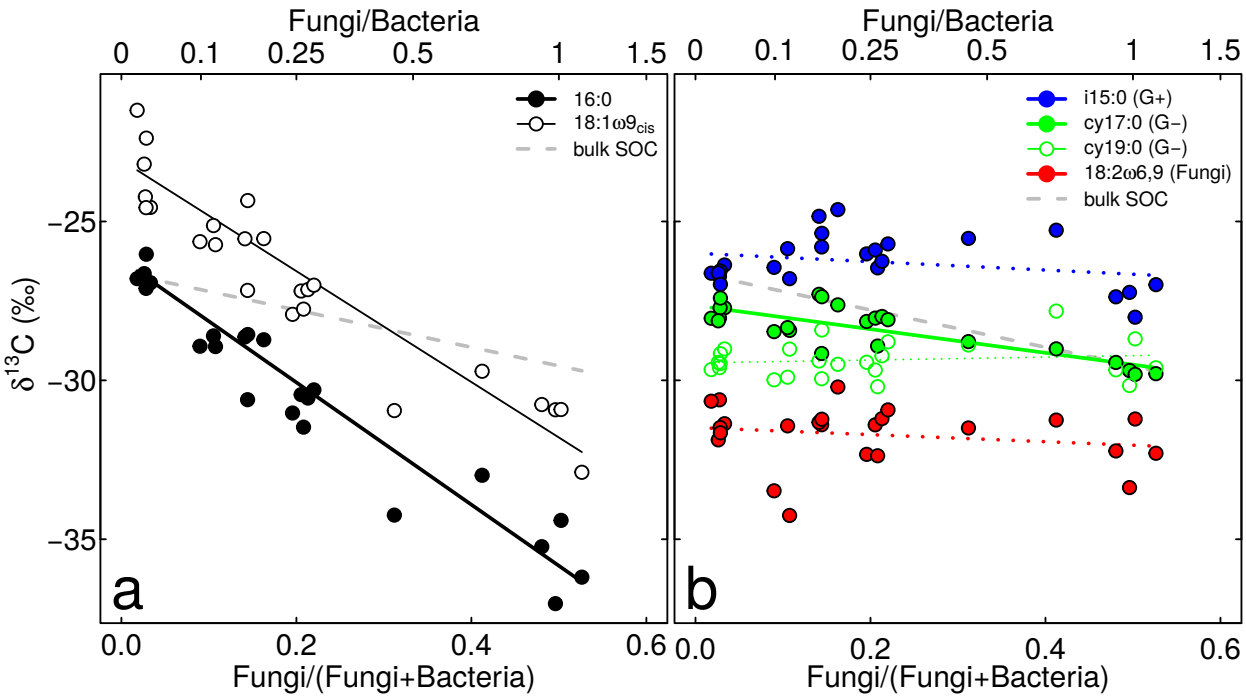

Figure 2.4 Correlation between δ^{13}C of two general PLFA (a) and four group specific PLFA (b) with the ratio of fungal/(fungal+bacterial) PLFA. Solid lines indicate linear regressions where a significant correlations was detected; dotted lines indicate linear fittings where no significant correlation was found. The dashed grey lines indicate the linear regression between $\delta^{13}C_{SOC}$ and fungal/(fungal+bacterial) PLFA.

of fungi or bacteria exhibit little to no variation with depth, the increase in δ^{13}C of 16:0 and 18:1ω9cis could not be explained by changes in the δ^{13}C of one or the other of these groups if, for example, shifts in community structure or substrate use with depth had an important influence on the δ^{13}C of microbial biomass.

The enrichment of ^{13}C of bacterial relative to fungal PLFA is a result of differences in biomass δ^{13}C between these two groups, and not because of a stronger discrimination against ^{13}C during fatty acid biosynthesis ($\Delta^{13}C_{\text{PLFA-biomass}} = \delta^{13}C_{\text{PLFA}}$-$\delta^{13}C_{\text{biomass}}$) in fungi relative to bacteria. Fatty acids were consistently depleted in ^{13}C by 2-4 ‰ relative to bulk biomass in both fungal and bacterial cultures, which is generally attributed to the fractionation associated with decarboxylation of pyruvate to acetyl-CoA, the main building block for fatty acids [DeNiro and Epstein, 1977, Hayes, 2001]. Congruent with this, available

literature values (presented for 16:0 in Table 2.2b) do not indicate any consistent difference in the fractionation of PLFA or total fatty acids relative to bulk microbial biomass between these two groups. In fungal cultures the $\delta^{13}C$ values of 16:0, 18:1ω9cis , and 18:2ω6,9 typically fell within 2.5 ‰ of the bulk cell [Abraham and Hesse, 2003]. A similar but perhaps slightly greater fractionation between fatty acid and biomass has been observed in aerobic cultures of heterotrophic bacteria ($\Delta^{13}C_{PLFA\text{-}biomass}$ = -3 to +0.8 ‰). A much larger fractionation ($\Delta^{13}C_{PLFA\text{-}biomass}$ = -14.7 to -10.4 ‰), however, was found in bacteria that utilize the serine pathway which is active under anaerobic conditions [Teece et al., 1999]. Together, the available data from culture studies suggests that if $\Delta^{13}C_{PLFA\text{-}biomass}$ differs between fungi and bacteria, the discrimination against ^{13}C in PLFA relative to biomass would be stronger in bacteria than in fungi. As such the $\delta^{13}C$ of bacterial biomass based upon their PLFA would lead to an underestimation of biomass $\delta^{13}C$ in bacteria relative to fungi, suggesting we could have underestimated the difference in the $\delta^{13}C_{biomass}$ of these two groups using these biomarkers in our study.

The consistent enrichment of ^{13}C in PLFA indicative of bacteria relative to those indicative of fungi in all horizons (Fig. 2.3a), across which substrate identity and microbial community structure varied, suggests that differences in $\delta^{13}C$ between fungal and bacterial biomass are driven by fundamental differences in metabolisms of these microbial groups. For example, fungi and bacteria likely differ in how C is allocated into different classes of microbial compounds (e.g. microbial cell walls, extracellular enzymes and polysaccharides, osmolytic compounds; Schimel and Schaeffer [2012]). This is consistent with results from Abraham et al. [1998], who reported that when grown on the same substrate, fungal PLFA 16:0 was depleted by 1.1-6.0 ‰ compared to bacterial 16:0. Results from the current study suggest that investigation into the mechanisms that may lead to differences in soil microbial $\delta^{13}C$ from natural environments are warranted given the potential significance of exploiting these signatures to further link bacterial and fungal activity to soil C cycling.

2.4.2 Soil $\delta^{13}C_{PLFA}$ values are driven by their fungal or bacterial origin, not by $\delta^{13}C_{SOC}$

The constant $\delta^{13}C$ values of PLFA indicative of fungi or bacteria across all soil horizons show that though $\delta^{13}C_{PLFA}$ of individual strains grown in culture on a single C source can exhibit large variability [Abraham et al., 1998], $\delta^{13}C_{PLFA}$ may vary little in natural environments where diverse organic substrates are available to complex microbial communities. Similar observation have been made in marine estuarine sediments [Bouillon and Boschker, 2006]. Constancy of fungal and bacterial PLFA across depth further suggests that the $\delta^{13}C$ of fungal and bacterial biomass were in part decoupled from the increase of bulk $\delta^{13}C_{SOC}$ with depth. This is consistent with the constant $\delta^{13}C$ values of fungal mycelia observed between 0 and 30 cm depth in spruce and mixed forest soil [Wallander et al., 2004]. The $\delta^{13}C$ of general PLFA produced by both fungi and bacteria, indicative of $\delta^{13}C_{biomass}$ of the soil microbial community as a whole, increased with depth but to a much larger extent (7.6-8.3 ‰ from L to B horizon) than bulk SOC (2.8 ‰; Fig. 2.3b). In spite of the correlation between the $\delta^{13}C$ of general PLFA and $\delta^{13}C_{SOC}$, the variation in the $\delta^{13}C$ of general PLFA could not have been driven by $\delta^{13}C_{SOC}$. If that were the case, we would have observed increased $\delta^{13}C$ values in deeper soil horizons not only in general PLFA, but also in PLFA specific to one or more microbial groups. More likely, the increased $\delta^{13}C$ of general PLFA with depth was driven by a greater bacterial relative to fungal source of these PLFA in deeper horizons, as fungi:bacteria ratios decreased by over an order of magnitude from L to B horizons and were highly correlated with the $\delta^{13}C$ of general PLFA as discussed above.

While fungi and bacteria might consume distinct substrates with different isotopic signatures, the lack of a soil horizon effect on the $\delta^{13}C$ of fungal and bacterial biomass observed here suggests that the substrates consumed by each group of soil microorganisms had similar isotopic signatures across all soil horizons. Bulk SOM therefore is a poor representative of the substrates actually taken up by soil microorganisms in situ. Our data thus suggest that

isotopic signatures of soil microorganisms are driven by substrates of common $\delta^{13}C$, found throughout soil horizons, rather than by bulk $\delta^{13}C_{SOC}$ signature of the soil horizon within which the microorganisms reside. This is feasible if the same substrate, with a constant $\delta^{13}C$ signature, were available for microbial uptake in all soil horizons. Indeed, plant transfer of photosynthate to mycorrhizal fungi likely represents such a substrate source, as do root exudates and fine root litter [Wallander et al., 2004]. A mobile SOC fraction percolating through horizons also could provide such a substrate source, and our field sites are characterized by relatively high precipitation and exhibit significant vertical DOC fluxes from the organic to the mineral horizons (10-30 g C m^{-2} $year^{-1}$; Edwards unpublished data). This is congruent with reports that in situ heterotrophic soil respiration can be derived from modern C even in deep mineral soil horizons containing centuries old SOC and even when root inputs were excluded [Phillips et al., 2013]. Substrate transport across soil horizons can also occur via fungal mycelia [Strickland and Rousk, 2010] and perhaps via actinobacterial mycelia, but this mechanism is unlikely in the B horizon where we detected only marginal amounts of fungal or actinobacterial PLFA.

2.4.3 Increased necromass $\delta^{13}C$ driven by fungal:bacterial ratios may contribute to increased $\delta^{13}C_{SOC}$ with depth

The difference in $\delta^{13}C$ between fungal and bacterial PLFA is a strong indicator that $\delta^{13}C$ of C pools influenced by microbial activity such as CO_2, DOC, and SOC are influenced by the identity of the microbial group contributing to the pool. The main trends observed in our study—the depletion of ^{13}C in fungal relative to bacterial biomass and the independence of specific $\delta^{13}C_{PLFA}$ from the increase of $\delta^{13}C_{SOC}$ with depth—have important implications for our conceptual understanding of soil C fluxes as well as the origin of SOC and its variation in $\delta^{13}C$ (Fig. 2.1). Ex situ laboratory incubation experiments, which dominate the study of microbial substrate use patterns, rely on the assumption that soil microorganisms primarily

consume SOC that is located within 'their own' soil horizon (Fig. 2.1a). The reliance on this assumption occurs because other substrates available in situ are excluded in such experiments through the separation of soil horizons, pre-incubating soils to remove labile C sources liberated by the disturbance required for experimental setup, and exclusion of litter leachates or root exudates. Such experiments inevitably generate data supporting the idea that microbial biomass in deeper soil horizons is enriched in ^{13}C due to microbial access to and use of more ^{13}C enriched SOC with depth. In contrast, our in situ study suggests the δ^{13}C value of microbial biomass as a whole can be more enriched in ^{13}C in deeper soil horizons as a result of a shift in fungal to bacterial dominance—a feature common to many of the world's soils [e.g. Schnecker et al., 2015].

Deeper soil horizons are traditionally viewed as exhibiting a greater bulk $\delta^{13}C_{SOC}$ value due to the enrichment of ^{13}C during diagenesis, associated losses of ^{13}C-depleted compounds from the soil system [Nadelhoffer and Fry, 1988, Nakamura et al., 1990, Fig. 2.1a] or increasing proportions of ^{13}C enriched compounds of microbial origin with depth [Boström et al., 2007]. Our results imply that the gradual shift from fungal to bacterial dominance with increasing depth, and changes in the δ^{13}C of bulk necromass as a result of that shift, can contribute to the more ^{13}C enriched SOC in deeper soil horizons (Fig. 2.1b). The δ^{13}C of bulk SOC therefore would not only depend on the quantity of material of microbial origin in SOC, but the fungal or bacterial identity of its microbial precursors as well. Thus, the δ^{13}C of microbial biomass likely exerts some influence on the δ^{13}C of SOC with depth, rather than conversely.

2.5 Acknowledgments

We thank Jamie Warren for laboratory assistance; Thalia Soucy-Giguère for help with field sampling; Birgit Wild, Lucia Fuchslueger, Frances Podrebarac, and Scarlett Vallaire for

helpful conversation and comments on the manuscript; and Frances Podrebarac for providing the soil profile pictures used in Fig. 2.1. We furthermore thank three anonymous reviewers who helped to substantially improve the manuscript. Our study was funded by the Natural Sciences and Engineering Research Council of Canada, the Center for Forestry Science and Innovation (Department of Natural Resources, Government of Newfoundland and Labrador), the Canada Research Chairs program, and the Humber River Basin Project (Government of Newfoundland and Labrador).

Table 2.2 Compiled literature values of $\delta^{13}C_{PLFA}$ expressed as the difference in $\delta^{13}C$ ($\Delta^{13}C$) among (a) fungal and bacterial PLFA within soil samples and (b) among PLFA and bulk biomass in cultures of fungi and heterotrophic bacteria. The differences in the $\delta^{13}C$ derived from the weighted mean of all PLFA attributed to the groups (e.g. Bacteria, fungi, Gram negative Bacteria, Gram positive Bacteria) is also provided in each case from the data provided in this study and Churchland et al. [2013].

PLFA	Reference	Range ($\Delta^{13}C$)	Ecosystem/Strain	Comments
(a) Fungal (18:2ω6,9) vs. bacterial PLFA in soil samples				
All bacteria		bacteria-fungi		
weighted mean	This study	2.4 to 4.3‰	Boreal forest soil	
	Churchland et al. [2013]	1.2 to 2.2‰	Temperate forest soil	Clearcut >forested
Gram positive bacteria		bacteria-fungi		
weighted mean	This study	4.3 to 6.4‰	Boreal forest soil	
i15:0-18:2ω6,9	Kramer and Gleixner [2006]	7.6‰	Agricultural soil	
	This study	3.2 to 7.5‰	Boreal forest soil	
	Steinbeiss et al. [2009]	3.3 to 6.6‰	Agricultural & forest soil	
	Streit et al. [2014]	2.6 to 5.1‰	Alpine forest soil	Inter-annual difference
	Billings and Ziegler [2008]	3.7 to 3.8‰	Temperate forest soil	
	Baum et al. [2009]	-1.5 to 5.3‰	Temperate forest soil	Before litterfall >after litterfall
	Esperschütz et al. [2011]	-3.5 to 1.6‰	Glacier forefield	
Gram negative bacteria		bacteria-fungi		
weighted mean	This study	2.1 to 3.8‰	Boreal forest soil	
16:1ω7-18:2ω6,9	Baum et al. [2009]	2.1 to 10.1‰	Temperate forest soil	Before litterfall >after litterfall
	Kramer and Gleixner [2006]	6.4‰	Agricultural soil	
	Streit et al. [2014]	2.8 to 6.8‰	Alpine forest soil	Inter-annual difference
	Billings and Ziegler [2008]	4.0 to 5.1‰	Temperate forest soil	Fertilized >control
	This study	2.8 to 7.1‰	Boreal forest soil	
	Steinbeiss et al. [2009]	2.1 to 5.5‰	Agricultural & forest soil	
	Esperschütz et al. [2011]	-3.4 to -0.3‰	Glacier forefield	

PLFA	Reference	Range ($\Delta^{13}C$)	Ecosystem/Strain	Comments
(b) PLFA vs. bulk biomass in cultures				
Fungi		PLFA-biomass		
16:0	Abraham et al. [1998]	-3.7 to +2.4‰	Fusarium solani	4 substrates
	Abraham and Hesse [2003]	-1.0 to +2.4‰	4 fungal species	4 substrates
	Cowie et al. [2009]	-2.9 to +3.1‰	Acremonium sp.	Heterotrophic enriched culture from acid mine drainage
18:2ω6,9	Abraham and Hesse [2003]	-0.2 to +2.5‰	4 fungal species	4 substrates
	Cowie et al. [2009]	-3.1 to +0.8‰	Acremonium sp.	Heterotrophic enriched culture from acid mine drainage
Heterotrophic bacteria		PLFA-biomass		
16:0	Londry and Marais [2003]ab	-16 to +3‰	4 sulfate reducing bacteria	Substrate: acetate or lactate
	Zhang et al. [2003]ab	-14.2 to -5.6‰	2 Fe(III) reducing species	Substrate: acetate or lactate
	Teece et al. [1999]ac	-10.3‰	Shewanella putrefaciencs	Substrate: lactate (anaerobic)
	L. Kohl, unpublished	-3.0 to -0.8‰	Pseudomonas fluorescence	Substrate: cellobiose
	Teece et al. [1999]b	-2.0‰	Shewanella putrefaciencs	Substrate: lactate (aerobic)
	Wick et al. [2003]	-0.7‰	Mycobacterium sp.	Substrate: glucose
	Zhang et al. [2002]a	+0.1 to +0.8‰	Thermatoga maritima	Substrate: glucose
	Wick et al. [2003]	+5.3‰	Mycobacterium sp.	Substrate: anthracene
All fatty acids	Blair et al. [1985]c	-2.5‰	Escherichia coli	Substrate: glucose
	Monson and Hayes [1982]c	-3.2‰	Escherichia coli	Substrate: glucose

a The microbial cultures in this study were grown under anaerobic conditions, which can cause a much larger depletion of 13C in fatty acids compared bulk biomass than aerobic cultures Teece et al. [1999].

b In these studies the highest values for $\Delta^{13}C_{PLFA\text{-}biomass}$ were found in cultures grown on acetate, which is not a common substrate in soil, and where a smaller depletion of ^{13}C in PLFA was expected due to the direct generation of fatty acids from acetyl-CoA as opposed to the production from pyruvate [Hayes, 2001].

c These studies reported the $\delta^{13}C$ of fatty acids in the total lipid fraction. We report these studies because little data is available on the apparent fractionation between $\delta^{13}C_{PLFA}$ and $\delta^{13}C_{biomass}$ in bacteria, and the difference in $\delta^{13}C_{16:0}$ between PL and other lipid fractions is variable, but small on average [0.7‰ Abraham et al., 1998].

2.6 Online Resources

2.6.1 Online Resource 2.1 - Field sites

Table 2.S1 Location and characteristics of field sites studied herein. Table modified from Laganière et al. [2015].

Region	Site	Latitude	Longitude	Elevation (m)	MAT[1] (C)	MAP[1] (mm a^{-1})	PET[1] (mm a^{-1})	Tree species	Litterfall (kg ha^{-1} yr^{-1})	Basal area (m^2 ha^{-1})	Soil type
Eagle	Muddy Pond	53°33'01"N	56°59'13"W	145	0.0	1074	432	Abies balsamea	1260	37.2	Humo-ferric podzol
River	Sheppar's Ridge	53°03'25"N	56°56'02"W	170	0.0	1074	432	Abies balsamea	2275	50.1	Humo-ferric podzol
(cold)	Harry's Pond	53°35'12"N	56°53'21"W	136	0.0	1074	432	Abies balsamea	1151	38.2	Humo-ferric podzol
Grand	Slug Hill	48°00'39"N	58°54'16"W	215	5.2	1505	608	Abies balsamea	5889	44.7	Humo-ferric podzol
Codroy	Maple Ridge	48°00'28"N	58°55'14"W	165	5.2	1505	608	Abies balsamea	3732	48.4	Humo-ferric podzol
(Warm)	O'Reagan's	47°53'36"N	59°10'28"W	100	5.2	1505	608	Abies balsamea	3439	50.1	Humo-ferric podzol

[1] MAT; mean annual temperature; MAP, mean annual precipitation; PET, mean annual potential evapotranspiration. Meteorological data represent climate normals of 1981-2010 from Cartwright, NL and Doyles, NL weather station and was taken from Environment Canada [2014]. Potential evaporation was calculated according to Xu and Singh [2001] based on monthly temperature and precipitation normals.

2.6.2 Online Resource 2.2 - Additional methods

Elemental Analysis/isotope ratio mass spectroscopy (EA/IRMS)

Samples designated for chemical analysis were stored at 4 °C for up to 14 days during the field campaign, and then dried (60 °C for 48h) and ball-milled (Retsch Mixer Mill MM200). Bulk $\delta^{13}C_{SOC}$ values were analyzed with a Carlo Erba NA1500 Series II elemental analyzer coupled to a DeltaV Plus isotope ratio mass spectrometer (Thermo Scientific) at Memorial University, Newfoundland. The instrument precision (2 standard deviations (SD)) for $\delta^{13}C$ was $<0.5‰$ based on repeated analysis of reference materials (B2150, B2153, and B2155; Elemental Microanalysis, Okehampton, UK) with a mean offset $<0.2‰$ to certified values.

PLFA Extraction

Phospholipids were extracted using a modified Bligh-Dyer extraction followed by the separation of lipid classes with column chromatography using a silica stationary phase and alkaline methanolysis [Frostegård et al., 1993, White and Ringelberg, 1998, Ziegler et al., 2013]. The protocol was modified as followed: (1) We decreased the sample amount. (2) We increased the extraction times and sonicated the samples before each extraction step according to the protocol used by [Cooke et al., 2008]. (3) We applied a modified the solvent mixture to elute phospholipids from silica columns to optimize the recovery of phosphatidylcholine-derived fatty acids [Mills and Goldhaber, 2010].

Samples designated for PLFA analysis were kept on ice in the field and frozen at -18 °C after each fieldwork day. These samples were then freeze-dried and stored in air-tight sealed plastic bags at 5 °C until extraction. Samples from organic horizons (L, F, and H) were homogenized by gentle grinding with a mortar and pestle following careful removal of a few larger particles (twigs and roots $>$ 1 mm diameter). Mineral soils (B horizon) were sieved to 2 mm.

For extraction, 2 g organic soil or 10 g mineral soil were weighed into 50 mL and 32.4 mL of extractant mixture (1:2:0.8 methanol (MeOH) : dichloromethane (DCM) : phosphate buffer (pH 7.4; 40 mmol L^{-1}) were added. Samples were sonicated (1h min), horizontally shaken (200 rpm, 4h), centrifuged (20 min, 4000 rpm), and the supernatent fluid was transferred with a pasteur pipette into a clean 50 mL Kimex tube. Samples were re-extracted twice as described above, but with 16.2 mL extractant mixture and shaken first overnight and then for three hours. The supernatant extracts from the re-extractions were collected in a second 50 mL Kimax tube. The extractant volume in the two Kimax tubes was then evened out, and phase separation was initiated by adding 4mL water and 4mL DCM to each vial. Kimax tubes were then mixed by inverting them several times, and the phases were allowed to separation overnight.

On the next day, the lower, organic phases of the two vial per sample were combined in a fresh, pre-weighed Kimax tube. After weighing, the total extract was aliquoted into 2-4 clean, pre-weighed 18mL Kimax tubes. The weight of each vials was noted and used to calculate the fraction of the extract ultimately analyzed. The solvent was then removed by vacuum centrifugation (Thermo Savant SC250EXP).

For lipid class separation, dry samples were re-dissolved in a total of 8mL DCM and applied to glass SPE columns with 1g DCM rinsed silica (UniSil; Clarkson Chromatography products, South Williamsport, PA, USA). Neutral and glycolipids were removed by rinsing the column with 6 mL DCM and 12 mL acetone. Phospholipids were eluted with 6 mL methanol and then 6 mL of MeOH : DCM : water (3:5:2), and dried by vacuum centrifugation.

For analysis, phospholipid fatty acids were converted to their methyl esters by mild alkaline methanolysis. Samples were re-dissolved in 1mL MeOH:toluene (1:1) and 1mL methanolic KOH (0.2 mol L^{-1}). Both solutions were prepared from MeOH with known $\delta^{13}C$ value. Samples were allowed to react for 15min at 37 °C. After cooling down, samples were neutralized with 1 mL 0.2 mol L^{-1} acetic acid and extracted with 5mL water and 5mL

hexane:dimethylether (9:1). The upper organic phase was transferred to a new, clean tube, and the water phase re-extracted twice in the same way. The combined organic phases were then dried down under a flow of nitrogen gas and transferred with DCM into GC vials pre-loaded with a known amount of arachidonic acid ethylester.

The recovery of PLFA was determined in each extraction batch through duplicate extractions of samples from the F and B horizons with one replicate spiked with 130 µg di-17:0-phosphatidylcholine as described in [Ziegler et al., 2013]. We recovered 73% of this phospholipid with no significant differences between soil horizons or extraction batches. Background concentrations of 17:0 made up 0.6-1.2 mole% of the soil PLFA, and less than 10% of the added recovery standard.

Chromatographic methods

We quantified fatty acid methyl esters (FAMEs) by gas-chromatography/flame ionization detection (GC/FID; Agilent 6890A, Agilent Technologies, Mississauga, ON, Canada) and analyzed selected samples with gas chromatography/mass spectrometry (GC/MS; Agilent 6890N GC with 5975C MS, Agilent Techonogies, Mississauga,, Canada) for peak identification. Compound specific isotope analysis was conducted with gas chromatography/combustion/isotope ratio mass spectrometry (GC/IRMS) at Memorial University, St. John's, Canada. We used an Agilent 6890N gas chromatograph (Agilent Technologies, Mississauga, ON, Canada) coupled to a Thermo Delta V+ isotope ratio mass spectrometer through a GC Combustion III interface (both Thermo Scientific, Waltham, MA, USA). The stability and accuracy of GC/IRMS measurements was monitored by analyzing a reference mixture of 8 fatty acid methyl esters and ethyl esters ('F8'; A. Schimmelmann, Biogeochemical Laboratory, University of Indiana) before and after every 4-5 samples. The average $\delta^{13}C$ values measured were within 0.3‰ of the certified values for all components with a precision (2 SD) of <0.6‰ (n=24).

For GC/FID and GC/MS, FAMEs were separated using a BPX70 column (50m x 0.25mm ID x 0.25 μm film thickness, SGE Analytical Science, Austin, TX, USA). Samples were applied to the column by splitless injection at an oven temperature of 70 °C. After injection the oven temperature was increased at 10 °C min^{-1} to at temperature of 160 °C which was held constant for 5 minutes. The oven temperature was then further increased at 4 °C min^{-1} to the final temperature (260 °C), which was held for 15 min. Injector and FID detector were kept isothermal at 250 and 300 °C. Helium was used as a carrier gas at a flow rate of 1.3 ml min^{-1}. The MS was set to monitor ions with m/z between 50 and 550. For GC/IRMS, the same column type and temperature program described above were applied for GC/IRMS but using a 0.32mm ID column and a carrier gas flow of 1.5 ml min^{-1}. The isotopic signatures of FAMEs were corrected for methanol derived C. The $\delta^{13}C$ of the methanol used for the derivatization of fatty acids was determined with a TOC analyzer (OI Analytical Aurora 1030W) coupled to an isotope ratio mass spectrometer (Finnigan DeltaPlusXP) at G. G. Hatch Stable Isotope Laboratory (University of Ottawa) after diluting 1-2 μL MeOH in 30 mL NanoUV water.

2.6.3 Online Resource 2.3 - List of detected PLFA

Table 2.S3 List of PLFA detected in this study, their molecular weight (MW), assignment to microbial groups, and relative abundance (mol%). For bacterial PLFA we further indicated whether these PLFA are indicative for Gram positive bacteria (G+) or actinobacteria (Act.), or predominantly produced by gram negative bacteria (G-). Please note that the grouping of bacterial PLFA indicates predominant but not exclusive source organisms.

PLFA	MW ($g\ mol^{-1}$)	Group	Relative abundance[1]			
			L	F	H	B
15:0	256.43	Bacteria (G+)	0.86±0.08	1.06±0.09	1.15±0.20	0.69±0.11
i-15:0	256.43	Bacteria (G+)	2.48±0.62	4.64±0.42	5.52±0.58	4.87±0.80
a-15:0	256.43	Bacteria (G+)	1.70±0.45	2.46±0.17	2.53±0.43	2.81±0.47
15:1	254.41	Bacteria (G+)	0.04±0.01	0.11±0.01	0.15±0.05	0.20±0.07
i-16:0	270.45	Bacteria (G+)	1.06±0.42	1.97±0.59	2.06±0.34	2.12±0.39
br-16:0	270.45	Bacteria (G+)	0.01±0.02	0.04±0.03	0.04±0.02	0.18±0.03
17:0	284.48	Bacteria (G+)	0.91±0.11	1.45±1.74	0.61±0.05	0.81±0.09
i-17:0	284.48	Bacteria (G+)	0.32±0.15	0.67±0.15	0.94±0.20	1.62±0.14
br-17:0a	284.48	Bacteria (G+)	0.02±0.01	0.07±0.02	0.08±0.05	0.39±0.17
br-17:0b	284.48	Bacteria (G+)	3.14±0.60	3.29±0.40	2.89±0.44	2.28±0.38
br-17:1	282.47	Bacteria (G+)	0.52±0.15	1.31±0.16	1.51±0.21	2.63±0.38
10Me-16:0	284.48	Bacteria (Act.)	1.27±0.68	3.39±0.48	3.48±0.63	3.28±0.40
10Me-17:0	298.51	Bacteria (Act.)	0.32±0.16	0.49±0.14	0.48±0.13	0.54±0.12
10Me-18:0	312.53	Bacteria (Act.)	0.23±0.11	0.27±0.08	0.53±0.20	1.19±0.35
16:1ω7	268.44	Bacteria (G-)	4.21±0.48	6.26±0.97	6.35±1.06	5.75±0.97
cy17:0	282.47	Bacteria (G-)	1.76±0.38	2.12±0.18	2.20±0.47	3.90±0.91
18:1ω9trans	296.49	Bacteria (G-)	0.15±0.04	0.39±0.05	0.56±0.09	0.92±0.17
18:1ω7	296.49	Bacteria (G-)	5.82±0.73	7.90±1.05	10.26±2.07	18.34±1.79
cy-19:0a	310.52	Bacteria (G-)	0.15±0.05	0.58±0.12	0.67±0.16	0.46±0.11
cy-19:0b	310.52	Bacteria (G-)	3.31±0.76	5.93±1.27	8.76±1.83	14.55±3.65
16:1a[2]	268.44	Bacteria	0.41±0.18	0.87±0.14	1.00±0.24	1.39±0.19
16:1b[2]	268.44	Bacteria	0.25±0.09	0.44±0.06	0.46±0.10	0.89±0.14
16:1c[2]	268.44	Bacteria	1.34±0.32	2.25±0.33	2.54±0.53	3.27±0.59
18:1ω5	296.49	Bacteria	0.83±0.10	1.53±0.17	1.87±0.28	2.07±1.66
18:2ω6	294.48	Fungi	21.57±3.38	11.18±1.48	7.37±1.53	1.93±0.34
18:3ω3	292.46	Fungi	4.30±1.49	1.02±0.26	0.69±0.14	0.15±0.07
18:2a	294.48	Fungi	0.28±0.07	0.67±0.12	0.68±0.23	0.52±0.19
18:2b	294.48	Eukaryote	0.13±0.09	0.23±0.14	0.19±0.14	0.19±0.06
18:3ω6	292.46	Eukaryote	0.47±0.07	0.90±0.23	0.69±0.19	0.09±0.05
20:2	322.53	Eukaryote	0.23±0.07	0.17±0.04	0.10±0.05	0.04±0.04
20:3a	320.51	Eukaryote	0.41±0.04	0.71±0.13	0.63±0.18	0.12±0.06
20:3b	320.51	Eukaryote	0.23±0.06	0.13±0.03	0.07±0.04	0.04±0.03
20:4ω6	318.50	Eukaryote	1.58±1.26	0.69±0.11	0.48±0.05	0.19±0.04
20:5ω3	316.48	Eukaryote	0.58±0.34	0.24±0.07	0.14±0.03	0.05±0.03
22:6ω3	342.52	Eukaryote	0.11±0.03	0.07±0.03	0.06±0.03	0.01±0.01
14:0	242.40	General	0.96±0.20	0.93±0.16	0.93±0.19	0.52±0.14
16:0	270.45	General	17.88±1.54	13.85±1.52	12.04±1.09	9.75±0.84
18:0	298.51	General	3.32±0.56	2.21±0.58	1.66±0.86	1.91±0.86
18:1ω9cis	296.49	General	12.28±1.51	11.40±1.13	11.74±1.17	5.87±0.54
20:0	326.56	Unknown	0.99±0.29	1.23±0.44	1.41±0.39	0.64±0.17
21:0	340.59	Unknown	0.16±0.03	0.19±0.02	0.21±0.04	0.10±0.02
22:0	354.62	Unknown	1.68±0.59	2.35±1.28	2.11±0.53	0.76±0.17
23:0	368.64	Unknown	0.27±0.04	0.31±0.04	0.30±0.01	0.18±0.06
24:0	382.67	Unknown	1.35±0.37	1.91±0.85	1.74±0.31	1.72±0.32
25:0	396.70	Unknown	0.12±0.03	0.11±0.02	0.10±0.01	0.06±0.02
		Sum G+ bacteria	11.06±2.61	17.08±3.79	17.50±2.57	18.59±3.04
		Sum Actinobacteria	1.82±0.94	4.16±0.71	4.50±0.96	5.01±0.87
		Sum G- bacteria	15.40±2.45	23.19±3.65	28.80±5.68	43.92±7.60
		Sum (all bacteria)	31.12±6.69	49.51±8.84	56.66±10.36	75.15±14.10
		Sum Fungi	25.87±4.88	12.19±1.75	8.06±1.67	2.08±0.40
		Sum other Eukaryote	4.02±2.03	3.81±0.89	3.03±0.95	1.26±0.51
		Fungi:Bacteria	0.864±0.243	0.248±0.041	0.144±0.037	0.027±0.005
		Fungi:(Fungi+Bacteria)	0.455±0.080	0.198±0.027	0.125±0.028	0.027±0.005

1 Presented as means per soil horizon with errors indicating one standard deviation of the mean.

2 The unsaturation location was not verified via known standard for these three fatty acids. They are, however, likely to be 16:1ω11, 16:1ω9, and 16:1ω5, respectively, given their retention times.

2.6.4 Online Resource 2.4 - Total, fungal, and bacterial PLFA concentration

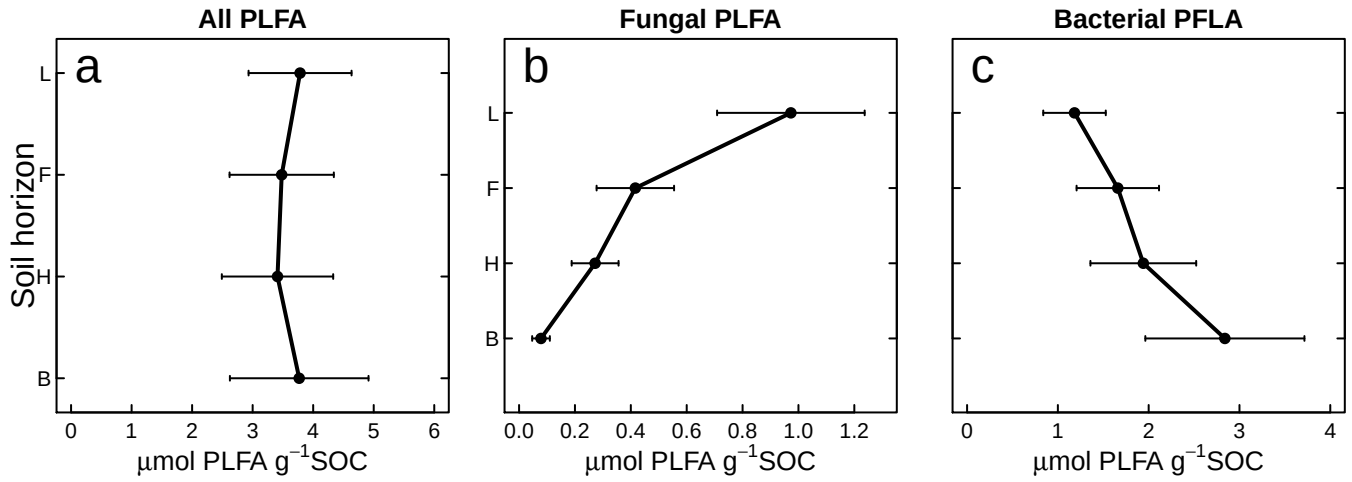

Figure 2.S4 Concentrations of total PLFA (a), fungal PLFA (b), and bacterial PLFA (c) in the soil profiles. Error bars indicate standard deviations of the means.

2.6.5 Online Resource 2.5 - Microbial community structure

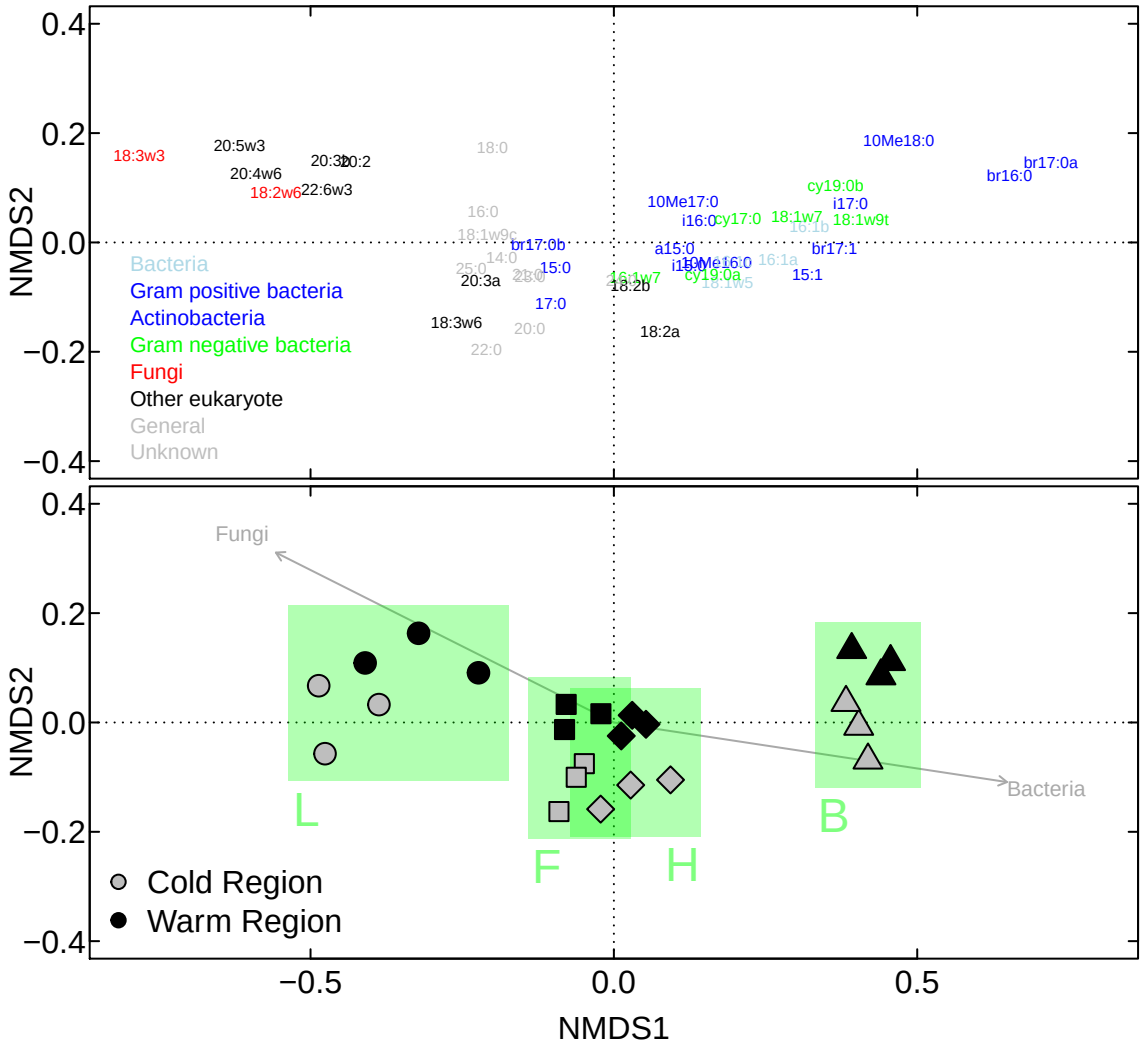

Figure 2.S5 Non-metric multidimensional scaling (NMDS) based on the relative abundance (mol%) of 45 individual PLFA. PFLA factor loadings are presented in the top panel and the PLFA composition of the individual samples is shown in the bottom plot.

2.6.6 Online Resource 2.6 - Relationship between $\delta^{13}C_{PLFA}$ and $\delta^{13}C_{SOC}$ for each individual PLFA.

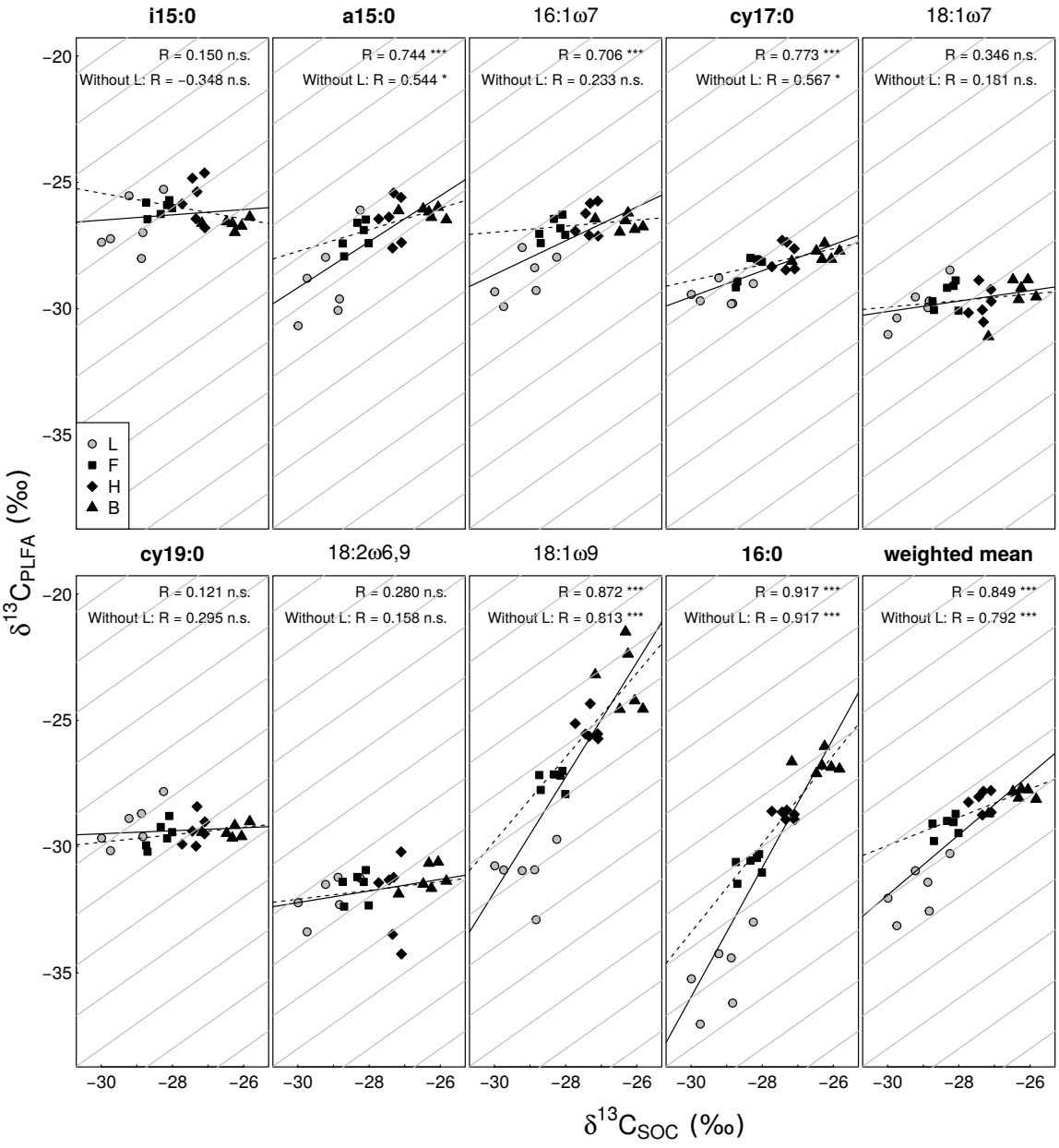

Online Resource 2.S6 Relationship between $\delta^{13}C_{PLFA}$ and $\delta^{13}C_{SOC}$ for each individual PLFA. Solid black lines represent linear regressions for which correlation coefficients (R) and significance levels (*, $p<0.05$; **, $p<0.01$, *, $p<0.001$; n.s., $p>0.05$) are provided in the top right corners. Dashed black lines represent regressions after removing L horizon samples, which often were relatively depleted and drove regressions. Grey lines represent a slope of 1.

2.6.7 Online Resource 2.7 - $\delta^{13}C_{PLFA}$ profiles in the six studied sites.

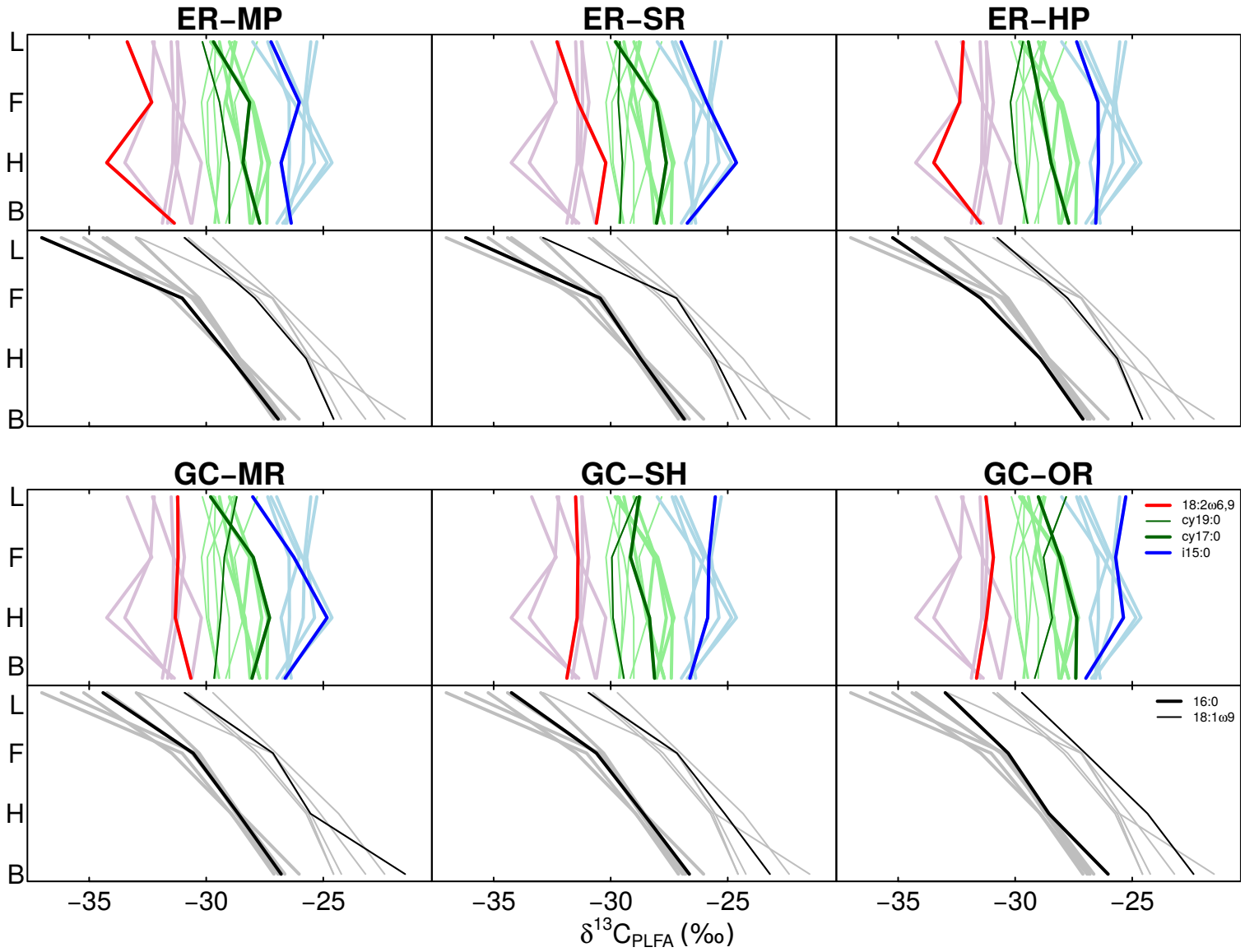

Online Resource 2.S7 $\delta^{13}C_{PLFA}$ profiles in the six studied sites. Profiles for each site are presented with the profiles from the other sites plotted in the background. The main trend - $\delta^{13}C$ values of sepecific PLFA exhibited little variation with depth while $\delta^{13}C$ values of general PLFA strongly increased with depth - was found in each of the soil profiles studied.

Chapter 3

Soil organic matter chemistry and bioreactivity are attributed to inputs not diagenesis across a boreal forest latitudinal gradient

Lukas Kohl[1], Michael Philben[1], Kate A. Edwards[2], Frances A. Podrebarac[1], Jamie Warren[1], Susan E. Ziegler[1]

[1]Department of Earth Sciences, Memorial University, St. John's, NL A1B 3X5, Canada

[2]Natural Resources Canada, Canadian Forest Service, Atlantic Forestry Centre, 26 University Drive, Corner Brook, A2H 6J3, NL, Canada

A revised version of this chapter is currently under review for publication in Global Change Biology. Supporting Information 3.1 to 3.7 is provided is provided on pages 88 to 100. Raw data for Figs. 3.2 and 3.3 is provided on pages 102 - 104.

Abstract

The chemical composition of soil organic matter (SOM) is an important factor affecting the turnover and fate of SOM. Soil warming experiments and cross site studies both indicate that climate influences SOM composition, but disagree in whether this effect is mediated through climate affecting plant inputs or the transformation of SOM over time (diagenesis). Here, we characterized the chemical composition of trapped plant litter and SOM across a boreal forest latitudinal transect in Atlantic Canada. In this transect, SOM in soils that developed under a warmer climate exhibits lower decomposition rates at a given temperature (bioreactivity) than SOM from cooler-climate soils. We investigated whether this difference in bioreactivity resulted from climate affecting SOM chemistry through its influence on plant litter inputs, on the diagenesis of SOM, or both. Elemental, isotopic, nuclear magnetic resonance, and total amino acid analysis of the organic soil horizons (L, F, H) across forest sites within each of three climate regions indicated that (1) climate history and decomposition affect distinct parameters of SOM chemistry, (2) regional differences in SOM bioreactivity were associated with proportions of carbohydrates, plant waxes and lignin, and (3) regional differences in SOM chemistry were associated with chemically distinct litter inputs and not derived from different levels of diagenesis. Climate effects on the composition of vascular plant litter chemistry, however, explained only part the regional differences in SOM chemistry, most notably the higher protein content of SOM from more southern regions. Instead, greater proportions of lignin and aliphatic compounds and smaller proportions of carbohydrates at more southern sites were explained by a mixing model that accounted for the higher proportion of moss litter in more northern regions. These results indicate that climate induced changes in moss inputs can be a significant control on SOM cycling boreal forest soils.

3.1 Introduction

Soils organic matter (SOM) is the largest pool of reduced carbon in terrestrial ecosystems [Jobbágy and Jackson, 2000]. The chemical, physical, and biological properties of SOM (SOM quality) are tightly connected to past and future climate. SOM quality controls the rate at which CO_2 is released from soils via soil respiration [Waksman and Gerretsen, 1931, Sollins et al., 1996, Leifeld and Fuhrer, 2005], thus affecting the global carbon cycle and climate feedbacks. Conversely, SOM quality itself is determined by the conditions, including climate, under which a given soil has developed [Zech et al., 1989, Franzluebbers et al., 2001, Pisani et al., 2014] and will undoubtedly respond to future climate. Understanding how climate affected SOM properties in the past can, therefore, help us predict if soils will act as a source or sink for CO_2 in a warmer future.

Climate affects SOM quality through two major processes. First, climate is a major determinant of the vegetation cover overlying a soil, including species composition and plant physiology. Changes in climate therefore lead to changes in the quantity and composition of plant litter inputs to soils. This, in turn, can explain the differences in SOM chemistry observed in soils that developed under different climate regimes found in cross-site studies. The differences in SOM chemistry observed along an elevation gradient, for example, were also found when plant communities typical of the different altitude zones planted in close proximity (i.e., exposed to the same climate) [Quideau et al., 2001]. Furthermore, SOM bioreactivity, defined as the rate at which SOM carbon is mineralized when incubated at a given temperature, varied more strongly with forest type than with climate [Fissore et al., 2008, Laganière et al., 2013].

It remains unclear to which extent climate affects SOM properties through its effect on litter inputs in the absence of a change of the dominant species. Such changes could occur if climate affects either the litter chemistry of the dominant species, or the abundance or

composition of litter produced by the understory vegetation. In boreal forests the proportions of moss and vascular plant litter will likely change with climate. Vascular plant net primary production (NPP) in boreal forests decreases with latitude and increases with temperature [Gower et al., 2001]. Moss NPP, in contrast, is similar in boreal and artic ecosystems and decreases towards the southern extreme of the boreal zone due to greater canopy shading [Turetsky, 2003]. Climate change will thus lead to greater litter inputs from vascular plant and equal or lesser inputs from mosses. As nonvascular plants, mosses exhibit a distinctly different chemical composition than vascular plants, including coniferous trees, in boreal forests [Hobbie, 1996, Philben et al., 2014, Butler et al., in preparation]. Changes in the proportion of moss and vascular plant litter inputs may represent a key factor regulating climate effects on SOM chemistry in boreal forests even when dominant vegetation, defined by tree species, remains the same.

Second, differences in SOM quality of soils that formed under distinct climate regimes may also originate from differences in the degree of diagenetic alteration, i.e., the change of SOM chemistry over time by both biological decomposition and physiochemical processes including leaching and aggregation. Soil warming experiments, which manipulate only the below-ground component of an ecosystem, have demonstrated that the physiochemical and biological properties of SOM are altered with warming. Soil respiration rates can decrease, for example, after multiple years of warming [Melillo et al., 2002], indicating that the acclimation of SOM to a warmer temperature causes a decrease in soil bioreactivity. This decrease in bioreactivity was accompanied by a change in the chemical composition of SOM [Feng et al., 2008, Pisani et al., 2015], most notably increased concentrations of cutin derived compounds, and lower concentrations of lignin and carbohydrates [Feng et al., 2008]. In other ecosystems, however, *in situ* experimental warming caused an increase in soil respiration without reducing SOM bioreactivity possibly attributed to shifts in microbial substrate use [Streit et al., 2014], and some soil warming experiments did not detected a change in SOM chemistry [Schnecker

et al., 2016].

These two processes, different inputs and degrees of diagenesis, provide mechanisms for how climate affects SOM chemistry and thus SOM bioreactivity. In the first case, changes in climate prompt changes in vegetation that alter the chemical nature of inputs to the soil. In the latter case, climate changes predominantly affect belowground processes and, therefore, how SOM chemistry changes over time. The relative role of these two mechanisms in controlling SOM chemistry remains unclear. This is especially true for moderate warming scenarios leads to changes in plant productivity and physiology; and potentially in under-story species composition, but do not lead to a change in the dominant species. This uncertainty in the origin of the chemical changes in SOM, therefore, makes it difficult to interpret SOM chemistry for the purposes of assessing the impact of future climate warming.

Climate transects allow us to trade time for space. By comparing similar sites along natural climate gradients we can study how past climate shaped ecosystem properties like the quantity and chemical composition of SOM stocks, and how these properties might change under a different climate in the future. In boreal forest regions such studies have highlighted the role of climate in controlling SOM properties [Vucetich et al., 2000, Santruckova et al., 2003, Sjögersten et al., 2003, Kane et al., 2005, Meyer et al., 2006, Preston et al., 2006, Cannone et al., 2008, Norris et al., 2011], but it remains unclear if this is due to effects of temperature and moisture on vegetation or on diagenesis. In continental transects, where greater temperature is associated with stronger moisture limitation, significant changes in SOM properties (e.g. C:N, NMR, tannins) are more attributable to how site condition control rates of decomposition, and less on the differences in the chemical nature of the inputs [Preston et al., 2006, Norris et al., 2011]. However, across boreal forest ecosystems moisture and other climate variables also control moss biomass [Vitt, 1990] and therefore the moss' contribution to soil inputs. The fact that (1) moisture regime can impact both the source of SOM and its mineralization and (2) shifts in the source of SOM can include changes in

the proportion of vascular versus nonvascular plants make it particularly difficult to identify the controls over SOM chemistry in boreal forest ecosystems. The mesic boreal forests of Atlantic Canada feature a latitudinal climate gradient in which mean annual temperature (MAT) and precipitation (MAP) decrease with latitude. As greater precipitation compensates for the increased evapotranspiration, these forests are therefore characterized by similar moisture across a temperature gradient, which allowed us to explore the effects of increasing temperature in the absence of greater water limitation predicted for this region [van Oldenborgh et al., 2013]. By studying the chemistry of SOM in these forests we investigated the proportional role of changes in diagenesis and vegetation in response to climate warming in the absence of changes in the moisture regime.

The goal of this study was to determine to what extent variations in SOM chemistry along a climate transect of mesic boreal forest sites originated (1) from different litter input types and quantities or (2) from differences in the quantity and quality of chemical alteration during its residence under distinct climate regimes (diagenesis). Previous work in this transect has shown that the bioreactivity of SOM decreases with greater depth and climate warming along this transect [Laganière et al., 2015, ; Supporting Information 3.1]. Here, we explore how the chemical composition of SOM varies along gradients of climate (latitude) and increasing diagenetic alteration (soil depth). We exploited the 'decomposition continuum', often noted in the study of soil profiles [Melillo et al., 1989], as a gradient of increasing diagenesis to determine how SOM chemistry changes due to diagenesis in these forests. We then used this forest site-specific understanding of diagenetic indicators to assess drivers of regional variations in SOM chemistry. If regional differences in SOM chemistry resulted from different litter inputs, the diagenesis (D) and latitude (L) effects, those observed by depth and region respectively, would affect distinct parameter of SOM chemistry (Fig 3.1a, 3.1b). A parameter that is controlled by input type, for example, could exhibit a decreasing trend with depth, signifying how it behaves with increased diagenesis, but no change with latitude, signifying

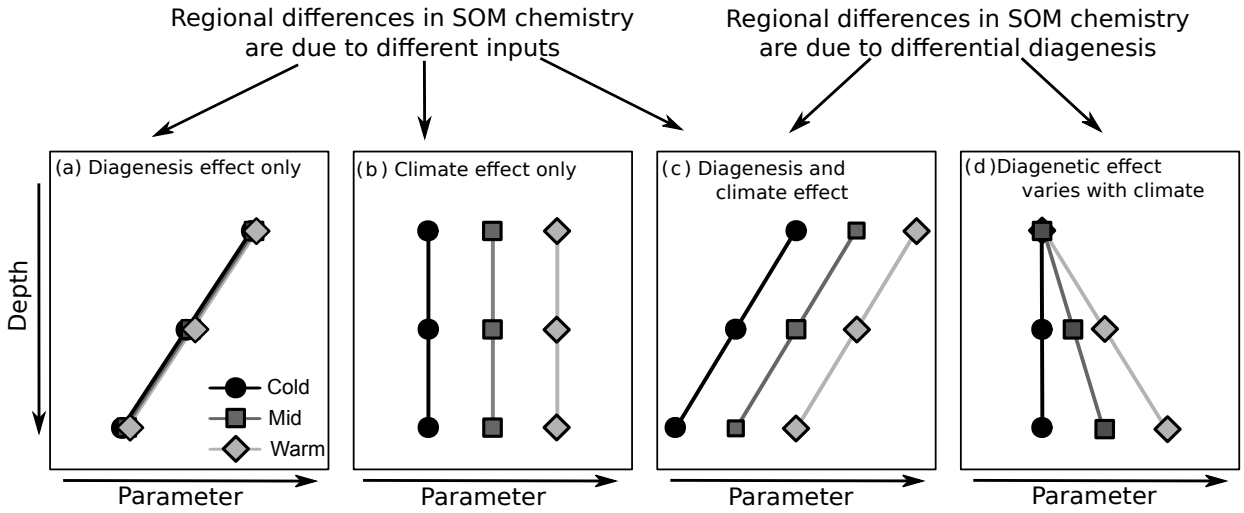

Figure 3.1 Conceptional figure how parameters of SOM chemistry would vary with depth and latitude if regional differences in SOM chemistry were driven by different inputs (a-c) or different diagenesis (c-d).If regional differences result from different inputs, we expect some parameters to be affected by diagenesis, but not latitude, and thus to vary with depth only (a), while other parameters would be affected by inputs and thus vary with latitude only (b). Both scenarios allow for parameters that are affected by both depth and latitude (c). Differences acquired during diagenesis would be indicated by regional differences increasing with exposure time (and thus with depth), as indicated by an effect of depth and latitude (d).

that it is not impacted of changing input type or quantity across climate regions (Fig. 3.1a). Alternatively, a parameter may not change with depth and only change with region due to effects of different inputs by climate region (Fig. 3.1b), or could exhibit added effects on the same parameter where inputs fix initial difference noted throughout the profile that changes with depth due to diagenesis (Fig. 3.1c). In contrast, if regional differences are acquired via climate driven differences in diagenesis, we would expect that region and depth would affect the same parameters (Fig 3.1c), and that differences between regions would increase with depth (Fig 3.1d). Using this approach, we report three key findings, (1) regional differences in SOM chemistry are largely driven by inputs, not diagenesis in these forests; (2) these regional differences are consistent with differences in SOM bioreactivity across climate regions; and (3) these differences likely result from different proportions of moss relative to conifer needle litter inputs to soils.

3.2 Material and Methods

3.2.1 Field sites

The Newfoundland and Labrador Boreal Ecosystem Latitudinal Transect (NL-BELT) is a boreal climate transect located in Atlantic Canada. We studied nine field sites (Table 3.1) of mesic boreal forests which were located in three watersheds ('regions'). More southern regions are characterized by higher MAT (5.2 C) and MAP (1570 mm a^{-1}) than more northern regions (0.0 C MAT, 1040 m a^{-1} MAP), resulting in similar soil moisture conditions across the transect [Ziegler et al., 2017]. More southern sites exhibited more narrow C:N ratios in needle foliage, plant litter, and soils indicating that accelerated nitrogen cycling in more southern regions [Philben et al., 2016] has led to greater availability of N in all components of the ecosystem. These trends are consistent with the anthropogenic changes that are predicted to occur in this ecosystem over the next decades, i.e., higher temperatures, precipitation, and allochthonous nitrogen inputs [Gruber and Galloway, 2008, Price et al., 2013, van Oldenborgh et al., 2013]. The three field sites in each region were selected for their similar forest type and successional stage (mature *Abies balsamea* stands), soil properties (well-drained podzols), and disturbance regime (insect outbreak). The transect thus represents incarnations of *Abies balsamea* dominated forests that developed under different climate regimes, where understory vegetation developed in accordance with the local climate. This transect thus also represent a climate change scenario for a managed forest, where the dominant species is determined by afforestation, but the forest is left to develop in response to the local climate conditions in all other regards.

3.2.2 Field sampling

At each field site, we collected samples from three replicate plots (10 m diameter) as described previously [Laganière et al., 2015, Ziegler et al., 2017]. Soil samples for chemical analyses

Table 3.1 Location and characteristics of field sites studied herein. Table updated from Ziegler et al. [Chapter 2 and 2017]

Region	Site	Latitude	Longitude	Elevation (m)	MAT[1] (C)	MAP[1] (mm a^{-1})	PET[1] (mm a^{-1})	Tree species	Litterfall (g m^{-2} yr^{-1})	Basal area (m^2 ha^{-1})	SOM in LFH (kg SOM-C m^{-2})	Soil type
Eagle	Muddy Pond	53°33'01"N	56°59'13"W	145	0.0	1074	432	Abies balsamea	126	37.2	2.43	Humo-ferric podzol
River	Sheppar's Ridge	53°03'25"N	56°56'02"W	170	0.0	1074	432	Abies balsamea	228	50.1	2.16	Humo-ferric podzol
(Cold)	Harry's Pond	53°35'12"N	56°53'21"W	136	0.0	1074	432	Abies balsamea	115	38.2	1.95	Humo-ferric podzol
Salmon	Hare Bay (HB)	51°15'21"N	56°8'18"W	31	2.0	1224	489	Abies balsamea	469	63.2	3.13	Humo-ferric podzol
River	Tuckamore (TM)	51°9'51"N	56°0'15"W	16	2.0	1224	489	Abies balsamea	321	39.2	3.15	Humo-ferric podzol
(Mid)	Catch-A-Feeder (CF)	51°5'21"N	56°12'16"W	38	2.0	1224	489	Abies balsamea	1942[2]	34.0	2.51	Humo-ferric podzol
Grand	Slug Hill	48°00'39"N	58°54'16"W	215	5.2	1505	608	Abies balsamea	589	48.4	2.88	Humo-ferric podzol
Codroy	Maple Ridge	48°00'28"N	58°55'14"W	165	5.2	1505	608	Abies balsamea	373	44.7	3.23	Humo-ferric podzol
(Warm)	O'Reagan's	47°53'36"N	59°10'28"W	100	5.2	1505	608	Abies balsamea	344	50.1	2.91	Humo-ferric podzol

[1] MAT; mean annual temperature; MAP, mean annual precipitation; PET, mean annual potential evapotranspiration. Meteorological data represent climate normals of 1981-2010 from Cartwright, NL, [Site for SR], NL, and Doyles, NL weather station and was taken from Environment Canada [2014]. Potential evaporation was calculated according to Xu and Singh [2001] based on monthly temperature and precipitation normals.

[2] Field site affected by windfall.

were collected in June 2011 as described in detail by Laganière and others Laganière et al. [2015]. Briefly, at three random locations in each plot all living biomass including green mosses was removed and a 20x20 cm rectangle was cut out of the organic horizons. These samples were then manually separated into the L, F, and H soil horizons (Oe, Oa, and Oi horizons in the US soil nomenclature) and pooled into one composite sample per soil horizon and plot. This sampling resulted in a set of 81 samples (27 plots x 3 soil horizons) which were further pooled into 27 samples (9 sites x 3 horizons) for some analyses.

Subsamples of the L horizon material were manually separated into foliar litter, woody material (including cones), and mosses. The dry mass of each such fraction was measured or estimated when the separation of compacted material was not possible, and is reported as rounded to the closest 5%, as present in traces (assigned 1%), or as absent (0%). Foliar, woody, and moss litter were then re-combined and all samples were then homogenized for chemical analysis using a Siebtechnik rock pulverizer. Litter trap samples were collected between June 2011 and June 2013 as described in [Ziegler et al., 2017]. Briefly, 3 litter traps with an area of 0.34 m2 were installed at each plot. The trapped material was collected at least three times per year and sorted into different types of material (green needles, brown needles, deciduous leaves, twigs, cones). Each fraction was dried and weighed separately. Chemical analysis was conducted on pooled samples representing the annual litter-fall input at each field site.

3.2.3 Chemical analysis

3.2.3.1 Soil organic matter

Elemental contents of carbon and nitrogen (%C, %N, C:N) and their stable isotope ratios (δ^{13}C, δ^{15}N) were analyzed for each plot and soil horizon (n=81) as described in Chapter 2. The C:N ratio was calculated as the molar ratio of C and N contents. For better comparison with %N, the inverted C to N ratios (N:C) are depicted in Fig. 3.3. Solid state nuclear

magnetic resonance (CP-MAS NMR) spectra were measured for samples of L, F, or H horizon material pooled for each site (n=27). Samples were analyzed using a Bruker AVANCE II 600 MHz with a MASHCCND probe. All samples were run at 600.33 MHz (1H) or 150.96 MHz (^{13}C) and spun at 20 kHz at 298 K. Spectra were deconvoluted using the software 'DM Fit' based on a 19 component model. These peak were then assigned to 7 functional groups (alkyl-C, methoxy-C, N-alkyl-C, O-alkyl-C, Di-O-alkyl-C, aromatic C, carbonyl-C) based on Wilson [1987] and Preston et al. [2009], and expressed as percent of the total area of all components. We furthermore calculated the alkyl:O-alkyl ratio, an indicator that typically increases with greater diagenesis, as alkyl-C/(O-alkyl-C + di-O-alkyl-C + methoxy-C) [Preston et al., 2009]. Spectra are provided in Supporting Information 3.2.

Concentrations and composition of total hydrolysable amino acids (THAA) were retrieved from Philben et al. [2016]. The analysis was conducted in samples of L, F, or H horizon material pooled for each site (n=27). We included four parameters describing the abundance and composition of THAA, i.e., the proportions of organic carbon and nitrogen present in the form of THAA (%C as THAA, %N as THAA); the degradation index (DI) which represents the first dimension of a principal component analysis of the composition of THAA; and the relative abundance of glycine among THAA (mol% gly). Hydrolysable amino acids accounted for >40% of N in these soil horizons [Philben et al., 2016]. The abundance and composition of THAAs, therefore, provide a means to study the chemistry of organic N in these soils and a proxy for the origin and past processing of organic matter in general [Hedges et al., 1994, Shen et al., 2014, Philben et al., 2016].

3.2.3.2 Litterfall

Litter samples were analyzed with the same methods as SOM (EA/IRMS, THAA, CP-MAS-NMR). With all three methods, pooled samples representing the annual litterfall of each plot were analyzed. For EA/IRMS, fractions of the litterfall (i.e., green needles, brown

needles, deciduous litter, twigs, bark, and cones) were analyzed separately at the plot level as described by Podrebarac et al. [in preparation]. For CP-MAS NMR, a pooled sample representing the annual weighted input of the different types of foliar litterfall (green needles, brown needles, deciduous litter) inputs of each site was analyzed. For THAA, a pooled sample representing the total litterfall, including both foliar and woody litter, was analyzed for each site.

Litter traps do not collect of moss litter inputs to soils. We therefore estimated the chemical composition of the total above-ground litter including both moss and vascular plant detritus based on the composition of the L-horizon material. We calculated this based on the measured composition of foliar litter for each site, measurements of mosses collected in two regions of the transect, and literature values for woody material (Supporting information 3.3).

3.2.4 Bioreactivity of intact LFH profiles

To test if the parameters of SOM chemistry that varied by region can predict the bioreactivity of field soils, we assessed if these parameters could explain the respiration rates of intact cores of the organic soil (i.e., the unseparated L, F, and H horizons) measured in a separate incubation experiment [Podrebarac et al., 2016]. Since these soil cores comprise the entire organic soil layer, we would expect respiration rates to depend on SOM properties with climate history (latitude) whereas we excluded SOM properties that change during diagenesis (i.e., vary with depth). We updated the dataset retrieved from Podrebarac and others [Podrebarac et al., 2016] to include results from the mid latitude region of the climate transect (SR). The complete dataset comprised of the cumulative respiration of 81 soil cores from 27 sites, incubated for 467 days at 5 °C, 10 °C, or 15 °C and 60% water holding capacity, is provided in Supporting Information 3.4.

3.2.5 Data Analysis

3.2.5.1 Climate and diagenesis effects on SOM chemistry

To characterize the nature of regional differences in SOM chemistry and distinguish between differences that originate from dissimilar inputs and differences that originate in differential diagenetic alteration, we conducted a comparative analysis of the individual parameters of SOM chemistry. First, we applied a two-way analysis of variance (ANOVA) to determine if the parameter differed among soil horizons or regions. We then tested if the differences between regions and/or soil horizons detected by ANOVA represented a consistent increase or decrease with depth or latitude (as opposed to merely random differences between regions and/or soil horizons) by calculating the Spearman's correlation coefficient (Spearman's ρ) of each parameter with both soil horizon and region. A ρ-value close to 0 indicates that the parameter varies independently of depth or latitude, whereas a ρ-value close to -1 or +1 indicates that the parameter exhibited a monotonic increase or decrease with depth or latitude. For both ANOVA and Spearman correlation tests, we report the test metric (% variance explained and ρ-values, respectively) regardless of statistical significance to allow for a comparison of region/depth effects on both affected and unaffected parameters.

To test if the proportions of moss, foliar litter, and woody material in the L layer varied among regions, we used the non-parametric Kruskal-Wallis test followed by a Nemenyi post-hoc test as normality and heteroscedasticity could not be assumed.

3.2.5.2 Relation between SOM bioreactivity and SOM chemistry

We conducted a correlative analysis to evaluate if the regional variations in SOM chemistry among field sites could explain the observed differences in bioreactivity. We included six parameters of SOM chemistry that varied with latitude (%methoxy-C, %O-alkyl-C, %Di-O-alkyl-C, %alkyl-C, %N, %C as THAA) in this analysis. Two other parameters that varied

with latitude were excluded because they did not represent a chemical property that directly affects bioreactivity (δ^{15}N) or were redundant with %N (C:N). For each parameter, we combined the values measured in the individual soil horizons by calculating a weighted average value for the entire organic layer of each site site as described in Supporting Information 3.5. A multiple regression analysis to distinguish which of these six parameters had the strongest effect on bioreactivity was not possible because the six parameters were inter-correlated (Supporting Information 3.6). We therefore used the first principal component of the six parameters ('PCA1'), representing 84% of their total variance, as a predictor to evaluate their combined effect on bioreactivity, and calculating the regressions between cumulative respiration (log transformed) and PCA1 for each incubation temperature. We furthermore calculated the fraction of site level variance in cumulative respiration in the complete dataset (all temperature treatments) explained by each of the six parameters as well as by PCA1 (Supporting Information 3.7). All statistical analysis was conducted using statistical programming environment R version [R Development Core Team, 2015].

3.3 Results

3.3.1 Chemical composition and bioreactivity of isolated soil horizons

The analyzed parameters of SOM chemistry exhibited distinct trends with depth and latitude. Soil carbon contents (%C) decreased with depth and slightly decreased with latitude (Fig. 3.2a), whereas δ^{13}C values increased with depth but was unaffected by latitude (Fig 3.2b). In contrast, soil nitrogen content and δ^{15}N values increased with depth but also decreased with latitude (Figs. 3.2c,3.2d). Three of the functional groups identified via NMR were affected by latitude, not depth; %methoxy-C decreased with latitude whereas %O-alkyl-C and %di-O-alkyl-C increased with latitude, indicative of lower lignin:carbohydrate ratios in more northern regions (3.2e,3.2f,3.2g). Three other functional groups were affected

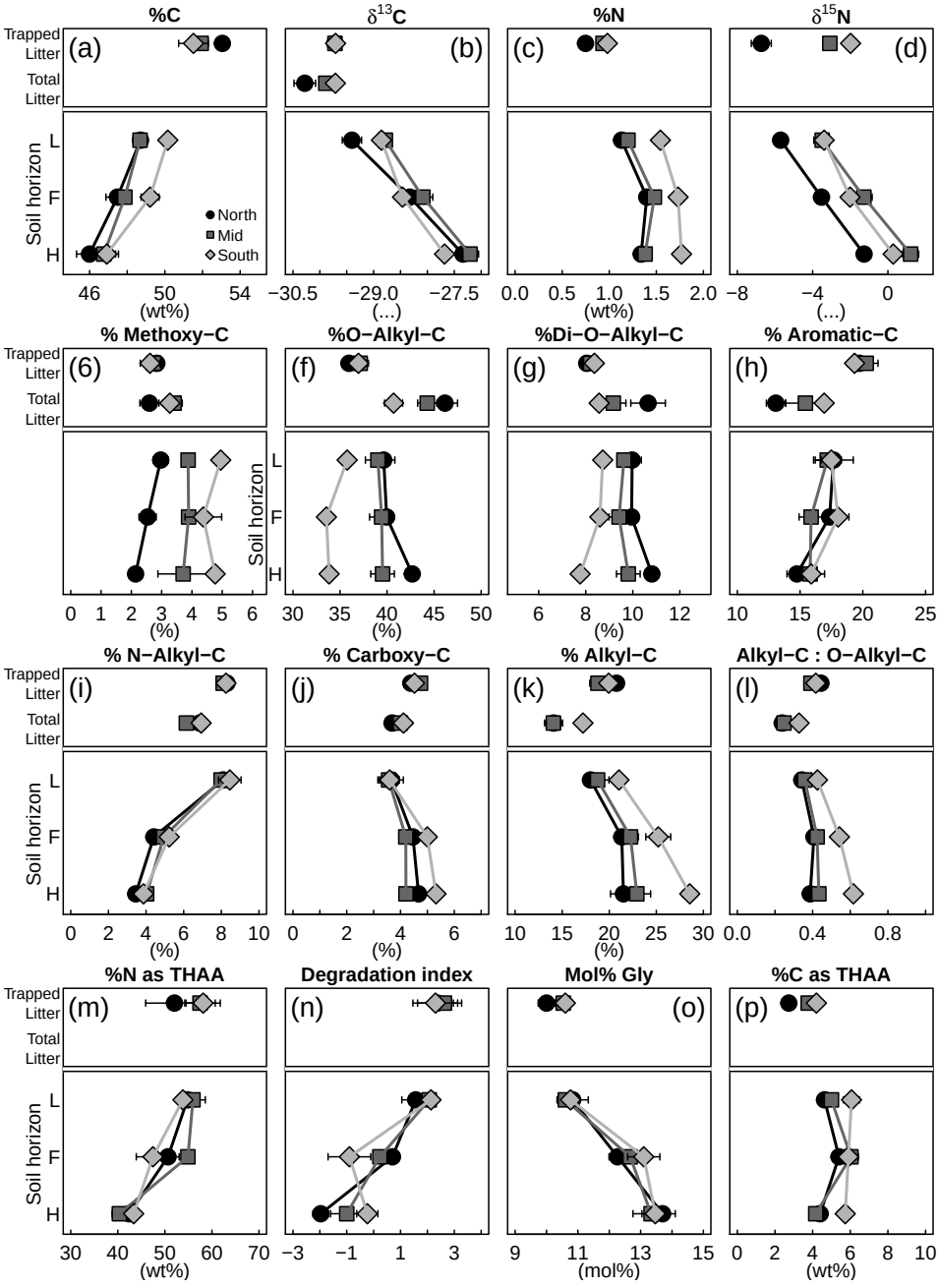

Figure 3.2 Depth profiles of parameters of SOM chemistry covered in this paper. (a-d) elemental concentrations and stable isotope values of carbon and nitrogen; (e-l) abundance of functional groups in CP-MAS NMR spectra; (m-p) parameters describing the concentration and composition of total hydrolyzeable amino acis (THAA; data from Philben and others (2016)). Colors indicate field regions: black, northernmost region, dark grey, mid region, light grey, southernmost region. Trapped litter, measured litter samples collected in traps. Total litter, estimate for all inputs to SOM chemistry taking into account foliar litter, woody litter, and moss litter (see Supporting Information 3). L,F,H, organic soil horizons.

by depth, but not latitude; %aromatic-C and %N-alkyl-C decreased with depth, whereas %carbonyl-C increased with depth (Figs. 3.2h,3.2i,3.2j). The %alkyl-C and alkyl:O-alkyl were affected by both latitude and depth with greater values detected in more southern regions and in deeper soil horizons (Figs. 3.2k,3.2l). The %N as THAA, DI and decreased with depth but did not differ between regions (Figs. 3.2m,3.2n). Mol% gly increased with depth but did not differ among regions (Fig. 3.2o), whereas %C as AA decreased with latitude, but did not change with depth (Fig. 3.2p).

3.3.2 Categorization of parameters of SOM chemistry by variance with depth and latitude

The parameters included in this study fell into three groups with regard to how the variance was explained by latitude and depth (Fig 3.3a) enabling our investigation of the potential source of each as described in Fig. 3.1. Variables that differ by soil horizon and/or regions typically exhibited a monotonous increase or decrease with depth and/or latitude as indicated by significant Spearman correlations (Figs. 3.3b,3.3c).

The %N as THAA and THAA composition (DI and mol% gly), %carbonyl-C and %N-alkyl-C, and $\delta^{13}C$ were all explained by depth alone. Three parameters exhibited a monotonous increase with depth (%carbonylC, $\delta^{13}C$, and mol% gly; Fig 3.3b) and three a monotonous decrease (DI, %N as THAA, %amino-C; Fig 3.3b), but none of these parameters increased or decreased with latitude (Fig 3.3c). In contrast, 3 NMR parameters representing the relative carbohydrate and lignin concentrations (%O-alkyl-C, %Di-O-alkyl-C, %methoxy-C) were explained by region alone (Fig 3.3a). None of these parameters exhibited a monotonous increase or decrease with depth (Fig 3.3b), but %O-alkyl-C and %di-O-alkyl-C increased with latitude, whereas %methoxy decreased with latitude (Fig 3.3c).

The variances of %C, %N, $\delta^{15}N$, C:N (plotted as N:C for better comparability with %N), %C as THAA, and alkyl:O-alkyl were explained by both latitude and depth, but

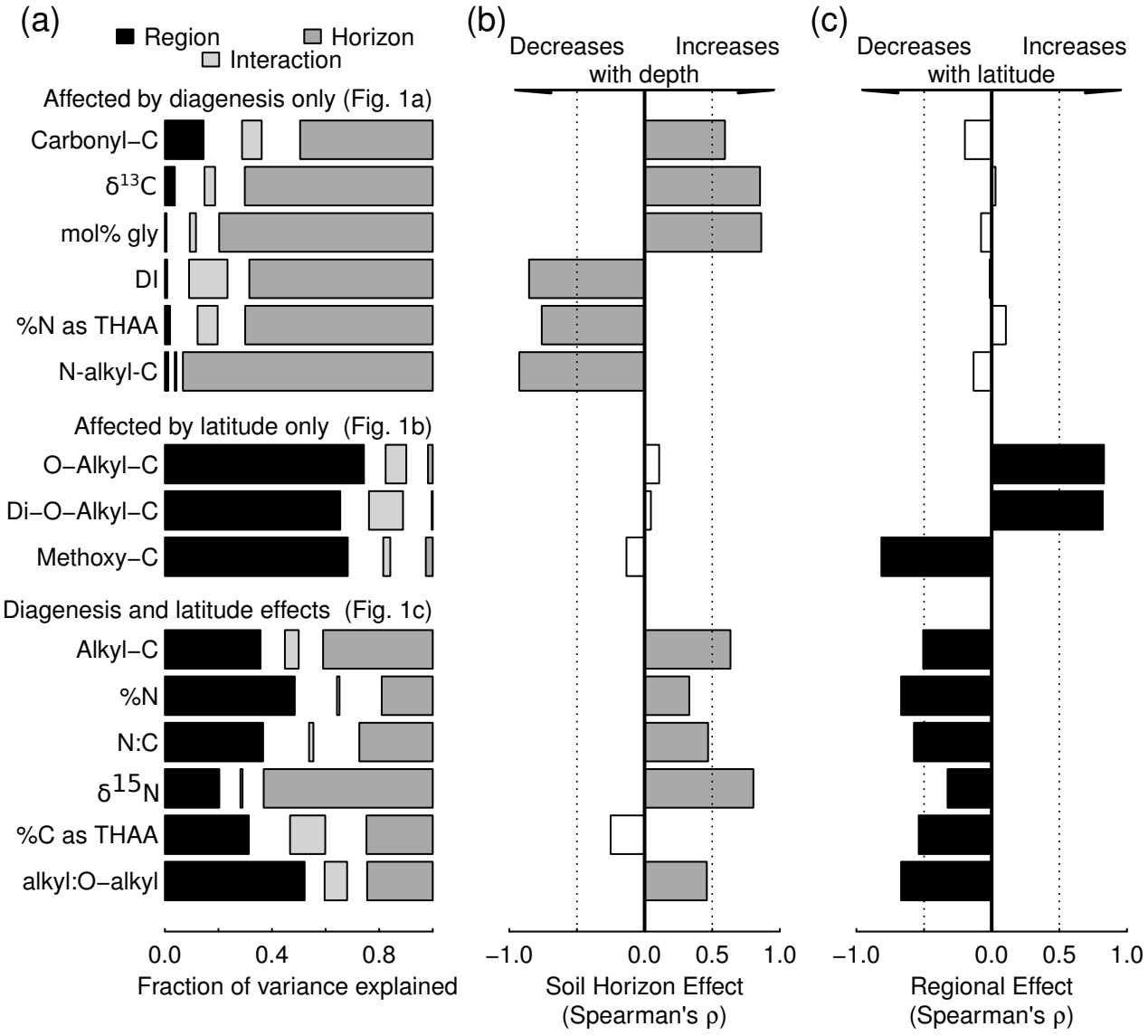

Figure 3.3 Parameters of SOM chemistry grouped according to how they vary with depth and latitude. Parameters for which these two factors together explained less than 50% of the total variance were excluded. (a) Fraction of variance of each parameter explained by the factors soil horizon and region. (b,c) Spearman correlation coefficient (ρ) between the parameter and latitude (b) or depth (c). A ρ close to +1 or -1 indicates a monotonous increase or decrease of the parameter with depth or latitude, while a ρ close to 0 indicates independence of the parameter from depth or latitude.

did not exhibit a significant interactive effect of latitude and depth (LxD). Five of these parameters exhibited a monotonous decrease with depth (%C, %N, δ^{15}N, N:C, and alkyl:O-alkyl; Fig 3.3b), and all six parameters exhibited a significant decrease with latitude (Fig 3.3c). Noteworthy, none of the variables exhibited a significant LxD effect, which would indicate that the regional differences in SOM chemistry either become larger (differential diagenetic alteration) or converge with increasing decomposition associated with organic horizon depth. Taken together, the studied parameters thus exhibited the pattern expected if latitude and diagenesis were to affect SOM chemistry independently (Fig. 3.1a-c), indicating that regional differences in SOM chemistry were largely driven by different inputs to SOM, not by differential diagenesis.

3.3.3 Evidence for effects of SOM chemistry on bioreactivity

The first principal component (PCA1) of the six main parameters varying by region (%methoxy-C, %O-alkyl-C, %Di-O-alkyl-C, %alkyl-C, %N, %C as THAA) explained 46.7% of the variance in bioreactivity at site level (Supporting Information 3.7). This predictor thus explained a similar fraction of variance as the factor 'region' (54.4%).

Bioreactivity was negatively correlated to PCA1 for soil cores incubated at 15 °C (r=-0.72, p=0.025) and 10 °C (r=-.67, p=0.05). In soil cores incubated at 5°C, the relation between PCA1 and bioreactivity followed the same trends, although they were not significantly correlated (r=-0.47, p=0.200) due to the higher variance among individual soil cores (Fig. 3.5). Taking into account the strong inter-correlation among the six parameters of SOM chemistry that varied by region (all $r > 0.46$; Supporting Information 3.6), we could not determine which of the parameters may explain the differences in bioreactivity individually. This group of six parameters, however, collectively explained the observed regional differences in SOM bioreactivity.

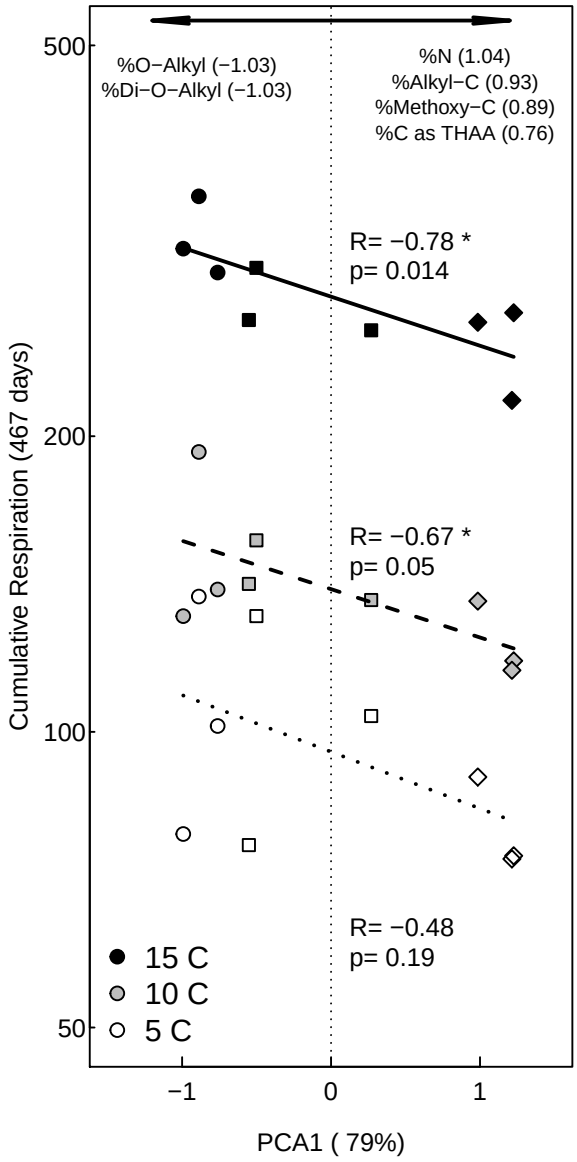

Figure 3.4 Effect of SOM chemistry on the bioreactivity of SOM in intact soil cores. PCA1 represents the first principal component of parameters of SOM chemistry that differed with latitude. For each parameter, the weighted mean among L, F, and H horizons was calculated for each site (see supplement). PCA1 explained 79% of the total variance of these six parameters. The regression between PCA and the cumulative respiration was calculated separately for each incubation temperature (open symbols, 5 °C; grey symbols,10 °C; black symbols, 15 °C). Diamonds, northern region; squares, mid region; circles, southern region. Note the logarithmic scale of the dependent variable (cumulative respiration). The variables used to generate the PCA and their factor loadings versus PCA1 are stated on top of the figure..

3.3.4 Composition of litter inputs to soils

In trapped litter, which included vascular plant litter but not moss litter, the majority of chemical parameters did not exhibit significant differences between three regions (%C, δ^{13}C, %N as AA, DI, mol% gly, and all functional groups in NMR spectra; Fig. 3.2). Trapped litter from more southern sites, however, exhibited higher %N, δ^{15}N, and %C as THAA values (Figs. 3.3d, 3.2e, 3.2p) and more narrow C:N ratios (not shown). Differences in the chemical composition of the litter collected in litter traps trapped thus explained higher nitrogen and protein abundance in SOM from more southern sites, but not their higher concentrations of lignin and aliphatic compounds or their lower concentrations of carbohydrates.

Estimates of the composition of the litter inputs to soils based upon the L horizon composition showed that if woody litter and moss litter are accounted for (in addition to needle litter), the total litter inputs in more southern sites contained higher proportions of O-alkyl-C and di-O-alkyl-C, and lower proportions of alkyl-C and methoxy-C, and lower alkyl:O-alkyl ratios (Total litter in top panel of Figs. 3.2e, 3.2f, 3.2g, 3.2k, 3.2l). For %O-alkyl-C, %di-O-alkyl-C, %alkyl-C, and alkyl:O-alkyl, the differences among regions in total litter inputs were similar to those observed in L-horizon SOM, even though all sites exhibited higher proportions of O-alkyl-C and lower proportions of alkyl-C in litter inputs compared to L-horizon SOM (Figs. 3.2e, 3.2f, 3.2k, 3.2l). For %methoxy-C, the difference observed between the two most extreme regions was more than twice as high in L-horizon SOM than in our estimate for total litter inputs (%methoxy-C was 67% higher southernmost region compared to the northernmost region in L horizon SOM, but only 26% higher in the total litter inputs estimate; Fig 3.2g).

Taken together, the parameters that differed between regions in SOM fell into three groups in regards to whether these differences were also reflected in the litter inputs or not. Regional differences in parameters dependent on N concentrations (%N, C:N, %C as THAA) and δ^{15}N could be explained by chemically different vascular plant litter. In contrast, the

regional differences in %O-alkyl-C, %di-O-alkyl-C, %alkyl-C, and alkyl:O-alkyl could be explained by the different proportions of moss and vascular plant litter. The differences in %methoxy-C, however, were only partially explained by differences in litter chemistry.

3.4 Discussion

3.4.1 SOM chemistry is largely determined by litter inputs, not diagenesis

Results from in-situ soil warming experiments demonstrate that a change in soil temperatures alone can alter SOM chemistry and its bioreactivity [Melillo et al., 2002, Feng et al., 2008, Pisani et al., 2015]. Cross-sites studies, in contrast, indicate that differences in vegetation (and thus litter inputs) affect SOM chemistry more strongly than other differences associated with climate [Quideau et al., 2001] suggesting the need to reconcile whole ecosystem soil responses to climate change. Clarifying the origins of SOM chemistry in the context of the boreal forest climate transect studied here enables knowledge required to understand the controls on SOM cycling and fate in boreal forest ecosystems critical to predictive understanding of climate change. In this transect, more southern regions were characterized by higher temperatures, precipitation, and N availability (Table 3.1). The transect thus features a combined gradient of three environmental conditions that represent upcoming environmental changes in this region. Similar SOM stocks across this forest transect suggest that acceleration of SOM decomposition with climate warming will be compensated by greater productivity [Ziegler et al., 2017] and decreasing bioreactivity [Laganière et al., 2015]. Here, we investigated how the differences in SOM bioreactivity across this climate gradient are manifested in SOM chemistry to assess whether regional differences in SOM chemistry were inherited from chemically distinct litter inputs, or acquired over time as diagenesis acted differently under different environmental conditions.

We addressed this question of the origin of SOM chemistry by studying how SOM varies

along a gradient of increasing diagenesis (i.e., from L to H horizons) in each of the field sites of this transect. If regional differences in SOM chemistry were to develop over time due to diagenetic alteration under different climatic conditions as suggested by some *in situ* warming experiments, we would expect (1) climate history (latitude) to affect the same parameters of SOM chemistry as diagenesis (depth), and (2) these regional differences to increase with greater diagenetic alteration (from shallow to deep soil horizons). The parameters of SOM chemistry that differ with climate in these forests, however, turn out to be different from those that vary with diagenesis. Furthermore, the differences between regions in SOM chemistry do not increase with depth, and thus indicate that the regional difference in SOM chemistry and bioreactivity observed along this transect primarily resulted from chemically distinct litter inputs to SOM.

The field sites that form this transect were selected among mature stands of *Abies balsamea* forests with similar stand history, disturbance regime, soil types and drainage. As such, we constrained the dominant tree species, but allowed local environmental conditions to form the under-story vegetation composition and tree physiology. This represents a typical scenario for managed forests, where the composition of tree species is determined during afforestation, but climate effects are allowed to play out freely thereafter. Our study demonstrated that even in the absence of a change in dominant over-story vegetation, changes in SOM chemistry are primarily mediated through aboveground processes that lead to different litter inputs, rather than through climate effects on SOM diagenesis.

3.4.2 The diagenetic state of SOM did not vary with climate

In spite of the different climate regimes in the three regions, SOM in each of the L, F, or H horizons appear to have undergone a similar extent of diagenetic alteration based upon the chemical composition. This was evidenced by the fact that all parameters that change with depth in these forest soils exhibited a similar change from the L to H horizons in all

regions (no interactive effect of depth and latitude), and that most of these parameters did not differ among regions at all (Fig. 3.3). In contrast, chemical parameters indicative of diagenetic alteration of SOM have been found to change to a greater extent in depth profiles of more southern, warmer relative to northern Jack Pine boreal forests and attributed to SOM losses with climate warming [Norris et al., 2011]. The consistent SOM stocks in the mesic forests studied here suggest that, in contrast to the drier Jack Pine forests, inputs keep pace with losses and contribute to the lack of change in depth profile SOM chemistry associated with diagenetic alteration. The contrast in these studies signifies the need for regional understanding (e.g. drier, inland versus mesic, coastal) of forest soil responses to climate change as has been suggested with the response of trees to climate change [Charney et al., 2016].

The trends in SOM chemistry with soil depth were consistent with those typically associated with increasing diagenetic alteration, thus validating our use of the depth gradients observed to assess the role of differential diagenesis in regulating soil chemistry across climate regions. Increases in $\delta^{13}C$ and $\delta^{15}N$ and decreases in C:N with diagenesis are commonly observed soils and other environments [Nadelhoffer and Fry, 1988]. The change in the composition of THAA with depth, represented by the decreases in the THAA-based DI as well as the increase of mol% glycine have been associated with the microbial processing of organic matter in a range of terrestrial and aquatic ecosystems [Hedges et al., 1994, Dauwe et al., 1999, Shen et al., 2014, Philben et al., 2016]. The decrease in %N-alkyl-C with depth, observed in the NMR results, is consistent with the lower proportion of soil N as THAA that occurs during decomposition of natural organic matter [Philben et al., 2016]. The increase of %carbonyl-C with depth can be associated with oxidation of functional groups while increasing abundance of %alkyl-C with greater depth likely represent the accumulation of hydrophobic compounds (i.e., long chained aliphatic lipids) during diagenesis [Baldock et al., 1992, Quideau et al., 2000]. For example, the leaching of more water soluble compounds

from the organic layer likely constitute an important process in the formation of SOM under these precipitation-rich climates [Chapter 2, Bowering et al., in review, Edwards et al., in preparation].

Unlike %alkyl-C and %carbonyl-C, the relative abundance of carbon functional groups representing lignin and carbohydrates (%O-alkyl-C, %di-O-alkyl-C, and %methoxy-C) did not change with depth. This stands in contrast to the increase of %methoxy-C and decrease in %O-alkyl-C and %Di-O-Alkyl-C that typically occurs during litter decomposition [Preston et al., 2009] in association with the retention of lignin and loss of carbohydrates that together make up more than 50 % of the litter dry mass [Berg and McClaugherty, 2008]. Our results thus suggest that decadal scale changes to SOM chemistry in the organic horizons of these forests are primarily associated with the relatively small soil organic nitrogen (SON) pool, whereas a major part of soil organic carbon (SOC) exhibited relatively few observable changes during diagenesis.

3.4.3 Regional differences in SOM chemistry resulted from differences in moss-derived and N content of litter

Our finding that the differences in SOM chemistry along a climate transect of *Abies balsamea* dominated forests soils occurred due to differences in litter inputs agree with cross-site studies that span multiple different vegetation types [Quideau et al., 2001]. We showed that even within a highly constrained transect where sites were selected for the same forest type, climate effects on vegetation had a stronger effect on SOM chemistry compared to climate effects on soil diagenesis.

We identified three central mechanisms through which climate and N availability likely caused the chemical composition of litter inputs to differ among regions, thus indicating that these mechanisms may lead to a change in SOM chemistry of these forests in the future.

1. SOM from more northern regions inherited lower protein contents and lower $\delta^{15}N$

values from the vascular plant litter, explaining the lower %N, %C as THAA, and δ^{15}N values, and the higher C:N ratios in SOM from the more northern sites. The lower C:N ratios and higher δ^{15}N values in SOM from more southern site, therefore, should not be interpreted as indicative of more decomposed SOM. The decrease of litter N contents with latitude, rather, resulted from a greater N resorption during needle senescence [Podrebarac et al., in preparation] in response to lower N availability due to slower N recycling at higher latitude sites [Philben et al., 2016]. This is consistent with a global trend towards greater N limitation in high latitude ecosystems [Zechmeister-Boltenstern et al., 2015] and signifies how soil nutrient cycling can regulate the variation in elemental and isotopic composition of SOM with climate change.

2. The higher proportion of moss litter relative to needle litter in more northern regions (Fig. 3.5) led to SOM that was chemically more similar to moss litter. Compared to vascular plants, mosses contain higher proportions of carbohydrates and lower proportions of aliphatic compounds (waxes) and no guaiacyl- and syringyl-type lignins [Butler et al., in preparation]. Higher proportion of moss inputs thus explained the higher proportions of O-alkyl-C and di-O-alkyl-C, and the lower proportion of alkyl-C in SOM at more northern sites. This is not only supported by the unique chemical composition of the nonvascular moss in relation to the vascular needle inputs but also because none of these parameters differed among the needle litter from the different regions (Fig. 3.2). Greater moss inputs also led to lower lignin contents at higher latitude, however, the differences in the proportion of moss relative to vascular plant litter could not fully explain the full magnitude of the difference in %methoxy-C observed between regions (Fig. 3.5g).

3. The majority of litter mass is lost during the initial decomposition stages, and only a small fraction (20 - 30%) of the litter mass input is incorporated into organic layer SOM

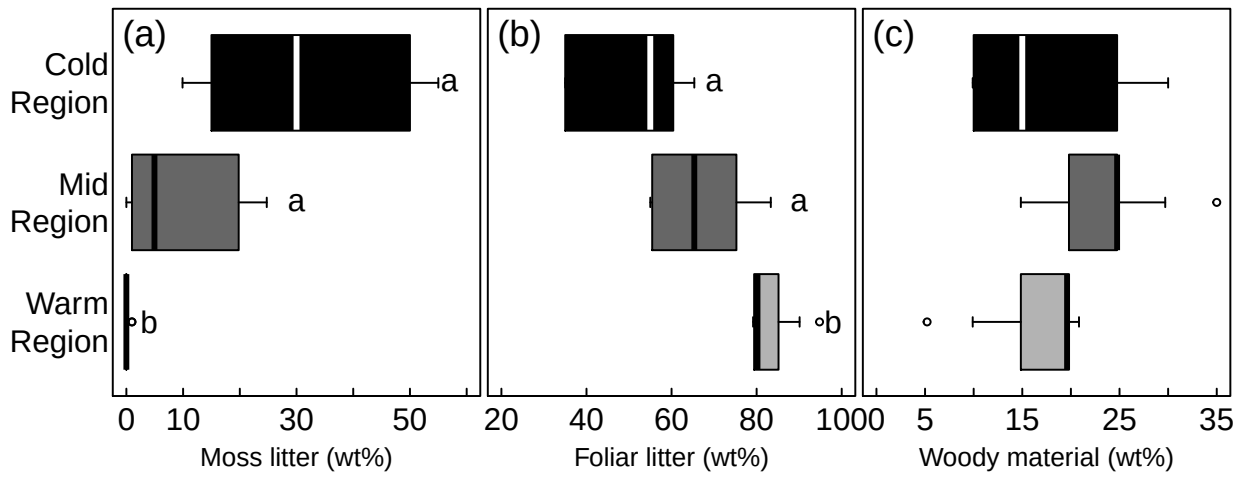

Figure 3.5 Composition of L layer material. L layer material was separated into foliar litter, woody material and moss litter. Letters indicate significant differences among regions.

[Berg et al., 1996, Prescott, 2010]. Environmental conditions affect which chemical components of the initial litter are preferentially decomposed, and which remain to be incorporated into SOM [Wickings et al., 2012]. Further, high N availability has been shown to inhibit the degradation of lignin [Jeffries et al., 1981, Melillo et al., 1989]. The higher N concentrations in southern regions thus could have led to a stronger accumulation at of lignin during the initial litter decomposition stage, thus explaining the high proportions of %methoxy-C found in the southernmost region compared to our estimate for total litter inputs in that region.

The significant role of inputs and their initial decomposition in controlling the SOM chemistry of these forests stresses the need to carefully assess soil inputs in our use of chemical knowledge to understand the response of soil biogeochemistry to climate change.

3.4.4 Moss contributions mediate the climate effect on SOM chemistry and its bioreactivity

Our study revealed that the chemical and biological properties of SOM in these organic horizons are determined by litter inputs resulting from differences in climate history. Taken

together our results suggest that chemical differences, such as the relative abundance of lignin, carbohydrates, and aliphatic compounds, were primarily determined by the proportion of moss and vascular plant litter and had the greatest influence on SOM bioreactivity. The inter-correlation among these parameters, however, prevented us from identifying which chemical properties are responsible for the increase of bioreactivity with latitude. Instead, we evaluated if this relationship is consistent with the current understanding of the effects of different SOM properties on decomposition.

The bioreactivity of SOM increased with the proportion of carbohydrates (%O-alkyl-C and %di-O-alkyl-C) and decreased with the proportion of lignin (%methoxy-C) and aliphatic compounds (%alkyl-C). This is consistent with decomposition of carbohydrate being metabolically favorable compared to that of lignin and plant waxes [von Lützow et al., 2006, Kuzyakov et al., 2015]. Surprisingly, bioreactivity also decreased with %N and THAA as %C. Higher N concentrations can alleviate the N limitation of microbial decomposers in organic soil horizons [Mooshammer et al., 2014], and have often been associated with increased rates of decomposition and therefore SOM bioreactivity. The opposite trend observed in our study likely emphasizes the strong influence of the vascular versus nonvascular plant inputs along this climate gradient in controlling the SOM chemistry and its bioreactivity. The elevated N availability associated with the warmer study sites [Philben et al., 2016] and evidenced by the greater N and protein content of the vascular plant litter in the warmer forests did not positively correlate with SOM bioreactivity. However, those C features that typically distinguish the non-vascular moss tissues from vascular plant tissues, abundance of carbohydrates relative to lignin and waxes, were correlated with SOM bioreactivity, as expected.

Our observations, therefore, suggest that the proportion of nonvascular (moss) and vascular plant litter was the key parameter driving the chemical and biological properties of SOM in these forests. SOM was degraded faster, under controlled conditions, if it was de-

rived to a larger extent from moss litter relative to vascular plant litter. This result stands in contrast to the slower decomposition rates of fresh moss litter relative to vascular plant litter in both field (litterbag) and laboratory studies [Hobbie, 1996, Hagemann and Moroni, 2015, Butler et al., in preparation]. Given what we observed, the moss litter properties responsible for initially slow or inhibited decomposition are lost over time. For example, a number of moss species have been shown to produce antimicrobial compounds [Banerjee and Sen, 1979, Basile et al., 1999, Dey and De, 2011, Nikolajeva et al., 2012]. Perhaps these compounds are leached out of moss litter during initial decomposition, leaving behind moss-derived SOM that is chemically more labile than vascular plant-derived SOM.

The climate induced changes in moss versus vascular plant inputs and its ramifications for SOM chemistry and bioreactivity stress the importance of accounting for moss litter inputs which are often missed using typical litter trap methods. Moss NPP accounts on average for 20% of the total NPP of upland boreal forests [Turetsky et al., 2010]. However, this values varies considerably across forest stands [Bisbee et al., 2001, Gower et al., 2001] likely in response to climate [Vitt, 1990], and moss NPP can exceed vascular plant NPP locally [Bonan and Van Cleve, 1992, Frolking et al., 1996, Gower et al., 1997, 2001]. Mosses are not collected in litter traps, and quantifying of moss NPP (relative to vascular plants) is difficult, labor intensive, and prone to errors [Yuan et al., 2014]. Moss litter production thus remains poorly constrained for most boreal ecosystems. Moss NPP, however, is similar in boreal and arctic ecosystems [Turetsky, 2003], whereas vascular plant NPP in boreal forests decreases with latitude [Gower et al., 2001] . It is therefore likely that the proportion of moss litter relative to plant litter will decrease with warming. Our study showed that chemical properties of SOM associated with moss litter strongly vary among field sites, and that these variations have meaningful effects on the overall bioreactivity of SOM.

3.5 Acknowledgements

We thank Jerome Laganiere and Thalia Soucy-Giguere for field sampling and Rachelle Dove for help with laboratory work. Andrea Skinner, Sara Thompson, Dave Meade, and Danny Pink assisted with litterfall collection and processing. This study was funded by the Natural Sciences and Engineering Research Council of Canada, the Canadian Forest Service (Natural Resources Canada) the Center for Forestry Science and Innovation (Department of Fisheries, Forestry and Agrifoods, Government of Newfoundland and Labrador), the Canada Research Chairs program, and the Humber River Basin Project (Government of Newfoundland and Labrador).

3.6 Supporting Information

3.6.1 Supporting Information 3.1 - Bioreactivity of isolated soil horizons

Respiration rates of isolated L,F, and H horizon were measured in an incubation experiment conducted for a previous study [Laganière et al., 2015]. Briefly, the samples of the organic soil horizon in the northernmost and southernmost region of the NL-BELT transect were collected during a field campaign in October 2011. These samples were then separated into L, F, and H horizons, and incubated for 480 days at 5, 10, or 15 °C and 60 % water holding capacity. Respiration rates were measured at six time points during the incubation experiment. Bioreactivity (R_{10}) was defined as the daily respiration at 10 °C, and temperature sensitivity (Q_{10}) was defined as the factor by which respiration increases if temperature increases by 10 °C. We calculated R_{10} and Q_{10} according to equations S1-S3, where *Temp* stands for the incubation temperature, and *Resp* stands for average respiration over the course of the incubation experiment in mg CO_2-C g^{-1} SOM-C d^{-1}. Figure S1 shows how Bioreactivity decreases with from shallow to deep soil horizons, and from cold to warm sites regions. Temperature sensitivity, in contrast, decreased with depth, but did not differ among regions.

$$Resp = R_{10} \cdot Q_{10}^{\frac{Temp}{10}-1} \tag{3.S1}$$

$$R_{10} = e^{intercept(\frac{Temp}{10}-1,\ log(Resp))} \tag{3.S2}$$

$$Q_{10} = e^{slope(\frac{Temp}{10}-1,\ log(Resp))} \tag{3.S3}$$

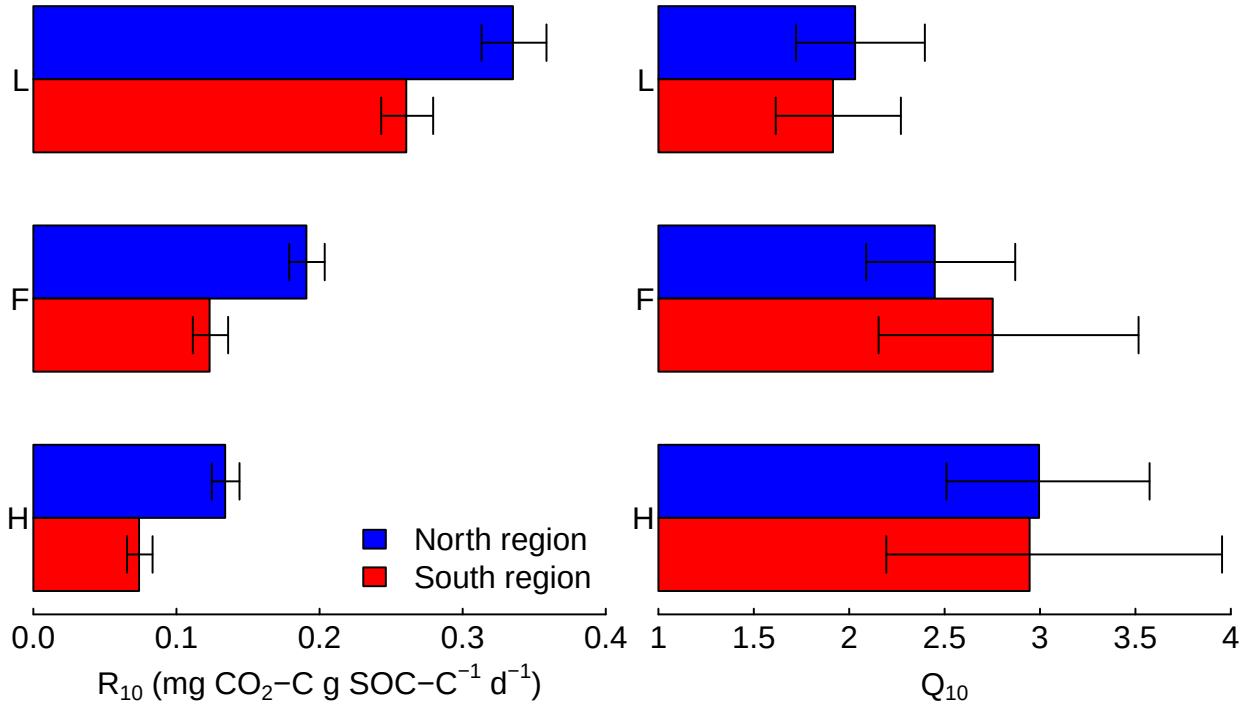

Figure 3.S1 Bioreactivity and temperature sensitivity of respiration of isolated soil horizons from the northernmost (blue) and southernmost (red) regions of the transect. Error bars indicate standard errors. Data from Laganière et al. [2015].

3.6.2 Supporting Information 3.2 - CP-MAS NMR spectra

Figures 3.S2 and 3.S3 provide CP-MAS ^{13}C-NMR spectra of soil organic matter (Fig. 3.S2) and of needle litter and moss litter (Fig. 3.S3). Figures 3.S4 and 3.S5 provides examples of the peak deconvolution models and the assignment of spectra regions to functional groups. The four deconvoluted spectra shown are from samples of the most shallow and deepest soil horizons from the northernmost and southernmost sites, thus representing the most extreme soil sample studied in this chapter.

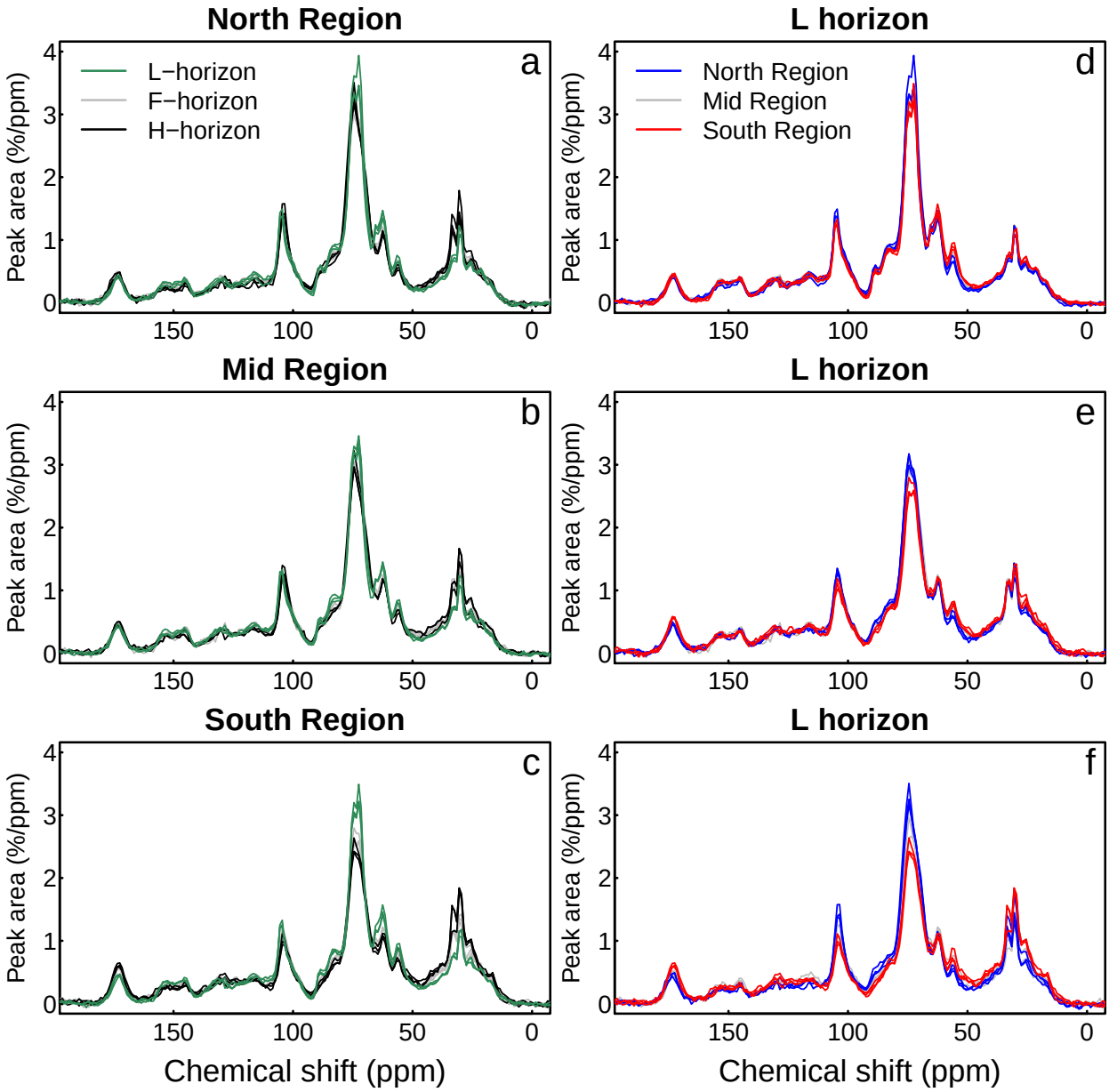

Figure 3.S2 CP-MAS spectra of the distinct soil horizons and regions. (a-c) Comparison of the spectra of the distinct soil horizons (L, F, and H) in each region. (d-f) Comparison of the different samples of the same soil horizon from distinct regions. Data has been processed for baseline correction, normalization to a total peak area of 100% · ppm. The plotted spectra represent samples from the three replicate sites in each region.

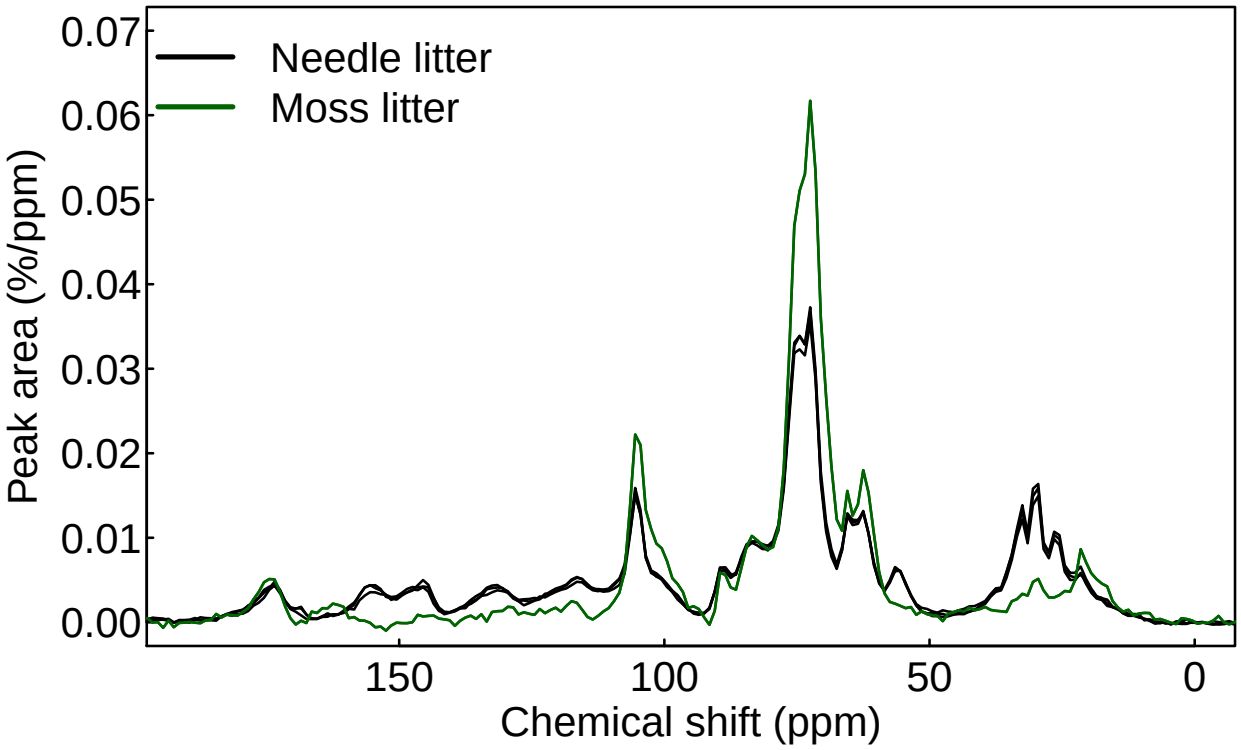

Figure 3.S3 CP-MAS ^{13}C-NMR spectra of vascular plant and moss litter samples from the boreal forest transect studied herein. The plotted spectra (black) represents the average for needle litter from the three sites in each of the three regions (n=9), the plotted spectra represent the average spectra litter from three replicate field sites in each region. Moss litter was collected at field sites in the southernmost and the mid region (n=4). Each sample was composed of a representative mixture of the moss species present in the region. Although moss species differed between sites, the difference in their NMR spectra was smaller than the line width in this figure.

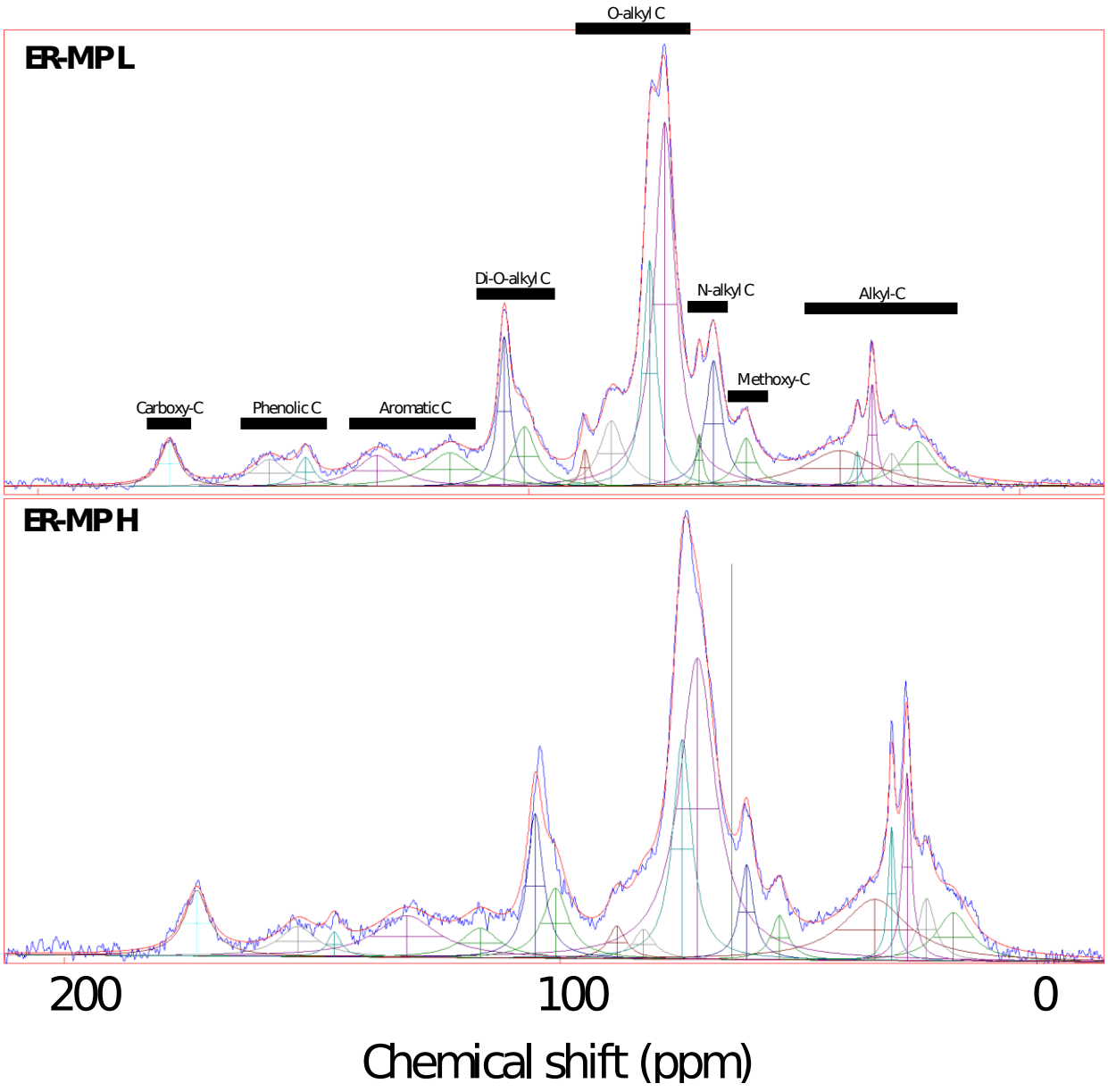

Figure 3.S4 Assignment of functional groups to spectral regions and examples of deconvoluted CP-MAS ^{13}C NMR spectra from L and H horizon in the northernmost region.

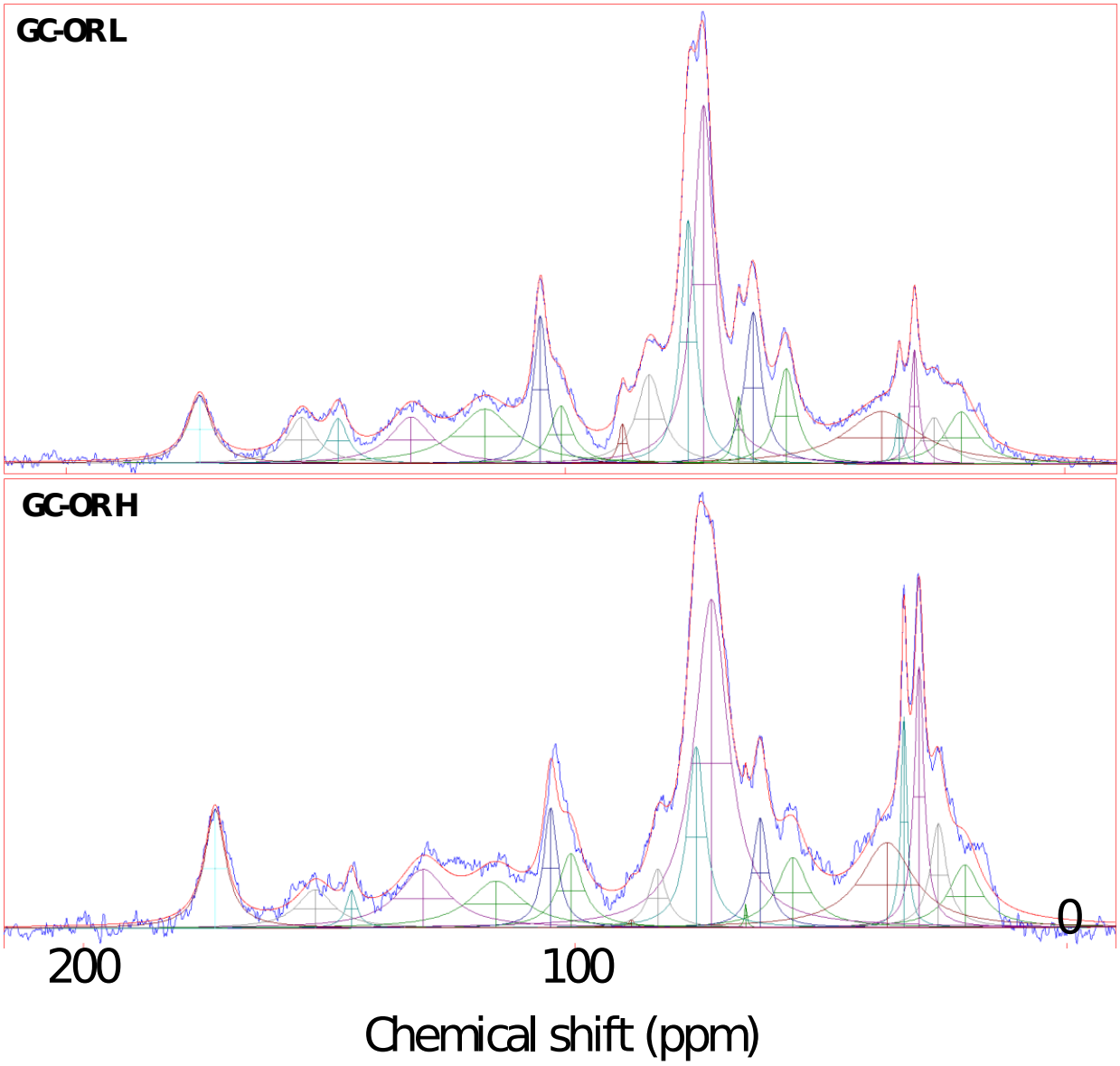

Figure 3.S5 Examples of deconvoluted CP-MAS ^{13}C NMR spectra from L and H horizon in the southernmost region.

3.6.3 Supporting Information 3.3 - Estimated chemical composition of total detritus inputs

The chemical composition of litter inputs to the L layer were calculated according to equation 3.S4 based on the composition of the material in the L layer, where f_{foliar}, f_{woody}, and f_{moss} indicates the fraction of the L horizon identified as foliar, woody, and moss litter and x_{foliar}, x_{woody}, and x_{moss} indicates any of the geochemical measures for these fractions (e.g. NMR components).

$$x_{inputs} = x_{foliar} * f_{foliar} + x_{woody} * f_{woody} + x_{moss} * f_{moss} \quad (3.S4)$$

For this calculation, values for x_{foliar} were measured for each plot, values for x_{moss} were taken from mosses collected in two of the regions [Butler et al., in preparation], and x_{woody} was based on literature values as described in [Ziegler et al., 2017]. Raw data and all literature values are provided in the table below.

Table 3.S1 Calculated composition of total litter inputs.

	Foliar litter			Woody material	Moss	Total litter inputs			L horizon		
Region	North	Mid	South			North	Mid	South	North	Mid	South
$\delta^{13}C$ (‰)	-29.7	-29.7	-29.7	[1]	-31.5	-30.3	-29.9	-29.7	-29.4	-28.8	-28.9
O-alkyl (%)	35.9	37.0	37.0	60	55.3	46.1	44.3	40.7	39.6	39.0	35.8
di-O-alkyl (%)	8.0	8.2	8.4	9.5	15.6	10.7	9.2	8.6	10.0	9.8	7.8
methoxy (%)	2.8	2.7	2.6	6.7	0	2.6	3.4	3.3	2.1	3.7	4.8
aromatic (%)	19.7	20.3	19.3	4.5	7.0	13.1	15.4	16.9	17.7	17.2	17.5
amino (%)	8.3	8.1	8.2	0	8.25	6.8	6.1	6.9	8.1	8.0	8.5
carbonyl-C (%)	4.4	4.7	4.5	2	3.4	3.7	4.0	4.1	3.7	3.6	3.6
alkyl (%)	20.8	18.8	19.9	3	9.1	14.1	14.1	17.2	18.0	18.8	21.0
alkyl/O-alkyl (%)	0.44	0.39	0.42	0.04	0.13	0.24	0.25	0.33	0.34	0.35	0.43

[1] $\delta^{13}C$ were measured in pooled samples that included both foliar litter and woody material.

3.6.4 Supporting Information 3.4 - Bioreactivity of intact soil cores

This dataset has been updated from Podrebarac et al. [2016] to include soil cores from the middle region (SR). Respiration rates were measured at six time points during the incubation experiment. Bioreactivity (R_{10}) was defined as the daily respiration at 10 °C, and temperature sensitivity (Q_{10}) was defined as the factor by which respiration increases if temperature increases by 10 °C. We calculated R_{10} and Q_{10} as described in Supporting Information 3.4.

Table 3.S2 Bioreactivity of intact soil cores.

Region	Site	Plot	Cumulative respiration (mg CO2-C g^{-1} SOC)			R_{10}	Q_{10}	R^2 [a]
			5°C	10°C	15°C			
ER	MP	1	89	135	314	156	3.5	0.98
		2	80	132	343	154	4.3	0.98
		3	67	127	274	132	4.1	1.00
	SR	1	79	142	292	148	3.7	1.00
		2	105	144	298	165	2.8	0.97
		3	120	134	291	167	2.4	0.92
	HP	1	137	203	319	207	2.3	1.00
		2	165	205	337	225	2.0	0.98
		3	110	171	397	196	3.6	0.98
SR	CF	1	87	195	402	189	4.6	1.00
		2	209	183	328	233	1.6	0.74
		3	97	92	160	113	1.6	0.81
	HB	1	104	111	260	144	2.5	0.89
		2	99	169	269	165	2.7	1.00
		3	108	129	241	150	2.2	0.95
	TM	1	97	106	272	142	2.8	0.90
		2	48	154	239	121	4.9	0.97
		3	83	165	277	156	3.3	1.00
GC	MR	1	90	117	321	150	3.6	0.95
		2	56	135	229	120	4.1	0.99
		3	78	102	252	126	3.2	0.95
	SH	1	95	166	206	148	2.2	0.97
		2	99	129	246	146	2.5	0.97
		3	76	113	332	142	4.4	0.97
	OR	1	72	110	227	122	3.1	0.99
		2	112	152	265	169	2.2	0.97
		3	31	84	161	74	5.3	0.99

[a] R^2 indicates the coefficient of determination between log(respiration) and temperature.

3.6.5 Supporting Information 3.5 - Average SOM chemistry for intact soil profiles

The chemical composition of intact soil profiles was calculated as the weighted mean of each soil horizons equation 3.S5, where x_{LFH} stands for the average value of parameter x in an intact soil profile, x_L, x_F, and x_H stand for the measured values of x in the L, F, and H horizons, and f_L, f_F, and f_H stand for the proportion of organic carbon present in the L, F, and H layer as a fraction of the sum of these three horizons.

$$x_{LFH} = x_L * f_L + x_F * f_F + x_H * f_H \tag{3.S5}$$

3.6.6 Supporting Information 3.6 - Correlations among parameters of litter chemistry used to predict bioreactivity, and commulative respiration at three temperatures

Table 3.S3 Correlation coefficients (R) between parameters of SOM chemistry across sites.

	%Methoxy-C	%O-Alkyl-C	%Di-O-Alkyl-C	%Alkyl-C	%N	%C as THAA	cum resp 5C	cum resp 10C
cum resp 15C	**-0.711***	**0.669***	**0.78***	-0.552	**-0.681***	**-0.732***	**0.672***	**0.809****
cum resp 10C	-0.561	0.568	0.644	-0.552	-0.541	-0.519	**0.872****	
cum resp 5C	-0.281	0.542	0.531	-0.547	-0.359	-0.286		
%C as THAA	0.463	-0.598	-0.580	0.480	**0.753***			
%N	**0.789***	**-0.927*****	**-0.908*****	**0.791***				
%Alkyl-C	0.597	**-0.909*****	**-0.802****					
%Di-O-Alkyl-C	**-0.857****	**0.935*****						
%O-Alkyl-C	**-0.708***							

Numbers in bold represent significant correlations. Asterisks indicate significance levels (*, $p<0.05$; **, $p<0.01$; ***, $p<0.001$).

3.6.7 Supporting Information 3.7 - Evaluation of the effect of regional differences in SOM chemistry on bioreactivity

To evaluate parameters of SOM chemistry as a predictors of bioreactivity, we tested their significance in a model that also accounted for the exponential increase of respiration with temperature:

$$\log R_{i,j,k} = \beta_T \cdot Temp_i + \beta_S \cdot [predictor]_j + \epsilon_{i,j,k} \tag{3.S6}$$

In this model, $R_{i,j,k}$ stands for the average respiration rate of the microcosms from plot k at site j incubated at temperature i. This model assumes constant temperature sensitivity (Q_{10}) of respiration across regions. Allowing for variations of Q_{10} among sites or regions did not improve the predictive power of any tested model.

We compared the variance of continuous variables (df=2) to that explained by region (df=3), to the maximal variance explainable at site level (i.e., predictor=Site; df=9), and to the variance explained by temperature only (df=1). To compare models accounting for different degrees of freedom we calculated Akaike's information criterion (AIC) for each model.

Table 3.S4 Predition of site-level variation in bioreactivity by parameters of SOM chemistry.

Predictor	df	ESS	RSS	% site-level variance explained	AIC[1]	ANOVA Group[2]	AIC group2
None	1	15.89	7.13	0%	39.0	a	a
C:N ratio	2	16:33	6.68	20.9%	35.8	b	b
%Alkyl-C	2	16.67	6.35	36.8%	31.6	b	c
%Methoxy-C	2	16.70	6.31	38.3%	31.2	b	c
PCA1[3]	2	16.88	6.14	46.7%	28.9	bc	d
Region	3	17.04	5.98	54.4%	28.7	c	d
%O-Alkyl-C	2	16.92	6.09	48.7%	28.3	bc	de
%Di-O-alkyl-C	2	17.07	5.95	55.6%	26.4	bcd	e
Site	9	18.01	5.01	100%	26.4	d	f

[1]AIC, Akaike's information criterion

[2]Significant difference in model performance, either $p<0.05$ in ANOVA, or AIC difference >2

[3]First component of a principal component analysis of %Alkyl, %O-Alkyl, %Di-O-Alkyl, %Methoxy-C, %N, and %C as THAA. PCA1 explained 79% of the total variance of these six variables.

3.7 Raw data

Table 3.S5 Raw data for Fig. 3.2: Elemental concentrations and stable isotope values

Region	Site	Soil horizon	%C		δ^{13}C		%N		δ^{15}N	
			mean	SD	mean	SD	mean	SD	mean	SD
		L	48.8	0.5	-29.7	0.7	1.04	0.05	-6.3	0.5
	MP	F	48.5	0.9	-28.2	0.3	1.35	0.08	-4.0	0.4
		H	47.3	2.1	-27.1	0.8	1.35	0.24	-2.0	0.4
Eagle		L	49.3	0.6	-29.0	0.4	1.19	0.14	-5.4	0.3
River	SR	F	47.9	1.1	-28.4	0.3	1.41	0.12	-3.1	1.0
(Cold)		H	46.1	0.9	-27.3	0.4	1.25	0.03	-1.4	0.2
		L	48.0	0.7	-29.5	0.5	1.16	0.07	-5.3	1.0
	HP	F	46.0	2.5	-28.4	0.3	1.44	0.20	-3.5	1.0
		H	44.7	2.6	-27.6	0.3	1.42	0.14	-1.4	0.9
		L	48.0	0.3	-28.9	0.2	1.23	0.02	-3.2	0.7
	CF	F	47.2	1.0	-27.9	0.6	1.40	0.12	-1.5	1.4
		H	46.0	2.3	-27.1	0.7	1.46	0.02	0.7	2.1
Salmon		L	48.7	1.1	-29.0	0.1	1.31	0.12	-2.6	1.2
River	HB	F	48.4	0.5	-28.6	0.4	1.64	0.05	-0.2	0.7
(Mid)		H	46.8	2.4	-27.5	0.2	1.44	0.08	2.0	0.9
		L	49.3	1.0	-28.4	0.1	1.06	0.18	-4.7	1.3
	TM	F	48.1	0.2	-27.8	0.4	1.40	0.03	-2.1	1.3
		H	47.5	1.0	-27.0	0.5	1.25	0.09	0.9	0.3
		L	50.2	0.1	-29.1	0.2	1.47	0.05	-3.0	0.5
	MR	F	49.6	1.3	-28.8	0.2	1.78	0.16	-1.8	0.2
		H	46.4	3.1	-27.9	0.5	1.73	0.19	-0.1	0.6
Grand		L	50.1	0.6	-28.8	0.1	1.48	0.02	-3.4	0.1
Codroy	SH	F	49.1	2.2	-28.4	0.1	1.70	0.20	-2.1	0.5
(Warm)		H	46.5	0.4	-27.6	0.1	1.66	0.12	0.9	0.3
		L	50.1	0.1	-28.6	0.3	1.68	0.19	-3.8	0.2
	OR	F	49.0	1.2	-28.2	0.1	1.72	0.20	-2.2	0.1
		H	47.8	1.5	-27.6	0.3	1.92	0.19	0.1	0.6

Table 3.S6 Raw data for Fig. 3.2: relative abundance of functional groups in CP-MAS NMR spectra.

Region	Site	Soil horizon	%O-alkyl-C	%Di-O-alkyl-C	%Methoxy-C	%Aromatic C	%N-alkyl-C	%Carbonyl-C	%Alkyl-C	Alkyl:O-Alkyl
		L	42.0	10.7	2.9	14.6	8.0	2.9	18.9	0.45
	MP	F	40.2	10.3	2.2	16.6	4.3	4.5	21.9	0.55
		H	42.1	10.7	1.9	13.6	3.4	4.3	24.0	0.57
Eagle		L	38.1	9.5	3.4	18.7	8.7	3.7	18.0	0.47
River	SR	F	40.7	9.5	3.1	17.6	4.7	4.2	20.3	0.50
(Cold)		H	43.2	10.9	1.9	16.3	3.8	4.6	19.3	0.45
		L	38.9	9.7	2.6	19.8	7.5	4.4	17.1	0.44
	HP	F	39.0	10.0	2.3	17.9	4.3	4.7	21.8	0.56
		H	42.7	10.9	2.6	14.3	3.2	5.1	21.2	0.50
		L	41.7	10.2	3.9	15.8	7.9	3.1	17.4	0.42
	CF	F	42.0	10.3	3.9	14.8	4.3	4.3	20.7	0.49
		H	37.6	9.1	5.3	17.9	3.2	4.6	21.8	0.58
Salmon		L	37.7	9.2	3.9	19.0	8.3	4.4	17.7	0.47
River	HB	F	38.5	9.2	4.2	15.1	5.4	4.1	23.5	0.61
(Mid)		H	39.1	9.6	3.5	13.9	4.1	4.1	25.8	0.66
		L	37.7	9.5	3.9	16.7	7.8	3.2	21.2	0.56
	TM	F	37.9	8.9	3.6	17.8	5.1	4.2	22.6	0.60
		H	41.9	10.8	2.4	15.7	4.1	4.0	21.2	0.51
		L	36.1	8.7	5.4	16.4	9.6	3.0	20.9	0.58
	MR	F	33.0	8.2	5.2	16.4	5.3	4.8	27.1	0.82
		H	32.7	7.3	4.8	15.8	4.5	5.3	29.7	0.91
Grand		L	36.3	9.1	4.6	17.1	7.8	3.6	21.6	0.60
Codroy	SH	F	33.7	9.0	3.2	18.3	5.0	4.9	25.9	0.77
(Warm)		H	34.4	8.3	4.6	15.5	3.3	5.0	28.9	0.84
		L	35.0	8.4	4.8	19.0	7.9	4.2	20.6	0.59
	OR	F	34.0	8.7	4.7	19.4	5.4	5.3	22.7	0.67
		H	34.5	7.7	5.0	16.3	3.8	5.7	27.1	0.79

Table 3.S7 Raw data for Fig. 3.2: Composition of total hydrolyzable amino acids

Region	Site	Soil horizon	%N as THAA	DI	Mol% Gly	%C as THAA
Eagle River (Cold)	MP	L	52.5	1.0	11.0	4.0
		F	53.7	1.1	11.9	5.4
		H	45.4	-1.5	12.9	4.5
	SR	L	59.3	2.6	9.9	5.3
		F	52.3	0.4	12.1	5.7
		H	40.9	-1.9	14.0	4.2
	HP	L	52.5	1.1	11.6	4.6
		F	46.0	0.6	12.8	5.1
		H	41.0	-2.5	14.2	4.5
Salmon River (Mid)	CF	L	57.4	2.0	10.5	5.4
		F	54.2	0.1	13.0	5.7
		H	37.5	-0.4	13.4	4.2
	HB	L	50.9	2.6	10.7	5.0
		F	56.6	0.2	12.4	6.8
		H	42.8	-2.2	14.3	4.5
	TM	L	59.6	1.6	10.6	4.6
		F	53.9	0.4	12.6	5.6
		H	40.7	-0.4	12.3	3.8
Grand Codroy (Warm)	MR	L	53.8	2.0	10.9	5.8
		F	40.4	-2.1	14.1	4.9
		H	42.7	-1.0	14.3	5.3
	SH	L	51.5	2.2	10.9	5.5
		F	51.5	0.6	12.4	6.6
		H	42.7	0.0	12.9	5.6
	OR	L	56.2	2.2	10.5	6.9
		F	50.5	-1.2	12.8	6.2
		H	45.1	0.3	13.2	6.3

Chapter 4

Regional differences in soil organic matter chemistry develop at the litter to soil interface

Lukas Kohl[1], Kate A. Edwards[2], Sharon A. Billings[3], Jamie Warren[1], Susan E. Ziegler[1]

[1]Department of Earth Sciences, Memorial University, St. John's, NL A1B 3X5, Canada

[2]Natural Resources Canada, Canadian Forest Service, Atlantic Forestry Centre, 26 University Drive, Corner Brook, A2H 6J3, NL, Canada

[3]Department of Ecology and Evolutionary Biology, Kansas Biological Survey, University of Kansas, 2101 Constant Ave., Lawrence, 66047, KS, USA

This chapter is intented for publication in Biogeosciences

Abstract

Environmental conditions can profoundly affect how the chemical composition of plant litter changes during decomposition. Here, we investigate the changes in plant litter chemistry during decomposition, and microorganisms that mediate this litter processing, along a latitudinal transect of boreal forests. We studied how plant litter from each region changed chemically in a one-year litterbag experiment. Decomposition changed litter chemistry in distinct ways in the different regions of the transect, so that initially similar litter acquired novel regional differences in its chemical composition despite similar degrees of mass loss. Litter from more northern regions exhibited increasing proportions of alkyl-C compounds (plant waxes and aliphatic lipids), while litter in more southern regions exhibited greater enhancement of lignin concentrations, as suggested by an increasing proportion of methoxy-C compounds. To investigate if these different decomposition trends resulted from differences in the composition and substrate use patterns of the microorganisms present in the litter to soil interface of these sites, we analyzed the composition of phospholipid fatty acids in the L horizon (0-2cm depth) and their natural abundance stable carbon isotope values ($\delta^{13}C_{PLFA}$). More southern regions exhibited lower fungi:bacteria ratios, indicating a latitudinal shift in microbial community composition. Higher $\delta^{13}C_{PLFA}$ values observed in more southern regions indicate a potential climate driven shift of microbial substrate use towards more labile compounds classes. F:B and $\delta^{13}C_{PLFA}$ values were correlated with C:N ratios, suggesting that the shift in substrate use was driven by higher nitrogen concentrations. Taken together our results suggest that in these forests litter decomposition is a key process largely influenced by litter nitrogen availability, and during which initially similar litter acquires regionally distinct chemical composition.

4.1 Introduction

Global annual litter fall is estimated to account for approximately 60 Pg of carbon (C) [Janzen, 2004]. These plant litter inputs to soil profiles can have positive or negative effects on soil organic matter (SOM) stocks. Plant litter can be sequestrated into SOM, and thus replenish SOM stocks [Prescott, 2010]. Inputs of relatively labile plant litter, however, can also stimulate the decomposition of more

stable SOM ('priming effect'), thus increasing losses of SOM [Bingeman et al., 1953, Kuzyakov et al., 2000]. The chemical composition of litter inputs is an important factor determining to which extent these inputs stimulate SOM sequestration or decomposition [Cotrufo et al., 2013, Stewart et al., 2015, Kuzyakov et al., 2015] and a key control on the chemical and biological properties of the SOM [Quideau et al., 2001, Chapter 3].

To predict how future climate changes will affect the quantity and chemical composition SOM, we therefore need to understand not only how climate affects the quantity and quality of litter produced by vegetation, but also how climate affects the processing of this litter during decomposition. Traditionally, it has been assumed that the chemistry of litter residuals can be predicted based upon the initial chemical composition of fresh litter and the mass loss alone, independent of the climate under which decomposition occurs [Coûteaux et al., 1995, Quideau et al., 2005, Mathers et al., 2007, Berg and McClaugherty, 2008, Preston et al., 2009]. However, recent studies provided evidence that the conditions during decomposition can affect how litter chemistry changes during decomposition, thus contradicting the classical concept [Steffen et al., 2007, Filley et al., 2008, Baumann et al., 2009, Wallenstein et al., 2010, Wickings et al., 2011, 2012]. The decomposition of initially identical plant litter at sites subjected to different land management practices can, for example, result in chemically distinct litter residuals after decomposition [Wickings et al., 2011, 2012]. Similarly, N fertilization prompted changes in the litter residual chemistry after 150 days laboratory incubation in low-N litter types [Baumann et al., 2009].

Key biotic agents of litter decomposition, soil microorganisms, excrete extracellular enzymes that break down distinct plant polymers (e.g., lignin and cellulose; [e.g. Sinsabaugh, 2010, Mooshammer et al., 2014]), and ultimately control which litter components are preferentially degraded or preserved during decomposition [Moorhead and Sinsabaugh, 2006]. A useful tool for examining this phenomenon is the stable carbon isotope value of microbial biomass ($\delta^{13}C_{biomass}$) which reflects, in part, the $\delta^{13}C$ of the substrates a microorganism had consumed. As such, $\delta^{13}C_{biomass}$ may allow inferences about substrate use shifts within a given microbial community [e.g., Coffin et al., 1990, Abraham et al., 1998, Cifuentes and Salata, 2001]. This approach is typically used in combination with the introduction of isotopically distinct substrates, either through the direct amendment of

labelled compounds [e.g., Waldrop and Firestone, 2004, Rinnan and Bååth, 2009, Rinnan et al., 2013] or indirectly through manipulating the $\delta^{13}C$ value of vegetation as in C3/C4 crop change or free air CO_2 enrichment experiments [Billings and Ziegler, 2005, 2008, Streit et al., 2014]. $\delta^{13}C$ values, however, also vary naturally among the plant polymers due to isotopic fractionation during biosynthesis. Indeed, the range of compound specific stable isotope values in the same plant can span 10-14‰ [Glaser, 2005]. As a general trend, chemically more labile compounds typically exhibit higher $\delta^{13}C$ values (pectin > hemicellulose > amino acids and sugars > cellulose > lignin; Glaser [2005]), with lignin typically exhibiting a depletion in ^{13}C relative to cellulose of 2-6‰ [Benner et al., 1987, Hobbie and Werner, 2004]. A similar trend has been observed in organic C residing in soil fractions, which are often used as a coarse index of substrate lability (water soluble > acid soluble > acid insoluble Biasi et al. [2005]).

Monitoring natural variations of $\delta^{13}C_{biomass}$ provides a complementary approach to detect changes in microbial substrate use patterns that provides two key advantages over label-tracing studies. First, the disturbance required for the introduction of labelled substrates can be avoided (Chapter 2). Second, this approach allows passive sampling and, therefore, can be used in studies requiring larger spatial replication [e.g., Churchland et al., 2013], and those not initially planned for stable isotope labelling studies. An increasing number of studies therefore use $\delta^{13}C$ values of respired CO_2, microbial biomass (i.e., the fraction of soil carbon that is solubilized by chloroform fumigation), or microbial biomarkers to investigate how microbial substrate use varies in response to climate and other variables [e.g. Andrews et al., 2000, Biasi et al., 2005, Cusack et al., 2011, Churchland et al., 2013].

Anthropogenic activity is predicted to lead to warming and increased N deposition in most forest ecosystems [Galloway et al., 2004, van Oldenborgh et al., 2013]. High latitude ecosystems, including boreal forests, are predicted to undergo above average warming [van Oldenborgh et al., 2013], which in turn can accelerate the natural N cycle [Hobbie et al., 2002, Philben et al., 2016] and increase N availability during litter decomposition [Podrebarac et al., 2016]. Greater temperatures and greater N availability both have the potential to change microbial substrate use patterns, and ultimately the chemical composition of the litter residuals incorporated into SOM. Kinetic theory predicts

that the decomposition of more stable organic matter - characterized by higher activation energy - becomes more favorable at greater temperatures [Conant et al., 2011]. This has been supported by a decrease of $\delta^{13}C$ values of respired CO_2 when the same soil was incubated at a higher temperature, suggesting the decomposition of a more stable carbon fraction [Andrews et al., 2000, Biasi et al., 2005], and by incubation experiments with labelled substrates of varying lability [Li et al., 2012, 2013, Ziegler et al., 2013]. In contrast, greater N availability shifts microbial substrate use towards the decomposition of more labile C substrates [DeForest et al., 2004, Craine et al., 2007], consistent with an increase in $\delta^{13}C_{biomass}$ after N fertilization and decreased activities of phenoloxidases, i.e., enzymes that degrade lignin and other complex carbon sources [Cusack et al., 2011].

Climate transects allow us to trade time for space, and enable observations of how future climate changes will affect soils, and the microbial processes that influence them. In contrast to experimental warming, climate transects capture both direct climate effects like changes in temperatures and precipitation, and indirect climate effects like changes in vegetation or climate driven increases in N availability. The Newfoundland and Labrador Boreal Ecosystem Latitudinal Transect (NL-BELT) is a transect of mesic balsam fir forests along the coast of Atlantic Canada [Ziegler et al., 2017]. Previous work on this transect has indicated that SOM stocks will be maintained in a warmer climate despite accelerated SOM decomposition [Ziegler et al., 2017]. The persistence of SOM stocks in spite of warming partly results from increased plant litter production [Ziegler et al., 2017], supported by increased soil N cycling and availability [Philben et al., 2016]. Another factor contributing to this persistence is that SOM from soils that developed under a warmer climate exhibits lower bioreactivity, i.e., is decomposed more slowly at a given temperature [Laganière et al., 2015]. We recently linked this difference in bioreactivity to changes in SOM chemistry that result from distinct litter inputs to SOM along the transect (Chapter 3). The differences in SOM chemistry stand in contrast to the apparently identical chemical composition of fresh vascular plant litter in all transect regions. Some differences in the SOM chemistry can be attributed to different proportions of moss and vascular plant inputs, whereas the the origin of other differences in SOM chemistry, specifically greater lignin concentrations in the warmer region, could not be explained moss inputs alone. In chapter 3 we therefore suggested that these differences may result from

the distinct processing of litter in the different regions of the transect due to the differences in temperature or nitrogen availability.

Here, we tested two hypotheses regarding the origin of regional difference in SOM chemistry along this transect; (1) litter has a similar initial composition in all regions of the transect, but is processed differently along the transect, resulting in chemically distinct litter residues, and (2) any distinction in litterfall processing results from compositionally distinct decomposer communities with distinct substrate use patterns. To test the first hypothesis, we conducted a one-year litterbag experiment with the local litter in each of the regions. We analyzed the chemical composition of this litter before and after decomposition by solid state nuclear magnetic resonance (CP-MAS-^{13}C-NMR) to assess if the changes in litter chemistry associated with decomposition differed among regions. To test the second hypothesis, we collected L-horizon samples in each region and analyzed the composition and δ^{13}C value of microbial biomass in these samples via phospholipid fatty acids (PLFA). We expected that temperature and N availability would exert opposite effects on microbial substrate use, such that increased temperatures in the more southern regions would shift microbial substrate use towards more stable compounds, i.e., soil microorganisms would degrade more lignin relative to carbohydrates. PLFA from more southern regions, therefore, would exhibit more negative δ^{13}C values. In contrast, greater nitrogen availability in more southern regions would shift microbial substrate use towards more labile substrates, resulting in higher $\delta^{13}C_{PLFA}$ values. This study, therefore, aims to determine whether nitrogen or temperature effects dominate the regional response of microbial substrate use in this transect.

4.2 Material and Methods

4.2.1 Field sites and sampling

This study focused on 9 field sites located in three watershed ('regions') in western Newfoundland and southeastern Labrador that form part of the Newfoundland and Labrador Boreal Ecosystem Latitudinal Transect (NL-BELT). All field sites are located within mature balsam fir (*Abies balsamea*) stands on well drained humo-ferric podzols. More southern sites are characterized by greater

mean annual temperatures (5.2 C), and higher mean annual precipitation (1575 mm a^{-1}) compared to more northern sites (0.0 C MAT, 1040 mm a^{-1} MAP; Table 3.1). More southern sites, furthermore, exhibited greater nitrogen concentrations in foliage, litter, and soils [Podrebarac et al., in preparation], likely due to accelerated soil N cycling [Philben et al., 2016]. Northern sites were characterized by higher moss cover, moss productivity, and moss derived litter in the top soil horizon, (Chapter 3, K. Buckridge pers. comm.).

4.2.2 Litterbag experiment

Needle litter was collected from the three sites in each region in late August 2012 , corresponding with the end of the growing season. Low branches were clipped from mature balsam forests trees (>10 cm diameter at breast hight) that were already loosing needles. After red and brown needles were manually removed, the branches were dried at 30 °C before needles were manually stripped. The needles from the three sites in each region were then mixed and 18 litter bags were filled with 5 g needles (dry weight equivalent). The litter bags were constructed using woven polypropylene fabric (Lumite style 6065400) with 0.25 mm x 0.5 mm mesh [Trofymow and CIDET Working Group, 1998]. Six such litter bags, containing the litter from the respective region, were placed at each of the nine field sites in between late October and mid December 2012. The litterbags were pinned to the ground with wire to ensure contact to the soil, and retrieved after 11-12 months exposure. To determine mass loss, the initial and retrieved litter were dried at 55 °C for 48h. Litter samples were then homogenized for chemical analysis using a Wiley Mini Mill 3383-L20 (Thomas Scientific, Swedesboro, NJ; mesh size 60).

Solid state NMR analysis was conducted as described in chapter 3. For each region, we analyzed one sample of initial litter (n=3) and three samples of decomposed litter that were pooled from the six replicate litter bags retrieved for each site (n=9). NMR spectra were deconvoluted using the software 'dmfit' to yield relative peak areas for 8 functional groups given as % of the total resolved peak area. The functional groups assessed and their chemical shift regions via NMR were alkyl-C (21-33 ppm), methoxy-C (56 ppm), N-alkyl-C (62-65ppm), O-alkyl-C (72-89), di-O-alkyl-C (100-105 ppm), aromatic C (117-132 ppm), phenolic C (146-155 ppm), carboxylic C (174 ppm). We

furthermore calculated the ratio of alkyl:O-alkyl carbon as alkyl-C/(O-alkyl-C + di-O-alkyl-C + methoxy-C) [Preston et al., 2009]

4.2.3 Soil analysis

The PLFA analysis conducted herein expands upon the a previous study that measured PLFA concentrations and $\delta^{13}C_{PLFA}$ in the L, F, H, and B horizons at six locations in two most extreme regions of this transect (Chapter 2). This preliminary analysis suggested that PLFA composition (fungi:bacteria ratios) and $\delta^{13}C$ values in the most shallow L horizon (0-2 cm) exhibited larger variance than in underlying horizons (F, H, B). Here, we expanded the spatial replication to a total of 26 L horizon samples from 9 sites across the three 3 regions. We compare these values to the results from deeper soil horizons reported in Chapter 2.

Soil samples were collected during a two week field campaign in late June and early July 2011. At each field site, samples were collected in three permanent sampling plots (n=27). At each plot, three 20x20 cm squares were cut out of the organic soil layer at random locations after removal of all living vegetation. These samples were then manually separated into L, F, and H horizons, pooled for each plot, and divided into subsamples for geochemical and PLFA analysis.

Samples for geochemical analysis were kept on ice during the field trip, dried (60°C for 48h), and ball milled (Retsch Mixer Mill MM200) before analysis. Soil elemental concetrations (%C, %N) and bulk stable carbon isotope values ($\delta^{13}C_{SOC}$) were analyzed by elemental analysis - isotope ratio mass spectrometry (EA-IRMS) as described in Chapter 2. One outlying %N value (>3 σ from mean of region) was excluded from all analyses.

Samples for PLFA analysis were kept on ice in the field and frozen at -18 °C after each day of field work. Samples were then freeze dried and stored in air-tight bags at +5 °C. Before analysis, samples were manually homogenized with mortar and pestle. For consistency, we closely followed the methods for PLFA extraction and analysis described in Chapter 2. Briefly, lipids were extracted with a modified Bligh-Dyer protocol, and phospholipids were isolated by solid phase extraction on silica columns, and converted to their fatty acid methyl esters (FAMEs). FAMEs were quantified by gas chromatography / flame ionization detection (GC/FID), and compound specific $\delta^{13}C$ values

were measured by gas chromatography / isotope ratio mass spectroscopy (GC/IRMS). Selected samples were analyzed by gas chromatography / mass spectroscopy (GC/MS) to confirm peak identification. Recoveries were determined by duplicate extraction, with one replicate spiked with 130 µg di-17:0-phosphatidylcholine. We found consistent recoveries of 72±3% (range 67-75%).

We quantified 25 individual PLFA in each sample (Table 4.S1), which were assigned to fungi, Gram positive bacteria, Gram negative bacteria, Actinobacteria, eukaryotic, or non-specific (general). The fungi:bacteria ratio (F:B) was calculated as the molar ratio of fungi/(Gram positive + Gram negative + actinobacteria). Compound specific δ^{13}C values were measured for 10 individual PLFA, i.e., i15:0 and a15:0 (Gram positive bacteria); 16:1ω7, 18:1ω7, cy17:0, and cy19:0 (Gram negative bacteria); 18:2w6,9 and 18:3w3,6,9 (fungi); as well as 16:0 and 18:1w9 (general). To study how the δ^{13}C values of PLFA varied relative to bulk SOM, we calculated $\Delta^{13}C_{\text{PLFA-SOM}}$ for each individual PLFA according to eq. 4.1.

$$\Delta^{13}C_{PLFA-SOC} = \delta^{13}C_{PFLA} - \delta^{13}C_{SOC}. \tag{4.1}$$

The weighted mean $\delta^{13}C_{\text{PLFA}}$ and $\Delta^{13}C_{\text{PLFA-SOC}}$ values were calculated according to equation 4.2 and 4.3, where c_i stands for the concentration of individual PLFA i, n_i for the number of C atoms of this PLFA, and $\delta^{13}C_i$ for its stable carbon isotope value.

$$\delta^{13}C_{PLFA(mean)} = \frac{\sum c_i \cdot n_i \cdot \delta^{13}C_i}{\sum c_i \cdot n_i} \tag{4.2}$$

$$\Delta^{13}C_{PLFA-SOC(mean)} = \frac{\sum c_i \cdot n_i \cdot (\delta^{13}C_i - \delta^{13}C_{SOC})}{\sum c_i \cdot n_i} \tag{4.3}$$

4.2.4 Statistical analysis

To test if litter mass loss differed among the three regions a mixed effect model with 'region' as a fixed effect and site-in-region as a random effect was used. To compare if the proportions of functional groups differed between litter exposed in the different regions we applied a one-way analyses of variance (ANOVA) followed by Tukey HSD post-hoc tests. The samples of initial litter (one from

each region) exhibited highly similar NMR spectra. We therefore grouped these samples together so that we compared four groups (initial litter, 1-year north region, 1-year mid region, 1-year south region).

We tested if PLFA concentration, composition, $\Delta^{13}C_{PLFA\text{-}SOC}$ values differed between regions with Kruskal-Wallis tests and Nemenyi post-hoc tests. These non-parametric tests were used to reduce the effect of ecological or analytical outliers. The relationship of PLFA composition and carbon stable isotope values with N availability was assessed by testing for Pearson correlations of the C:N ratio with F:B, $\delta^{13}C_{PLFA}$, and $\Delta^{13}C_{PLFA\text{-}SOC}$.

To further test if regional differences in L horizon samples were larger than in underlying horizons, we applied a two-way ANOVA with region and soil horizon as fixed effects. The mid region was excluded from this analysis because only L horizon samples had been analyzed in this region. Variance among samples was greater in L horizons compared to underlying horizons. We applied ANOVA nonetheless because F statistics are conservative when the number of replicates is greater in the more variable group (Zimmerman 2004), as was the case in our study. The actual chance of a false positive is therefore smaller than indicated by the p-values calculated in these tests. All statistical analysis was conducted in the statistical programming environment R version 3.2.3 [R Development Core Team, 2015]. Results are stated as mean ± one standard deviation (σ) unless indicated otherwise.

4.3 Results

4.3.1 Litterbag experiment

Mass loss rates of local needle foliage decreased with increasing latitude from 0.097±0.003% d-1 in the southernmost region to 0.082±0.001% d^{-1} in the northernmost region (Fig 4.1a). The total mass loss, however, varied only slightly (33.5± 1.0%, 28.3± 0.4%, and 29.7±0.4% in the southernmost, mid, and northernmost regions, respectively; Fig 4.1b) as slower mass loss in the northernmost region was compensated by slightly longer exposure (12 months) compared to the two more southern regions (11 months).

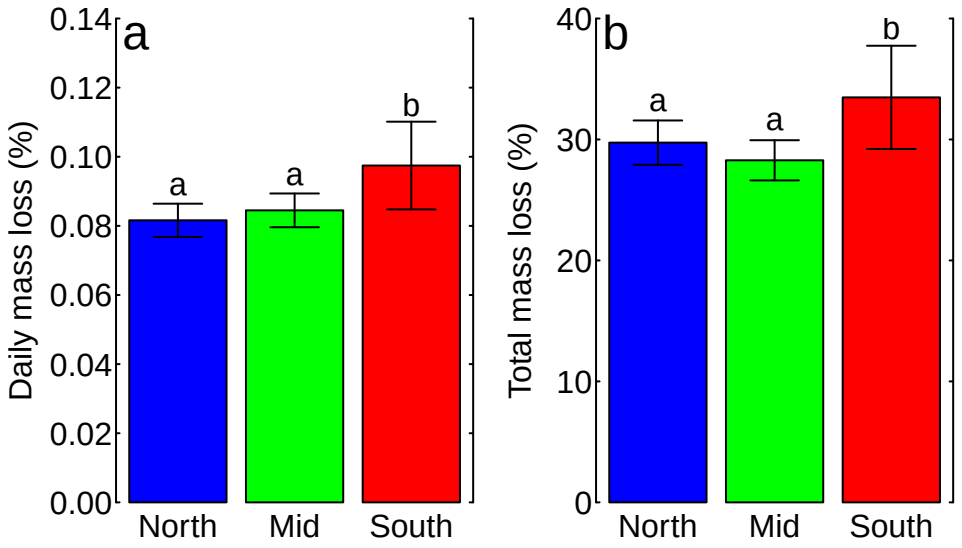

Figure 4.1 Mass loss of needle litter from sites located in the three regions following 11-12 months exposure in litter bags. (a) Daily mass loss rates calculated accounting for the different exposure times. (b) Mass loss over entire exposure time. Note that litterbags at more northern sites were exposed slightly longer (12 vs. 11 months). Letters indicate significant differences among regions according to Tukey HSD, using Site-in-Region as a random factor.

The NMR spectra of initial litter from all three regions were highly similar (Fig. 4.S1a), consistent with the results of our analysis of three years of litterfall from these sites (Chapter 3). The spectra were dominated by a large double peak in the O-alkyl region (72 and 75 ppm), representing carbohydrates. Further peaks were detected in the alkyl (26, 30, and 33 ppm; likely derived from plant waxes and lipids), in the methoxy (56 ppm; mainly lignin), N-alkyl (63 and 65 ppm, mainly protein), di-O-alkyl (98 and 105 ppm, carbohydrates), aromatic (116 and 131 ppm), phenolic (145 and 156 ppm; lignin and tannin), and carboxyl (174 ppm) regions (assignment based on Preston et al. [2000]).

Needle litter from all regions exhibited some common changes in NMR spectra during decomposition. In all regions, the O-alkyl and phenolic peaks decreased during decomposition, whereas the carboxylic peak increased slightly (Figs 4.2, 4.S1). In addition to these general changes, we also observed changes specific to the three field regions. Litter in the two northern regions, but not the southernmost region, exhibited a significant increase in the proportions of alkyl carbon (Fig 4.2). This increase occurred in particular at 20-25 ppm and 38ppm, i.e., separate from the main alkyl

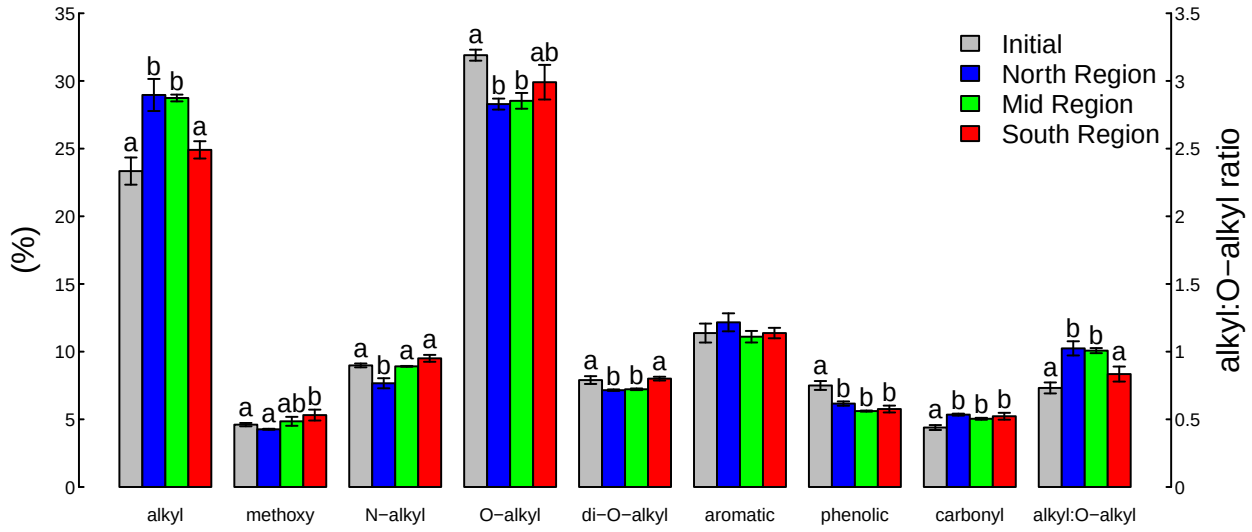

Figure 4.2 Relative abundance of functional groups and the alkyl:O-alkyl ratio derived from the MAS-CP-^{13}C-NMR results of the initial litter (grey, all regions combined), and of litter decomposed for 11-12 months in the north (blue), mid (green), or south (red) region of the transect. Letters indicate significant differences among regions using a Tukey HSD. The three samples of initial litter, one composite sample derived from all sites within each region, exhibited highly similar NMR spectra (see also Fig. 4.S1) and were combined for statistical analysis and compared to the three spatial replicates per region of litter recollected after after 11-12 months decomposition at distinct field sites in each of the regions. Letters indicate significant differences between regions (Tukey HSD test).

peaks (Fig 4.S1). In contrast, the proportion of methoxy carbon increased in the two southern, but not the northernmost region, the proportion of N-alkyl carbon decreased in the northernmost region, but not the two more southern regions, and O-alkyl carbon and di-O-alkyl carbon decreased in the two northern regions (Fig 4.2). The decomposed litter from more northern regions therefore exhibited greater abundances of methoxy carbon and N-alkyl carbon compared to decomposed litter from more southern regions (Fig 4.2, 4.S1).

4.3.2 L-horizon PLFA analysis

The 26 analyzed L horizon samples had an average PLFA concentration of 3.4 ± 0.5 mmol PLFA g-1 SOC (Fig 4.3a) with no significant differences among regions (F=1.54, p=0.243). The PLFA composition, in contrast, differed among regions. Soils from more northern sites contained greater proportions of fungal PLFA, and lower proportions of Gram positive, Gram negative and actinobacterial PLFA compared to the two southern regions (Fig 4.3b, Table 4.S1). In consequence, the two

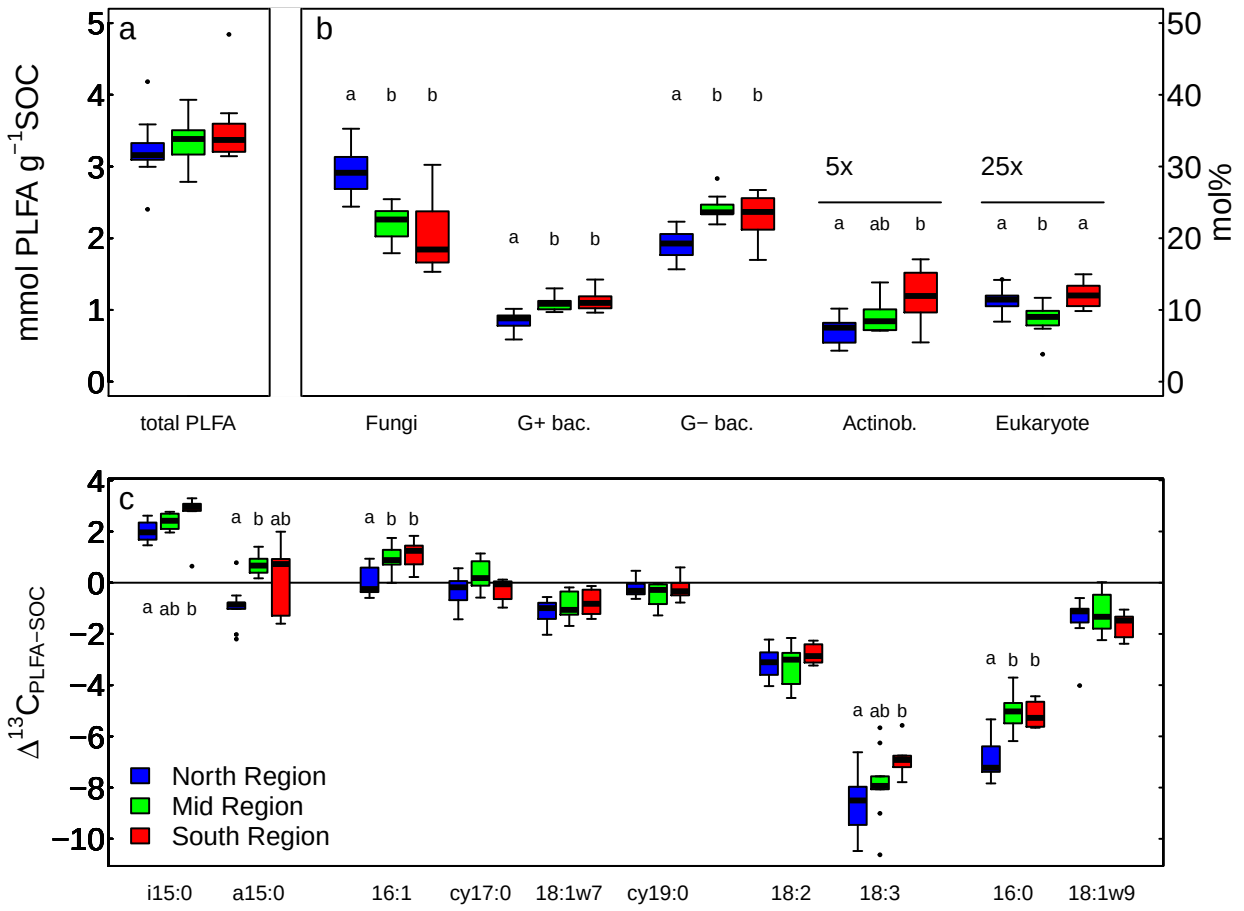

Figure 4.3 Concentration (a), mole percent (b), and stable carbon isotope values relative to bulk soil organic carbon ($\Delta^{13}C_{PLFA\text{-}SOC}$; c) values of phospholipid fatty acids (PLFA) in L horizon samples from three regions along a boreal forest latitudinal transect. Boxplots depict the mean (bold horizontal line), inter-quartile range (box) and the range of observed values (whiskers) except suspected outliers (dots). Letters indicate significant differences among regions assessed using Kruskal-Wallis and Nemenyi post-hoc tests.

southern sites exhibited lower F:B ratios than the northernmost region (Fig 4.4a, 4.4d).

PLFA from the north region exhibited more negative weighted mean $\delta^{13}C_{PLFA}$ values (-32.8‰) than PLFA from the mid and south regions (both -31.1‰, F=19.7, p<0.001). Part of this difference was explained by more negative $\delta^{13}C_{SOC}$ values in the north region (both -29.4‰) than in the mid and south regions (-28.8‰; F=6.85, p=0.005). The difference between the two most extreme regions in $\delta^{13}C_{PLFA}$ (1.7 ± 0.7‰ (95% CI)), however, was significantly larger than the difference in $\delta^{13}C_{SOC}$ (0.6 ± 0.4‰ (95% CI)). Therefore, PLFA in the north region were also more ^{13}C-depleted

Table 4.1 Regional difference in the $\delta^{13}C$ values of the phospholipid fatty acids relative to soil organic carbon ($\Delta^{13}C_{PLFA\text{-}SOC}$) and correlation with C:N.

	$\Delta^{13}C_{PLFA\text{-}SOC}$ (median)			Difference[1]	Correlation with C:N	
	North	Mid	South	South-North	R	Slope[2]
G+ bacteria						
i15:0	+2.0‰	+2.4‰	+3.0‰	+1.0‰ **	-0.42*	-0.041
a15:0	-0.8‰	+0.7‰	+0.7‰	+1.5‰ *	-0.32	-0.057
G+ bacteria						
16:17	-0.2‰	+0.9‰	+1.2‰	+1.4‰**	-0.59**	-0.068
cy17:0	-0.2‰	+0.2‰	-0.1‰	+0.1‰	-0.06	-0.006
18:17	-1.0‰	-1.1‰	-0.8‰	+0.3‰	-0.27	-0.021
cy19:0	-0.3‰	-0.3‰	-0.3‰	±0.0‰	-0.02	-0.001
Fungi						
18:26	-3.1‰	-3.0‰	-2.9‰	+0.2‰	-0.30	-0.031
18:33	-8.5‰	-7.9‰	-6.9‰	+1.8‰*	-0.57**	-0.122
General						
16:0	-7.2‰	-5.0‰	-5.3‰	+1.9‰**	-0.60**	-0.102
18:19	-1.1‰	-1.3‰	-1.5‰	-0.4‰	+0.13	0.016
Weighted mean	-3.7‰	-2.6‰	-2.3‰	+1.3‰**	-0.58**	-0.075

[1] Asterisks indicates significance levels for the Kruskal-Wallice test. *, $p<0.05$; **, $p<0.01$, ***, $p<0.001$.
[2] 2Slope is stated in ‰ per C:N unit.

relative to the bulk SOC ($\Delta^{13}C_{PLFA\text{-}SOC}$ = -3.4‰) than PLFA in the mid and south regions (-2.4‰ and -2.3‰, respectively; F=9.07, p=0.001). The F:B ratio and PLFA stable carbon isotope values (weighted mean $\delta^{13}C_{PLFA}$ and $\Delta^{13}C_{PLFA\text{-}SOC}$) were correlated to C:N ratios (Figs. 4.4,4.5), with more nitrogen rich samples containing more bacteria relative to fungi, and more ^{13}C-enriched PLFA.

This difference in weighted mean $\Delta^{13}C_{PLFA\text{-}SOC}$ values might have resulted from either (1) differences in the $\delta^{13}C_{biomass}$ values of one or more groups of microorganisms (fungi, G- bacteria, G+ bacteria), or (2) differences in community composition alone, e.g., different proportion of ^{13}C-enriched bacteria relative to ^{13}C-depleted fungi (Chapter 2). The $\Delta^{13}C_{PLFA\text{-}SOC}$ values of individual PLFA specific to fungi and bacteria indicate variations of the $\delta^{13}C_{biomass}$ of these groups independent of their abundance or of fungi:bacteria ratios. Among the ten individual PLFA analyzed, five (i15:0, a15:0, 16:0, 16:1, and 18:3) exhibited 1.0 to 1.9‰ higher $\Delta^{13}C_{PLFA\text{-}SOC}$ in the south regions compared to the north region (Table 4.1). Four of these PLFA (i15:0, 16:0, 16:1w7, 18:3) exhibited a negative correlation for $\Delta^{13}C_{PLFA\text{-}SOC}$ with the C:N ratio (Fig. 4.5) with slopes between 0.041 and 0.122‰ per C:N unit (Table 4.1). The $\Delta^{13}C_{PLFA\text{-}SOC}$ values of the other five individual PLFA (18:1w7, 18:1w9, 18:2, cy17:0, cy19:0) did not differ between regions and were not correlated with

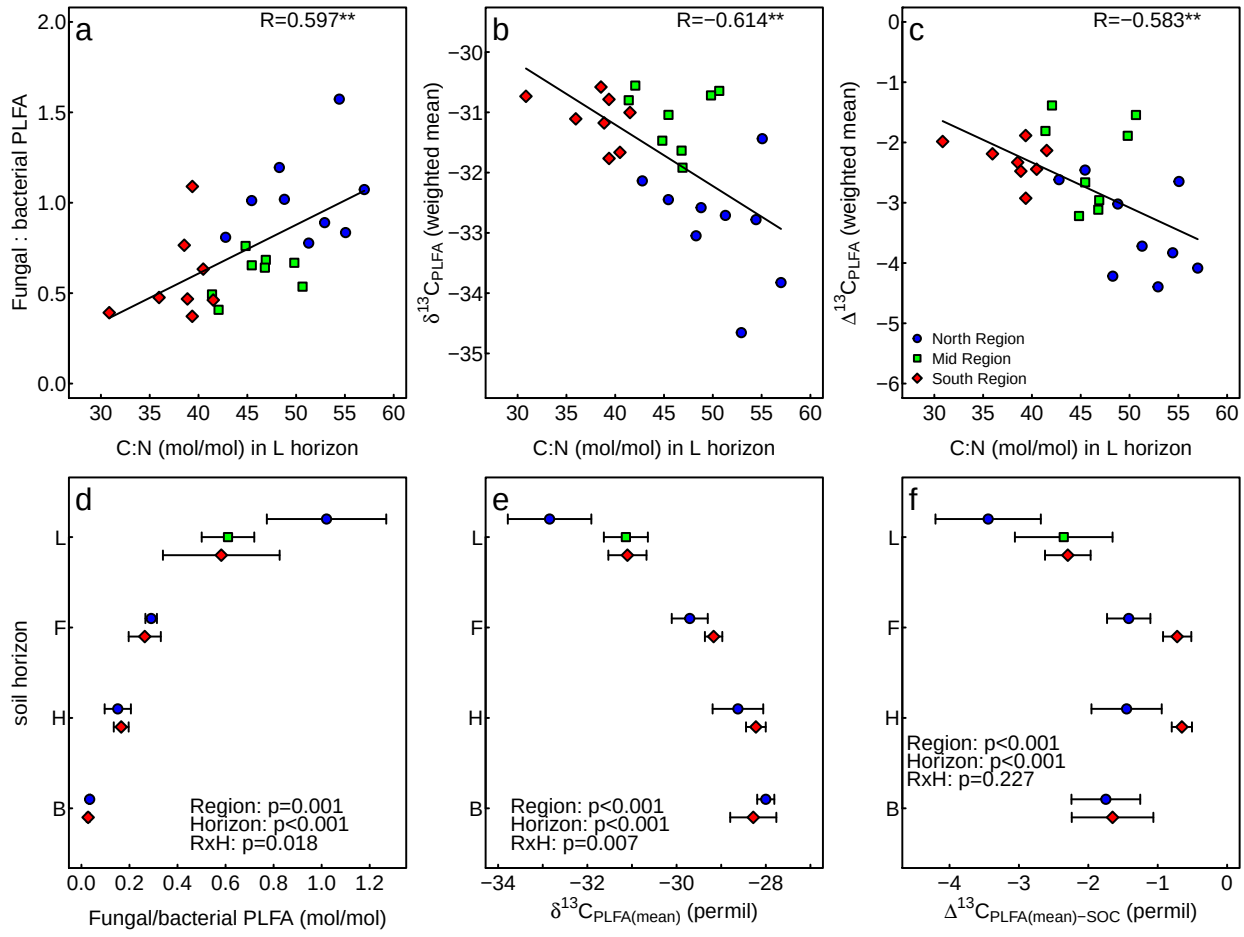

Figure 4.4 Correlation between F:B, $\delta^{13}C_{PLFA}$, and $\Delta^{13}C_{PLFA\text{-}SOC}$ with C:N in L horizon, and comparison of these three measures in L horizons and deeper soil horizons. (a-c) Correlation between the ratio of fungal to bacterial PLFA (a; F:B) and the weighted mean stable carbon isotope value of PLFA in absolute terms (b; $\delta^{13}C_{PLFA}$) and relative to bulk soil organic carbon (c; $\Delta^{13}C_{PLFA\text{-}SOC}$) with C:N in L horizon samples (n=25). (d-f) Comparison of the F:B, $\delta^{13}C_{PLFA}$), and ($\Delta^{13}C_{PLFA\text{-}SOC}$) values in L horizon samples presented herein (n=26) with deeper soil horizons at the two most extreme regions (n=6; data from Chapter 2). Values represent the regional mean and error bars indicate one standard deviation.

C:N ratios. The extent to which the $\Delta^{13}C_{PLFA\text{-}SOC}$ values of individual PLFA differed with latitude or C:N ratios did not differ significantly among PLFA associated with Gram positive bacteria, Gram negative bacteria, or fungi (Table 4.1). The greater weighted mean $\Delta^{13}C_{PLFA\text{-}SOC}$ values in more southern regions therefore resulted at least partially from higher $\Delta^{13}C_{biomass\text{-}SOC}$ values of both fungal and bacterial biomass, and not just from different proportion of fungi and bacteria across the regions.

We compared F:B, $\delta^{13}C_{PLFA}$ and $\Delta^{13}C_{PLFA\text{-}SOC}$ values from the L horizons to previous results

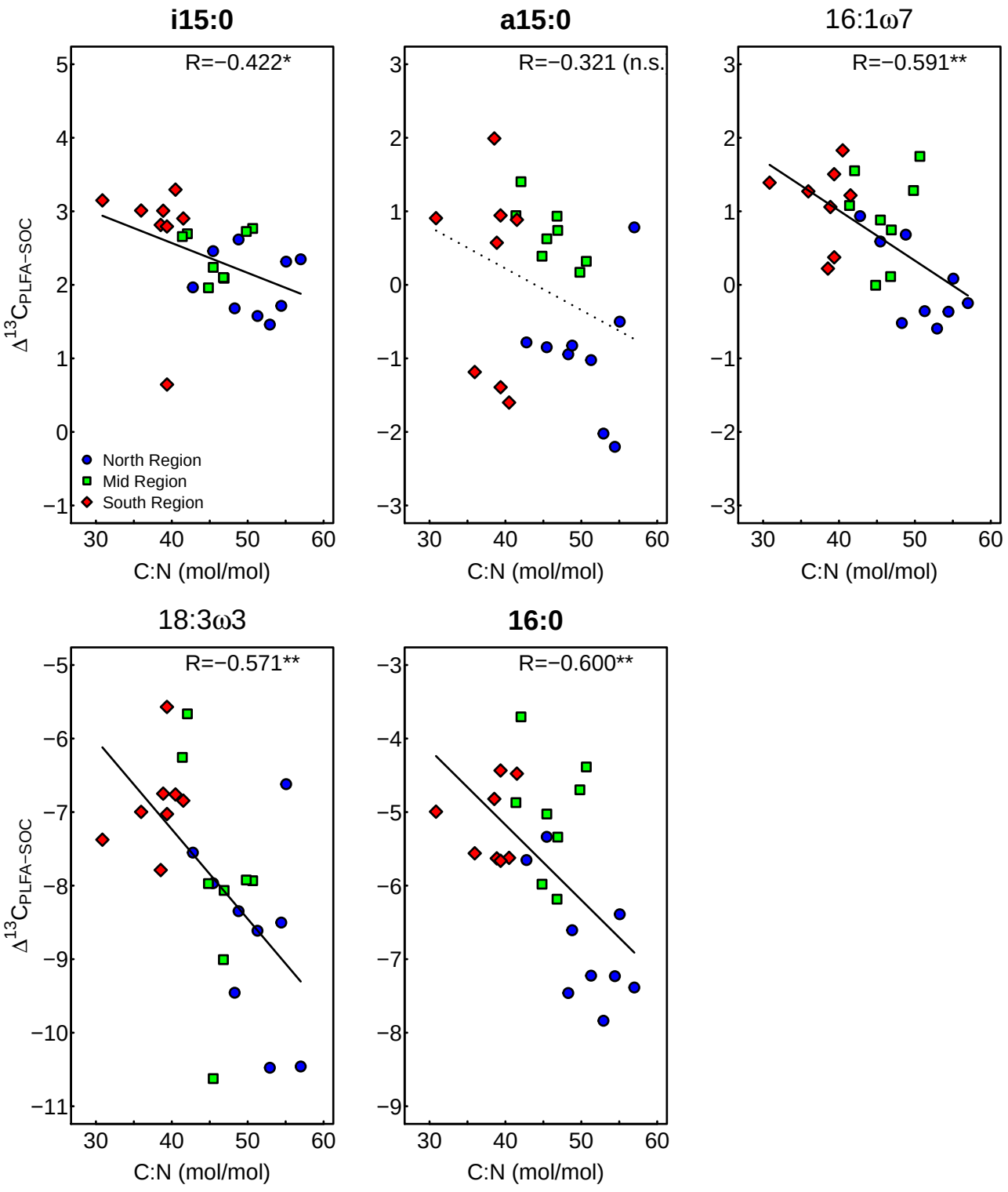

Figure 4.5 Correlation of $\Delta^{13}C_{PLFA\text{-}SOC}$ of five individual PLFA with the C:N ratio to demonstrate the observed relationship for both group specific and general PLFA. Only individual PLFA that exhibited differences among the three regions of the transect (Fig 3c) are presented. The other 5 individual PLFA did not vary among regions or covary with C:N. Dashed lines indicate linear regression trendlines in cases where no significant correlation was detected.

from deeper soil horizons to investigate if the regional differences in microbial community composition and substrate use were largely limited to the L horizon. Indeed, the regional differences in F:B and $\delta^{13}C_{PLFA}$ for the L horizons found in this study were greater than those observed in deeper soil horizons reported in Chapter 2 (Fig 4.4d, 4.4e). This was confirmed by a Region x Depth interaction in the 2-way ANOVAs (F=4.67, p=0.008 for F:B and F=4.94, p=0.006 for $\delta^{13}C_{PLFA}$). Regional differences in $\Delta^{13}C_{PLFA\text{-}SOC}$ values also decreased with depth (1.2‰ in L, 0.6‰ in F and H, no difference in B; Fig. 4.4f), but the Depth x Region interaction was not significant (F= 0.87, p=0.46).

4.4 Discussion

4.4.1 Climate influences how litter chemistry changes during decomposition

The chemical composition of needle litter inputs to SOM differ among the regions of this transect, likely due to the different climate regimes. This climate effect, however, was imprinted upon litter chemistry during decomposition rather than during plant growth. Fresh needle foliage from each of the three regions of this transect exhibited similar NMR spectra, but the same litter exhibited distinct NMR spectra after one year of in-situ decomposition. This confirmed our first hypothesis that litter is processed differently in the different regions of this transect.

Our finding that the needle litter collected in each of the three regions of the transect exhibited highly similar NMR spectra (Fig S1a) was consistent with our previous analysis of multiple years of litterfall samples from each of the field sites (Chapter 3). It is also consistent with an implicit assumption common in literature that the intra-specific variation of CP-MAS NMR spectra among litter of the same species but from different sites (e.g., in response to different climates) is negligible compared to the strong variation among distinct species. While there is a surprisingly lack of data available regarding this question, it is supported by the results presented by Preston et al. [2000]. Our previous work in this transect, however, also showed that litter from more southern regions exhibited higher %N and amino acid concentrations [Philben et al., 2016]. These greater N concentrations likely result from the accelerated turnover of N in warmer soils [Hobbie et al., 2002,

Philben et al., 2016] and stronger N retention in the warmer forests [Podrebarac et al., 2016]. This suggests that increasing needle N concentration might be a key driver of secondary climate effects that influence the chemistry and fate of SOM due to their effects on litter decomposition in the future.

The changes in litter chemistry during one year of decomposition can be grouped into (1) general decomposition trends that occurred in litter at all field sites and (2) climate effects that led to distinct changes in each of the regions. In all regions, litter exhibited a decrease in the proportions of O-alkyl-C and phenolic C and an increase in the proportion of carboxyl-C (Figs. 4.2, 4.S1), consistent with other litter decomposition studies [Preston et al., 2009]. More specifically, a decrease in O-alkyl-C during decomposition has been reported in all studied litter, and represents the decreasing concentration of carbohydrates in litter [Preston et al., 2009]. The phenolic C peaks at 145 and 156 ppm represent phenolic groups common to lignin and tannins [Preston et al., 2000]. In our study, the decrease of these two peaks was not matched by a decrease in the methoxy carbon peak, also representing lignin, suggesting that the decreases in the proportion of phenolic-C may be more attributed to a decrease in tannin concentrations with litter decomposition. Decreasing abundances of the 145 and 156 ppm peaks and tannin concentrations have been reported during the decomposition of some deciduous and coniferous tissues (aspen and tamarack) [Preston et al., 2009].

Despite similar mass loss (29 to 34%) and typical features of chemical change in litter common to all regions we observed regionally distinct changes in chemistry with decomposition that differed among the climate regions. After one year of decomposition, needle litter in the more southern regions exhibited greater proportions of methoxy-C and lower proportions of alkyl-C compared to more northern regions (Fig 2, S1), suggesting greater accumulation of lignin and less accumulation of plant waxes in more southern sites. These results stand in contrast to the effect of warming effect on forest floor organic matter found by Feng et al. [2008], who found increased lignin decomposition, and greater retention of cuticular waxes in warmed soils. However, the effect of warming on soil organic matter chemistry can be modulated by nitrogen fertilization [Pisani et al., 2015], which co-varies MAT across the regions studied in the current work. Specifically, the greater N needle

foliage in the southern region is associated with stronger lignin accumulation. Decreases in lignin decomposition after N fertilization has been reported in both pure cultures and field studies [Jeffries et al., 1981, DeForest et al., 2004]. Such stronger accumulation of lignin during litter decomposition is also consistent with the greater proportion of methoxy-C in southern-most SOM compared to more northern regions (Chapter 3). The greater proportion of methoxy-C in southern SOM, however, could not be explained by differences in the vascular plant litter, which exhibited similar proportions of methoxy-C in all regions across the transect (Chapter 3). Similarily, distinct proportions of moss litter inputs explained only one third of the greater proportion of methoxy-C in more southern soil (Chapter 3). Therefore the suppression of lignin decomposition in more southern sites, likely by greater N abundance, observed here could explain the higher proportion of methoxy-C found in the more southern soils.

These results are consistent with controlled experiments demonstrating regionally distinct changes of litter chemistry during decomposition. For example, distinct changes in litter chemistry were found when a single litter type was decomposed in plantations with different land use practices [Wickings et al., 2011, 2012]. In a similar way, N fertilization led to distinct changes in litter chemistry observed in some litter types [Baumann et al., 2009]. Here, by studying litter decomposition along a climate transect, we demonstrated that this effect is relevant under field conditions, that it contributes to the climate impacts on soils, and that it is prone to change with climate in the future.

4.4.2 Climate influences fungi:bacteria ratios and microbial substrate use through its effect on N-availability

Litter decomposition is affected by both the initial litter and environmental conditions during decomposition. By exposing the local litter from each region to decomposition within this region we evaluated ecosystem scale effects of climate on litter decomposition, capturing a range of direct (greater MAT and MAP) and indirect (greater N concentrations) climate effects. The litterbag experiment therefore demonstrated that climate causes distinct changes in litter chemistry along this transect. In contrast, our study of L horizon microbial communities and their $\delta^{13}C_{biomass}$ provides

further insight into how this climate effect on litter chemistry occurred. More specifically, these data indicated that potential climate induced increases in L-horizon N concentrations can cause a decrease in soil F:B ratio and shifts in substrate use congruent with the consumption of more labile C substrates by litter decomposers.

Incubation experiments showed that soils incubated at a higher temperature respire CO_2 with more negative $\delta^{13}C$ values; several investigators have interpreted such findings as a temperature-driven shift of microbial substrate use towards the decomposition of more stable substrates [Andrews et al., 2000, Biasi et al., 2005]. Our analysis of $\delta^{13}C_{PLFA}$ as a proxy for $\delta^{13}C_{biomass}$ found no evidence for this effect under the field conditions of a latitudinal transect. We did not observe a decrease in $\delta^{13}C_{PLFA}$ with climate warming along this transect. This was likely due to two reasons. First, the temperature range used by [Andrews et al., 2000, Biasi et al., 2005] was substantially larger (>20 C) than in our transect (5.2 C). Second, incubation experiments measure only direct temperature effects, whereas in situ studies incorporate the effects associated with long-term changes in ecosystem properties in response to climate such as increasing N concentrations. Our study indicates these nutrient-driven secondary climate effects can be more important than direct temperature effects under field conditions.

Our results indicate that the climate effect on the microbial decomposer community were primarily driven by greater N concentrations in more southern sites. Consistent with the N mining hypothesis [Craine et al., 2007], soils with greater N concentrations and lower C:N ratios exhibited greater $\delta^{13}C_{PLFA}$ values (Figs 4b-c, 5), consistent with the consumption of more labile substrates by soil microbiota. A similar increase in $\delta^{13}C_{PLFA}$ was found in a N fertilization experiment where N fertilization also led to a decrease in the activities of phenoloxidases, i.e., enzymes degrading lignin and other complex C compounds [Cusack et al., 2011]. Sites with higher N concentrations also exhibited smaller fungi:bacteria ratios. Fungi have often been associated with the degradation of lignin, in particular in fresh plant material [Strickland and Rousk, 2010]. Lower proportions of fungal relative to bacteria, therefore, are consistent with a shift of microbial substrate use from lignin to more labile and more ^{13}C-enriched plant compounds.

4.4.3 The litter inputs to L horizon interface represents a key step for climate impacts controlling SOM chemistry

Transects along gradients of expected climate changes allow us to trade time for space in order to study how ecosystems will change in the future. In the transect studied here, the forest sites within the more southern regions are characterized by greater temperature, precipitation and N availability, and are used as scenarios for how comparable but colder, northern forest could develop in a future warmer, wetter, and more N rich future. Our study of this transect provides an integrated picture of how carbon cycling may change when the forest ecosystem as a whole undergoes warming. This is different from more controlled experiments, where only belowground components are warmed or where soils are incubated under laboratory conditions. Most notably, this transect features a moderate gradient in N concentrations, representing greater N availability at more southern sites. Allochthonous N deposition decreases with latitude along this transect with total N deposition (wet + dry) decreasing by 0.05 to 0.25 g N m^{-2} a^{-1} from the southernmost to the northernmost region of the transect (Vanden Boer unpubl. data), which is in line with global estimates for the region [Vet et al., 2014]. This additional N input in more southern regions, however, represents $<$10% of the differences in annual litterfall nitrogen content, which is 3.5 g N m^{-2} a^{-1} higher in the southernmost than in the northernmost region. This indicates that the majority of the greater N uptake by primary producers in more southern regions is met through N cycling [Podrebarac et al., 2016], not by allochtonous inputs. The greater N concentration of litter and SOM in more southern region is, therefore, primarily an indirect effect of climate, rather than of the greater N deposition. Such an increase in N availability as an indirect effects of warming is consistent with global trends towards greater N limitation at higher latitude [Zechmeister-Boltenstern et al., 2015] and common in boreal ecosystems [Hobbie et al., 2002]. The impact of this decrease in N limitation due to warming is clearly observed in the decreased N content of the foliage and needle litter with increasing latitude in the sites studied here [Podrebarac et al., 2016] which appears to have ramification for how those inputs contribute to SOM chemistry.

Our results indicate that the litter to soil interface is a key zone in which the climate effects on

decomposition is imprinted upon SOM chemistry. This zone receives inputs of similar needle litter in terms of C chemistry in all regions, but produces chemically distinct SOM. The distinct chemical properties associated with the decomposition of litter, and resulting from climate induced shifts in microbial communities and their substrate use, appear to be largely preserved within underlying soil horizons, at least within the organic soil layer (Chapter 3). SOM chemistry is a key control over the rate at which SOM is decomposed under given environmental conditions (SOM bioreactivity), in particular in the absence of a mineral phase on which SOM could be stabilized [von Lützow et al., 2006]. The greater accumulation of lignin in the litter/soil interface likely contributes to the lower SOM bioreactivity in more southern site (Chapter 3). Regional differences in microbial community composition and substrate use patterns were detected in the L horizon, but not in the underlying soil horizons (Figs. 4.4d,4.4e,4.4f). We thus provide several lines of evidence that suggest predicted changes in climate represented in this transect will lead to changes in how vascular plant litter is processed during early diagenesis and how this is relevant to soil C storage in these forests.

In addition to regionally distinct changes of in litter chemistry during decomposition, changes in understory vegetation litter inputs, and specifically the proportions of non-vascular plant (moss) and needle litter inputs, have also been identified as an important control on the SOM chemistry in the organic soil horizons across this transect (Chapter 3). For some compound classes, both initial litter decomposition and moss versus needle inputs can explain the observed chemical differences. For example, lignin was more abundant in southern soils due to both greater accumulation during litter decomposition, and due to lesser proportions of lignin-poor moss litter inputs (Chapter 3). In other cases, the mechanisms had opposite effects. Alkyl-C (plant waxes and aliphatic lipids), for example, was accumulated more strongly in the northern forests, but not strongly enough to overcome the greater inputs of low alkyl-C moss litter in those colder forests (Chapter 3). Unlike vascular plant litter, moss litter exhibits few changes in NMR spectra during decomposition [Butler et al., in preparation]. The relative importance of these two climate effects – changes in the proportion of vascular and non-vascular plant inputs versus changes in how vascular plant litter during decomposition - therefore depends greatly on the relative importance of mosses in different boreal forests. Initial litter decomposition therefore might represent an even more important step controlling SOM

chemistry in many other forests, where moss litter inputs are of lesser importance. Evidence that suggest moss abundance will decrease with warming in boreal forests further emphasizes the role of the initial stages of litter decomposition in controlling soil C chemistry (Chapter 3).

In summary, this study examined where, when, and in which way climate effects can shape SOM chemistry. The decomposition occurring in the most shallow soil horizon (L) and the moss layer, and within the first years after litterfall was critical to the climate induced differences observed in soil chemistry across these mesic boreal forests. This is where indirect climate effects control how litter is processed during decomposition, in particular effects of N availability on microbial community composition and microbial substrate use patterns. In contrast, little additional differences in SOM chemistry were acquired in the deeper horizons of the organic layer, consistent with similar microbial communities and substrate use patterns in these horizons (Chapter 2). In other words, climate effects are rapidly imprinted upon SOM chemistry, and preserved largely unmodified for the turn-over time of the organic soil horizons (decades in H horizons).

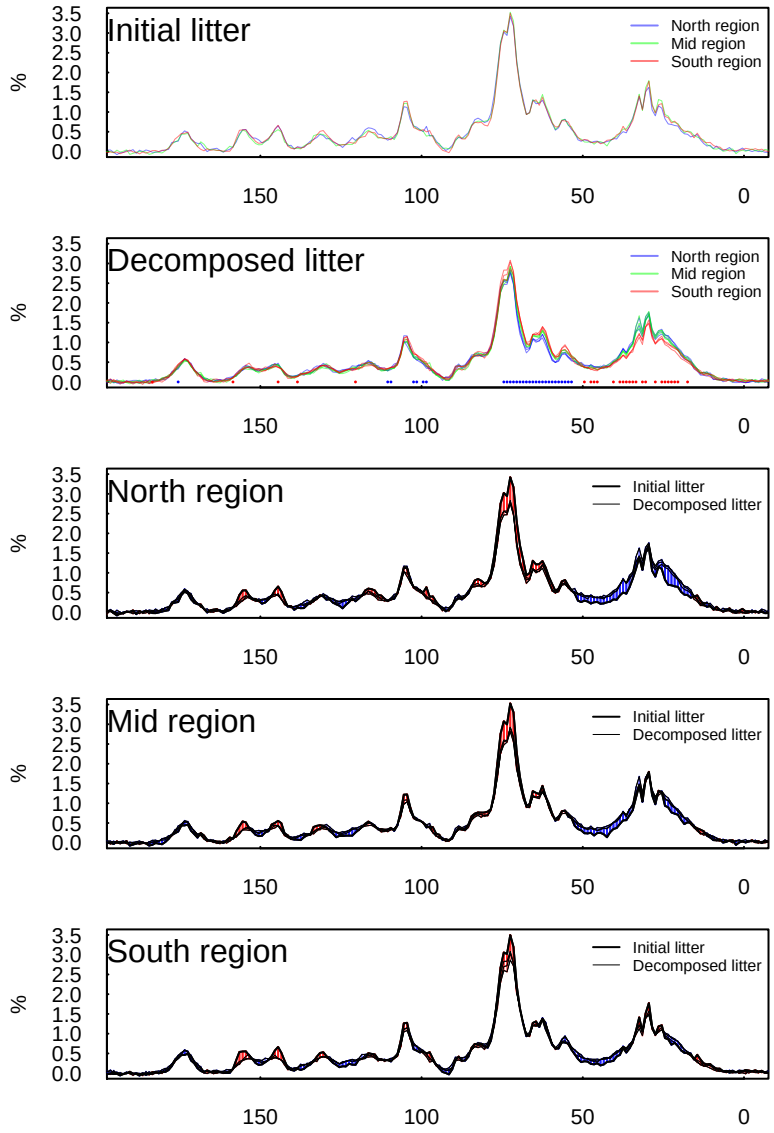

Figure 4.S1 CP-MAS NMR spectra of fresh and decomposed litter. (a) NMR spetra of needle foliage collected in three regions of a climate transect and used for the decompostion experiment. Note the similarity of NMR spectra. (b) NMR spectra of local litter after 11-12 months of in-situ decomposition at three replicate regions. Red and blue dots below the spectrum indicate chemical shifts where a monotonous increase (red) or decrease (blue) with latitude was found (Spearman correlation test for each ppm step). (c,e,f) Comparison of NMR spectra before and after decomposition in each regions. Blue areas indicate spectral regions that decreased in abundance during decomposition, red areas spectral regions that increased during decomposition. All spectra have been normialized to a total area of 100 pmm $\times$ %.

Table 4.S1 Concentrations of individual PLFA in L horizon soil samples from three regions in µmol g^{-1} SOC.

	Northern Region (ER)		Mid Region (SR)		Southern Region (GC)	
	mean	SD	mean	SD	mean	SD
Gram positive bacteria						
i15:0	124	51	135	26	154	51
a15:0	72	26	102	13	93	29
15:0	32	8	39	4	33	8
i16:0	52	29	43	7	58	16
i17:0	25	22	19	2	30	23
br17:0	65	39	28	4	88	54
br19:0	18	21	14	3	16	13
Gram negative bacteria						
16.1w7	173	48	221	37	218	78
16:1a	23	16	20	4	34	21
16.1b	14	9	15	2	19	13
16:1c	63	28	66	9	88	45
cy17:0	72	29	90	9	102	61
18:1b	312	229	265	27	384	265
18:1c	38	13	31	5	67	81
cy19:0	249	243	120	28	246	198
Actinobacteria						
10Me-16:0	72	44	43	15	95	43
10Me-17:0	16	6	19	3	15	3
Fungi						
18:2w6.9	487	317	652	108	429	302
18:3w3.6.9	95	86	93	29	59	51
Eukaryots						
18:3w6.9.12	15	7	12	3	19	14
20:0	33	10	41	7	39	17
General						
14:0	33	16	58	10	39	19
16:0	549	203	671	75	567	210
18:0	94	27	135	15	104	58
18:1w9c	359	87	415	54	413	135
Sum all PLFA	3087	678	3347	333	3409	1050
Sum Fungi	582	399	745	129	487	354
Sum G+ bacteria	371	141	367	50	459	147
Sum G- bacteria	923	559	808	101	1123	712
Sum Actinobacteria	89	49	62	17	110	44
Sum Eukaryotes	15	7	12	3	20	14
Fungi:Bacteria	0.42	0.53	0.60	0.77	0.29	0.39

Chapter 5

Exploring the metabolic potential of microbial communities in ultra-basic, reducing springs at The Cedars, CA, USA: Experimental evidence of microbial methanogenesis and heterotrophic acetogenesis

Lukas Kohl[1], Emily Cumming[1], Alison Cox[1], Amanda Rietze[1], Liam Morrissey[1], Susan Q. Lang[2], Andreas Richter[3], Shino Suzuki[4], Kenneth H. Nealson[5], Penny L. Morrill[1]

[1]Department of Earth Sciences, Memorial University, St. John's, NL A1B 3X5, Canada

[2]Department of Earth and Ocean Sciences, University of South Carolina, Columbia, SC 29208, USA

[3]Division of Terrestrial Ecosystem Research, Department of Microbiology and Ecosystem Science, University of Vienna, 1090 Vienna, Austria

[4]Microbial and Environmental Geomicrobiology, Japan Agency for Marine-Earth Science and Technology, Kochi, 783-8502, Japan

[5]Department of Earth Sciences, University of Southern California, Los Angeles, CA 90089, USA

This chapter was originally published in the Journal of Geophysical Research - Biogeosciences 124:13-26. [Kohl et al., 2016]. The Supporting Information provided with the original publication can be found on pages 163 to 169.

Abstract

Present-day serpentinization generates groundwaters with conditions (pH>11, Eh<-550mV) favorable for the microbial and abiotic production of organic compounds from inorganic precursors. Elevated concentrations of methane, C_2-C_6 alkanes, acetate, and formate have been detected at these sites, but the microbial or abiotic origin of these compounds remains unclear. While geochemical data indicate that methane at most sites of present-day serpentinization is abiogenic, the stable carbon, hydrogen, and clumped isotope data as well as the hydrocarbon gas composition from The Cedars, CA, USA, are consistent with a microbial origin for methane. However, there is no direct evidence of methanogenesis at this site of serpentinization. We report on laboratory experiments in which the microbial communities in fluids and sediments from The Cedars were incubated with ^{13}C labeled substrates. Increasing methane concentrations and the incorporation of ^{13}C into methane in live experiments, but not in killed controls, demonstrated that methanogens converted methanol, formate, acetate (methyl group), and bicarbonate to methane. The apparent fractionation between methane and potential substrates ($\alpha^{13}C_{CH_4\text{-}CO_2(g)}$=1.059 to 1.105, $\alpha^{13}C_{CH_4\text{-acetate}}$=1.042 to 1.119) indicated that methanogenesis was dominated by the carbonate reduction pathway. Increasing concentrations of volatile organic acid anions indicated microbial acetogenesis. $\alpha^{13}C_{CO_2(g)\text{-acetate}}$ values (0.999 to 1.000), however, were inconsistent with autotrophic acetogenesis, thus suggesting that acetate was produced through fermentation. This is the first study to show direct evidence of microbial methanogenesis and acetogenesis by the native microbial community at a site of present-day serpentinization.

5.1 Introduction

5.1.1 Geochemistry of Serpentinization-Associated Fluids

Serpentinization is the geochemical alteration of ultramafic rocks in contact with water [Moody, 1976]. The oxidation and hydration of these rocks generates ultra-basic and highly reducing fluids (pH>11; Eh<-550mV) with elevated concentrations of H_2 and Ca^{2+} [Barnes et al., 1967, Sleep et al., 2004, McCollom and Seewald, 2013, Schrenk et al., 2013]. Conditions in fluids in many serpentinizing systems are amenable to the abiotic reduction of inorganic carbon to simple organic compounds through Fisher-Tropsch type reactions [McCollom, 2013]. Elevated concentrations of methane and C_2-C_6 alkanes along with acetate and formate have been detected in many serpentinization-associated fluids [Lang et al., 2010, Etiope and Sherwood Lollar, 2013]. The H_2 generated through serpentinization may support chemolithotrophic life in the deep biosphere [Bach and Edwards, 2003, Sleep et al., 2004].

Present-day serpentinization occurs along the axis of slow spreading marine ridges [Kelley et al., 2005], in ancient seafloor deposits in billions-of-year-old Precambrian shield rocks [Sherwood Lollar et al., 1993], and terrestrially at sites where ocean crust has been obducted and exposed above sea level [Barnes et al., 1967, Neal and Stanger, 1983, Abrajano et al., 1990, Fritz et al., 1992, Hosgörmez, 2007, Morrill et al., 2013, Szponar et al., 2013, Sánchez-Murillo et al., 2014]. Where serpentinization-associated fluids discharge to the surface at marine vents and terrestrial springs, Ca^{2+} precipitates as travertine ($CaCO_3$), forming chimneys (marine sites) or pools (terrestrial sites). These structures act as portals that allow the exchange of material between surface and subsurface and provide a window through which researchers can study subsurface ecosystems. These sites of discharge are characterized by steep gradients of pH and redox potentials, which supply the energy that can power dense microbial life as seen in the biofilms of the carbonate chimneys of the Lost City hydrothermal field [Kelley, 2005, Schrenk et al., 2013] and elsewhere.

There has been recent interest, largely generated by Kelemen and Matter [2008], in the potential of terrestrial ultramafic deposits for use in CO_2 sequestration. These projects are based on the injection of CO_2 into ophiolitic groundwaters to stimulate CaCO3 precipitation [Kelemen and Matter, 2008]. Biotic and abiotic processes that convert inorganic carbon to CH_4 and other organic species may compete with this $CaCO_3$ precipitation. Furthermore, if CH_4 is a by-product of CO_2 sequestration, the higher radiative forcing of CH_4 produced compared to CO_2 consumed could lead to a negative net greenhouse gas balance of such CO_2 sequestration projects.

5.1.2 Microbial Processes in Serpentinization-Associated Fluids

The H_2 generated through serpentinization is a source of energy that may be utilized by chemosynthetic microorganisms, such as autotrophic methanogens (equation 5.1a) or acetogens (equation 5.1b).

$$CO_3^{2-} + 4H_2 + 2H^+ \rightarrow CH_4 + 3H_2O \tag{5.1a}$$

$$2CO_3^{2-} + 4H_2 + 3H^+ \rightarrow CH_3COO^- + 4H_2O \tag{5.1b}$$

Heterotrophic methanogens can utilize H_2 to reduce organic C_1 compounds like formate and methanol (equations 5.2a and 5.2b).

$$HCOO^- + 3H_2 + H^+ \rightarrow CH_4 + 2H_2O \tag{5.2a}$$

$$CH_3OH + H_2 \rightarrow CH_3COO^- + H_2O \tag{5.2b}$$

Furthermore, reducing conditions and high concentrations of acetate make fluids associated with serpentinization amenable to heterotrophic methanogenesis through the disproportionation of acetate (equation 5.3).

$$CH_3COO^- + H_2O \rightarrow CH_4 + CO_3^{2-} + H^+ \tag{5.3}$$

Microbial life (bacteria and archaea) has been found in serpentinization-associated fluids discharging at hydrothermal vents and ultra-basic springs [Schrenk et al., 2004, Brazelton et al., 2006, 2012, Blank et al., 2009, Suzuki et al., 2013, Szponar et al., 2013, Tiago and Veríssimo, 2013, Sánchez-Murillo et al., 2014, Woycheese et al., 2015, Meyer-Dombard et al., 2015, Quéméneur et al., 2015] and in subsurface ecosystems directly accessed through drilling [Daae et al., 2013, Crespo-Medina et al., 2014]. These microorganisms may produce, mineralize, or transform the organic compounds in such fluids. Thus far, it remains unclear to what degree the organic compounds in these fluids are produced by biogenic or abiogenic processes, and how microbial activity modifies the composition of these organic compounds McCollom and Seewald [2007], Schrenk et al. [2013].

So far, efforts to distinguish between biogenic and abiogenic origins of organic compounds in serpentinization-associated fluids focused on methane and other low molecular weight hydrocarbon gases. $\delta^{13}C_{CH_4}$ and $\delta^{2}H_{CH_4}$ values indicate that despite the potential for microbial methanogenesis, the primary source of methane is nonmicrobial (i.e., abiotic or thermogenic) at most terrestrial sites of serpentinization of Phanerozoic age [Neal and Stanger, 1983, Abrajano et al., 1990, Fritz et al., 1992, Sherwood Lollar et al., 1993, 2002, Hosgormez et al., 2008, Proskurowski et al., 2008, Etiope et al., 2011, 2013, Szponar et al., 2013, Suda et al., 2014]. Additionally, methanogens were rarely found in the metagenome of terrestrial serpentinization-associated ecosystems; however, their detection is becoming more common [Blank et al., 2009, Sánchez-Murillo et al., 2014, Quéméneur et al., 2015, Woycheese et al., 2015]. To our knowledge, no successful isolation of methangens from such a site has been reported.

Microbial methanogenesis, however, has not been ruled out as a source of methane at

The Cedars, a complex of ultra-basic, reducing springs located in Sonoma County, CA, USA [Morrill et al., 2013]. At this site, the stable isotope values ($\delta^{13}C_{CH_4}$=-68‰and $\delta^{2}H_{CH_4}$=-333‰) and the CH_4/C_{2+} ($<10^3$) of methane and other gaseous hydrocarbons exsolving from one spring (NS1) were typical of microbially sourced methane [Morrill et al., 2013, Wang et al., 2015], whereas the $\delta^{13}C$ values and CH_4/C_{2+} ratios at two other springs (BSC and CS1/GPS) were more enriched in ^{13}C and had $CH_4/C_{2+}<10^3$, suggesting a mixture of microbial and nonmicrobial methane [Morrill et al., 2013]. A microbial origin of methane is further indicated by nonequilibrium methane "clumped isotope" values ($\Delta^{13}CH_3D$) [Wang et al., 2015]. A study of the microbial diversity at The Cedars detected only a single archaeal OTU (Phylotype Ced_A01), which was present in springs fed by both deep groundwater and in springs fed by a mixture of deep and shallow groundwaters [Suzuki et al., 2013]. This OTU belongs to the order Methanosarcinales; however, the sequence was not part of any known methanogen or anaerobic methanotroph clades. So far, it remains unclear whether "Phylotype Ced_A01" is capable of methanogenesis.

Because stable carbon and hydrogen isotope values of methane, and microbial community surveys provide indirect evidence for microbial methanogenesis, we conducted a series of microcosm experiments (Table 5.1) to test for direct evidence of the metabolic potential of the microbial communities present at The Cedars. We designed these laboratory experiments to (a) test whether microbial communities native to springs and sediments at The Cedars are capable of methanogenesis under high-pH conditions, (b) investigate the range of substrates that can be utilized by methanogens, and (c) provide empirical estimates of the apparent fractionation of carbon and hydrogen isotopes in microbial methanogenesis under conditions similar to those found at The Cedars.

Table 5.1 Overview over microcosm experiments.

Experiment	Treatment	Sampling date	Total Vial Volume	Suspended Sedinement	Fluid	Mineral Nutrients	CAPS buffer	Initial pH	Headspace[1]	Natural Abundance Substrate[2]	^{13}C-labeled substrate[2]	$HgCl_2$
Formate	Live	July 2014	100 ml	2 ml	30 ml	14 ml	14 ml	11-12	32 ml N2	1.18 mM formate	–	–
	Killed	July 2014	100 ml	2 ml	30 ml	14 ml	14 ml	11-12	32 ml N2	1.18 mM formate	–	100 mg/L
	^{13}C-labeled Live	July 2014	100 ml	2 ml	30 ml	14 ml	14 ml	11-12	32 ml N2	0.88 mM formate	3 µM ^{13}C-formate	–
	^{13}C-labeled Killed	July 2014	100 ml	2 ml	30 ml	14 ml	14 ml	11-12	32 ml N2	0.88 mM formate	3 µM ^{13}C-formate	100 mg/L
Acetate	Live	July 2014	100 ml	2 ml	30 ml	14 ml	14 ml	11-12	32 ml N2	1.18 mM acetate	–	–
	Killed	July 2014	100 ml	2 ml	30 ml	14 ml	14 ml	11-12	32 ml N2	1.18 mM acetate	–	100 mg/L
	$^{13}C_1$-labeled Live	July 2014	100 ml	2 ml	30 ml	14 ml	14 ml	11-12	32 ml N2	0.88 mM acetate	3 µM $^{13}C_1$-acetate	–
	$^{13}C_1$-labeled Killed	July 2014	100 ml	2 ml	30 ml	14 ml	14 ml	11-12	32 ml N2	0.88 mM acetate	3 µM $^{13}C_1$-acetate	100 mg/L
	$^{13}C_2$-labeled Live	July 2014	100 ml	2 ml	30 ml	14 ml	14 ml	11-12	32 ml N2	0.88 mM acetate	3 µM $^{13}C_2$-acetate	–
	$^{13}C_2$-labeled Killed	July 2014	100 ml	2 ml	30 ml	14 ml	14 ml	11-12	32 ml N2	0.88 mM acetate	3 µM $^{13}C_2$-acetate	100 mg/L
Methanol	Live	July 2014	100 ml	2 ml	30 ml	14 ml	14 ml	11-12	32 ml N2	1.18 mM methanol	–	–
	Killed	July 2014	100 ml	2 ml	30 ml	14 ml	14 ml	11-12	32 ml N2	1.18 mM methanol	–	100 mg/L
	^{13}C-labeled Live	July 2014	100 ml	2 ml	30 ml	14 ml	14 ml	11-12	32 ml N2	0.88 mM methanol	3 µM ^{13}C-methanol	–
	^{13}C-labeled Killed	July 2014	100 ml	2 ml	30 ml	14 ml	14 ml	11-12	32 ml N2	0.88 mM methanol	3 µM ^{13}C-methanol	100 mg/L
Bicarbonate	Live	July 2014	100 ml	2 ml	30 ml	14 ml	14 ml	11-12	32 ml N2	1.18 mM bicarbonate	–	–
	Killed	July 2014	100 ml	2 ml	30 ml	14 ml	14 ml	11-12	32 ml N2	1.18 mM bicarbonate	–	100 mg/L
	^{13}C-labeled Live	July 2014	100 ml	2 ml	30 ml	14 ml	14 ml	11-12	32 ml N2	0.88 mM bicarbonate	3 µM ^{13}C-bicarbonate	–
	^{13}C-labeled Killed	July 2014	100 ml	2 ml	30 ml	14 ml	14 ml	11-12	32 ml N2	0.88 mM bicarbonate	3 µM ^{13}C-bicarbonate	100 mg/L
Nutrients	Live	August 2013	160 ml	10 ml	60 ml	14 ml[3]		11-12	86 ml air	1160 ppm CO	–	–
	Killed	August 2013	160 ml	10 ml	60 ml	14 ml[3]		11-12	86 ml air	1160 ppm CO	–	100 mg/L
	^{13}C-labeled Live	August 2013	160 ml	10 ml	60 ml	14 ml[3]		11-12	86 ml air	1160 ppm CO	116 ppm ^{13}C-CO	–
	^{13}C-labeled Killed	August 2013	160 ml	10 ml	60 ml	14 ml[3]		11-12	86 ml air	1160 ppm CO	116 ppm ^{13}C-CO	100 mg/L

[1] Microcosms with N_2 headspace were prepared anaerobically in a nitrogen filled glove bag. Microcosms with air headspace were aerated during preparation.
[2] Final concentration in solution (formate, acetate, methanol, bicarbonate) or headspace (CO).
[3] A buffered mineral medium was used for this experiment.

5.2 Site Description

The Cedars refers to a block of peridotite (3.5km wide, 6.4km long, and 1–2km deep) situated in the northwestern section of Sonoma County, CA, USA (N38° 37' 14.84", W123° 08' 02.13").The Cedars is located in the interior of an ultramafic zone that is part of the North California Coastal Range. The peridotite was obducted onto the continent before or during the middle of the Jurassic [Coleman, 2000], which makes it a relatively young ophiolite. For a detailed description of The Cedars see Barnes et al. [1967] and Coleman [2000]. Ultra-basic and reducing groundwater discharges from multiple points along the talus slopes and creek beds within the ophiolite. Many of these springs create ultra-basic reducing pools within travertine and bubble with hydrogen and methane-rich gas mixtures. Multiple springs in close proximity make up spring complexes such as the Barnes Spring Complex (BS). The geochemistry of many of these springs was published in Morrill et al. [2013], whose 6 year study noted little variation in the geochemistry of the springs within a complex and over time. A brief summary of the geochemical characteristics of the fluids discharging from the BS is provided in Table 5.2.

5.3 Material and Methods

5.3.1 Bicarbonate and Organic Acid Amended Microcosms

We conducted a set of microcosm experiments to test if the microbial communities in spring fluids and carbonate sediments at The Cedars were capable of converting amended substrates to methane. The carbonate was of particular interest because a previous laboratory study found that microorganisms isolated from The Cedars were not able to grow without the addition of solid calcium carbonate and reported that the microorganisms aggregated on the surface of the carbonate [Suzuki et al., 2014]. Spring fluid and carbonate sediment were

Table 5.2 Physical and chemical characteristics of spring BS5.

Parameter	Unit	Sampling date	Mean[1]	1σ[1]	Source
Temperature	C	2007-2012	17.4	0.5	[Morrill et al., 2013]
pH		2007-2012	11.6	0.1	[Morrill et al., 2013]
Eh	mV	2007-2012	-585	33	[Morrill et al., 2013]
Conductivity	µS cm^{-1}	2007-2012	870	70	[Morrill et al., 2013]
DOC	mmol L^{-1}	2013	0.13		This study
$\delta^{13}C_{DOC}$	‰	2013	-17.8		This study
TIC	mmol L^{-1}	2007-2012	0.07		[Morrill et al., 2013]
$\delta^{13}C_{TIC}$	‰	2007-2012	-32.6		[Morrill et al., 2013]
$\delta^{13}C_{CH_4}$	‰	2014	-63.5		This study
$\delta^{2}H_{CH_4}$	‰	2013-2014	-346	7	[Wang et al., 2015]; this study
$\Delta^{13}CH_3D$	‰	2013-2014	-3.2	0.4	[Wang et al., 2015]
Formate	µmol L^{-1}	2013-2014	<1 to 1.5		This study
Acetate	µmol L^{-1}	2013-2014	47.5	2.3	This study
Propionate	µmol L^{-1}	2013-2014	<1		This study
Butyrate	µmol L^{-1}	2013-2014	2.8	0.4	This study
Lactate	µmol L^{-1}	2013-2014	<1		This study
$\delta^{2}H_{H_2O}$	‰	2007-2013	-37		[Morrill et al., 2013]
$\delta^{18}O_{H_2O}$	‰	2007-2013	-5.7		[Morrill et al., 2013]

[1] Mean and one standard deviations among values measured in samples collected at different dates.

collected from Barnes Spring 5 (BS5) in July 2014. Fluid was collected in 1L glass bottles prefilled with N_2. The bottles were completely submerged in the ultra-basic reducing pool of BS5 before opening the bottle to allow the pool fluid to replace the gas in the bottle, leaving <50 mL gas headspace. The bottle was then capped while submerged. Carbonate sediment slurry from the bottom of the ultra-basic pool was captured in multiple sterile 50 mL falcon tubes, which were sealed underwater without headspace and kept sealed until experimental setup. Microcosms were prepared using an anaerobic, N_2-filled glove bag within 7 days after sampling. We tested the redox potential of the water during setup to confirm that its Eh (-602 mV) was similar to the redox potential measured previously in the field (-612 mV) [Morrill et al., 2013]. A total of 54 microcosms were assembled in 100 mL serum vials by mixing 2 mL of sediment slurry with 30mL of reducing water. We furthermore added 14 mL of 15 $mmolL^{-1}$ N-cyclohexyl-3-aminopropanesulfonic acid (CAPS) buffer and 14mL of mineral element solution growth (DSMZ medium 81) to each microcosm to match field conditions (pH11–12) and ensure that chemoautotrophs were not nutrient limited. Each

microcosm thus contained 68 mL fluid and 32 mL headspace. Vials were then capped with blue butyl septa that were conditioned as described by Oremland et al. [1987].

The microcosms were randomly assigned to four substrate amendment experiments: formate, acetate, methanol, and bicarbonate (Table 5.1). The formate, methanol, and bicarbonate amendment experiments each consisted of four experimental treatments: Live, ^{13}C-labeled Live, Killed, and ^{13}C-labeled Killed. All treatments were conducted in three replicate microcosms. Live and Killed treatments received 0.8mL of a 100 mM solution of the respective carbon substrate, ^{13}C-labeled Live and ^{13}C-labeled Killed treatments received 0.2 mL of 1 mM solution of the 99% ^{13}C labeled substrate (Cambridge Isotope Laboratories) and 0.6 mL of a solution of the nonlabeled substrate (100 mM). Killed, and ^{13}C-Killed treatments furthermore received a saturated $HgCl_2$ solution (7.5% w/v) such that their final $HgCl_2$ concentrations were 100 mgL^{-1}. Microbial methanogenesis thus would be indicated by the production of ^{13}C enriched methane in ^{13}C-labeled Live microcosms relative to Live microcosms. The absence of such an enrichment in ^{13}C-Killed relative to Killed microcosms would further demonstrate that the labeled substrate was not abiotically converted to methane.

In the acetate amendment experiment, we added either acetate with natural abundance of ^{13}C or one of two position-specific labeled isotopomers of acetate (i.e., $^{13}CH_3COO^-$ and $CH_3{}^{13}COO^-$), resulting in six experimental treatments (Live, $^{13}C_1$-labeled Live, $^{13}C_2$-labeled Live, Killed, $^{13}C_1$-labeled Killed, and $^{13}C_2$-labeled Killed). Given that acetate fermentation (equation 5.3) leads to the position-specific production of methane and inorganic carbon (i.e., the methyl group is converted to methane and the carboxyl group is converted to $CO_3{}^{2-}$), acetate fermentation would produce methane enriched in ^{13}C (relative to "Live" microcosms) in $^{13}C_2$-labeled Live microcosms but not $^{13}C_1$-labeled Live microcosms.

Methane concentrations were monitored in the incubations, and stable isotope values of CH_4 were measured at the beginning and the end of each experiment. Experiments were

terminated when sufficient methane for $\delta^{13}C$ and $\delta^{2}H$ analysis was produced in the headspace. Formate, acetate, and bicarbonate amended microcosms were terminated sooner (91 days) than the methanol amended microcosms (198 days) because CH_4 was produced at a faster rate in these experiments. Microcosms were then opened and sampled for the analysis of concentrations and $\delta^{13}C$ of total inorganic carbon (TIC), volatile organic acid (VOA) anions, and the water's stable hydrogen and oxygen isotope values ($\delta^{2}H_{H_20}$ and $\delta^{18}O_{H_20}$).

5.3.2 Nutrient Amended Microcosms

Another microcosm experiment was set up using material collected in August 2013. The experiment was initially intended to test for microbial carbon monoxide utilization. However, no detectable amounts of CO were fixed or oxidized (Figure 5.S1). We therefore refer to these microcosms as "nutrient amended." We report on this experiment here because it demonstrated that methanogenesis also occurred spontaneously and in the absence of amended substrates.

Twelve microcosms were constructed by transferring 10 mL of suspended sediment, 60mL fluid, and 14mL of mineral element solution (buffered to pH 11–12 with 15 mmol L^{-1} CAPS) to 160 mL serum vials. The microcosms thus contained a total fluid volume of 74mL and a headspace of 86mL. The microcosms were allowed to equilibrate with lab air during experimental setup. They were then capped with blue butyl septa, and 200 μL carbon monoxide (CO) was added to the headspace of each vial. Additional details of the experimental setup are described by Morrill et al. [2014].

The 12 microcosms were randomly assigned to one of four treatments, i.e., Live, Killed, ^{13}C-labeled Live, and ^{13}C-labeled Killed (n=3). Microbial activity was inhibited in Killed and ^{13}C-Killed microcosms by adding a saturated $HgCl_2$ solution, resulting in a final concentration of ∼100 mg L^{-1} $HgCl_2$. Ten microliters of isotopically labeled CO (99% ^{13}C; Sigma Aldrich) was added to ^{13}C-labeled Live and ^{13}C-labeled Killed microcosms. The microcosms

were stored at room temperature and repeatedly analyzed for headspace concentrations and $\delta^{13}C$ of CO and CH_4. After 434 days, the microcosms were opened, and Live microcosms were sampled to measure concentrations and $\delta^{13}C$ of TIC and VOA anions as well as $\delta^{2}H_{H_2O}$ and $\delta^{18}O_{H_2O}$ values.

5.3.3 Chemical Analysis

5.3.3.1 Gas Analysis

CH_4 and CO concentrations were analyzed using an SRI 8610 gas chromatograph (GC) equipped with a flame ionization detector (FID) with a methanizer using a Carboxen 1010 (30 mx0.32 mm inside diameter, 15µm film thickness) capillary column and He as the carrier gas following procedures determined previously [Morrill et al., 2014]. To separate CO_2, CO, and CH_4, the oven temperature was held constant at 35 °C for 3.8 min then increased by 25 °C min^{-1} to a final temperature of 110 °C, which was held constant for 5 min. Carbon and hydrogen stable isotope values of methane ($\delta^{13}C_{CH_4}$ and $\delta^{2}H_{CH_4}$) were analyzed by gas chromatography-combustion-isotope ratio mass spectrometry and by gas chromatography-pyrolysis-isotope ratio mass spectrometry, respectively, using an 6890°N gas chromatograph (Agilent technologies) coupled to a Delta V Plus isotope ratio mass spectrometry (IRMS) with a conflo III interface (Thermo Scientific) either through a GC combustion unit (GC/C III; Thermo Scientific) or through a high temperature micropyrolysis furnace (GC/TC; Thermo Scientific). The same column and temperature program as described above was applied to separate H_2, CH_4, CO, and CO_2. The total analytical errors (1σ) of $\delta^{13}C_{CH_4}$ and $\delta^{2}H_{CH_4}$ were ± 0.5 ‰ and ± 5 ‰, respectively, which incorporates both the internal reproducibility on triplicate injections and the analytical error associated with the instrumentation [Ward et al., 2004, Sherwood Lollar et al., 2007].

5.3.3.2 Volatile Organic Acid Anions

Samples for volatile organic acid (VOA) analysis were collected in 15 mL centrifuge tubes (VWR), frozen immediately on dry ice, and stored at -20 °C until analysis. VOA anions (formate, acetate, propionate, butyrate, and lactate) were quantified by high-performance liquid chromatography (HPLC) as described in Morrill et al. [2014] with a detection limit of 0.5 μmol L^{-1} in field samples collected during the field trip in August 2013. In all other samples VOA anions were quantified by ion chromatography using a ThermoScientific ICS-2100 ion chromatograph fitted with a conductivity detector. Sample aliquots were loaded with a 10μL loop and separated on AS11-HC analytical (250 x 4 mm) and guard (50 x 4 mm) columns (Dionex). Separations were performed over a total run time of 33.5 min at a flow rate of 1.5 mL min^{-1} using potassium hydroxide in a multistep gradient elution program, starting from 5 min equilibration time at 1 mM KOH, an isocratic hold from 0-7 min at 1 mM, linear ramp from 7-16 min from 1-15 mM, isocratic hold from 16-20 min at 15 mM, linear ramp from 20-25 min from 15-25 mM, linear ramp from 25-33 min from 25-60 mM, and a final 0.5 min hold at 60 mM. All eluent passed through a continuously regenerated trap column to ensure high eluent purity. All separations were performed with columns and conductivity detector at 30 °C. Eluent was suppressed using an AERS 500 (4 mm) operating at 223 mA. The detection limit was 1 μmol L^{-1}. The method provided a highly linear response (all R^2>0.995) between 1 and 100 μmol L^{-1}. Matrix effects (e.g., interference of elevated chloride concentrations) were determined to be <5%.

Compound-specific carbon stable isotope values ($\delta^{13}C$) of organic acids were analyzed with ion chromatography (Dionex Corporation ICS-3000) coupled to a Delta V Advantage isotope ratio mass spectrometer by a liquid chromatography IsoLink Interface (Thermo Fisher Scientific) [Wild et al., 2010, Berry et al., 2013]. Samples were acidified with phosphoric acid to remove bicarbonate and separated on a Nucleogel Sugar 810H column (Macherey-Nagel) at 75 °C with 0.5 mL min^{-1} 20 mM phosphoric acid eluent. The eluting compounds

were converted to CO_2 at 99 °C with 50 µL min^{-1} of each of 0.5 mol L^{-1} sodium persulfate and 1.7 mol L^{-1} phosphoric acid. For standardization see Wild et al. [2010]. All IC-IRMS measurements deviated less than 1.5‰ from EA/IRMS measurements.

5.3.3.3 Total Inorganic Carbon (TIC), Dissolved Organic Carbon (DOC), and Water Analyses

Field samples were analyzed for the concentrations and $\delta^{13}C$ of TIC and TOC at the G.G. Hatch Stable Isotope Laboratory (University of Ottawa, Ontario, Canada) with an OI Analytical AURORA 1030 TOC Analyzer interfaced to a ThermoElectron Delta Plus XP IRMS for analysis by continuous flow. TIC samples generated in the microcosm experiments were analyzed at Memorial University with an OI Analytical AURORA 1030 TOC Analyzer coupled to a MAT252 isotope ratio mass spectrometer (IRMS) via a Conflo III interface. In both laboratories, the analytical precision was 1% and ±0.1‰ for concentration and $\delta^{13}C$, respectively. $\delta^{2}H$ and $\delta^{18}O$ values of water samples were analyzed by laser cavity ring-down spectroscopy at Isotope Tracer Technologies, Mississauga, OT, Canada. The analytical precision (1σ) for $\delta^{2}H$ and $\delta^{18}O$ was ± 1‰ and ±0.1‰, respectively.

5.3.4 Data Analysis

5.3.4.1 Nomenclature

All stable isotope ratios are reported in delta notation ($\delta^{13}C$ and $\delta^{2}H$) relative to international standards V-PDB for carbon and V-SMOW for hydrogen isotopes:

$$\delta^{n}X = \frac{R_{sam}}{R_{std}} - 1 \tag{5.4}$$

where X is the element (i.e., C, H, or O), n is the heavy isotope (i.e., 13, 2, and 18, respectively) of the element, and R_{sam} and R_{std} are the ratio of heavy to light isotopes for

the sample and standard, respectively [Coplen, 2011]. Apparent isotopic fractionation (α $\alpha^{13}C_{CH4\text{-}TOC}$, $\alpha^{13}C_{CH_4\text{-}acetate}$, $\alpha^{13}C_{CH4\text{-}formate}$, and $\alpha^{2}H_{CH4\text{-}H_2O}$) were calculated as

$$\alpha^n X_{a-b} = \frac{\delta^n X_a + 1000}{\delta^n X_b + 1000} \tag{5.5}$$

5.3.4.2 Mass Balance

The fraction of microbially produced methane was calculated as

$$f_{microbial} = \frac{[CH_4]_{microbial}}{[CH_4]_{total}} = \frac{[CH_4]_{Live} - [CH_4]_{Killed}}{[CH_4]_{Live}} \tag{5.6}$$

The $\delta^{13}C$ value of microbially produced methane was calculated using equation 5.7a:

$$\begin{aligned} \delta^{13}C_{microbial} = \frac{\delta^{13}C_{Live} \times [CH_4]_{Live} - \delta^{13}C_{Killed} \times [CH_4]_{Killed}}{[CH_4]_{Live} - [CH_4]_{Killed}} = \\ = \frac{\delta^{13}C_{Live} - \delta^{13}C_{Killed} \times (1 - f_{microbial}]}{f_{microbial}} \end{aligned} \tag{5.7a}$$

Low (<21 μmol L^{-1}) initial background and "killed" microcosm methane concentrations prevented determination of $\delta^2H_{CH_4}$ for these aliquots. We therefore assumed that δ^2H of the background methane was the same as that of methane collected during the field campaign (equation 5.7b).

$$\begin{aligned} \delta^{2}H_{microbial} = \frac{\delta^{2}H_{Live} \times [CH_4]_{Live} - \delta^{2}H_{Field} \times [CH_4]_{Killed}}{[CH_4]_{Live} - [CH_4]_{Killed}} = \\ = \frac{\delta^{2}H_{Live} - \delta^{2}H_{Field} \times (1 - f_{microbial}]}{f_{microbial}} \end{aligned} \tag{5.7b}$$

5.3.4.3 Conversion Between $\delta^{13}C_{CO_2}$ and $\delta^{13}C_{TIC}$

Literature values for the $\delta^{13}C$ of inorganic carbon are reported inconsistently as either headspace CO_2 ($\delta^{13}C_{CO_2(g)}$) or total inorganic carbon ($\delta^{13}C_{TIC}$; i.e., the total acid purgeable

CO_2, also referred to as CO_2). For ultra-basic springs, the $\delta^{13}C$ is typically reported for TIC. To compare the apparent fractionation of stable carbon isotopes across studies, we converted between $\alpha^{13}C_{CH4\text{-}TIC}$ and $\alpha^{13}C_{CH4\text{-}CO_2(g)}$ according to equation 5.8.

$$\alpha^{13}C_{CH4-TIC} = \alpha^{13}C_{CO_2(g)-CH4} \times \alpha^{13}C_{TIC-CO_2(g)} \tag{5.8}$$

The fractionation between TIC and headspace CO_2 ($\alpha^{13}C_{TIC\text{-}CO_2(g)}$) was calculated based on literature values as described in the supporting information. $\alpha^{13}C_{TIC\text{-}CO_2(g)}$ is close to 1 and not sensitive to temperature at pH$<$5 (Figure S2). Measurements of $\delta^{13}C_{TIC}$ and $\delta^{13}C_{CO_2(g)}$ thus lead to similar results at low pH sites like wetlands. This is not the case for neutral to basic systems, where $\alpha^{13}C_{TIC\text{-}CO_2(g)}$ varies significantly with pH and temperature (Figure 5.S2).

5.3.4.4 Statistical Analysis

We applied Welch t tests to compare treatments (Live and ^{13}C-labeled Live versus Killed and ^{13}C-labeled Killed for concentrations; n=6–9, or ^{13}C-labeled Live versus Live for $\delta^{13}C$ values; n=3). Given large variance among the treatment group but little variance among control group (i.e., heteroscedasticity), we furthermore calculated the 95% confidence interval of the control group (Killed and ^{13}C-Killed for concentrations; Live for $\delta^{13}C$ values) and noted individual replicates of the treatment group (Live/^{13}C-labeled Live for concentrations; ^{13}C-labeled Live for $\delta^{13}C$) falling outside of this range. All statistical analysis was conducted using the statistical programming environment R version 3.0.2 [R Development Core Team, 2015].

5.4 Results

5.4.1 Methane Concentrations

Headspace methane concentrations in nutrient amended microcosms (CO utilization experiment) were below the detection limit (<1 μmol L^{-1}) at the beginning of the experiment. This lack of detectable CH_4 in these microcosms was expected because they were left open to the air during their setup. In this temporary open system most methane could have been removed from the experimental liquid and headspace. Over the duration of the experiment (434 days), CH_4 concentrations in CO amended microcosms increased toward 76 to 90 μmol L^{-1} in the Live and ^{13}C-labeled Live treatments but remained below the detection limit throughout the experiment in the Killed and ^{13}C-Killed treatments (Figure 5.1a).

A small amount of methane (4.2 to 19.3 μmol CH_4 L^{-1}) was detected initially in the headspace of the microcosms amended with bicarbonate, acetate, formate, and methanol. This background concentration of methane likely resulted from the equilibration of dissolved CH_4 from the liquid phase into the headspace of the microcosms. Unlike in the initially oxic nutrient amended microcosms, the other substrate amended microcosms were assembled rapidly with a minimum fluid exposure to the N_2 atmosphere of the glovebag (Table 5.1). The loss of CH_4 during this type of setup was limited. In the Killed and ^{13}C-Killed treatments of substrate amended experiments, CH_4 concentrations remained constant (7.5 - 21 μmol L^{-1}) over the duration of the experiment. Live and ^{13}C-labeled Live treatments of the same experiment exhibited increasing methane concentrations such that the final concentrations of methane was on average 650%, 470%, and 490% higher in Live/^{13}C-labeled Live treatments compared to Killed/^{13}C-labeled Killed treatments in the formate, acetate, and bicarbonate amended experiments, respectively (Figure 5.1a). The final methane concentrations, however, varied between replicate microcosms, ranging from 8.6 to 179.3 μmol L^{-1}.

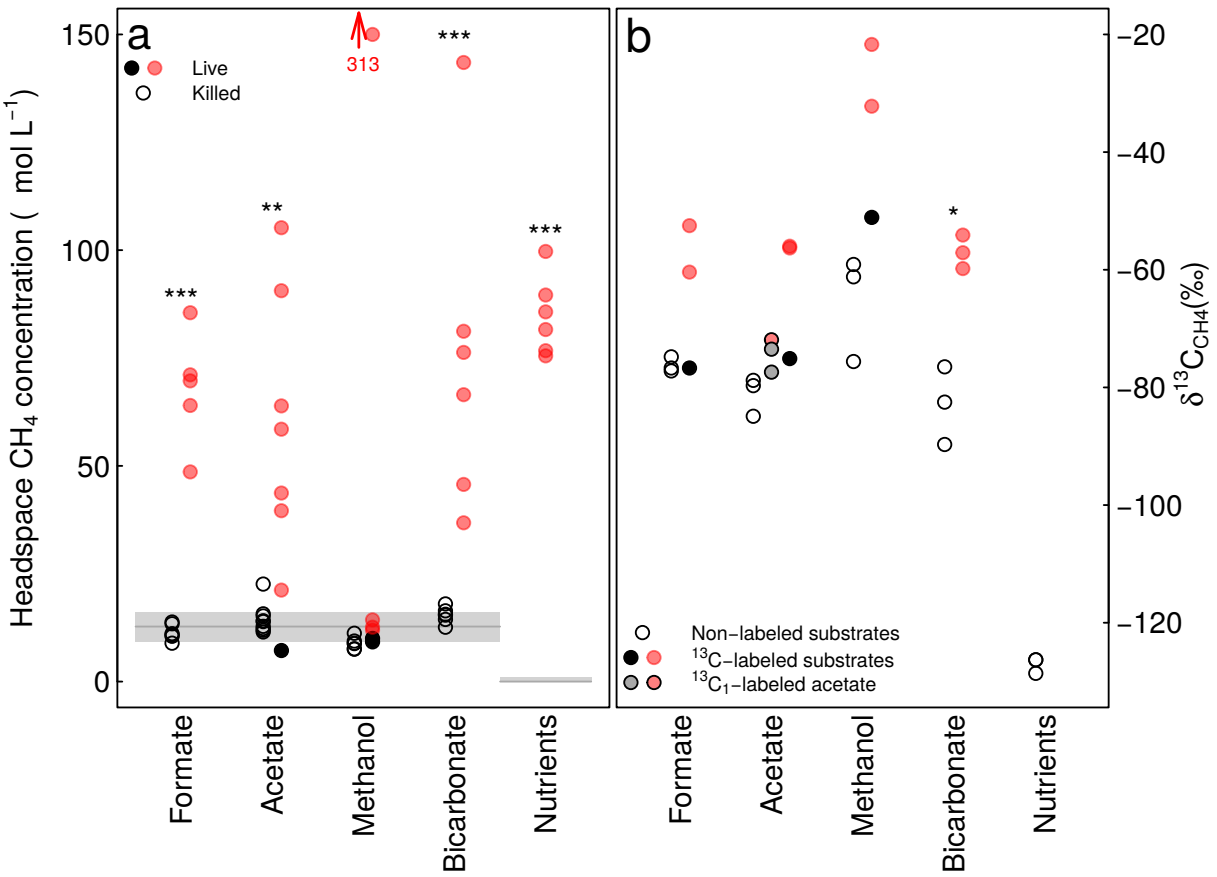

Figure 5.1 (a) Final headspace methane concentrations in microcosms amended with substrates (formate, acetate, methanol, and bicarbonate). (b) Final measured $\delta^{13}C_{CH_4}$ of headspace methane. Open symbols indicate microcosms amended with non-labeled substrates. Black symbols indicate microcosms amended with ^{13}C-labeled including C2-labeled acetate ($^{13}CH_3COO^-$). Grey symbols indicate microcosms amended with C1-labeled acetate ($CH_3{}^{13}COO^-$). Asterisks indicate significant differences between mean values in Live/^{13}C-labeled Live versus Killed/^{13}C-labeled Killed microcosms (Figure 5.1a) or ^{13}C-labeled Live versus Live microcosms (Figure 5.1b; *, p value <0.05; **, p value <0.01; ***, p value <0.001). Red symbols indicate measurements outside of the 95% confidence interval of the corresponding Killed controls (Figure 5.1a) or of natural abundance Live microcosms (Figure 5.1b).

Among the Live/^{13}C-labeled Live microcosms amended with methanol, five out of six replicates exhibited a small but significant increase in headspace methane concentrations relative to Killed/^{13}C-Killed controls (+30%; T=2.6, p=0.031 when the sixth replicate is excluded), while the sixth replicate exhibited a large increase in headspace methane concentrations (313.6 μmol CH_4 L^{-1} or 3400% higher than Killed/^{13}C-Killed microcosms; Figure 5.1a).

5.4.2 Measured $\delta^{13}C_{CH_4}$ and $\delta^{2}H_{CH_4}$ Values

Initial $\delta^{13}C_{CH_4}$ values were similar in all substrate amended microcosms regardless of the amended substrate or the treatment ($\delta^{13}C_{CH_4}$ = -61.5 ± 1.5‰ (1σ)). Final $\delta^{13}C_{CH_4}$ values in microcosms amended with ^{13}C labeled substrates (^{13}C-labeled Live) were more positive compared to microcosms amended with natural abundance substrates (Live; Figure 5.1b), demonstrating the conversion of the ^{13}C labeled substrates to CH_4. No difference between Killed and ^{13}C-Killed microcosms was observed (-61.2 versus -61.7‰), demonstrating that this conversion did not occur abiotically. The enrichment of ^{13}C in methane in ^{13}C-labeled Live treatments was variable among the individual microcosms. Nevertheless, for each substrate tested at least two out of three of the ^{13}C-labeled Live microcosms showed $\delta^{13}C_{CH_4}$ values 15‰ (formate), 25‰ ($^{13}C_2$-acetate, bicarbonate), or 30‰ (methanol) higher than in the corresponding Live microcosms, thus demonstrating the microbial conversion of each of the amended substrates to methane (Figure 5.1b). In contrast to $^{13}C_2$-acetate amended microcosms, $\delta^{13}C_{CH_4}$ in microcosms amended with $^{13}C_1$ acetate were only slightly higher relative to microcosms amended with unlabeled acetate (-74.2 versus -81.1‰). This position-specific conversion of the methyl, but not the carboxyl group of acetate to methane, demonstrates that acetate fermentation was the dominant pathway converting acetate to methane in this microcosms.

In substrate amended experiments, $\delta^{13}C_{CH_4}$ values of Killed and ^{13}C-Killed treatments neither varied between amended substrates nor changed over the duration of the experiments (-61.9 to -60.8‰). These values are similar to the $\delta^{13}C$ of exsolving methane collected at other BS springs in the field (-63.5‰), consistent with our assumption that the methane found in Killed controls resulted from dissolved background methane partitioning into the headspace of the sealed microcosm. At the end of the experiments, most Live microcosms amended with natural abundance substrates contained ^{13}C depleted CH_4 compared to field samples and to Killed microcosms, with formate, acetate, and bicarbonate amended micro-

Table 5.3 Calculated methane concentrations and stable isotope values of the microbial methane produced in the live experiments

Amendment	Treatment	Replicate	Measured[1]			Calculated Microbial[2]		
			$[CH_4]$	$\delta^{13}C_{CH_4}$	$\delta^{2}H_{CH_4}$	$[CH_4]$	$\delta^{13}C_{CH_4}$	$\delta^{2}H_{CH_4}$
			µM	‰	‰	µM	‰	‰
Formate + Nutrients	^{13}C-labeled Live	1	48.6	-52.5	-381	37.2	-49.7	-415
		2	64.0	-76.7	-	52.6	-80.0	-
		3	176.9	-60.4	-391	165.5	-60.3	-402
	Natural abundance Live	1	85.5	-76.7	-345	74.1	-79.1	-342
		2	71.1	-74.8	-	59.7	-77.4	-
		3	69.7	-77.2	-	58.3	-80.3	-
Acetate + Nutrients	$^{13}C_1$-labeled Live	1	43.7	-77.4	-	29.3	-85.2	-
		2	63.9	-71.9	-350	49.5	-74.9	-346
		3	179.3	-73.5	-387	164.9	-74.5	-396
	$^{13}C_2$-labeled Live	1	90.6	-75.1	-	76.2	-77.6	-
		2	105.2	-56.3	-380	90.8	-55.4	-394
		3	21.2	-56.0	-	6.8	-44.2	-
	Natural abundance Live	1	58.5	-79.7	-	44.1	-85.6	-
		2	7.2	-84.9	-	-7.23	-[3]	-
		3	39.6	-78.8	-	25.2	-88.6	-
Bicarbonate + Nutrients	^{13}C-labeled Live	1	36.8	-59.8	-	21.4	-58.0	-
		2	76.3	-57.1	-	60.9	-55.8	-
		3	45.7	-54.2	-	30.3	-50.0	-
	Natural abundance Live	1	143.5	-89.7	-363	128.1	-92.9	-365
		2	81.2	-82.5	-	65.8	-87.2	-
		3	66.5	-76.5	-	51.1	-80.7	-
Methanol + Nutrients	^{13}C-labeled Live	1	10.0	-51.1	-	1.1	+31.0	-
		2	12.6	-32.2	-	3.7	+37.7	-
		3	14.3	-21.7	-	5.4	+43.5	-
	Natural abundance Live	1	313.6	-75.6	-380	304.7	-76.0	-389
		2	11.9	-61.2	-	3.0	-61.1	-
		3	9.2	-59.1	-	0.3	-	-
Nutrients only	^{13}C-labeled Live	1	99.7	n.a.	n.a.	99.7	-	-
		2	76.7	n.a.	n.a.	76.7	-	-
		3	75.5	n.a.	n.a.	75.5	-	-
	Natural abundance Live	1	85.7	-126.3	-343	85.7	-126.3	-343
		2	81.6	-128.6	-356	81.6	-128.6	-356
		3	89.6	-126.3	-351	89.6	-126.3	-351

[1] n.a., not analyzed; -, below detection limit (Amplitude of m/z = 2 below 1000mV corresponding to 50-100 µmol CH4 L-1).
[2] Microbial methane concentrations in the live treatments were calculated by subtracting the methane concentration measured in the Live treatments from the average methane concentration in the Killed controls. The isotope value of the microbial methane was determined using isotopic mass balance (equations 5.7a, 5.7b). -, not applicable.
[3] Microcosms accidentally vented.

cosms exhibiting $\delta^{13}C_{CH_4}$ values of -77.2 to -74.8‰, -84.9 to -78.8‰, and -92.9 to -80.7‰, respectively. Live methanol amended microcosms exhibited only slightly lower $\delta^{13}C_{CH_4}$ values relative to Killed controls. Where quantifiable, $\delta^{2}H_{CH_4}$ ranged between -390 and -350‰, similar to field samples (-354‰).

5.4.3 δ^{13}C and δ^{2}H of Microbially Produced Methane

The calculated $\delta^{13}C_{CH_4}$ values of the microbially produced methane varied by ∼15‰ among the different nonlabeled substrate amendment experiments (Table 5.3) ranging from -92.9 to -80.7‰ (bicarbonate), -86.6 to -86.5‰ (acetate), and -80.3 to -77.4‰ (formate).

Only one methanol amended microcosm produced sufficient CH_4 for a reliable calculation, resulting in a similar value as formate derived CH_4 (-76.0‰). In contrast, methane produced in microcosms amended with nutrients only, which was exclusively microbially produced during the incubation (no background of exsolving methane), was substantially more depleted in ^{13}C (-128.6 to -126.3‰). The calculated $\delta^2H_{CH_4}$ values of microbial methane ranged -392 to -340‰ and did not exhibit any systematic variability by amended substrate.

5.4.4 Concentrations and $\delta^{13}C$ of Volatile Organic Acids (VOA) Anions

We observed the microbial production of VOAs in bicarbonate and methanol amendment experiments, as indicated by elevated concentrations of VOA anions in Live relative to Killed microcosms and relative to field concentrations (Figures 5.2a and 5.2b). In the bicarbonate amendment experiment, Live treatments exhibited 4–6 times higher concentrations of all VOA anions compared to Killed microcosms (Figure 5.2a). Furthermore, the composition of VOA anions was different in Live and Killed microcosms. In Killed microcosms and in field samples VOA anions were dominated by acetate (73% VOA carbon) with traces of formate (10%) and butyrate (17%), whereas propionate was not detected. Conversely, Live microcosms contained significant amounts of propionate (20% of the total VOA carbon).

We could not detect any incorporation of the amended ^{13}C-bicarbonate into acetate as $\delta^{13}C_{acetate}$ did not differ significantly between microcosms amended with ^{13}C labeled and natural abundance bicarbonate (-21.0 ± 2.2‰ versus -20.0 ± 1.5‰; Figure 3). This indicates that acetogenesis did not occur autotrophically (equation 5.1b).

Concentrations of VOA anions in the formate and acetate amended microcosms represented the substrate that was added (data not shown). Due to the necessary dilution, other organic acids could not be quantified in these experiments. In microcosms amended with natural abundance acetate or formate, $\delta^{13}C$ values of the amended VOA anion (formate: -25.9‰; acetate -43.0‰) did not differ between Live and Killed microcosms and were close to those of the added substrate (formate: -26.3‰; acetate 45.8‰). In microcosms amended

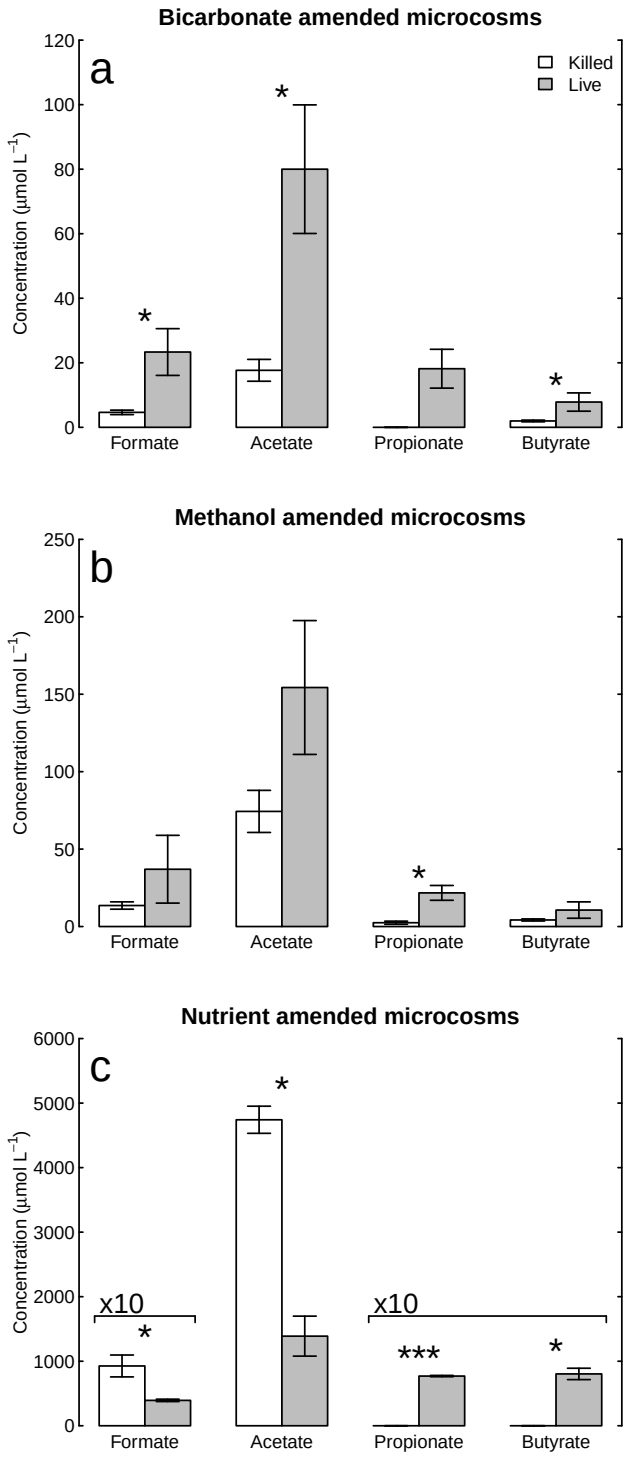

Figure 5.2 Concentrations of organic acids measured at the end of Live (grey) and Killed (white) treatments for each substrate amendment experiment. Error bars indicate ± one standard error. Asterisks indicate a significant difference between Live and Killed (*, p value <0.05; **, p value <0.01; ***, p value <0.001; n = 3). Ten times, tenfold concentrations plotted for better legibility. Organic acid concentrations in formate and acetate amended microcosms not shown.

with ^{13}C labeled acetate or formate, $\delta^{13}C$ values of the amended VOA anion differed between ^{13}C-labeled Live and ^{13}C-labeled Killed microcosms. $\delta^{13}C$ values of acetate and formate in ^{13}C-labeled Killed microcosms were much higher (i.e., >200‰); however, in the ^{13}C-labeled Live microcosms the same anions had similar or only slightly higher $\delta^{13}C$ values (formate: -26.4 to -25.0‰; acetate -41.3 to +5.8‰) compared to the natural abundance Live microcosms (Figure 5.3). This indicates that the $\delta^{13}C$ of acetate and formate decreased over time in ^{13}C- labeled Live, but not in ^{13}C-labeled Killed treatments, i.e., these organic acids were either isotopically diluted due to microbial turnover or microbial activity mediated the equilibration with other carbon species present in the microcosms (e.g., carbonates added with the sediment).

In the nutrient amendment experiment, concentrations of acetate and formate in both Live and Killed treatments were >20 times elevated (Figure 5.2c) relative to field samples (i.e., the fluid used to construct these microcosms; Table 5.2), suggesting that these anions can also be produced in these systems even when microbial activity is inhibited. Formate and acetate concentrations were higher in Killed than in Live microcosms, suggesting a biological consumption of these anions or the biotic inhibition of their abiotic production. In contrast, propionate and butyrate were found only in Live microcosms, indicating that these anions were microbially produced. $\delta^{13}C$ values of acetate in unamended microcosms (-25.4 ± 0.8‰) were slightly more depleted compared to those in bicarbonate amended microcosms (-21.0 ± 2.2‰; Figure 5.3).

5.4.5 Stable Isotope Values of Water and Inorganic Carbon

$\delta^{2}H_{H_2O}$ values of all microcosms ranged -44 to -42‰, similar to the $\delta^{2}H_{H_2O}$ values of field samples of spring and surface waters at The Cedars (-41 to -39‰) [Morrill et al., 2013]. $\delta^{13}C_{TIC}$ values of natural abundance substrate amended microcosm experiments ranged from -17.3 to -10.4‰ (Figure 5.3). These values are significantly higher than the $\delta^{13}C_{TIC}$ found

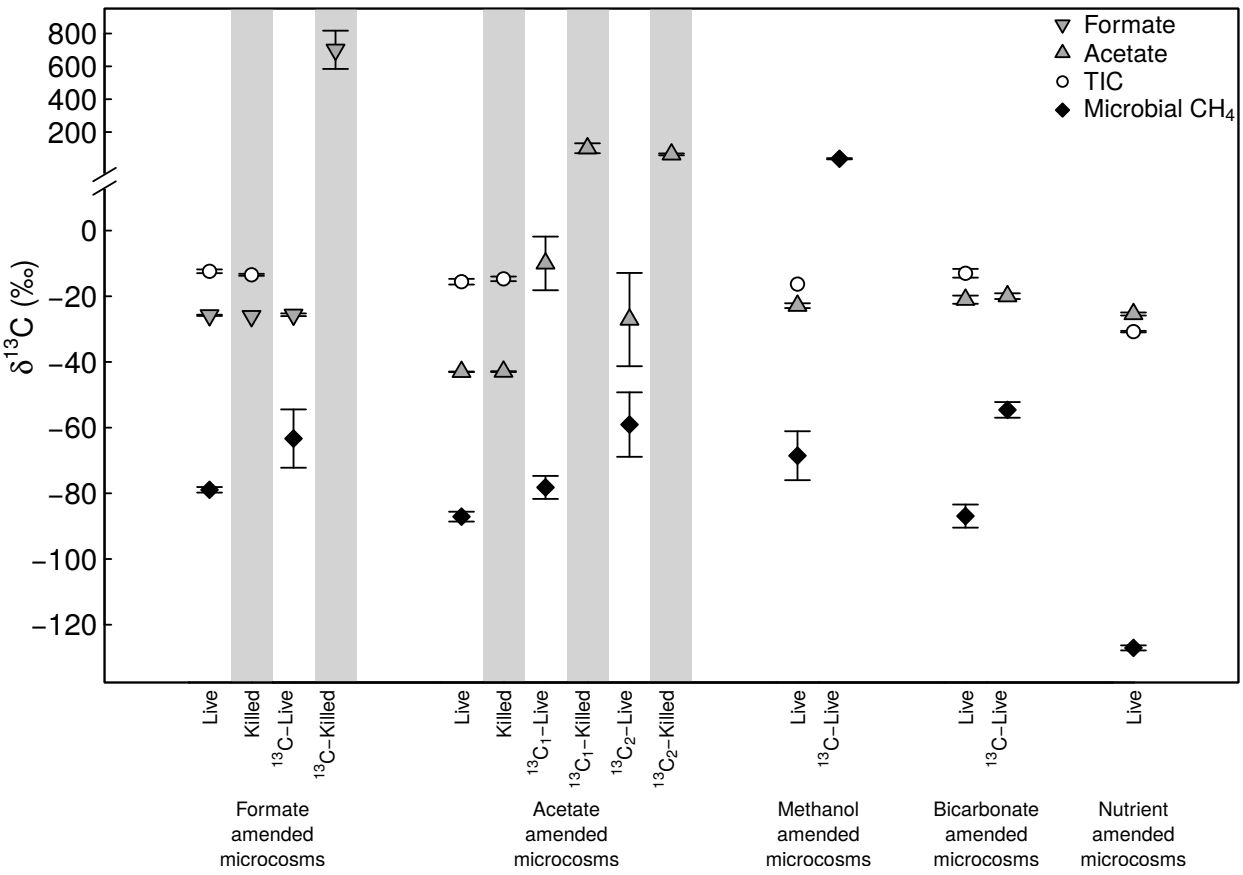

Figure 5.3 Comparison of the $\delta^{13}C$ values of microbially produced methane (calculated) with the available $\delta^{13}C$ values of potential substrates, i.e., TIC and of the most abundant VOA anions (formate where amended and acetate in all other experiments). Grey shaded areas indicate $HgCl_2$ killed controls. Error bars indicate standard errors.

in field samples of the BS5 spring water (-32.6‰) [Morrill et al., 2013]. $\delta^{13}C_{TIC}$ in nutrient amended microcosms ranged from -31.2 to -30.4‰ in nutrient amended microcosms, similar to field samples (Figure 5.3).

5.5 Discussion

5.5.1 Microbial Methanogenesis

Our microcosm experiments demonstrate methanogenesis by native microbial communities in spring water and/or the carbonate sediment at The Cedars despite the potential limita-

tions of taking a field sample and isolating it in laboratory bottles. Microbial methanogenesis was evidenced by increasing methane concentrations in Live microcosms but not in $HgCl_2$-Killed controls (Figure 1a). The incorporation of ^{13}C from labeled substrates into methane demonstrates that the microbial communities at this site are capable of converting both inorganic carbon and a range of organic substrates to methane (Figure 5.1b). To our knowledge, this is the first study to directly demonstrate the potential for microbial methanogenesis by an endemic microbial community of a terrestrial site of present-day serpentinization with labeled substrate experiments. Our results complement geochemical and microbial diversity data indicating that microbial methanogenesis might be a significant source of methane at The Cedars, including low $\delta^{13}C_{CH_4}$ values (<-62‰) [Morrill et al., 2013] and $\delta^{2}H_{CH_4}$ values (-346‰) [Wang et al., 2015, and this study], high C_1/C_{2+} ratios (>10^2) [Morrill et al., 2013], nonequilibrium $\Delta^{13}CH_3D$ ratios [Wang et al., 2015], and the detection of potentially methanogenic uncultivated archaea in The Cedars springs with the 16S rRNA gene sequencing survey [Suzuki et al., 2013].

The presence of a microbial community capable of methanogenesis at The Cedars stands in contrast to other terrestrial sites with serpentinization-associated groundwaters/springs. We recently reported the absence of microbial methanogenesis in a similar experiment with material collected from ultra-basic, reducing springs at The Tablelands, NL, Canada [Morrill et al., 2014], which is consistent with the absence of geochemical indicators of microbial methanogenesis at that site [Szponar et al., 2013], and the lack of genomic evidence for methanogens [Brazelton et al., 2012].

5.5.2 $\delta^{13}C$ and $\delta^{2}H$ of Microbial Methane Indicate the Dominance of Autotrophic Methanogenesis

Our results indicate that the microbial communities in our microcosms converted both inorganic carbon and a range of organic substrates to methane. Further insight into which

substrates were predominantly converted to methane can be generated from the δ^2H and δ^{13}C values of microbially produced methane. Naturally occurring methane typically exhibits more negative δ^2H and less negative δ^{13}C values when produced through the acetate fermentation pathway (equation 5.3) than when produced through carbonate reduction pathway (equations (1a) and (1b)) [Whiticar et al., 1986]. Plotting $\delta^{13}C_{CH_4}$ versus $\delta^2H_{CH_4}$ thus has been used to distinguish sources of naturally occurring CH_4 (i.e., microbial, thermogenic, and abiogenic) and methanogenic pathways (i.e., acetate fermentation, and carbonate reduction). However, the fields used for sourcing are expanding with more available data [Etiope and Sherwood Lollar, 2013]. Additionally, such a plot considers only absolute $\delta^{13}C_{CH_4}$ and $\delta^2H_{CH_4}$ values, which are not only a function of formation pathway but also the isotopic composition of the reactants and secondary processes.

Apparent fractionation factors between microbially produced methane and potential methanogenic substrates can help to further elucidate the dominant pathway in our microcosm experiment. We note that apparent fractionation factors compare empirically observed differences in the stable isotope values of coexisting species. These factors do not necessarily indicate the isotopic fractionation associated with the conversion of these substrates to methane. Carbonate, for example, besides being a substrate used by autotrophic methanogens, can also be the coproduct of methanogenesis through acetate fermentation and both the product (heterotrophic respiration) and the substrate (autotrophic acetogenesis) of competing pathways. Empirically determined fractionation factors, typically reported from microbial culture studies [Valentine et al., 2004, and references therein], thus represent maximum values for the apparent isotopic fractionation expected by the process in nature and might be diminished by the enrichment of the ^{13}C or ^{2}H in the substrate in closed systems like our microcosms. Furthermore, stable isotope values of substrates might change over the duration of an experiment. However, this was not the case in the nonlabeled treatments of our study, as similar δ^{13}C values of substrates (acetate, formate, and TIC) in Live and

Killed microcosms (Figure 5.3 and Table 5.4) indicate that microbial activity did not lead to a change in the $\delta^{13}C$ values of these substrates.

With this in mind, our analysis suggests that methanogenesis in our microcosms was likely dominated by the carbonate reduction pathway (equation (1a)). Figure 4a compares the $\alpha^{13}C_{actetate/formate\text{-}CH_4(micr)}$ and $\alpha^{13}C_{CO_2(g)\text{-}CH_4(micr)}$ to available literature values from culture studies [Valentine et al., 2004]. The apparent fractionation between microbially produced methane and inorganic carbon ($\alpha^{13}C_{CO_2(g)\text{-}CH_4(micr)}$) ranged 1.062–1.067, 1.069–1.073, and 1.068–1.078 in formate, acetate, and bicarbonate amended microcosms. These values are consistent with the reported fractionation during carbonate reduction (red area) [Valentine et al., 2004]. In contrast, $\alpha^{13}C_{acetate\text{-}CH_4(micr)}$ values (1.056–1.059 and 1.068–1.078 for acetate and bicarbonate amended microcosms) are much higher than can be explained by the fractionation observed during acetate fermentation (blue area) [Valentine et al., 2004]. We note that Valentine et al. [2004] compared the $\delta^{13}C_{CH_4}$ to the $\delta^{13}C$ of the methyl group of acetate, while we measured the $\delta^{13}C$ of the whole acetate molecule. To account for this different methodology, we compared our observed apparent fractionation with the highest observed $\alpha^{13}C_{acetate\text{-}CH_4}$ (1.022) [Valentine et al., 2004] combined with the highest observed depletion of ^{13}C in the methyl group of acetate relative to the total molecule (1.012 [Thomas, 2008]; blue dashed line in Figure 5.4a). Even after this correction, the observed $\alpha^{13}C_{acetate\text{-}CH_4}$ in all our microcosms is higher than what can be explained by acetate fermentation (Figure 5.4a).

The apparent fractionation of stable hydrogen isotopes observed in our microcosms ($\alpha^{2}H_{H_2O\text{-}CH_4}$=1.46), was larger than observed at sites where carbonate reduction is assumed to dominate (1.15 - 1.40; Figure 4b) or the fractionation factors observed in pure cultures by Valentine et al. [2004] (1.16 - 1.43). Larger $\alpha^{2}H_{H_2O\text{-}CH_4}$ values (1.67 $\pm$ 0.05), however, have been observed in early culture experiments conducted with high concentrations of H_2 [Balabane et al., 1987], and it has been suggested that the strong depletion of ^{2}H in CH_4 in these

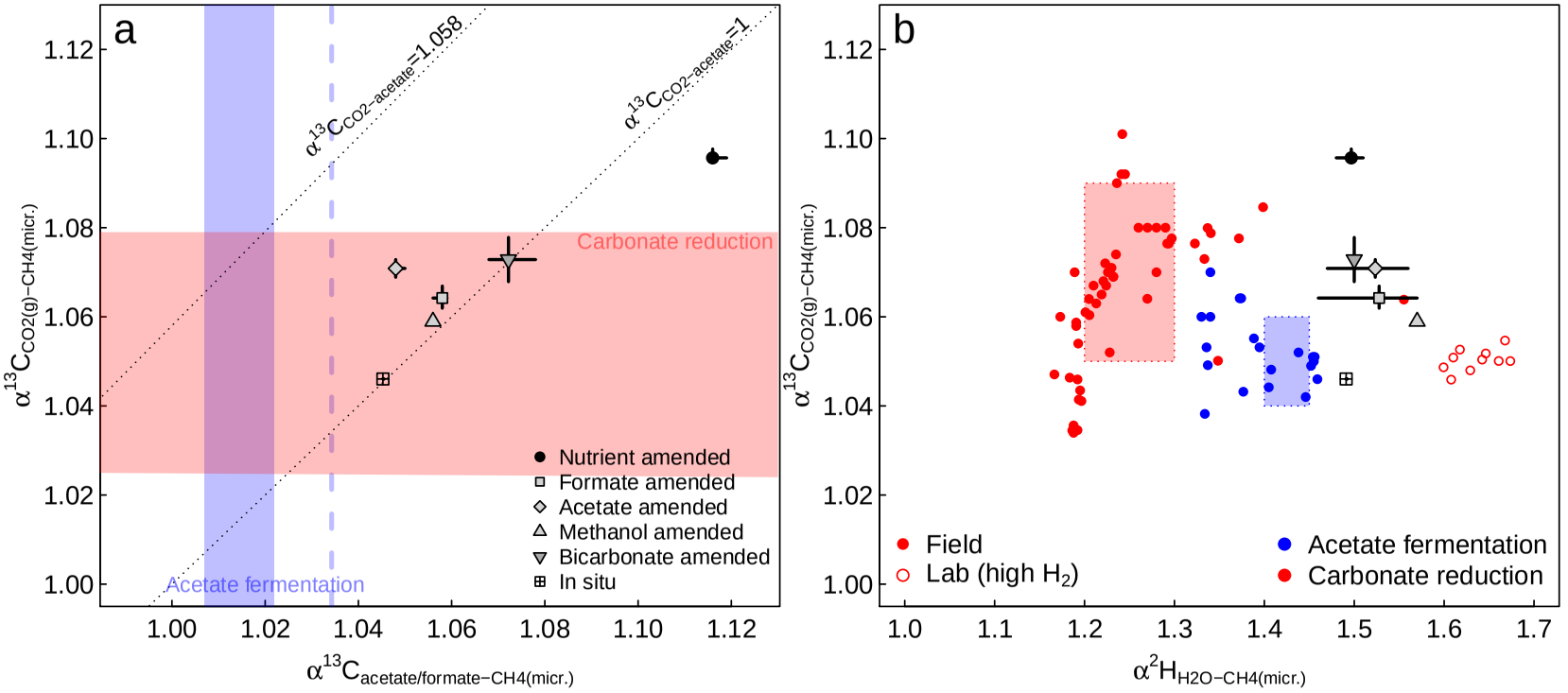

Figure 5.4 (a)Apparent isotopic fractionation between microbially produced methane and potential substrates ($\alpha^{13}C_{CO_2(g)\text{-}CH_4(micr)}$ and $\alpha^{13}C_{acetate/formate\text{-}CH_4(micr)}$). Error bars indicate the range of observed values. The shaded areas indicate the ranges of isotopic fractionation factors associated with carbonate reduction (red) acetate fermentation (blue) determined in culture studies [Valentine et al., 2004]. The vertical dashed blue line indicates the maximum fractionation between acetate and methane after taking into account intramolecular isotopic ordering in acetate (see text). The apparent fractionation observed in this study falls within the range observed during carbonate reduction and exceeds the fractionation observed during acetate fermentation.$\delta^{13}C_{acetate}$ could not be determined for field samples, alternativelywe used the average $\delta^{13}C$ value of acetate produced in bicarbonate and nutrient amended microcosms -23‰). Diagonal lines indicated the fractionation between inorganic carbon and acetate associated with autotrophic acetogenesis (equations 5.2a and 5.2b; $\alpha^{13}C_{CO_2(g)\text{-}acetate}$= 1.058 [Gelwicks et al., 1989]) and heterotrophic acetogenesis/terminal respiration ($\alpha^{13}C_{CO_2(g)\text{-}acetate}$ ~1 [Heuer et al., 2009]). (b)Apparent isotopic fractionation between methane and potential substrates ($\alpha^{2}H_{CH_4\text{-}H_2O}$ versus $\alpha^{13}C_{CH_4\text{-}TIC}$) observed in this study (grey symbols with error bars). Closed symbols indicate literature data of field samples fromenvironments wheremethane is understood to be primarily produced through carbonate reduction (equations 5.1a and 5.1b; red symbols) or acetate fermentation (equation 5.3; blue symbols). Raw data are provided in Table 5.S1. The shaded rectangles represent the areas where the fractionation factors for these two pathways have plotted previously according to Whiticar et al. [1986]. Open symbols indicate methane produced in cultures of carbonate reducing methanogens [Balabane et al., 1987]

Table 5.4 Apparent isotopic fractionation factors (α) between methane and H_2O or inorganic carbon[1].

Substrate & Treatment	Replicate	TIC	$\delta^{13}C_{TIC}$	$\delta^{2}H_{H_2O}$	$\delta^{18}O_{H_2O}$	$\alpha^{13}C_{TIC\text{-}CH_4}$		$\alpha^{13}C_{CO_2(g)\text{-}CH_4}$[3]		$\alpha^{2}H_{H_2O\text{-}CH_4}$	
						total	microbial	total	microbial	total	microbial
		mM	‰	‰	‰	methane	methanea	methane	methane	methane	methane
Formate Live	1	0.9	-13.2	-43.5	-7.3	1.069	1.072	1.061	1.063		
	2	0.7	-12.7	-43.7	-7.3	1.067	1.070	1.059	1.062	1.46-1.57[2]	1.45-1.57[2]
	3	0.9	-11.3	-43.6	-7.3	1.071	1.075	1.063	1.067		
Formate Killed	1	0.6	-13.6	-43.8	-7.4	1.051	-	1.043	-	-	-
	2	0.6	-13.9	-	-	1.051	-	1.043	-	-	-
	3	0.6	-12.9	-	-	1.052	-	1.044	-	-	-
Acetate Live	1	2.3	-14.8	-43.3	-7.2	1.071	1.077	1.062	1.069		
	2	5.0	-17.3	-43.5	-7.3	1.074	-[4]	1.066	-	1.47-1.55[2]	1.46-1.56[2]
	3	1.9	-14.6	-43.2	-7.3	1.070	1.081	1.062	1.073		
Acetate Killed	1	0.6	-14.1	-43.5	-7.3	1.051	-	1.043	-	-	-
	2	0.6	-13.9	-	-	1.050	-	1.042	-	-	-
	3	3.8	-16.1	-	-	1.048	-	1.040	-	-	-
Methanol Live	1	1.9	-16.3	-43.2	-7.3	1.064	1.065	1.059	1.059	1.57	1.57
	2	-	-	-	-	-	-	1.042	-	-	-
	3	-	-	-	-	-	-	1.040	-	-	-
Methanol Killed	1	-	-	-	-	1.050	-	1.042	-	-	-
	2	-	-	-	-	1.050	-	1.042	-	-	-
	3	-	-	-	-	1.051	-	1.043	-	-	-
Bicarbonate Live	1	4.3	-14.8	-43.1	-7.3	1.082	1.086	1.074	1.078	1.50	1.5
	2	4.2	-13.8	-43.5	-7.3	1.075	1.080	1.067	1.072	-	-
	3	1.1	-10.4	-43.6	-7.3	1.072	1.076	1.063	1.068	-	-
Bicarbonate Live	1	5.3	-15.1	-43.8	-7.3	1.050	-	1.043	-	-	-
	2	1.2	-11.6	-	-	1.054	-	1.046	-	-	-
	3	3.6	-14.5	-	-	1.051	-	1.043	-	-	-
Nutrient ammended Live	1	32.1	-30.4	-42.3	-6.5	1.110	1.110	1.102	1.102	1.48	1.48
	2	34.4	-30.7	-42.6	-7.2	1.112	1.112	1.105	1.105	1.51	1.51
	3	34.1	-31.2	-42.5	-7.2	1.109	1.109	1.101	1.101	1.50	1.50
Nutrient ammended Killed	1	-	-	-	-	-	-	-	-	-	-
	2	-	-	-	-	-	-	-	-	-	-
	3	-	-	-	-	-	-	-	-	-	-

[1] -, not analyzed / not applicable.

[2] Calculated based on $\delta^{2}H_{CH_4}$ values from ^{13}C labeled and natural abundance microcosms with sufficiently high CH_4 concentrations (Table 5.2) and $\delta^{2}H_{H_2O}$ values from natural abundance microcosms (this table). The stated range is based on the range of $\delta^{2}H_{CH_4}$ values observed in individual microcosms (3 replicates per treatment). Variations of $\delta^{2}H_{H_2O}$ among replicate microcosms were negligible (<0.3 ‰; four replicates per treatment).

[3] $\alpha^{13}C_{CO_2(g)\text{-}TIC}$ was calculated based on literature values (see supplemental methods). The sensitivity of $\alpha^{13}C_{CO_2(g)\text{-}TIC}$ to variations in temperature and pH in the range expected in our microcosms experiment was <0.002 (pH 8-11, 20-24 °C).

[4] Microcosm accidentially vented during incubation.

experiments was due to the incorporation of H_2-derived hydrogen into CH_4 [Burke, 1993]. H_2 is present in the reducing fluids and bubbling gases at The Cedars at concentrations 5 times higher than methane (∼35% in the bubbling gases) [Morrill et al., 2013]. We did not measure H_2 concentrations in the headspace of our microcosms; however, assuming that H_2 was introduced into microcosms at the same rate as methane, initial headspace concentrations of H_2 would have been on the order of 50 μmol L^{-1}, corresponding to a partial pressure of ∼100 Pa. This is far below the concentrations hypothesized to cause the depletion of H_2 in carbonate derived methane in Balabane et al. [1987]. Such an effect, however, might be relevant in the field, where H_2 is present at much higher partial pressures.

Noteworthy, culture studies on autotrophic methanogens have been conducted at neutral pH only. There is a consensus that the carbon and hydrogen isotopic fractionation depends on growth conditions and, in particular, the reversability of the methanogenesis reaction [Valentine et al., 2004]. However, little is known about how this fractionation is affected by the extra and/or intracellular pH, e.g., through proton availability. Further culture experiments with methanogens at high pH are sorely needed to further understand the isotope systematics of microbially produced methane in serpentinization-associated springs.

5.5.3 The Role of VOA Anions in Serpentinization-Associated Springs

Our results show that the total concentration of VOA anions in microcosms was affected by microbial production, consumption, and turnover. Microbial acetogenesis in bicarbonate and methanol amended microcosms was evidenced by elevated concentrations of C_1-C_4 VOA anions in Live treatments relative to Killed treatments and concentrations in field samples (which represent the material used to construct the microcosms).

Microbial acetogenesis can occur autotrophically (equation 5.1b) or heterotrophically. The $\delta^{13}C$ values of acetate in Live microcosms were inconsistent with autotrophic methanogenesis because (a) ^{13}C labeled bicarbonate was not incorporated into acetate (Figure 5.3)

and (b) acetate was not depleted in ^{13}C relative to inorganic carbon ($\alpha^{13}C_{CO_2(g)\text{-acetate}}$ =0.999 - 1.000; Figure 5.4a). Such a depletion would be expected given that autotrophic acetogenesis strongly discriminates against ^{13}C ($\alpha^{13}C_{CO_2(g)\text{-acetate}}$ =1.058 [Gelwicks et al., 1989]; Figure 5.4a). We therefore conclude that acetate in the bicarbonate amended microcosms was generated through heterotrophic acetogenesis, a process not associated with relevant isotopic fractionation effects (i.e., $\delta^{13}C_{\text{organic matter}} \sim \delta^{13}C_{\text{acetate}} \sim \delta^{13}C_{CO_2(g)}$; [Heuer et al., 2009]).

Microbial turnover (simultaneous production and consumption) of acetate was indicated by the isotopic dilution of the amended ^{13}C labeled acetate during the incubation due to the microbial production of nonlabeled acetate. Decreasing $\delta^{13}C_{\text{acetate}}$ values during the incubation were evidenced by the lower $\delta^{13}C_{\text{acetate}}$ values in ^{13}C-labeled Live microcosms compared to ^{13}C-labeled Killed microcosms (where $\delta^{13}C_{\text{acetate}}$ represents the initially amended ^{13}C-acetate) (Figure 5.3). We can exclude that this decrease in $\delta^{13}C_{\text{acetate}}$ occurred through the microbially mediated equilibration with inorganic carbon described by Thomas [2008] because only the carboxylic carbon of acetate equilibrates with inorganic carbon, and we observed that $\delta^{13}C_{\text{acetate}}$ decreased equally in microcosms amended carboxylic ^{13}C-labeled acetate and methyl ^{13}C labeled acetate.

Our results further show that ^{13}C labeled formate was isotopically diluted or equilibrated with inorganic carbon in ^{13}C-labeled Live but not ^{13}C-Killed microcosms. A microbially catalyzed equilibration ($CO_3^{2-}+H_2+H^+ \leftrightarrow HCOO^-+H_2O$) could explain the complete loss of the ^{13}C label in formate observed in ^{13}C-labeled Live but not in ^{13}C-Killed microcosms.

Our observation that acetate and formate concentrations strongly increased during incubation in both Live and Killed treatments of the nutrient amended microcosms indicates the abiotic production of these VOA anions. The composition of these tentatively abiotic VOA anions (Figure 5.2c) was similar to field samples from this study (Table 5.1) as well as at other sites of serpentinization [Lang et al., 2010, Crespo-Medina et al., 2014, Morrill et al., 2014], i.e., dominated by acetate with traces of formate and (at some sites) butyrate but not

propionate. In contrast, the microbially produced VOA anions found in this study contained elevated proportions of propionate and butyrate (Figures 5.2a–5.2c). The composition of VOA anions thus might provide insight into their origin and/or processing in field studies.

VOA are present at elevated concentrations in both terrestrial and marine serpentinization-associated fluids and can account for >50% of the dissolved organic carbon at these sites [Lang et al., 2010, Morrill et al., 2014]. They can be present in higher concentrations than gaseous hydrocarbons in these springs and make up a substantial and so far underestimated flux of reduced carbon from reducing springs. Our results show that VOA anions are rapidly produced and consumed and suggest that VOA-based metabolic pathways might play an important role in the carbon cycling of ultra-basic reducing springs. While our experiments were not designed to ultimately resolve the biogeochemistry of VOA anions, our results clearly show that further research into the origin and fate of these compounds is warranted.

5.5.4 Conclusions

Microcosms experiments can provide direct evidence that a microbial process like methanogenesis occurs under favorable conditions, thus demonstrating the metabolic capability of the native microbial communities. Such experiments do not necessarily imply that methanogenesis occurs under field conditions which may differ from those chosen for laboratory incubation. Most importantly, our substrate use experiments required us to provide a sufficiently high concentration of labeled substrates to detect the incorporation of ^{13}C into methane. We thereby increased the concentrations of VOA anions about twentyfold. However, it is highly likely that the conditions for methanogenesis can be met under in situ conditions as evidenced by the fact that methanogenesis occurred spontaneously in nutrient amended microcosms, even after exposing the microcosms to air during setup.

The main substrate for heterotrophic methanogenesis (acetate) is readily available in situ. Concentrations of dissolved organic carbon are higher in the spring fluids compared to the

adjacent Austin Creek [Morrill et al., 2013] and acetate accounts for >50% of this DOC (Table 5.2). Elevated concentrations of formate and acetate were also found at other terrestrial and marine serpentinization-associated fluids [Lang et al., 2010, Crespo-Medina et al., 2014, Morrill et al., 2014]. Our results, however, indicate that methanogenesis was dominated by carbonate reduction. At the high pH and Ca^{2+} concentrations in serpentinization-associated groundwaters, dissolved inorganic carbon is limited, as reflected in low TIC concentrations (Table 5.2). Autotrophic methanogenesis in serpentinization-associated groundwaters therefore is likely limited by the carbonate availability.

This finding has a direct consequence for proposed CO_2 sequestration projects. If autotrophic methanogenesis is indeed limited by the availability of inorganic carbon, the injection of CO_2 in ophiolitic ground water could result in increased microbial methanogenesis, thus creating a source of CH_4 with a radiative forcing higher than the sequestrated CO_2.

5.6 Acknowledgments

The authors would like to thank David McCrory and Roger Raiche and The Cedars Friends for all of their inspirational support and great help over the years and for allowing us access to The Cedars. The authors would also like to thank David Wang, Annette Rowe, and Heidi Kavanagh for their help in the field and during experimental setup as well as Birgit Wild, Jamie Warren, Trevor VanderBoer, and Geert van Biesen for their help with IC, HPLC/IRMS, and GC/IRMS measurements. We thank Birgit Wild and two anonymous reviewers for their comments on the manuscript. This research was funded by Morrill's Natural Science and Engineering Council (NSERC) Discovery grant.

5.7 Supporting Information

Calculation of $\alpha^{13}C_{TIC\text{-}CO_2(g)}$

To determine $\alpha^{13}C_{TIC\text{-}CO_2(g)}$, we first calculated the speciation of inorganic carbon (IC) as a function of the pH and absolute temperature (T). We therefore calculated the two acid dissociation constants of carbonic acids:

$$pK_1 = -log(\frac{[H^+] \times [HCO_3^-]}{[H_2CO_3]}) = 1.1 \times 10^{-4} \times (T - 273.15)^2 - 0.012 \times (T - 273.15) + 6.58 \quad (5.S1a)$$

$$pK_2 = -log(\frac{[H^+] \times [CO_3^{2-}]}{[HCO_3^-]}) = 9 \times 10^{-5} \times (T - 273.15)^2 - 0.0137 \times (T - 273.15) + 10.62 \quad (5.S1b)$$

(Drever [1997] after Clark and Fritz [1997])

Carbonate speciation was calculated assuming that the concentration of the least abundant species was negligible. We calculated the proportion of H_2CO_3, HCO_3^-, and CO_3^{2-} as follows:

$$f_{H_2CO3} = f_{CO_2(aq)} = \frac{[H_2CO_3]}{([HCO_3^-] + [H_2CO_3])} = \frac{10^{(pK_1 - pH)}}{1 + 10^{(pK_1 - pH)}} \quad (5.S2a)$$

$$f_{HCO_3^-} = f_{CO_2(aq)} = \frac{[H_2CO_3]}{([HCO_3^-] + [H_2CO_3])} = \frac{10^{(pK_1 - pH)}}{1 + 10^{(pK_1 - pH)}} \quad (5.S2b)$$

$$f_{CO3^{2-}} = f_{CO_2(aq)} = \frac{[H_2CO_3]}{([HCO_3^-] + [H_2CO_3])} = \frac{10^{(pK_1 - pH)}}{1 + 10^{(pK_1 - pH)}} \quad (5.S2c)$$

Isotopic fractionation factors between headspace and dissolved IC species were calculated as following:

$$\alpha^{13}C_{CO_2(aq)-CO_2(g)} = e^{(-0.373\times10^3/T+0.19)/1000} \tag{5.S3a}$$

$$\alpha^{13}C_{HCO_3^--CO_2(g)} = e^{(9.552\times10^3/T-24.1)/1000} \tag{5.S3b}$$

$$\alpha^{13}C_{CO_3^{2-}-CO_2(g)} = e^{(-0.87\times10^6/T^2+3.4)/1000} \tag{5.S3c}$$

([Vogel et al., 1970, Mook et al., 1974, Deines et al., 1974])

The δ^{13}C of each IC fraction was calculated as

$$\delta^{13}C_{CO_2(aq)} = (\delta^{13}C_{CO_2(g)} + 1000) \times \alpha^{13}C_{CO_2(aq)-CO_2(g)} - 1000 \tag{5.S4a}$$

$$\delta^{13}C_{HCO_3^-} = (\delta^{13}C_{CO_2(g)} + 1000) \times \alpha^{13}C_{HCO_3^--CO_2(g)} - 1000 \tag{5.S4b}$$

$$\delta^{13}C_{CO_3^{2-}} = (\delta^{13}C_{CO_2(g)} + 1000) \times \alpha^{13}C_{CO_3^{2-}-CO_2(g)} - 1000 \tag{5.S4c}$$

The δ^{13}C of TIC was calculated as the weighted mean of each IC species,

$$\delta^{13}C_{TIC} = \delta^{13}C_{CO_2(aq)} \times f_{CO_2(aq)} + \delta^{13}C_{HCO_3^-} \times f_{HCO_3^-} + \delta^{13}C_{CO_3^{2-}} \times f_{CO_3^{2-}} \tag{5.S5}$$

Thus,

$$\alpha^{13}C_{TIC-CO_2(g)} = \frac{\delta^{13}C_{CO_2(aq)} \times f_{CO_2(aq)} + \delta^{13}C_{HCO_3^-} \times f_{HCO_3^-} + \delta^{13}C_{CO_3^{2-}} \times f_{CO_3^{2-}} + 1000}{\delta^{13}C_{CO_2(g)} + 1000)} \tag{5.S6}$$

Replacing $\delta^{13}C_{CO_2(aq)}$, $\delta^{13}C_{HCO_3^-}$, and $\delta^{13}C_{CO_3^{2-}}$ in S6 with terms from eq. S4a-c gives

$$\alpha^{13}C_{TIC-CO_2(g)} = \alpha^{13}C_{CO_2(aq)-CO_2(g)} \times f_{CO_2(aq)} + \alpha^{13}C_{HCO_3^--CO_2(g)} \times f_{HCO_3^-} + \delta^{13}C_{CO_3^{2-}} \times f_{CO_3^{2-}} \tag{5.S7}$$

Derivation for equations 5.7a-b:

$$f_{microbial} = \frac{[CH_4]_{micobial}[CH_4]_{total}}{=} \frac{([CH_4]_{Live} - [CH_4]_{Killed}}{CH_4]_{Live}} \tag{5.S8a}$$

$$\delta^{13}C_{microbial} * ([CH_4]_{Live} - [CH_4]_{Killed}) = \delta^{13}C_{Live} * [CH_4]_{Live} - \delta^{13}C_{Killed} * [CH_4]_{Killed} \tag{5.S8b}$$

$$\delta^{13}C_{microbial} * \frac{[CH_4]_{Live} - [CH_4]_{Killed}}{[CH_4]_{Live}} = \delta^{13}C_{Live} * \frac{[CH_4]_{Live}}{[CH_4]_{Live}} - \delta^{13}C_{Killed} * \frac{[CH_4]_{Killed}}{[CH_4]_{Live}} \tag{5.S8c}$$

$$\delta^{13}C_{microbial} * f_{microbial} = \delta^{13}C_{Live} - \delta^{13}C_{Killed} * (1 - f_{microbial}) \tag{5.S8d}$$

$$\delta^{13}C_{microbial} = \frac{\delta^{13}C_{Live} - \delta^{13}C_{Killed} * (1 - f_{microbial})}{f_{microbial}} \tag{5.S8e}$$

Derivation for equations 5.S2a-c:

$$K_1 = \frac{[H^+] \times [HCO_3^-]}{[H_2CO_3]} = 10^{-pH} \times \frac{[HCO_3^-]}{[H_2CO_3]} \tag{5.S9a}$$

$$\frac{1}{K_1} = 10^{pH} \times \frac{[H_2CO_3]}{[HCO_3^-]} \tag{5.S9b}$$

$$\log(\frac{1}{K_1}) = -\log(K_1) = pK_1 = pH + \log(\frac{[H_2CO_3]}{[HCO_3^-]}) \tag{5.S9c}$$

$$pK_1 - pH = \log(\frac{[H_2CO_3]}{[HCO_3^-]}) \tag{5.S9d}$$

$$[H_2CO_3] = [HCO_3^-] \times 10^{pK_1 - pH} \tag{5.S9e}$$

$$f_{H_2CO_3} = \frac{[H_2CO_3]}{[H_2CO_3] + [HCO_3^-]} = \frac{[HCO_3^-] \times 10^{pK_1 - pH}}{[HCO_3^-] + [HCO_3^-] \times 10^{pK_1 - pH}} = \frac{10^{pK_1 - pH}}{1 + 10^{pK_1 - pH}} \tag{5.S9f}$$

$$f_{H_2CO_3} = \frac{[HCO_3^-]}{[H_2CO_3] + [HCO_3^-]} = \frac{[HCO_3^-]}{[HCO_3^-] + [HCO_3^-] \times 10^{pK_1 - pH}} = \frac{1}{1 + 10^{pK_1 - pH}} \tag{5.S9g}$$

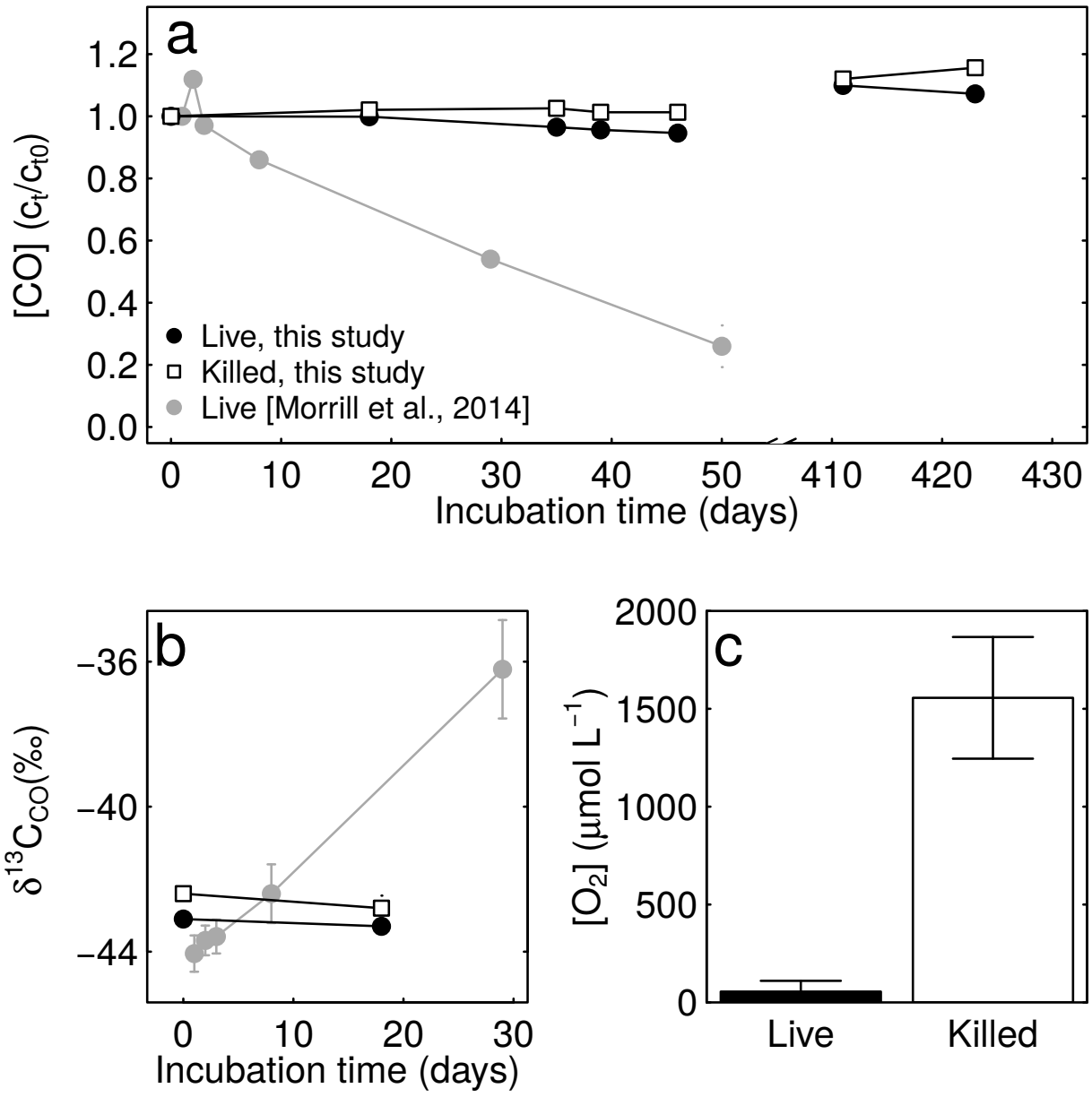

Figure 5.S1 Results of the carbon monoxide utilization experiment show that CO was not fixed/oxidized during the experiment. The difference in CO concentrations between the live (closed black circles) and killed controls (open black squares) as well as the change in CO concentrations over time remained within the GC/FID analytical error. Additionally the ^{13}CCO values after 0 and 17 days of incubation did not change (b). For comparison, results from [Morrill et al., 2014] (grey symbols), where CO utilization was indicated by decreasing concentrations of CO and the enrichment of ^{13}C in the remaining CO. The lack of CO utilization in this study was likely due to Live microcosms rapidly turned aerobic in this study, as indicated by be O_2 concentration in headspace after 11 days incubation (c). All error bars indicate standard errors.

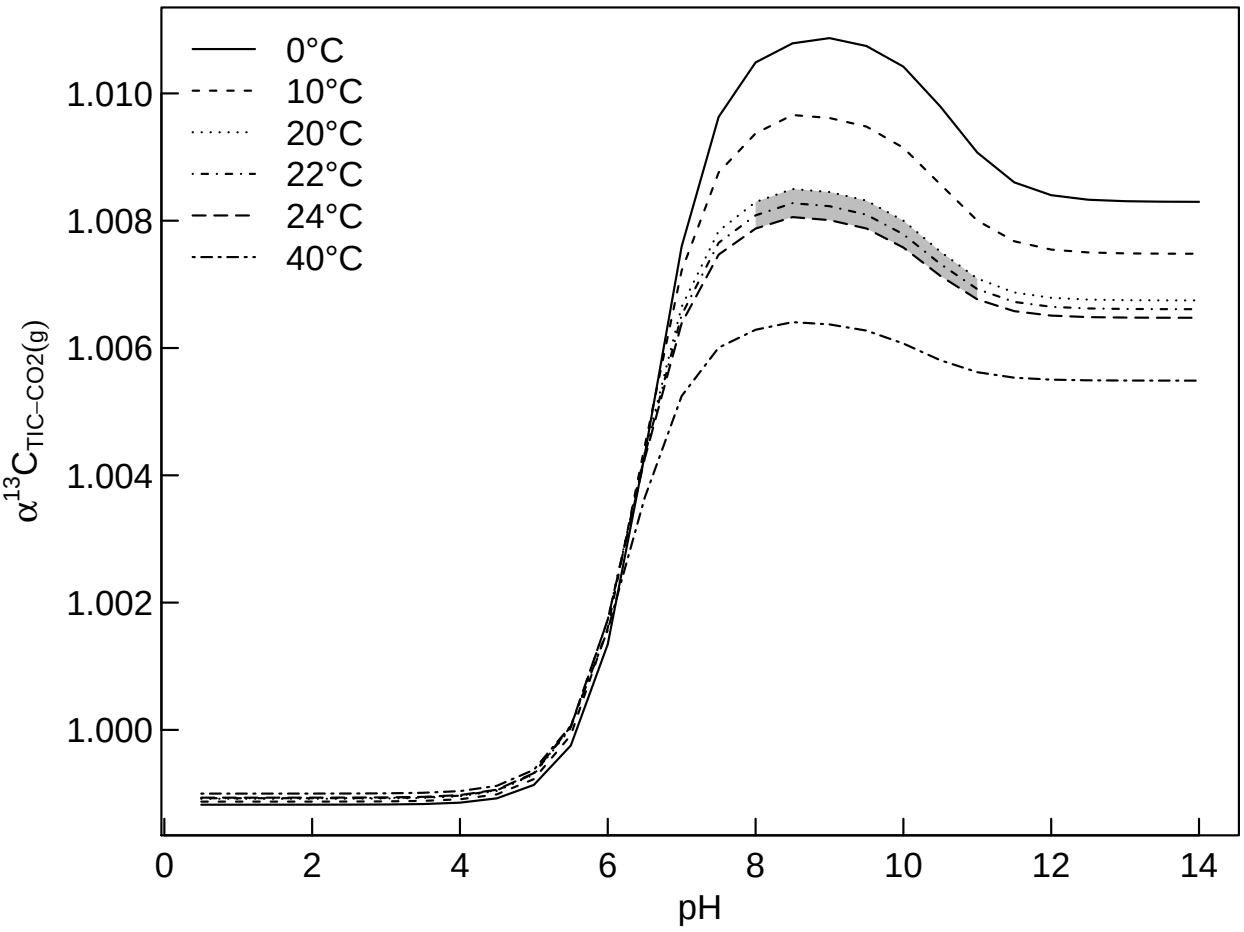

Figure 5.S2 Effect of Temperature and pH on $\alpha^{13}C_{TIC\text{-}CO_{2(g)}}$. The grey area indicates the range of conditions (pH 8-11, 20-24 °C) found in our microcosms experiments, corresponding to minimum $\alpha^{13}C_{TIC\text{-}CO_{2(g)}}$ value 1.0068 and a maximum $\alpha^{13}C_{TIC\text{-}CO_{2(g)}}$) value of 1.0085. We used 1.0076, the midpoint between these two values for our calculations. $\alpha^{13}C_{TIC\text{-}CO_{2(g)}}$ was calculated based on literature values as described in eq. 5.S1-5.S7.

Table 5.S1 Literature values for apparent fractionation among methane, water, and inorganic carbon.

Reference	lab or field	Pathway	pH	Temperature	$\alpha^{2}H_{H_2O\text{-}CH4}$	$\alpha^{13}C_{CO_2(g)\text{-}CH4}$ (lit.)[1]	$\alpha^{13}C_{TIC\text{-}CH4}$ (lit.)[1]	$\alpha\ ^{13}C_{CO_2(g)\text{-}CH4}$ (calc.)[2]
[Woltemate et al., 1984]	field	Acetate fermentation		17.5	1.459	1.046		
[Woltemate et al., 1984]	field	Acetate fermentation		17.5	1.446	1.042		
[Woltemate et al., 1984]	field	Acetate fermentation		18.5	1.452	1.049		
[Woltemate et al., 1984]	field	Acetate fermentation		18.5	1.454	1.051		
[Woltemate et al., 1984]	field	Acetate fermentation		18	1.456	1.051		
[Woltemate et al., 1984]	field	Acetate fermentation		18	1.455	1.050		
[Woltemate et al., 1984]	field	Acetate fermentation		17.5	1.459	1.046		
[Woltemate et al., 1984]	field	Acetate fermentation		19	1.438	1.052		
Claypool, Lyon and Friedman 1973[3]	field	Carbonate reduction			1.232	1.069		
Claypool, Lyon and Friedman 1973[3]	field	Carbonate reduction			1.219	1.065		
Claypool, Lyon and Friedman 1973[3]	field	Carbonate reduction			1.224	1.067		
Claypool, Lyon and Friedman 1973[3]	field	Carbonate reduction			1.228	1.070		
Claypool, Lyon and Friedman 1973[3]	field	Carbonate reduction			1.226	1.070		
Claypool, Lyon and Friedman 1973[3]	field	Carbonate reduction			1.232	1.069		
Claypool, Lyon and Friedman 1973[3]	field	Carbonate reduction			1.221	1.068		
Schoell 1982[3]	field	Carbonate reduction		5.2	1.235	1.074		
Schoell 1982[3]	field	Carbonate reduction		13.2	1.230	1.071		
Schoell 1982[3]	field	Carbonate reduction		17	1.223	1.072		
Schoell 1982[3]	field	Carbonate reduction		27.5	1.210	1.067		
Schoell 1982[3]	field	Carbonate reduction		34.6	1.205	1.064		
Schoell 1982[3]	field	Carbonate reduction		46.4	1.201	1.061		
Schoell 1982[3]	field	Carbonate reduction		12.9	1.213	1.063		
Schoell 1982[3]	field	Carbonate reduction		23.7	1.228	1.052		
Lien 1980[3]	field	Carbonate reduction		-1.3	1.236	1.090		
Lien 1980[3]	field	Carbonate reduction		-1.3	1.245	1.092		
Lien 1980[3]	field	Carbonate reduction		-1.3	1.241	1.092		
Lien 1980[3]	field	Carbonate reduction		-1.3	1.242	1.101		
Nakai 1974[3]	field	Carbonate reduction		44	1.193	1.054		
Nakai 1974[3]	field	Carbonate reduction		26.5	1.173	1.060		
Nakai 1974[3]	field	Carbonate reduction		17.5	1.189	1.070		
[Hornibrook et al., 1997]	field	Acetate fermentation	6.9	15	1.334		1.045	1.038
[Hornibrook et al., 1997]	field	Acetate fermentation	6.9	15	1.405		1.051	1.044
[Hornibrook et al., 1997]	field	Acetate fermentation	6.9	15	1.377		1.050	1.043
[Hornibrook et al., 1997]	field	Acetate fermentation	6.9	15	1.408		1.055	1.048
[Hornibrook et al., 1997]	field	Acetate fermentation	3.8	13.5	1.337		1.048	1.049
[Hornibrook et al., 1997]	field	Acetate fermentation	3.8	13.5	1.336		1.052	1.053
[Hornibrook et al., 1997]	field	Acetate fermentation	3.8	13.5	1.395		1.052	1.053
[Hornibrook et al., 1997]	field	Acetate fermentation	3.8	13.5	1.388		1.054	1.055
[Hornibrook et al., 1997]	field	Acetate fermentation	3.8	13.5	1.374		1.063	1.064
[Hornibrook et al., 1997]	field	Acetate fermentation	3.8	13.5	1.373		1.063	1.064
[Hornibrook et al., 1997]	field	Carbonate reduction	6.9	15	1.348		1.057	1.050
[Hornibrook et al., 1997]	field	Carbonate reduction	6.9	15	1.270		1.071	1.064
[Grossman et al., 1989]	field	Carbonate reduction	7.5	20[4]	1.191		1.066	1.058
[Grossman et al., 1989]	field	Carbonate reduction	8.1	20[4]	1.192		1.055	1.046
[Grossman et al., 1989]	field	Carbonate reduction	7.7	20[4]	1.191		1.067	1.058
[Grossman et al., 1989]	field	Carbonate reduction	8.7	20[4]	1.166		1.056	1.047
[Grossman et al., 1989]	field	Carbonate reduction	8.7	20[4]	1.188		1.043	1.034
[Grossman et al., 1989]	field	Carbonate reduction	8.1	20[4]	1.186		1.043	1.034
[Grossman et al., 1989]	field	Carbonate reduction	8.1	20[4]	1.192		1.043	1.034
[Grossman et al., 1989]	field	Carbonate reduction	8.2	20[4]	1.194		1.050	1.041

(Continued on next page)

Reference	lab or field	Pathway	pH	Temperature	$\alpha^{2}H_{H_2O\text{-}CH4}$	$\alpha^{13}C_{CO_2(g)\text{-}CH4}$ (lit.)[1]	$\alpha^{13}C_{TIC\text{-}CH4}$ (lit.)[1]	$\alpha\ ^{13}C_{CO_2(g)\text{-}CH4}$ (calc.)[2]
[Grossman et al., 1989]	field	Carbonate reduction	8.5	20[4]	1.197		1.050	1.041
[Grossman et al., 1989]	field	Carbonate reduction	8.7	20[4]	1.188		1.044	1.035
[Grossman et al., 1989]	field	Carbonate reduction	8.3	20[4]	1.195		1.052	1.043
[Grossman et al., 1989]	field	Carbonate reduction	8.4	20[4]	1.205		1.069	1.060
[Lansdown et al., 1992]	field	Carbonate reduction	3.5	15[4]	1.292		1.075	1.076
[Lansdown et al., 1992]	field	Carbonate reduction	3.5	15[4]	1.399		1.083	1.084
[Lansdown et al., 1992]	field	Carbonate reduction	3.5	15[4]	1.297		1.076	1.078
[Lansdown et al., 1992]	field	Carbonate reduction	3.5	15[4]	1.323		1.075	1.077
[Lansdown et al., 1992]	field	Carbonate reduction	3.5	15[4]	1.294		1.075	1.077
[Lansdown et al., 1992]	field	Carbonate reduction	3.5	15[4]	1.340		1.078	1.079
[Lansdown et al., 1992]	field	Carbonate reduction	3.5	15[4]	1.555		1.063	1.063
[Lansdown et al., 1992]	field	Carbonate reduction	3.5	15[4]	1.337		1.079	1.080
[Lansdown et al., 1992]	field	Carbonate reduction	3.5	15[4]	1.372		1.076	1.078
[Lansdown et al., 1992]	field	Carbonate reduction	3.5	15[4]	1.333		1.072	1.073
[Chasar et al., 2000]	field	Acetate fermentation	4		1.330	1.060		
[Chasar et al., 2000]	field	Acetate fermentation	4		1.340	1.060		
[Chasar et al., 2000]	field	Acetate fermentation	4		1.340	1.070		
[Chasar et al., 2000]	field	Carbonate reduction	4		1.280	1.070		
[Chasar et al., 2000]	field	Carbonate reduction	4		1.290	1.080		
[Chasar et al., 2000]	field	Carbonate reduction	4		1.280	1.080		
[Chasar et al., 2000]	field	Carbonate reduction	4		1.270	1.080		
[Chasar et al., 2000]	field	Carbonate reduction	4		1.260	1.080		
[Balabane et al., 1987]	lab	Carbonate reduction		34	1.608	1.046		
[Balabane et al., 1987]	lab	Carbonate reduction		34	1.610	1.051		
[Balabane et al., 1987]	lab	Carbonate reduction		34	1.599	1.049		
[Balabane et al., 1987]	lab	Carbonate reduction		34	1.618	1.053		
[Balabane et al., 1987]	lab	Carbonate reduction		34	1.674	1.050		
[Balabane et al., 1987]	lab	Carbonate reduction		34	1.668	1.055		
[Balabane et al., 1987]	lab	Carbonate reduction		34	1.661	1.050		
[Balabane et al., 1987]	lab	Carbonate reduction		34	1.629	1.048		
[Balabane et al., 1987]	lab	Carbonate reduction		34	1.642	1.050		
[Balabane et al., 1987]	lab	Carbonate reduction		34	1.646	1.052		

[1]Original ^{13}C stated in literature (either $\alpha^{13}C_{TIC\text{-}CH4}$ or $^{13}C_{CO_2(g)\text{-}CH4}$

[2] Converted as described in Supplemental Methods

[3] Cited after [Whiticar et al., 1986]

[4] assumed temperature

Chapter 6

Conclusions and Outlook

6.1 Carbon cycling in boreal forest soils

6.1.1 Conclusions

In the three chapters investigating boreal forest soil, this thesis provides a detailed survey of how soil organic matter chemistry and the composition and $\delta^{13}C$ values of microbial biomass vary in a latitudinal transect of mesic boreal forests. Taken together, the research presented in these chapters contributes to three distinct research domains, i.e., organic geochemistry, isotope geochemistry, and ecosystem ecology. First, from an organic geochemistry perspective, this thesis documented how climate history and diagenesis shape the chemistry of SOM in these soils. I showed that climate history and diagenesis affect distinct SOM properties, with climate history primarily influencing the lignin:carbohydrate ratio, whereas diagenesis primarily changes the composition of soil organic nitrogen. I furthermore showed that a warmer climate history and greater diagenetic alteration decrease the bioreactivity of SOM (Chapter 3).

Second, from an isotope geochemistry perspective, this thesis provided a detailed study of how the $\delta^{13}C$ values of phospholipid fatty acids (PLFA) vary with depth and latitude in these soils. As biomarkers specific to the living biomass of distinct groups of soils organisms, the $\delta^{13}C_{PLFA}$ values of these biomarkers therefore provided the means to document variations

in the natural abundance $\delta^{13}C$ values of the biomass of broad groups of microorganisms (fungi, Gram positive bacteria, and Gram negative bacteria), which allowed me to draw conclusionS about microbial substrate use patterns in undisturbed soils (Chapter 2 and 4). Third, from an ecosystem ecology perspective, this thesis identified the ecosystem processes through which climate warming will likely affect SOM properties in these soils. Most notably, warming will decrease the proportions of moss litter relative to vascular plant litter (Chapter 3). Warming will furthermore likely cause an increase in litter nitrogen concentrations, which in turn will change how litter is processed during its initial decomposition, that is, lignin will be accumulated more strongly during litter decomposition in a warmer future (Chapters 4). These changes will increase the bioreactivity of fresh plant litter, but decrease the bioreactivity of soil organic matter (Chapter 3).

6.1.2 Outlook

This thesis provided a detailed study of how $\delta^{13}C_{PLFA}$ varies along gradients of depth, latitude, and among microbial groups in these soils, along with examples of how such measurements can provide a novel window to study the cycling of carbon in intact soils. This prompts the question whether the findings in this thesis can be generalized to other soils, with three questions standing out as especially prone to direct future research.

First, what process causes absence of an increase of $\delta^{13}C$ values of fungal and bacterial PLFA with depth, in contrast to the increase of $\delta^{13}C_{SOC}$? How widespread does this pattern occur in different soil types? Does this pattern occur throughout the annual cycle? Does it also occur in deciduous forests with a distinct annual cycle of litterfall and decomposition, or is this phenomenon limited to the evergreen coniferous forests studied in this thesis? In Chapter 2, I suggested several mechanisms that could facilitate substrates availability across multiple soil horizons, including the transport of dissolved organic carbon with water percolating through the soil profile, root litter and exudates, and mycelial transport. Fu-

ture studies are needed explore to which degree these mechanisms are relevant under field conditions, e.g., though experiments that apply ^{13}C-labeled litter and CO_2 pulse-labelling. Furthermore, all such mechanisms imply that soil microorganisms consume recently fixated carbon substrates, even if they are located in soil horizons dominated by centuries old SOM. Studies that measure the radiocarbon age of dissolved organic carbon, microbial biomass, and respired CO_2 in mineral soil horizons will therefore help to quantify the consumption of 'young' (bomb-^{14}C) carbon in 'old' soil horizons dominated by pre-bomb carbon.

Second, which mechanism cause the depletion of ^{13}C in fungal relative to bacterial PLFA? This pattern could have resulted from a difference between fungal and bacterial substrate use patterns, from stronger discrimination against ^{13}C during substrate uptake into biomass or during PLFA biosynthesis. Distinguishing these mechanisms will require experiments that cultivate fungi and bacteria on various substrates under controlled conditions. In Chapter 2, I hypothesized that the depletion of fungal relative to bacterial biomass, in combination with lower fungi to bacteria ratios at greater depth, could provide a novel mechanism that contributes to the increase of $\delta^{13}C_{SOC}$ with depth. Future studies could further prove this mechanism by complementing measurements of $\delta^{13}C_{PLFA}$, indicative of the δ^{13}C values of living microbial biomass, with measurements of the δ^{13}C values of biomarkers indicative of microbial necromass, like amino sugars, sterols (e.g. ergosterol), or hopanoids. Such studies will also be helpful in assessing the degree to which soil properties are shaped by the proportions of the fungal and bacterial necromass inputs.

Third, how reliably can $\delta^{13}C_{PLFA}$ values predict microbial substrate use patterns? This thesis found a general consistency between $\delta^{13}C_{PLFA}$ values and changes in NMR spectra, but further research needs to compare $\delta^{13}C_{PLFA}$ values with other methods to determine microbial substrate use like the potential activities of extracellular enzymes, soil metatranscriptome and metaproteome analysis, as well as studies that compare $\delta^{13}C_{PLFA}$ to changes in SOM chemistry in decomposition experiments. While some such work on this question has been

presented in the past [Andrews et al., 2000; Biasi et al., 2005; Cusack et al., 2011], this method requires further studies covering a wider range of ecosystems and locations to be considered fully reliable.

More generally, this thesis demonstrates the potential of systematically comparing the variations of $\delta^{13}C_{PLFA}$ varies across ecosystems. Such attempts, however, currently remain limited by the sparse availability of $\delta^{13}C_{PLFA}$ data in literature, and in particular, the lack of raw data in many publications. This limited data availability stands in contrast to the popularity of $\delta^{13}C_{PLFA}$ analysis in many manipulative ecosystem studies, including soil warming experiments and FACE studies. The data from the control treatments of such experiments could provide a comprehensive basis to study the global and regional variations in $\delta^{13}C_{PLFA}$. Unfortunately, such data are rarely published in raw format and to my knowledge no specialized databases for such isotopic data of microbial biomarkers exist so far.

6.2 Serpentinization associated springs

6.2.1 Conclusions

Chapter 5 investigated the metabolic potential of the microbial communities at The Cedars, a site of present day serpentinization located in northern California. Based on the $\delta^{13}C$ values of methane and other geochemical indicators, Morrill et al. [2013] concluded that methane at The Cedars would be at of at least partially microbial origin. I therefore hypothesized that microorganisms at The Cedars would be capable of methanogenesis. This hypothesis was confirmed by labeled substrate tracing experiments, which is consistent with the microbiological and geochemical surveys of this site. The microcosm experiments conducted as part of Chapter 5 in this thesis furthermore provided evidence of the simultaneous microbial production and consumption of volatile organic acids at The Cedars.

The findings of Chapter 5 stand in direct contrast to results from The Tablelands, a

site of present day serpentinization located in western Newfoundland. At these site, we conducted experiments similar to those in Chapter 5 [Morrill et al., 2014]. These experiments found no evidence for the presence of methanogen in the microbial communities present at the Tablelands, which is consistent with stable carbon isotope values and other geochemical indicators at this site [Szponar et al., 2013]. Together, the microcosm experiments conducted with materials from The Cedars (Chapter 5) and The Tablelands [Morrill et al., 2014] thus experimentally confirmed the interpretation of stable isotope values of methane as indicators of contrasting sources of methane at these sites.

6.2.2 Outlook

The results presented in this thesis point out several questions for future research. Most importantly, it remains unclear why these sites feature microbial communities with such strikingly different metabolic capabilities, even though geochemical conditions are similar at both sites. Did this difference result from stochastic variations in the which microorganisms colonized each site (i.e., an island effect)? This seems rather implausible given the similarity of microbial communities in ultra-basic, reducing springs located a great geographical distance apart and in isolation [Brazelton et al., 2012, Schrenk et al., 2013, Suzuki et al., 2014]. Or are these differences due to some geochemical controls that makes The Cedars habitable to biogeochemically relevant populations of methanogens, while The Tablelands and most other terrestrial sites of serpentinization are not? A third possibility would be that methanogens are present in most such sites, but that their activity and abundance is limited by geochemical conditions, i.e., reducing environments that contain sufficient inorganic carbon to allow carbonate reducing methanogenesis.

Another line of future research opened in this thesis investigating the origin and fate of volatile organic acids (VOA) in sites of serpentinization. The measurements made over the course of this thesis indicate that the groundwaters discharging at The Cedars and

The Tablelands both contain elevated concentrations of acetate, along with other VOAs. While different sources of methane have been distinguished based on the stable carbon and hydrogen isotope values of methane [Whiticar et al., 1986, Whiticar, 1999, Etiope et al., 2013], no such tools are available to distinguish between biogenic and abiogenic acetate. Since the carboxylic-C group of acetate can be equilibrated by through microbial activity [Thomas, 2008], this will likely require the position specific analysis of stable carbon isotopes in acetate.

6.3 Natural abundance stable isotope values as a tool to study microbial processes

This thesis provided three examples of how stable isotope values can inform on microbial processes in undisturbed or unaccessible ecosystems.

1. Variation in the origins of microbial sources of SOM.
2. Diagenetic and climate controls on SOM chemistry and its relationship to microbial substrate use.
3. Sourcing methane and its relationship to the geochemistry of ultramafic springs.

Together, these examples from two strikingly different ecosystem demonstrate how variations in natural abundance stable isotope values are a powerful tool to study the role of microorganisms in the geochemical cycling of elements.

Bibliography

WR Abraham and C Hesse. Isotope fractionations in the biosynthesis of cell components by different fungi: a basis for environmental carbon flux studies. *FEMS microbiology ecology*, 46(1):121–8, 2003. doi: 10.1016/S0168-6496(03)00203-4.

WR Abraham, C Hesse, and O Pelz. Ratios of Carbon Isotopes in Microbial Lipids as an Indicator of Substrate Usage. *Applied and environmental microbiology*, 64(11):4202–4209, 1998.

TA Abrajano, NC Sturchio, BM Kennedy, GL Lyon, K Muehlenbachs, and JK Bohlke. Geochemistry of reduced gas related to serpentinization of the Zambales ophiolite, Philippines. *Applied Geochemistry*, 5(5-6):625–630, 1990. doi: 10.1016/0883-2927(90)90060-I.

TA Abrajano, DE Murphy, J Fang, P Comet, and JM Brooks. 13C/12C ratios in individual fatty acids of maarine mytilids with and without bacterial symbionts. *Organic Geochemistry*, 21(6/7):611–617, 1994. doi: 10.1016/0146-6380(94)90007-8.

TF Anderson and MA Arthur. Stable isotopes of oxygen and carbon and their application to sedimentological and paleoenvironmental problems. In MA Arthur, TF Anderson, IR Kaplan, J Veizer, and LS Land, editors, *Stable isotopes in sedimentary geology Vol. 10*, pages 1–150. SEPM Short Course, Columbia, SC, USA, 1983.

JA Andrews, R Matamala, KM Westover, and WH Schlesinger. Temperature effects on

the diversity of soil heterotrophs and the δ13C of soil-respired CO2. *Soil Biology and Biochemistry*, 32:699–706, 2000.

W Bach and KJ Edwards. Iron and sulfide oxidation within basalt ocean crust: Implications for chemolithoautotrophic microbial biomass production. *Geochimica et Cosmochimica Acta*, 67(20):3871–3887, 2003. doi: 10.1016/S0016-7037(00)00304-1.

M Balabane, E Galimov, M Hermann, and R Létolle. Hydrogen and carbon isotope fractionation during experimental production of bacterial methane. *Organic Geochemistry*, 11 (2):115–119, 1987. doi: 10.1016/0146-6380(87)90033-7.

JA Baldock, JM Oades, AG Waters, X Peng, AM Vassallo, and MA Wilson. Aspects of the Chemical Structure of Soil Organic Materials as Revealed by Solid-State 13 C NMR Spectroscopy. *Biogeochemistry1*, 16(1):1–42, 1992.

RD Banerjee and SP Sen. Antibiotic Activity of Bryophytes. *The Bryologist*, 82(2):141–153, 1979.

I Barnes, VC Lamarche, and G Himmelberg. Geochemical evidence of present-day serpentinization. *Science*, 156(3776):830–832, 1967. doi: 10.1126/science.156.3776.830.

A Basile, S Giordano, JA López Sáez, and RC Cobianchi. Antibacterial activity of pure flavonoids isolated from mosses. *Phytochemistry*, 52(8):1479–1482, 1999. doi: 10.1016/S0031-9422(99)00286-1.

F Bastida, JL Moreno, C Nicolás, T Hernández, and C García. Soil metaproteomics: A review of an emerging environmental science. Significance, methodology and perspectives. *European Journal of Soil Science*, 60(6):845–859, 2009. doi: 10.1111/j.1365-2389.2009.01184.x.

C Baum, M Fienemann, S Glatzel, and G Gleixner. Overstory-specific effects of litter fall on the microbial carbon turnover in a mature deciduous forest. *Forest Ecology and Management*, 258(2):109–114, 2009. doi: 10.1016/j.foreco.2009.03.047.

K Baumann, P Marschner, RJ Smernik, and JA Baldock. Residue chemistry and microbial community structure during decomposition of eucalypt, wheat and vetch residues. *Soil Biology and Biochemistry*, 41(9):1966–1975, 2009. doi: 10.1016/j.soilbio.2009.06.022.

R Benner, ML Fogel, KE Spargue, and RE Hodson. Depletion of 13C in lignin and its implications for stable carbon isotope studies. *Nature*, 329(6141):708–710, 1987. doi: doi:10.1038/329708a0.

B Berg and C McClaugherty. *Plant Litter. Decomposition, Humus Formation, Carbon Sequestration.* Springer, Berlin, 2008.

B Berg, M-B Johansson, G Ekbohm, C McClaugherty, F Rutigliano, and AV de Santo. Maximum decomposition limits of forest litter types: a synthesis. *Canadian Journal of Botany*, 74(5):659–672, 1996. doi: 10.1139/b96-084.

D Berry, B Stecher, A Schintlmeister, J Reichert, S Brugiroux, B Wild, W Wanek, A Richter, I Rauch, T Decker, A Loy, and M Wagner. Host-compound foraging by intestinal microbiota revealed by single-cell stable isotope probing. *Proceedings of the National Academy of Sciences of the United States of America*, 110(12):4720–4725, 2013. doi: 10.1073/pnas.1219247110.

C Biasi, O Rusalimova, H Meyer, C Kaiser, W Wanek, P Barsukov, H Junger, and A Richter. Temperature-dependent shift from labile to recalcitrant carbon sources of arctic heterotrophs. *Rapid communications in mass spectrometry*, 19(11):1401–8, 2005. doi: 10.1002/rcm.1911.

SA Billings and SE Ziegler. Linking microbial activity and soil organic matter transformations in forest soils under elevated CO2. *Global Change Biology*, 11(2):203–212, feb 2005. doi: 10.1111/j.1365-2486.2005.00909.x.

SA Billings and SE Ziegler. Altered patterns of soil carbon substrate usage and heterotrophic respiration in a pine forest with elevated CO 2 and N fertilization. *Global Change Biology*, 14(5):1025–1036, 2008. doi: 10.1111/j.1365-2486.2008.01562.x.

SA Billings, SE Ziegler, WH Schlesinger, R Benner, and DdB Richter. Predicting carbon cycle feedbacks to climate: Integrating the right tools for the job, 2012.

CW Bingeman, JE Verner, and WP Martin. The Effect of the Addition of Organic Materials on the Decomposition of an Organic Soil. *Soil Science Society Proceedings*, 17(1):34–38, 1953.

KE Bisbee, ST Gower, JM Norman, and EV Nordheim. Environmental controls on ground cover species composition and productivity in a boreal black spruce forest. *Oecologia*, 129 (2):261–270, 2001. doi: 10.1007/s004420100719.

N Blair, A Leu, E Muñoz, J Olsen, E Kwong, and D Des Marais. Carbon isotopic fractionation in heterotrophic microbial metabolism. *Applied and environmental microbiology*, 50 (4):996–1001, oct 1985.

JG Blank, SJ Green, D Blake, JW Valley, NT Kita, A Treiman, and PF Dobson. An alkaline spring system within the Del Puerto Ophiolite (California, USA): A Mars analog site. *Planetary and Space Science*, 57(5-6):533–540, 2009. doi: 10.1016/j.pss.2008.11.018.

R Bol, N Poirier, J Balesdent, and G Gleixner. Molecular turnover time of soil organic matter in particle - size fractions of an arable soil. *Rapid Communications in Mass Spectrometry*, 23:2551–2558, 2009. doi: 10.1002/rcm.4124.

GB Bonan and K Van Cleve. Soil temperature, nitrogen mineralization, and carbon source-sink relationships in boreal forests. *Canadian Journal of Forest Research*, 22:629–639, 1992.

M Bonkowski. Protozoa and plant growth: The microbial loop in soil revisited. *New Phytologist*, 162(3):617–631, 2004. doi: 10.1111/j.1469-8137.2004.01066.x.

B Boström, D Comstedt, and A Ekblad. Isotope fractionation and 13C enrichment in soil profiles during the decomposition of soil organic matter. *Oecologia*, 153(1):89–98, 2007. doi: 10.1007/s00442-007-0700-8.

S Bouillon and HTS Boschker. Bacterial carbon sources in coastal sediments : a cross-system analysis based on stable isotope data of biomarkers. *Biogeosciences*, 3:175–185, 2006.

K. Bowering, K. Edwards, and S.E. Ziegler. Dissolved organic carbon fluxes from soil organic horizons within mature and regenerating boreal forest stands. *Biogeochemistry*, in review.

WJ Brazelton, MO Schrenk, DS Kelley, and JA Baross. Methane- and sulfur-metabolizing microbial communities dominate the lost city hydrothermal field ecosystem. *Applied and Environmental Microbiology*, 72(9):6257–6270, 2006. doi: 10.1128/AEM.00574-06.

WJ Brazelton, B Nelson, and MO Schrenk. Metagenomic evidence for H2 oxidation and H2 production by serpentinite-hosted subsurface microbial communities. *Frontiers in Microbiology*, 2(January):268, jan 2012. doi: 10.3389/fmicb.2011.00268.

WJ Brazelton, PL Morrill, N Szponar, and MO Schrenk. Bacterial communities associated with subsurface geochemical processes in continental serpentinite springs. *Applied and environmental microbiology*, 79(13):3906–3916, apr 2013. doi: 10.1128/AEM.00330-13.

JT Brenna, TN Corso, HJ Tobias, and RJ Caimi. High-precision continuous-flow iso-

tope ratio mass spectrometry. *Mass spectrometry reviews*, 16(5):227–258, 1998. doi: 10.1002/(SICI)1098-2787(1997)16:5<227::AID-MAS1>3.0.CO;2-J.

PC Brookes. *The Potential of Microbiological Properties as Indicators in Soil Pollution Monitoring*, pages 229–254. Birkhaeuser Basel, Basel, 1993.

ID Bull, NR Parekh, GH Hall, P Ineson, and RP Evershed. Detection and classifcation of atmospheric methane oxidizing bacteria in soil. *Nature*, 405(1998):175–178, 2000.

RA Burke. Possible Influence of Hydrogen Concentration on Microbial Methane Stable. *Chemosphere*, 26(1-4):55–67, 1993.

S Butler, SA Billings, and SE Zieger. Decomposition dynamics and chemical composition of boreal upland forest moss tissues. in preparation.

N Cannone, D Wagner, HW Hubberten, and M Guglielmin. Biotic and abiotic factors influencing soil properties across a latitudinal gradient in Victoria Land, Antarctica. *Geoderma*, 144(1-2):50–65, 2008. doi: 10.1016/j.geoderma.2007.10.008.

ND Charney, F Babst, B Poulter, S Record, VM Trouet, D Frank, BJ Enquist, and MEK Evans. Observed forest sensitivity to climate implies large changes in 21st century North American forest growth. *Ecology Letters*, 2016. doi: 10.1111/ele.12650.

LS Chasar, JP Chanton, PH Glaser, and DI Siegel. Methane concentration and stable isotope distribution as evidence of rhizospheric processes: Comparison of a fen and bog in the Glacial Lake Agassiz Peatland complex. *Annals of Botany*, 86(3):655–663, 2000. doi: 10.1006/anbo.2000.1172.

C Churchland, SJ Grayston, and P Bengtson. Spatial variability of soil fungal and bacterial abundance: Consequences for carbon turnover along a transition from a forested to clear-cut site. *Soil Biology and Biochemistry*, 63:5–13, 2013. doi: 10.1016/j.soilbio.2013.03.015.

LA Cifuentes and GG Salata. Signicance of carbon isotope discrimination between bulk carbon and extracted phospholipid fatty acids in selected terrestrial and marine environments. *Organic Geochemistry*, 32:613–621, 2001. doi: doi:10.1016/S0146-6380(00)00198-4.

I Clark and P Fritz. *Environmental Isotopes in Hydrogeology*. Lewis Publishers, New York, 1997.

RB Coffin, DJ Velinsky, R Devereux, WA Prince, and LA Cifuentes. Stable carbon isotope analysis of nucleic acids to trace sources of dissolved substrates used by estuarine bacteria. *Applied and environmental microbiology*, 56(7):2012–2020, 1990.

RG Coleman. Propsecting for ophiolites along the Carlifornia continental margin. In *Ophiolites and Oceanic Crust: New Insights from Field Studies and the Ocean Drilling Program.*, pages 351–364. Geological Society of America, Bolder, Colorade, 2000.

FS Colwell and S D'Hondt. Nature and Extent of the Deep Biosphere. *Reviews in Mineralogy and Geochemistry*, 75(1):547–574, 2013. doi: 10.2138/rmg.2013.75.17.

RT Conant, MG Ryan, GI Ågren, HE Birge, EA Davidson, PE Eliasson, SE Evans, SD Frey, CP Giardina, F Hopkins, R Hyvönen, MUF Kirschbaum, JM Lavallee, J Leifeld, WJ Parton, MJ Steinweg, MD Wallenstein, JÅM Wetterstedt, and MA Bradford. Temperature and soil organic matter decomposition rates - synthesis of current knowledge and a way forward. *Global Change Biology*, 17:3391–3404, 2011. doi: 10.1111/j.1365-2486.2011.02496.x.

MP Cooke, HM Talbot, and T Wagner. Tracking soil organic carbon transport to continental margin sediments using soil-specific hopanoid biomarkers: A case study from the Congo fan (ODP site 1075). *Organic Geochemistry*, 39(8):965–971, 2008. doi: 10.1016/j.orggeochem.2008.03.009.

TB Coplen. Guidelines and recommended terms for expression of stable-isotope-ratio and

gas-ratio measurement results. *Rapid Communications in Mass Spectrometry*, 25(17): 2538–2560, 2011. doi: 10.1002/rcm.5129.

MF Cotrufo, MD Wallenstein, CM Boot, K Denef, and E Paul. The Microbial Efficiency-Matrix Stabilization (MEMS) framework integrates plant litter decomposition with soil organic matter stabilization: do labile plant inputs form stable soil organic matter? *Global Change Biology*, pages n/a–n/a, 2013. doi: 10.1111/gcb.12113.

M-M Coûteaux, P Bottner, and B Berg. Litter decomposition, climate and liter quality. *Trends in ecology and evolution*, 10(2):63–66, feb 1995.

BR Cowie, GF Slater, L Bernier, and LA Warren. Carbon isotope fractionation in phospholipid fatty acid biomarkers of bacteria and fungi native to an acid mine drainage lake. *Organic Geochemistry*, 40(9):956–962, 2009. doi: 10.1016/j.orggeochem.2009.06.004.

JM Craine, C Morrow, and N Fierer. Microbial nitrogen limitation increases decomposition. *Ecology*, 88(8):2105–13, aug 2007.

M Crespo-Medina, KI Twing, MDY Kubo, TM Hoehler, D Cardace, T McCollom, and MO Schrenk. Insights into environmental controls on microbial communities in a continental serpentinite aquifer using a microcosm-based approach. *Frontiers in Microbiology*, 5(November):1–9, 2014. doi: 10.3389/fmicb.2014.00604.

DF Cusack, WL Silver, MS Torn, SD Burton, and MK Firestone. Changes in microbial community characteristics and soil organic matter with nitrogen additions in two tropical forests. *Ecology*, 92(3):621–32, mar 2011. doi: 10.1890/10-0459.1.

FL Daae, I Økland, H Dahle, SL Jørgensen, IH Thorseth, and RB Pedersen. Microbial life associated with low-temperature alteration of ultramafic rocks in the Leka ophiolite complex. *Geobiology*, 11(4):318–339, 2013. doi: 10.1111/gbi.12035.

B Dauwe, JJ Middelburg, P Van Rijswijk, J Sinke, PMJ Herman, and CHR Heip. Enzymatically hydrolyzable amino acids in North Sea sediments and their possible implication for sediment nutritional values. *Journal of Marine Research*, 57(1):109–134, 1999. doi: 10.1357/002224099765038580.

J de Vrieze. The littlest farmhands. *Science*, 21(2):680–683, 2015.

JL DeForest, DR Zak, KS Pregitzer, and AJ Burton. Atmospheric nitrate deposition, microbial community composition, and enzyme activity in northern hardwood forests. *Soil Science Society of America Journal*, 68(1):132–138, 2004. doi: 10.2136/sssaj2004.1320.

P Deines, D Langmuir, and RS Harmon. Stable carbon isotope ratios and the existence of a gas phase in the evolution of carbonate ground waters. *Geochimica et Cosmochimica Acta*, 38(7):1147–1164, 1974. doi: 10.1016/0016-7037(74)90010-6.

MJ DeNiro and S Epstein. Mechanism of carbon isotope fractionation associated with lipid synthesis. *Science*, 197(4300):261–263, 1977. doi: 10.1126/science.327543.

DJ Des Marais. Isotopic Evolution of the Biogeochemical Carbon Cycle During the Precambrian. *Reviews in Mineralogy and Geochemistry*, 43(1):555–578, 2001. doi: 10.2138/gsrmg.43.1.555.

A Dey and JN De. Antifungal bryophytes: a possible role against human pathogens and in plant protection. *Research journal of Botany*, 6(4):129–140, 2011. doi: 10.3923/rjb.2011.129.140.

HJ Di, KC Cameron, and RG McLaren. Isotopic dilution methods to determine the gross transformation rates of nitrogen, phosphorus, and sulfur in soil: a review of the theory, methodologies, and limitations. *Soil Research*, 38(1):213–230, jan 2000.

RF Dias, KH Freeman, and SG Franks. Gas chromatography-pyrolysis-isotope ratio mass spectrometry: A new method for investigating intramolecular isotopic variation in low molecular weight organic acids. *Organic Geochemistry*, 33(2):161–168, 2002. doi: 10.1016/S0146-6380(01)00141-3.

P Dijkstra, A Ishizu, R Doucett, SC Hart, E Schwartz, OV Menyailo, and BA Hungate. 13C and 15N natural abundance of the soil microbial biomass. *Soil Biology and Biochemistry*, 38(11):3257–3266, 2006. doi: 10.1016/j.soilbio.2006.04.005.

JL Drever. *The Geochemistry of Natural Waters: Surface and Groundwaater Environments*. Prentice Hall, New Jersey, 3rd edition, 1997.

KA Edwards, K Bowering, A Skinner, and SE Ziegler. Field estimates of doc transport through organic soils of a boreal forest climate transect. in preparation.

JR Ehleringer, ED Schulze, H Ziegler, OL Lange, GD Farquhar, and IR Cowar. Xylem-tapping mistletoes: water or nutrient parasites. *Science*, 227(4693):1479–1481, 1985. doi: 10.1126/science.227.4693.1479.

JM Eiler. Paleoclimate reconstruction using carbonate clumped isotope thermometry. *Quaternary Science Reviews*, 30(25-26):3575–3588, 2011. doi: 10.1016/j.quascirev.2011.09.001.

JM Eiler, B Bergquist, I Bourg, P Cartigny, J Farquhar, A Gagnon, W Guo, I Halevy, A Hofmann, TE Larson, N Levin, EA Schauble, and D Stolper. Frontiers of stable isotope geoscience, 2014.

Environment Canada. *Canadian Climate Normals or Averages 1981-2010*. Fredericton, NB, Canada, 2014.

J Esperschütz, A Pérez-de Mora, K Schreiner, G Welzl, F Buegger, J Zeyer, F Hagedorn,

JC Munch, and M Schloter. Microbial food web dynamics along a soil chronosequence of a glacier forefield. *Biogeosciences*, 8(11):3283–3294, 2011. doi: 10.5194/bg-8-3283-2011.

G Etiope and B Sherwood Lollar. Abiotic methane on earth. *Reviews of Geophysics*, 51(2): 276–299, 2013. doi: 10.1002/rog.20011.

G Etiope, M Schoell, and H Hosgörmez. Abiotic methane flux from the Chimaera seep and Tekirova ophiolites (Turkey): Understanding gas exhalation from low temperature serpentinization and implications for Mars. *Earth and Planetary Science Letters*, 310 (1-2):96–104, 2011. doi: 10.1016/j.epsl.2011.08.001.

G Etiope, S Vance, LE Christensen, JM Marques, and I Ribeiro da Costa. Methane in serpentinized ultramafic rocks in mainland Portugal. *Marine and Petroleum Geology*, 45: 12–16, 2013. doi: 10.1016/j.marpetgeo.2013.04.009.

PG Falkowski, T Fenchel, and EF Delong. The microbial engines that drive Earth's biogeochemical cycles. *Science (New York, N.Y.)*, 320(5879):1034–9, may 2008. doi: 10.1126/science.1153213.

T Fenchel. The microbial loop - 25 years later. *Journal of Experimental Marine Biology and Ecology*, 366(1-2):99–103, 2008. doi: 10.1016/j.jembe.2008.07.013.

X Feng, AJ Simpson, KP Wilson, DD Williams, and MJ Simpson. Increased cuticular carbon sequestration and lignin oxidation in response to soil warming. *Nature Geoscience*, 1(12): 836–839, 2008. doi: 10.1038/ngeo361.

TR Filley, MK McCormick, SE Crow, K Szlavecz, DF Whigham, CT Johnston, and RN van den Heuvel. Comparison of the chemical alteration trajectory of Liriodendron tulipifera L. leaf litter among forests with different earthworm abundance. *Journal of Geophysical Research: Biogeosciences*, 113(1), 2008. doi: 10.1029/2007JG000542.

C Fissore, CP Giardina, RK Kolka, CC Trettin, GM King, MF Jurgensen, CD Barton, and SD Mcdowell. Temperature and vegetation effects on soil organic carbon quality along a forested mean annual temperature gradient in North America. *Global Change Biology*, 14 (1):193–205, 2008. doi: 10.1111/j.1365-2486.2007.01478.x.

AJ Franzluebbers, RL Haney, CW Honeycutt, MA Arshad, HH Schomberg, and FM Hons. Climatic influences on active fractions of soil organic matter. *Soil Biology and Biochemistry*, 33(7-8):1103–1111, 2001. doi: 10.1016/S0038-0717(01)00016-5.

P Fritz, ID Clark, J-C Fontes, MJ Whiticar, and E Faber. Deuterium and 13C evidence for low temperature production of hydrogen and methane in a highly alkaline groundwater environment in Oman. In K Maest, editor, *Water-rock Interaction*, pages 793–796. Rotterdam, 1992.

S Frolking, ML Goulden, SC Wofsy, S-M Fan, DJ Sutton, JW Munger, AM Bazzaz, BC Daube, PM Crill, JD Aber, LE Band, X Wang, K Savage, T Moore, and RC Harriss. Modelling temporal variability in the carbon balance of a spruce/moss boreal forest. *Global Change Biology*, 2(4):343–366, 1996. doi: 10.1111/j.1365-2486.1996.tb00086.x.

Å Frostegård, A Tunlid, and E Baarth. Communities from Two Soil Types Metals Phospholipid Fatty Acid Composition , Biomass , and Activity of Microbial Communities from Two Soil Types Experimentally Exposed to Different Heavy Metals. *Applied and environmental microbiology*, 59(11):3605–3616, 1993.

Å Frostegård, A Tunlid, and E Bååth. Use and misuse of PLFA measurements in soils. *Soil Biology and Biochemistry*, 43(8):1621–1625, dec 2010. doi: 10.1016/j.soilbio.2010.11.021.

B Fry, A Joern, and PL Parker. Grasshopper food web analysis: use of carbon isotope ratios to examine feeding relationships among terrestrial herbivores, 1978.

JN Galloway, FJ Dentener, DG Capone, EW Boyer, RW Howarth, SP Seitzinger, GP Asner, CC Cleveland, PA Green, EA Holland, DM Karl, AF Michaels, JH Porter, AR. Townsend, and CJ Vörösmarty. *Nitrogen cycles: Past, present, and future*, volume 70. 2004. ISBN 1434924130. doi: 10.1007/s10533-004-0370-0.

C Gawad, W Koh, and SR Quake. Single-cell genome sequencing: current state of the science. *Nature reviews. Genetics*, 17(3):175–188, 2016. doi: 10.1038/nrg.2015.16.

JT Gelwicks, JB Risatti, and JM Hayes. Carbon isotope effects associated with autotrophic acetogenesis. *Organic geochemistry*, 14(4):441–6, 1989.

B Glaser. Compound-specific stable-isotope (δ13C) analysis in soil science. *Journal of Plant Nutrition and Soil Science*, 168(5):633–648, 2005. doi: 10.1002/jpln.200521794.

S T Gower, J G Vogel, M Norman, C J Kucharik, and S J Steele. Carbon distribution and aboveground net primary production in aspen , jack pine , and black spruce stands in Saskatchewan and Manitoba , Canada. *Journal of Geophysical Research*, 102(D24): 29029–29041, 1997. doi: 10.1029/97JD02317.

ST Gower, O Krankina, and RJ Olson. Net primary production and carbon allocation patterns of boreal forest ecosystems. *Ecological Applications*, 11(5):1395–1411, 2001. doi: 10.1890/1051-0761(2001)011[1395:NPPACA]2.0.CO;2.

MC Graham, MA Eaves, JG Farmer, J Dobson, and AE Fallick. A Study of Carbon and Nitrogen Stable Isotope and Elemental Ratios as Potential Indicators of Source and Fate of Organic Matter in Sediments of the Forth Estuary, Scotland. *Estuarine, Coastal and Shelf Science*, 52(3):375–380, 2001. doi: 10.1006/ecss.2000.0742.

SA Grandy and JC Neff. Molecular C dynamics downstream: the biochemical decomposition sequence and its impact on soil organic matter structure and function. *The Science of the total environment*, 404(2-3):297–307, 2008. doi: 10.1016/j.scitotenv.2007.11.013.

TJ Griffis, SD Sargent, JM Baker, X Lee, BD Tanner, J Greene, E Swiatek, and K Billmark. Direct measurement of biosphere-atmosphere isotopic CO 2 exchange using the eddy covariance technique. *Journal of Geophysical Research*, 113(D08):D08304, 2008. doi: 10.1029/2007JD009297.

EL Grossman, BK Coffman, SJ Fritz, and H Wada. Bacterial production of methane and its influence on ground-water chemistry in east-central Texas aquifers. *Geology*, 17(6): 495–499, 1989. doi: 10.1130/0091-7613(1989)017<0495:BPOMAI>2.3.CO;2.

N Gruber and JN Galloway. An Earth-system perspective of the global nitrogen cycle. *Nature*, 451(7176):293–6, jan 2008. doi: 10.1038/nature06592.

U Hagemann and MT Moroni. Moss and lichen decomposition in old-growth and harvested high-boreal forests estimated using the litterbag and minicontainermethods. *Soil Biology and Biochemistry*, 87:10–24, 2015. doi: 10.1016/j.soilbio.2015.04.002.

JM Hayes. Factors controlling 13C contents of sedimentary organic compounds: Principles and evidence. *Marine Geology*, 113:111–125, 1993. doi: 10.1016/0025-3227(93)90153-M.

JM Hayes. Fractionation of Carbon and Hydrogen Isotopes in Biosynthetic Processes. *Reviews in Mineralogy and Geochemistry*, 43(March):225–277, 2001. doi: 10.2138/gsrmg.43.1.225.

JM Hayes, KH Freeman, BN Popp, and CH Hoham. Compound-specific isotopic analyses: a novel tool for reconstruction of ancient biogeochemical processes. *Organic geochemistry*, 16(4-6):1115–28, jan 1990. doi: 10.1016/0146-6380(90)90147-R.

JI Hedges, GL Cowie, JE Richey, PD Quay, R Benner, M Strom, and BR Forsberg. Origins and Processing of Organic-Matter in the Amazon River as Indicated by Carbohydrates and Amino-Acids. *Limnology and Oceanography*, 39(4):743–761, 1994. doi: 10.4319/lo.1994.39.4.0743.

VB Heuer, JW Pohlman, ME Torres, M Elvert, and KU Hinrichs. The stable carbon isotope biogeochemistry of acetate and other dissolved carbon species in deep subseafloor sediments at the northern Cascadia Margin. *Geochimica et Cosmochimica Acta*, 73(11): 3323–3336, 2009. doi: 10.1016/j.gca.2009.03.001.

S Hilli, S Stark, and J Derome. Carbon Quality and Stocks in Organic Horizons in Boreal Forest Soils. *Ecosystems*, 11(2):270–282, 2008. doi: 10.1007/s10021-007-9121-0.

EA Hobbie and RA Werner. Intramolecular, compound-specific, and bulk carbon isotope patterns in C3 and C4 plants: a review and synthesis. *New Phytologist*, 161:371–385, 2004. doi: 10.1046/j.1469-8137.2004.00970.x.

Sarah E Hobbie. Temperature and plant species control over litter decomposition in Alaska Tundra. *Ecological Monographs*, 66(4):502–522, 1996. doi: 10.2307/2963492.

SE Hobbie, KJ Nadelhoffer, and P Högberg. A synthesis: The role of nutrients as constraints on carbon balances in boreal and arctic regions. *Plant and Soil*, 242(1):163–170, 2002. doi: 10.1023/A:1019670731128.

ERC Hornibrook, FJ Longstaffe, and WS Fyfe. Spatial distribution of microbial methane production pathways in temperate zone wetland soils: Stable carbon and hydrogen isotope evidence. *Geochimica et Cosmochimica Acta*, 61(4):745–753, 1997. doi: 10.1016/S0016-7037(96)00368-7.

H Hosgörmez. Origin of the natural gas seep of Çirali (Chimera), Turkey: Site of the first Olympic fire. *Journal of Asian Earth Sciences*, 30(1):131–141, 2007. doi: 10.1016/j.jseaes.2006.08.002.

H Hosgormez, G Etiope, and MN Yalçin. New evidence for a mixed inorganic and organic origin of the Olympic Chimaera fire (Turkey): A large onshore seepage of abiogenic gas. *Geofluids*, 8(4):263–273, 2008. doi: 10.1111/j.1468-8123.2008.00226.x.

T Hothorn, F Bretz, and P Westfall. Simultaneous inference in general parametric models. *Biometrical Journal*, 50(3):346–363, 2008. doi: 10.1002/bimj.200810425.

Intergovernmental Panel on Climate Change. Working Group I Contribution to the IPCC Fifth Assessment Report Climate Change 2013: The Physical Science Basis. Summary for Policymakers, 2013.

HH Janzen. Carbon cycling in earth systems - A soil science perspective. *Agriculture, Ecosystems and Environment*, 104(3):399–417, 2004. doi: 10.1016/j.agee.2004.01.040.

TW Jeffries, S Choi, and TK Kirk. Nutritional Regulation of Lignin Degradation by Phanerochaete chrysosporium. *Applied and environmental microbiology*, 42(2):290–6, aug 1981.

EG Jobbágy and RB Jackson. The vertical distribution of soil organic carbon and its relation to climate and vegetation. *Ecological applications*, 10(April):423–436, 2000.

DB Johnson. Biodiversity and ecology of acidophilic microorganisms. *FEMS Microbiology Ecology*, 27(4):307–317, 1998. doi: 10.1016/S0168-6496(98)00079-8.

ES Kane, DW Valentine, EAG Schuur, and K Dutta. Soil carbon stabilization along climate and stand productivity gradients in black spruce forests of interior Alaska. *Canadian Journal of Forest Research*, 2129(April 2016):2118–2129, 2005. doi: 10.1139/X05-093.

K Kashefi. Temperature Limit for Life. *Science*, 301:934, 2003.

Peter B. Kelemen and Jürg Matter. In situ carbonation of peridotite for CO2 storage. 105 (45):17295–17300, 2008. ISSN 0027-8424. doi: 10.1073/pnas.0805794105.

DS Kelley. From the mantle to microbes - The lost city hydrothermal field. *Oceanography*, 18(3):21–45, 2005. doi: 10.5670/oceanog.2005.23.

DS Kelley, JA Karson, GL Früh-Green, DR Yoerger, TM Shank, DA Butterfield, JM Hayes, MO Schrenk, EJ Olson, G Proskurowski, M Jakuba, AS Bradley, B Larson, K Ludwig, D Glickson, K Buckman, AS Bradley, WJ Brazelton, K Roe, SM Bernasconi, MJ Elend, MD Lilley, JA Baross, RE Summons, and SP Sylva. A Serpentinite-Hosted Ecosystem: The Lost City Hydrothermal Field. *Science*, 307:1428–1434, 2005. doi: 10.1126/science.1102556.

L Kohl, J Laganière, KA Edwards, SA Billings, PL Morrill, G Van Biesen, and SE Ziegler. Distinct fungal and bacterial δ13C signatures as potential drivers of increasing δ13C of soil organic matter with depth. *Biogeochemistry*, 124(1-3):13–26, 2015. doi: 10.1007/s10533-015-0107-2.

L Kohl, E Cumming, A Cox, A Rietze, L Morrissey, SQ Lang, A Richter, S Suzuki, KH Nealson, and PL Morrill. Exploring the metabolic potential of microbial communities in ultra-basic, reducing springs at The Cedars, CA, US: Experimental evidence of microbial methanogenesis and heterotrophic acetogenesis. *Journal of Geophysical Research: Biogeosciences*, pages 1–18, 2016. doi: 10.1002/2015JG003233.

C Kramer and G Gleixner. Variable use of plant- and soil-derived carbon by microorganisms in agricultural soils. *Soil Biology and Biochemistry*, 38(11):3267–3278, 2006. doi: 10.1016/j.soilbio.2006.04.006.

C Kramer and G Gleixner. Soil organic matter in soil depth profiles: Distinct carbon preferences of microbial groups during carbon transformation. *Soil Biology and Biochemistry*, 40(2):425–433, 2008. doi: 10.1016/j.soilbio.2007.09.016.

JG Kuenen. Anammox bacteria: from discovery to application. *Nat Rev Micro*, 6(4):320–326, 2008.

Y Kuzyakov, JK Friedel, and K Stahr. Review of mechanisms and quantification of priming effects. *Soil Biology and Biochemistry*, 32:1485–1498, 2000. doi: 10.1016/S0038-0717(00)00084-5.

Y Kuzyakov, C Apostel, A Gunina, AM Herrmann, and M Dippold. Oxidation state, bioavailability and biochemical pathway define the fate of carbon in soil. In *EGU General Assembly Conference Abstracts*, volume 17 of *EGU General Assembly Conference Abstracts*, page 3533, 2015.

MT La Duc, A Dekas, S Osman, C Moissl, D Newcombe, and K Venkateswaran. Isolation and characterization of bacteria capable of tolerating the extreme conditions of clean room environments. *Applied and Environmental Microbiology*, 73(8):2600–2611, 2007. doi: 10.1128/AEM.03007-06.

J Laganière, D Paré, Y Bergeron, HYH Chen, BW Brassard, and X Cavard. Stability of Soil Carbon Stocks Varies with Forest Composition in the Canadian Boreal Biome. *Ecosystems*, 16(5):852–865, 2013. doi: 10.1007/s10021-013-9658-z.

J Laganière, F Podrebarac, SA Billings, KA Edwards, and SE Ziegler. A warmer climate reduces the bioreactivity of isolated boreal forest soil horizons without increasing the temperature sensitivity of respiratory CO2 loss. *Soil Biology and Biochemistry*, 84(November): 177–188, 2015. doi: 10.1016/j.soilbio.2015.02.025.

SQ Lang, DA Butterfield, M Schulte, DS Kelley, and MS Lilley. Elevated concentrations of formate, acetate and dissolved organic carbon found at the Lost City hydrothermal field. *Geochimica et Cosmochimica Acta*, 74(3):941–952, feb 2010. doi: 10.1016/j.gca.2009.10.045.

JM Lansdown, PD Quay, and SL King. CH4 production via CO2 reduction in a temperate

bog - A source of 13C-depleted CH4. *Geochimica et Cosmochimica Acta*, 56:3493–3503, 1992. doi: 10.1016/0016-7037(92)90393-W.

J Leifeld and J Fuhrer. The temperature response of CO2 production from bulk soils and soil fractions is related to soil organic matter quality. *Biogeochemistry*, 75(3):433–453, 2005. doi: 10.1007/s10533-005-2237-4.

CS Li and PA Hou. Bioaerosol characteristics in hospital clean rooms. *Science of the Total Environment*, 305(1-3):169–176, 2003. doi: 10.1016/S0048-9697(02)00500-4.

J Li, SE Ziegler, CS Lane, and SA Billings. Warming-enhanced preferential microbial mineralization of humified boreal forest soil organic matter: Interpretation of soil profiles along a climate transect using laboratory incubations. *Journal of Geophysical Research*, 117(G2):1–13, apr 2012. ISSN 0148-0227. doi: 10.1029/2011JG001769. URL `http://www.agu.org/pubs/crossref/2012/2011JG001769.shtml`.

J Li, SE Ziegler, CS Lane, and SA Billings. Legacies of native climate regime govern responses of boreal soil microbes to litter stoichiometry and temperature. *Soil Biology and Biochemistry*, 66:204–213, nov 2013. ISSN 00380717. doi: 10.1016/j.soilbio.2013.07.018.

KL Londry and DJD Marais. Stable Carbon Isotope Fractionation by Sulfate-Reducing Bacteria Stable Carbon Isotope Fractionation by Sulfate-Reducing Bacteria. 69(5), 2003. doi: 10.1128/AEM.69.5.2942.

AA Malik, V-N Roth, M Hébert, L Tremblay, T Dittmar, and G Gleixner. Linking molecular size, composition and carbon turnover of extractable soil microbial compounds. *Soil Biology and Biochemistry*, 100:66–73, 2016. doi: 10.1016/j.soilbio.2016.05.019.

NJ Mathers, RK Jalota, RC Dalal, and SE Boyd. 13C-NMR analysis of decomposing litter and fine roots in the semi-arid Mulga Lands of southern Queensland. *Soil Biology and Biochemistry*, 39(5):993–1006, 2007. doi: 10.1016/j.soilbio.2006.11.009.

TM McCollom. Laboratory Simulations of Abiotic Hydrocarbon Formation in Earth's Deep Subsurface. *Reviews in Mineralogy and Geochemistry*, 75(1):467–494, 2013. doi: 10.2138/rmg.2013.75.15.

TM McCollom and JS Seewald. Abiotic Synthesis of Organic Compounds in Deep-Sea Hydrothermal Environments on Abiotic Synthesis. *Nature Geoscience*, pages 382–401, 2007. doi: 10.1021/cr0503660.

TM McCollom and JS Seewald. Serpentinites, hydrogen, and life. *Elements*, 9(2):129–134, 2013. doi: 10.2113/gselements.9.2.129.

JM Melillo, JD Aber, AE Linkins, A Ricca, B Fry, and KJ Nadelhoffer. Carbon and nitrogen dynamics along the decay continuum: Plant litter to soil organic matter. *Plant and Soil*, 115(2):189–198, 1989. doi: 10.1007/BF02202587.

JM Melillo, PA Steudler, JD Aber, K Newkirk, H Lux, FP Bowles, C Catricala, A Magill, T Ahrens, and S Morrisseau. Soil warming and carbon-cycle feedbacks to the climate system. *Science*, 298(5601):2173–2176, 2002. doi: 10.1126/science.1074153.

H Meyer, C Kaiser, C Biasi, R Hämmerle, O Rusalimova, N Lashchinsky, C Baranyi, H Daims, P Barsukov, and A Richter. Soil carbon and nitrogen dynamics along a latitudinal transect in Western Siberia, Russia. *Biogeochemistry*, 81(2):239–252, 2006. doi: 10.1007/s10533-006-9039-1.

DR Meyer-Dombard, KM Woycheese, EN Yargıçoğlu, D Cardace, EL Shock, Y Güleçal-Pektas, and M Temel. High pH microbial ecosystems in a newly discovered, ephemeral, serpentinizing fluid seep at Yanartaş (Chimera), Turkey. *Frontiers in Microbiology*, 5 (January):1–13, 2015. doi: 10.3389/fmicb.2014.00723.

CT Mills and MB Goldhaber. On silica-based solid phase extraction techniques for isolating microbial membrane phospholipids: Ensuring quantitative recovery of

phosphatidylcholine-derived fatty acids. *Soil Biology and Biochemistry*, 42(7):1179–1182, jul 2010. doi: 10.1016/j.soilbio.2010.03.023.

CT Mills, GF Slater, RF Dias, SA Carr, CM Reddy, R Schmidt, and KW Mandernack. The relative contribution of methanotrophs to microbial communities and carbon cycling in soil overlying a coal-bed methane seep. *FEMS microbiology ecology*, 2013. doi: 10.1111/1574-6941.12079.

A Miltner, R Kindler, H Knicker, H-H Richnow, M Kästner, and M Thullner. Fate of bacterial biomass derived fatty acids in soil and their contribution to soil organic matter. *Organic Geochemistry*, 40(9):978–985, 2009. doi: 10.1016/j.orggeochem.2009.06.008.

A Miltner, P Bombach, B Schmidt-Brücken, and M Kästner. SOM genesis: microbial biomass as a significant source. *Biogeochemistry*, 111(1-3):41–55, 2011. doi: 10.1007/s10533-011-9658-z.

K. D. Monson and J. M. Hayes. Carbon isotopic fractionation in the biosynthesis of bacterial fatty acids - Ozonolysis of unsaturated fatty acids as a means of determining the intramolecular distribution of carbon isotopes. 46, 1982. ISSN 00167037. doi: 10.1016/0016-7037(82)90241-1.

JB Moody. Serpentinization: a review. *Lithos*, 9(2):125–138, 1976. doi: 10.1016/0024-4937(76)90030-X.

WG Mook, JC Bommerson, and WH Staverman. Carbon isotope fractionation between dissolved bicarbonate and gaseous carbon dioxide. *Earth and Planetary Science Letters*, 22(2):169–176, 1974. doi: 10.1016/0012-821X(74)90078-8.

DL Moorhead and RL Sinsabaugh. A theoretical model of litter decay and microbial interaction. *Ecological Monographs*, 76(2):151–174, 2006.

M Mooshammer, W Wanek, S Zechmeister-Boltenstern, and A Richter. Stoichiometric imbalances between terrestrial decomposer communities and their resources: mechanisms and implications of microbial adaptations to their resources. *Frontiers in microbiology*, 5 (February):22, 2014. doi: 10.3389/fmicb.2014.00022.

PL Morrill, G Lacrampe-Couloume, GF Slater, BE Sleep, EA Edwards, ML McMaster, DW Major, and B Sherwood Lollar. Quantifying chlorinated ethene degradation during reductive dechlorination at Kelly AFB using stable carbon isotopes. *Journal of Contaminant Hydrology*, 76(3-4):279–293, 2005. doi: 10.1016/j.jconhyd.2004.11.002.

PL Morrill, JG Kuenen, OJ Johnson, S Suzuki, A Rietze, AL Sessions, ML Fogel, and KH Nealson. Geochemistry and geobiology of a present-day serpentinization site in California: The Cedars. *Geochimica et Cosmochimica Acta*, 109:222–240, 2013. doi: 10.1016/j.gca.2013.01.043.

PL Morrill, WJ Brazelton, L Kohl, A Rietze, SM Miles, H Kavanagh, MO Schrenk, SE Ziegler, and SQ Lang. Investigations of potential microbial methanogenic and carbon monoxide utilization pathways in ultra-basic reducing springs associated with present-day continental serpentinization: the Tablelands, NL, CAN. *Frontiers in Microbiology*, 5 (November):1–13, 2014. doi: 10.3389/fmicb.2014.00613.

KJ Nadelhoffer and B Fry. Controls on Natural Nitrogen-15 and Carbon-13 Abundances in Forest soil organic matter. *Soil Science Society of America Journal*, 52:1633–1640, 1988. doi: 10.2136/sssaj1988.03615995005200060024x.

K Nakamura, Y Takai, and E Wada. Carbon isotopes of soil gases and related organic matter in an agroecosystem with special reference to paddy field. In EM Durrance, EM Galimov, ME Hinkle, GM Reimer, R Sugusaki, and SS Augustithis, editors, *Geochemistry*

of Gaseous Elements and Com- pounds, pages 455–484. Theophrastus Publications SA, Athens, Greece, 1990.

R Navarro-González, FA Rainey, P Molina, DR Bagaley, BJ Hollen, J de la Rosa, AM Small, RC Quinn, FJ Grunthaner, L Cáceres, B Gomez-Silva, and CP McKay. Mars-like soils in the Atacama Desert, Chile, and the dry limit of microbial life. *Science*, 302(5647): 1018–1021, 2003. doi: 10.1126/science.1089143.

C Neal and G Stanger. Hydrogen generation from mantle source rocks in Oman. *Earth and Planetary Science Letters*, 66:315–320, 1983. doi: 10.1016/0012-821X(83)90144-9.

JD Neufeld, MG Dumont, J Vohra, and JC Murrell. Methodological considerations for the use of stable isotope probing in microbial ecology. *Microbial ecology*, 53(3):435–442, apr 2007. doi: 10.1007/s00248-006-9125-x.

V Nikolajeva, L Liepina, Z Petrina, G Krumina, M Grube, and I Muiznieks. Antibacterial Activity of Extracts from Some Bryophytes. *Advances in Microbiology*, 02(03):345–353, 2012. doi: 10.4236/aim.2012.23042.

CE Norris, SA Quideau, JS Bhatti, and RE Wasylishen. Soil carbon stabilization in jack pine stands along the Boreal Forest Transect Case Study. *Global Change Biology*, 17(1): 480–494, 2011. doi: 10.1111/j.1365-2486.2010.02236.x.

S Ono, DT Wang, DS Gruen, B Sherwood Lollar, MS Zahniser, BJ McManus, and DD Nelson. Measurement of a Doubly Substituted Methane Isotopologue, (13)CH3D, by Tunable Infrared Laser Direct Absorption Spectroscopy. *Analytical chemistry*, 86(13):6487–94, 2014. doi: 10.1021/ac5010579.

RS Oremland, LG Miller, and MJ Whiticar. Sources and flux of natural gases from Mono Lake, California. *Geochimica et Cosmochimica Acta*, 51(11):2915–2929, 1987. doi: 10.1016/0016-7037(87)90367-X.

BJ Peterson, RW Howarth, and RH Garritt. Multiple stable isotopes used to trace the flow of organic matter in estuarine food webs. *Science*, 227(4692):1361–1363, 1985. doi: 10.1126/science.227.4692.1361.

M Philben, K Kaiser, and R Benner. Biochemical evidence for minimal vegetation change in peatlands of the West Siberian Lowland during the Medieval Climate Anomaly and Little Ice Age. *Journal of Geophysical Research: Biogeosciences*, 119(5):808–825, 2014. doi: 10.1002/2013JG002396.

M Philben, SE Ziegler, KE Edwards, R Kahler, and R Benner. Rates of soil organic nitrogen cycling increase with temperature and precipitation along a boreal forest latitudinal transect. *Biogeochemistry*, 127:397–410, 2016. doi: 10.1007/s10533-016-0187-7.

CL Phillips, KJ McFarlane, D Risk, and AR Desai. Biological and physical influences on soil 14CO2 seasonal dynamics in a temperate hardwood forest. *Biogeosciences*, 10(12): 7999–8012, 2013. doi: 10.5194/bg-10-7999-2013.

O Pisani, KM Hills, D Courtier-Murias, ML Haddix, EA Paul, RT Conant, AJ Simpson, GB Arhonditsis, and MJ Simpson. Accumulation of aliphatic compounds in soil with increasing mean annual temperature. *Organic Geochemistry*, 76:118–127, 2014. doi: 10.1016/j.orggeochem.2014.07.009.

O Pisani, SD Frey, AJ Simpson, and MJ Simpson. Soil warming and nitrogen deposition alter soil organic matter composition at the molecular-level. *Biogeochemistry*, 123(3):391–409, 2015. doi: 10.1007/s10533-015-0073-8.

FA Podrebarac, J Laganière, SA Billings, KA Edwards, and SE Ziegler. Soils isolated during incubation underestimate temperature sensitivity of respiration and its response to climate history. *Soil Biology and Biochemistry*, 93(February):60–68, 2016. doi: 10.1016/j.soilbio.2015.10.012.

FA Podrebarac, R Dove, SA Billiungs, Edwards KA, and Ziegler SE. Determining nutrient status along a boreal forest climate transect. in preparation.

WM Post, J Pastor, PJ Zinke, and AG Stangenberger. Global patterns of soil nitrogen storage. *Nature*, 317(6038):613–616, 1985. doi: 10.1038/317613a0.

CE Prescott. Litter decomposition: what controls it and how can we alter it to sequester more carbon in forest soils? *Biogeochemistry*, 101(1-3):133–149, 2010. doi: 10.1007/s10533-010-9439-0.

CM Preston, JA Trofymow, and the Canadian Intersite Decomposition Experiment Working Group. Variability in litter quality and its relationship to litter decay in Canadian forests. *Canadian Journal of Botany*, 78:1269–1287, 2000. doi: 10.1139/cjb-78-10-1269.

CM Preston, JS Bhatti, LB Flanagan, and C Norris. Stocks, chemistry, and sensitivity to climate change of dead organic matter along the Canadian boreal forest transect case study. *Climatic Change*, 74(1-3):233–251, 2006. doi: 10.1007/s10584-006-0466-8.

CM Preston, JR Nault, and JA Trofymow. Chemical Changes During 6 Years of Decomposition of 11 Litters in Some Canadian Forest Sites. Part 2. 13C Abundance, Solid-State 13C NMR Spectroscopy and the Meaning of "Lignin". *Ecosystems*, 12(7):1078–1102, 2009. doi: 10.1007/s10021-009-9267-z.

DT Price, RI Alfaro, KJ Brown, MD Flannigan, RA Fleming, EH Hogg, MP Girardin, T Lakusta, M Johnston, DW Mckenney, JH Pedlar, T Stratton, RN Sturrock, ID Thompson, JA Trofymow, and LA Venier. Anticipating the consequences of climate change for Canada's boreal forest ecosystems. *Environmental Reviews*, 365(December):322–365, 2013.

G Proskurowski, MD Lilley, JS Seewald, GL Früh-Green, EJ Olson, JE Lupton, SP Sylva, and DS Kelley. Abiogenic hydrocarbon production at lost city hydrothermal field. *Science*, 319(5863):604–7, 2008. doi: 10.1126/science.1151194.

M Quéméneur, A Palvadeau, A Postec, C Monnin, V Chavagnac, B Ollivier, and G Erauso. Endolithic microbial communities in carbonate precipitates from serpentinite-hosted hyperalkaline springs of the Voltri Massif (Ligurian Alps, Northern Italy). *Environmental science and pollution research international*, pages 13613–13624, 2015. doi: 10.1007/s11356-015-4113-7.

SA Quideau, MA Anderson, RC Graham, OA Chadwick, and SE Trumbore. Soil organic matter processes: characterization by 13C NMR and 14C measurements. *Forest Ecology and Management*, 138:19–27, 2000. doi: 10.1016/S0378-1127(00)00409-6.

SA Quideau, OA Chadwick, A Benesi, RC Graham, and MA Anderson. A direct link between forest vegetation type and soil organic matter composition. *Geoderma*, 104(1-2): 41–60, 2001. doi: 10.1016/S0016-7061(01)00055-6.

SA Quideau, RC Graham, SW Oh, PF Hendrix, and RE Wasylishen. Leaf litter decomposition in a chaparral ecosystem, Southern California. *Soil Biology and Biochemistry*, 37 (11):1988–1998, 2005. doi: 10.1016/j.soilbio.2005.01.031.

R Development Core Team. R: A Language and Environment for Statistical Computing, 2015. URL `http://www.r-project.org`.

JA Reuter, DV Spacek, and MP Snyder. High-Throughput Sequencing Technologies. *Molecular Cell*, 58(4):586–597, 2015. doi: 10.1016/j.molcel.2015.05.004.

R Rinnan and E Bååth. Differential utilization of carbon substrates by bacteria and fungi in tundra soil. *Applied and environmental microbiology*, 75(11):3611–3620, 2009. doi: 10.1128/AEM.02865-08.

R Rinnan, A Michelsen, and E Baath. Fungi benefit from two decades of increased nutrient availability in tundra heath soil. *PLoS ONE*, 8(2), 2013.

L Ruess and PM Chamberlain. The fat that matters: Soil food web analysis using fatty acids and their carbon stable isotope signature. *Soil Biology and Biochemistry*, 42(11): 1898–1910, 2010. doi: 10.1016/j.soilbio.2010.07.020.

MJ Russell, AJ Hall, and W Martin. Serpentinization as a source of energy at the origin of life. *Geobiology*, 8(5):355–71, 2010. doi: 10.1111/j.1472-4669.2010.00249.x.

R Sánchez-Murillo, E Gazel, EM M Schwarzenbach, M Crespo-Medina, MO O Schrenk, J Boll, and BC C Gill. Geochemical evidence for active tropical serpentinization in the Santa Elena Ophiolite, Costa Rica: An analog of a humid early Earth? *Geochemistry Geophysics Geosystems*, 18:1–16, 2014. doi: 10.1002/2014GC005356.Received.

H Santruckova, MI Bird, YN Kalaschnikov, M Grund, D Elhottova, M Simek, S Grigoryev, G Gleixner, A Arneth, E-D Schulze, and J Lloyd. Microbial characteristics of soils on a latitudinal transect in Siberia. *Global Change Biology*, 9(7):1106–1117, 2003. doi: 10.1046/j.1365-2486.2003.00596.x.

JPW Scharlemann, EVJ Tanner, R Hiederer, and V Kapos. Global soil carbon: understanding and managing the largest terrestrial carbon pool. *Carbon Management*, 5(1):81–91, 2014. doi: 10.4155/cmt.13.77.

J Schimel. Assumptions and Errors in the NH4+ Pool Dilution Technique for Measuring Mineralizaion and Immobilization. *Soil Biology and Biochemistry*, 28(6):827–828, 1996. doi: 10.1128/AEM.02280-15.Editor.

JP Schimel and SM Schaeffer. Microbial control over carbon cycling in soil. *Frontiers in microbiology*, 3(September):348, 2012. doi: 10.3389/fmicb.2012.00348.

WH Schlesinger. *Biogeochemistry. An analysis of global change*. Academic Press, San Diego, CA, USA, 1997.

WH Schlesinger and JA Andrews. Soil respiration and the global carbon cycle. *Biogeochemistry*, 48:7–20, 2000.

J Schnecker, B Wild, M Takriti, RJ Eloy Alves, N Gentsch, A Gittel, A Hofer, K Klaus, A Knoltsch, N Lashchinskiy, R Mikutta, and A Richter. Enzyme patterns in topsoil and subsoil horizons along a latitudinal transect in Western Siberia. *Soil Biology and Biochemistry*, 83:106–115, 2015. doi: 10.1016/j.soilbio.2015.01.016.

J Schnecker, W Borken, A Schindlbacher, and W Wanek. Little effects on soil organic matter chemistry of density fractions after seven years of forest soil warming. *Soil Biology and Biochemistry*, 103:300–307, 2016. ISSN 00380717. doi: 10.1016/j.soilbio.2016.09.003.

MO Schrenk, DS Kelley, SA Bolton, and JA Baross. Low archaeal diversity linked to subseafloor geochemical processes at the Lost City Hydrothermal Field, Mid-Atlantic Ridge. *Environmental Microbiology*, 6(10):1086–1095, 2004. doi: 10.1111/j.1462-2920.2004.00650.x.

MO Schrenk, WJ Brazelton, and SQ Lang. Serpentinization, Carbon, and Deep Life. *Reviews in Mineralogy and Geochemistry*, 75(1):575–606, 2013. doi: 10.2138/rmg.2013.75.18.

F Schubotz, JS Lipp, M Elvert, and K-U Hinrichs. Stable carbon isotopic compositions of intact polar lipids reveal complex carbon flow patterns among hydrocarbon degrading microbial communities at the Chapopote asphalt volcano. *Geochimica et Cosmochimica Acta*, 75(16):4399–4415, aug 2011. doi: 10.1016/j.gca.2011.05.018.

M Schulte, D Blake, T Hoehler, and T McCollom. Serpentinization and It's Implication for Life on Early Earth and Mars. *Astrobiology*, 6(2):364–376, 2006.

C Schurig, RH Smittenberg, J Berger, F Kraft, SK Woche, M-O Goebel, HJ Heipieper, A Miltner, and M Kaestner. Microbial cell-envelope fragments and the formation of soil

organic matter: a case study from a glacier forefield. *Biogeochemistry*, 113(1-3):595–612, 2012. doi: 10.1007/s10533-012-9791-3.

AL Sessions, SP Sylva, and JM Hayes. Moving-wire device for carbon isotopic analyses of nanogram quantities of nonvolatile organic carbon. *Analytical chemistry*, 77(20):6519–6527, 2005. doi: 10.1021/ac051251z.

Zachary Sharp. *Stable isotope geochemistry*. Pearson Prentice Hall, Upper Saddle River, 2007.

Y Shen, FH Chapelle, EW Strom, and R Benner. Origins and bioavailability of dissolved organic matter in groundwater. *Biogeochemistry*, 122(1):61–78, 2014. doi: 10.1007/s10533-014-0029-4.

B. Sherwood Lollar, SK Frape, P Fritz, SA Macko, JA Welhan, R Blomqvist, and PW Lahermo. Evidence for bacterially generated hydrocarbon gas in Canadian Shield and Fennoscandian Shield rocks. *Geochimica et cosmochimica acta*, 57(23-24):5073–5085, 1993.

B Sherwood Lollar, TD Westgate, JA Ward, GF Slater, and G Lacrampe-Couloume. Abiogenic formation of alkanes in the Earth's crust as a minor source for global hydrocarbon reservoirs. *Nature*, 416(6880):522–524, 2002. doi: 10.1038/416522a.

B Sherwood Lollar, K Voglesonger, L-H Lin, G Lacrampe-Couloume, J Telling, TA Abrajano, TC Onstott, and LM Pratt. Hydrogeologic controls on episodic H2 release from precambrian fractured rocks–energy for deep subsurface life on earth and mars. *Astrobiology*, 7 (6):971–986, 2007. doi: 10.1089/ast.2006.0096.

JA Silfer, MH Engel, SA Macko, and EJ Jumeau. Stable carbon isotope analysis of amino acid enantiomers by conventional isotope ratio mass spectrometry and combined gas chromatography/isotope ratio mass spectrometry. *Analytical Chemistry*, 63(4):370–374, 1991. doi: 10.1021/ac00004a014.

RL Sinsabaugh. Phenol oxidase, peroxidase and organic matter dynamics of soil. *Soil Biology and Biochemistry*, 42(3):391–404, 2010. doi: 10.1016/j.soilbio.2009.10.014.

S Sjögersten, BL Turner, N Mahieu, LM Condron, and PA Wookey. Soil organic matter biochemistry and potential susceptibility to climatic change across the forest-tundra ecotone in the Fennoscandian mountains. *Global Change Biology*, 9(5):759–772, 2003. doi: 10.1046/j.1365-2486.2003.00598.x.

NH Sleep, A Meibom, TH Fridriksson, RG Coleman, and DK Bird. H2-rich fluids from serpentinization: geochemical and biotic implications. *Proceedings of the National Academy of Sciences of the United States of America*, 101(35):12818–12823, 2004. doi: 10.1073/pnas.0405289101.

P Sollins, P Homann, and BA Caldwell. Stabilization and destabilization of soil organic matter: Mechanisms and controls. *Geoderma*, 74(1-2):65–105, 1996. doi: 10.1016/S0016-7061(96)00036-5.

KT Steffen, T Cajthaml, J Šnajdr, and P Baldrian. Differential degradation of oak (Quercus petraea) leaf litter by litter-decomposing basidiomycetes. *Research in Microbiology*, 158 (5):447–455, 2007. doi: 10.1016/j.resmic.2007.04.002.

S Steinbeiss, G Gleixner, and M Antonietti. Effect of biochar amendment on soil carbon balance and soil microbial activity. *Soil Biology and Biochemistry*, 41(6):1301–1310, 2009. doi: 10.1016/j.soilbio.2009.03.016.

Catherine E. Stewart, Pratibha Moturi, Ronald F. Follett, and Ardell D. Halvorson. Lignin biochemistry and soil N determine crop residue decomposition and soil priming. *Biogeochemistry*, 124(1):335–351, 2015. ISSN 1573515X. doi: 10.1007/s10533-015-0101-8.

R Stokke, I Roalkvam, A Lanzen, H Haflidason, and IH Steen. Integrated metagenomic and metaproteomic analyses of an ANME-1-dominated community in marine cold

seep sediments. *Environmental microbiology*, 14(5):1333–46, 2012. doi: 10.1111/j.1462-2920.2012.02716.x.

DA Stolper, AM Martini, M Clog, PM Douglas, SS Shusta, DL Valentine, AL Sessions, and JM Eiler. Distinguishing and understanding thermogenic and biogenic sources of methane using multiply substituted isotopologues. *Geochimica et Cosmochimica Acta*, 161:219–247, 2015. doi: 10.1016/j.gca.2015.04.015.

K Streit, F Hagedorn, D Hiltbrunner, M Portmann, M Saurer, N Buchmann, B Wild, A Richter, S Wipf, and RTW Siegwolf. Soil warming alters microbial substrate use in alpine soils. *Global change biology*, 20(1327-1338):1–12, 2014. doi: 10.1111/gcb.12396.

MS Strickland and J Rousk. Considering fungal:bacterial dominance in soils – Methods, controls, and ecosystem implications. *Soil Biology and Biochemistry*, 42(9):1385–1395, 2010. doi: 10.1016/j.soilbio.2010.05.007.

K Suda, Y Ueno, M Yoshizaki, H Nakamura, K Kurokawa, E Nishiyama, K Yoshino, Y Hongoh, K Kawachi, S Omori, K Yamada, N Yoshida, and S Maruyama. Origin of methane in serpentinite-hosted hydrothermal systems: The CH4–H2–H2O hydrogen isotope systematics of the Hakuba Happo hot spring. *Earth and Planetary Science Letters*, 386:112–125, 2014. doi: 10.1016/j.epsl.2013.11.001.

S Suzuki, S Ishii, A Wu, A Cheung, A Tenney, G Wanger, JG Kuenen, and KH Nealson. Microbial diversity in The Cedars, an ultrabasic, ultrareducing, and low salinity serpentinizing ecosystem. *Proceedings of the National Academy of Sciences*, 110(38):15336–15341, 2013. doi: 10.1073/pnas.1302426110.

S Suzuki, JG Kuenen, K Schipper, S van der Velde, S Ishii, A Wu, DY Sorokin, A Tenney, XY Meng, PL Morrill, Y Kamagata, G Muyzer, and KHh Nealson. Physiological and genomic features of highly alkaliphilic hydrogen-utilizing Betaproteobacteria

from a continental serpentinizing site. *Nature communications*, 5(May):3900, 2014. doi: 10.1038/ncomms4900.

N Szponar, WJ Brazelton, MO Schrenk, DM Bower, A Steele, and PL Morrill. Geochemistry of a continental site of serpentinization, the Tablelands Ophiolite, Gros Morne National Park: A Mars analogue. *Icarus*, 224(2):286–296, 2013. doi: 10.1016/j.icarus.2012.07.004.

MA Teece, ML Fogel, ME Dollhopf, and KH Nealson. Isotopic fractionation associated with biosynthesis of fatty acids by a marine bacterium under oxic and anoxic conditions. *Organic Geochemistry*, 30(12):1571–1579, 1999. doi: 10.1016/S0146-6380(99)00108-4.

RB Thomas. *Intramolecular Isotopic Variation in Acetate in Sediments and Wetland Soils*. PhD thesis, Pennsylvania State University, 2008.

SF Thornton and J McManus. Application of organic carbon and nitrogen stable isotope and C/N ratios as source indicators of organic matter provenance in estuarine systems: Evidence for the Tay Estuary, Scotland. *Estuarine, Coastal and Shelf Science*, 38(3): 219–233, 1994. doi: 10.1006/ecss.1994.1015.

I Tiago and A Veríssimo. Microbial and functional diversity of a subterrestrial high pH groundwater associated to serpentinization. *Environmental Microbiology*, 15(6):1687–1706, 2013. doi: 10.1111/1462-2920.12034.

JA Trofymow and CIDET Working Group. *The Canadian Intersite Decomposition Experiment Project and Site Establishment Report*. Victoria, BC, Canada, 1998. ISBN 0830-0453; Information Report BC-X-378.

MR Turetsky. The Role of Bryophytes in Carbon and Nitrogen Cycling. *The Bryologist*, 106 (3):395–409, 2003.

MR Turetsky, MC Mack, TN Hollingsworth, and JW Harden. The role of mosses in ecosystem succession and function in Alaska's boreal forest. *Canadian Journal of Forest Research*, 40(7):1237–1264, 2010. doi: 10.1139/X10-072.

DL Valentine. Biogeochemistry and microbial ecology of methane oxidation in anoxic environment: a review. *Antonie van leuwenhoek*, pages 271–282, 2001. doi: 10.1023/A:1020587206351.

DL Valentine, A Chidthaisong, A Rice, WS Reeburgh, and SC Tyler. Carbon and hydrogen isotope fractionation by moderately thermophilic methanogens. *Geochimica et Cosmochimica Acta*, 68(7):1571–1590, 2004. doi: 10.1016/j.gca.2003.10.012.

GJ van Oldenborgh, M Collins, J Arblaster, JH Christensen, J Marotzke, SB Power, M Rummukainen, and T Zhou. Atlas of Global and Regional Climate Projections. In TF Stocker, D Qin, G-K Plattner, M Tignor, SK Allen, J Boschung, A Nauels, Y Xia, V Bex, and PM Midgley, editors, *Climate Change 2013: The Physical Science Basis. Contribution of Working Group I to the Fifth Assessment Report of the Intergovernmental Panel on Climate Change*, pages 1311–1394. 2013. ISBN ISBN 978-1-107-66182-0. doi: 10.1017/CBO9781107415324.029.

R Vet, RS Artz, S Carou, M Shaw, CU Ro, W Aas, A Baker, VC Bowersox, F Dentener, C Galy-Lacaux, A Hou, JJ Pienaar, R Gillett, MC Forti, S Gromov, H Hara, T Khodzher, NM Mahowald, S Nickovic, PSP Rao, and NW Reid. A global assessment of precipitation chemistry and deposition of sulfur, nitrogen, sea salt, base cations, organic acids, acidity and pH, and phosphorus. *Atmospheric Environment*, 93:3–100, 2014. doi: 10.1016/j.atmosenv.2013.10.060.

DH Vitt. Growth and production dynamics of boreal mosses over climatic, chemical and

topographic gradients. *Botanical Journal of the Linnean Society*, 104:35–59, 1990. doi: 10.1111/j.1095-8339.1990.tb02210.x.

JC Vogel, PM Grootes, and WG Mook. Isotopic fractionation between gaseous and dissolved carbon dioxide. *Zeitschrift für Physik*, 230(3):225–238, 1970. doi: 10.1007/BF01394688.

M von Lützow, I Kogel-Knabner, K Ekschmitt, E Matzner, G Guggenberger, B Marschner, and H Flessa. Stabilization of organic matter in temperate soils: mechanisms and their relevance under different soil conditions - a review. *European Journal of Soil Science*, 57 (4):426–445, aug 2006. doi: 10.1111/j.1365-2389.2006.00809.x.

JA Vucetich, DD Reed, A Breymeyer, M Degórski, GD Mroz, J Solon, E Roo-Zielinska, and R Noble. Carbon pools and ecosystem properties along a latitudinal gradient in northern Scots pine (Pinus sylvestris) forests. *Forest Ecology and Management*, 136(1-3):135–145, 2000. doi: 10.1016/S0378-1127(99)00288-1.

EH Wahl, B Fidric, CW Rella, S Koulikov, B Kharlamov, S Tan, AA Kachanov, BA Richman, ER Crosson, BA Paldus, S Kalaskar, and DR Bowling. Applications of cavity ring-down spectroscopy to high precision isotope ratio measurement of 13C/12C in carbon dioxide. *Isotopes in Environmental and Health studies*, 42(1):21–35, 2006. doi: 10.1080/10256010500502934.

SA Waksman and FC Gerretsen. Influence of Temperature and Moisture Upon the Nature and Extent of Decomposition of Plant Residues by Microorganisms. *Ecology*, 12(1):33–60, 1931.

MP Waldrop and MK Firestone. Altered utilization patterns of young and old soil C by microorganisms caused by temperature shifts and N additions. *Biogeochemistry*, 67(2): 235–248, 2004.

H Wallander, H Göransson, and U Rosengren. Production, standing biomass and natural abundance of 15N and 13C in ectomycorrhizal mycelia collected at different soil depths in two forest types. *Oecologia*, 139(1):89–97, 2004. doi: 10.1007/s00442-003-1477-z.

MD Wallenstein, AM Hess, MR Lewis, H Steltzer, and E Ayres. Decomposition of aspen leaf litter results in unique metabolomes when decomposed under different tree species. *Soil Biology and Biochemistry*, 42(3):484–490, 2010. doi: 10.1016/j.soilbio.2009.12.001.

DT Wang, DS Gruen, B Sherwood Lollar, K-U Hinrichs, LC Stewart, JF Holden, AN Hristov, JW Pohlman, PL Morrill, M Könneke, KB Delwiche, and EP Reeves. Nonequilibrium clumped isotope signals in microbial methane. *Science*, 348(6223):428–431, 2015.

J Ward, GF Slater, DP Moser, L-H Lin, G Lacrampe-Couloume, AS Bonin, M Davidson, JA Hall, B Mislowack, RES Bellamy, TC Onstott, and B Sherwood Lollar. Microbial hydrocarbon gases in the Witwatersrand Basin, South Africa: Implications for the deep biosphere. *Geochimica et Cosmochimica Acta*, 68(15):3239–3250, aug 2004. doi: 10.1016/j.gca.2004.02.020.

LI Wassenaar. Evaluation of the origin and fate of nitrate in the Abbbotsford Aquifer using isotopes of 15N and 18O in NO3-. *Applied Geochemistry*, 10:391–405, 1995. doi: 10.1016/0883-2927(95)00013-A.

M Werth and Y Kuzyakov. 13C fractionation at the root–microorganisms–soil interface: A review and outlook for partitioning studies. *Soil Biology and Biochemistry*, 42(9):1372–1384, 2010. doi: 10.1016/j.soilbio.2010.04.009.

D White and D Ringelberg. Signature lipid biomarker analysis. In R.S. Burlage, editor, *Techniques in Microbial Ecology*, pages 255–272. Oxford University Press, Oxford, UK, 1998. ISBN 9780195092233.

MJ Whiticar. Carbon and hydrogen isotope systematics of bacterial formation and oxidation of methane. *Chemical Geology*, 161(1-3):291–314, 1999. doi: 10.1016/S0009-2541(99)00092-3.

MJ Whiticar, E Faber, and M Schoell. Biogenic methane formation in marine and freshwater environments: CO2 reduction vs. acetate fermentation—Isotope evidence. *Geochimica et Cosmochimica Acta*, 50(5):693–709, 1986. doi: 10.1016/0016-7037(86)90346-7.

WB Whitman, DC Coleman, and WJ Wiebe. Prokaryotes: the unseen majority. *Proc Natl Acad Sci U S A*, 95(12):6578–6583, 1998. doi: 10.1073/pnas.95.12.6578.

LY Wick, O Pelz, SM Bernasconi, N Andersen, and H Harms. Influence of the growth substrate on ester-linked phospho- and glycolipid fatty acids of PAH-degrading Mycobacterium sp . LB501T. *Environmental microbiology*, 5(8):672–680, 2003.

K Wickings, SA Grandy, SC Reed, and CC Cleveland. Management intensity alters decomposition via biological pathways. *Biogeochemistry*, 104(1-3):365–379, 2011. doi: 10.1007/s10533-010-9510-x.

K Wickings, SA Grandy, SC Reed, and CC Cleveland. The origin of litter chemical complexity during decomposition. *Ecology letters*, 15(10):1180–8, 2012. doi: 10.1111/j.1461-0248.2012.01837.x.

B Wild, W Wanek, W Postl, and A Richter. Contribution of carbon fixed by Rubisco and PEPC to phloem export in the Crassulacean acid metabolism plant Kalanchoë daigremontiana. *Journal of Experimental Botany*, 61(5):1375–1383, 2010.

MA Wilson. *N.M.R Techniques and Applications in Geochemistry and Soil Chemistry*. Pergamon Press, Oxford, UK, 1987.

I Woltemate, MJ Whiticar, and M Schoell. Carbon and hydrogen isotopic composition of bacterial methane in a shallow freshwater lake. *Limnology and Oceanography*, 29(5): 985–992, 1984. doi: 10.4319/lo.1984.29.5.0985.

K Woycheese, DR Meyer-Dombard, D Cardace, A Argayosa, and C Arcilla. Out of the dark: Transitional subsurface-to-surface microbial diversity in a terrestrial serpentinizing seep (Manleluag, Pangasinan, the Philippines). *Frontiers in Microbiology*, 6:1–12, 2015. doi: 10.3389/fmicb.2015.00044.

CY Xu and VP Singh. Evaluation and generalization of temperature based methods for calculating evaporation. *Hydrological processes*, 319:305–319, 2001.

Y Yang, CD Campbell, L Clark, CM Cameron, and E Paterson. Microbial indicators of heavy metal contamination in urban and rural soils. *Chemosphere*, 63(11):1942–1952, 2006. doi: 10.1016/j.chemosphere.2005.10.009.

W Yuan, S Liu, W Dong, S Liang, S Zhao, J Chen, W Xu, X Li, A Barr, TA Black, W Yan, ML Goulden, L Kulmala, A Lindroth, HA Margolis, Y Matsuura, E Moors, M van der Molen, T Ohta, K Pilegaard, A Varlagin, and T Vesala. Differentiating moss from higher plants is critical in studying the carbon cycle of the boreal biome. *Nature communications*, 5:4270, 2014. doi: 10.1038/ncomms5270.

W Zech, L Haumaier, and I Kogel-Knabner. Changes in aromaticity and carbon distribution of soil organic matter due to pedogenesis. *The Science of the Total Environment*, 81/82: 179–186, 1989.

S Zechmeister-Boltenstern, KM Keiblinger, M Mooshammer, J Peñuelas, A Richter, J Sardans, and W Wanek. The application of ecological stoichiometry to plant–microbial–soil organic matter transformations. *Ecological Monographs*, 85(2):133–155, 2015. doi: 10.1890/14-0777.1.

CL Zhang, Q Ye, A-L Reysenbach, D Götz, A Peacock, DC White, J Horita, DR Cole, J Fong, L Pratt, J Fang, and Y Huang. Carbon isotopic fractionations associated with thermophilic bacteria Thermotoga maritima and Persephonella marina. *Environmental microbiology*, 4(1):58–64, 2002.

CL Zhang, Y Li, Q Ye, J Fong, AD Peacock, E Blunt, J Fang, DR Lovley, and DC White. Carbon isotope signatures of fatty acids in Geobacter metallireducens and Shewanella algae. *Chemical Geology*, 195(1-4):17–28, 2003. doi: 10.1016/S0009-2541(02)00386-8.

SE Ziegler, SA Billings, CS Lane, J Li, and ML Fogel. Warming alters routing of labile and slower-turnover carbon through distinct microbial groups in boreal forest organic soils. *Soil Biology and Biochemistry*, 60:23–32, 2013. doi: 10.1016/j.soilbio.2013.01.001.

SE Ziegler, R Benner, SA Billings, KA Edwards, M Philben, X Zhu, and J. Laganiere. Climate change can accelerate carbon fluxes without changing soil carbon stocks. *Frontiers in Earth Sciences*, 5:2, 2017.